



UNIVERSITY OF
BIRMINGHAM

University of Birmingham

**DEVELOPMENT AND APPLICATIONS OF PROTON
TRANSFER REACTION MASS SPECTROMETRY FOR
MEDICINE**

By

PREMA DEVI CHELLAYAH

A thesis submitted to
The University of Birmingham
for the degree of

DOCTOR OF PHILOSOPHY

**School of Physics and Astronomy
The University of Birmingham
July 2018**

UNIVERSITY OF
BIRMINGHAM

University of Birmingham Research Archive

e-theses repository

This unpublished thesis/dissertation is copyright of the author and/or third parties. The intellectual property rights of the author or third parties in respect of this work are as defined by The Copyright Designs and Patents Act 1988 or as modified by any successor legislation.

Any use made of information contained in this thesis/dissertation must be in accordance with that legislation and must be properly acknowledged. Further distribution or reproduction in any format is prohibited without the permission of the copyright holder.

University of Birmingham

School of Physics and Astronomy
Doctor of Philosophy

PhD

Academic Year 2014 - 2018

PREMA DEVI CHELLAYAH

**DEVELOPMENT AND APPLICATIONS OF PROTON
TRANSFER REACTION MASS SPECTROMETRY FOR
MEDICINE**

Supervisor: Prof Chris Mayhew
2014-2018

This thesis is submitted in partial fulfilment of the requirements for the
degree of Physics and Astronomy

© University of Birmingham 2018. All rights reserved. No part of this
publication may be reproduced without the written permission of the
copyright owner.

ABSTRACT

This thesis reports the use of Proton Transfer Reaction-Mass Spectrometry (PTR-MS) in the health sciences. Here we provide the details on volatiles emitted from the shisha paste and when shisha paste undergoes combustion follows on from this, the analyses of which are aided by GC-MS (Gas Chromatography-Mass Spectrometry) measurements. This work presents the first PTR-MS study of shisha smoking, a poster for which won the best poster award at the Breath Research Conference in Zürich 2016. Presented first is a pre-investigation of two key compounds, menthol and vanillin, expected in some shisha pastes to determine the product ions together with related compounds that have differences in their functional groups. Details on the reactions of H_3O^+ with several fluorinated anaesthetics are presented, with the objective to provide details on which product ions should be monitored in a planned study of washout characteristics of anaesthetics following surgery. Breath washout characteristics for volatiles present in the blood following the ingestion of a peppermint oil capsule are presented, being part of a much larger European study dealing with breath standardisation. Here we present details on intra- and inter- individuals variability. The final results chapter looks at volatiles in breath samples of young men who have undergone a head trauma.

DEDICATION

My Family

ACKNOWLEDGEMENTS

This PhD was funded by the Health Ministry of Malaysia.

First and foremost, I would like to express my upmost gratitude and thanks to my supervisor Professor Dr Chris Mayhew. It has been an honor to be the first PhD student to be able to put his new title in my thesis as Professor Dr Chris Mayhew. I really appreciate his valuable input, skillful guidance and indomitable patience. Throughout his supervision, he has taught me, both consciously and unconsciously, how to be an excellent experimental physicist. He, has also given me opportunities to be part of the European research project in collaboration with the Univeristy of Innsbruck and has funded me so that I can attend International Breath analysis conferences. Through the contributions of his time and ideas, my Ph.D. experience has been a very stimulating, rewarding and treasured experience.

It is my pleasure to acknowledge the roles of several individuals who were instrumental for the completion of my Ph.D research. First of all, I want to thank my working colleagues and also my friend Dr. Raquel Fernandez del Rio and Kathleen Hynes (who also proof read my thesis), who encouraged me to keep going on this research project, being caring, helpful and being there for me over these years. The joy and enthusiasm they offered throughout my research was contagious and motivational , even during tough times in the pursuit of my Ph.D. I am forever grateful to them. We had many great and fun moments together.

I would also like to thank Dr John Thompson, who gave me many suggestions and advice on experimental works, especially on statistics. My sincere thanks to him in helping me by providing diffusion tubes for my ‘Isopene Calibration experiment’ and for his valuable discussions. My sincere thanks to David Howse, who helped me to proof read my thesis chapters and gave me moral support.

I would also like to thank Dr. Margaret O'Hara for her help and advice during the course of the breath analysis and who took initiative to collaborate with the Queen Elizabeth hospital's liver, anaesthetics and Neuro-Trauma research groups. Here, I am taking this opportunity to thank clinicians, paramedics and scientists from the Queen Elizabeth hospital, Birmingham who have cooperated with the Molecular research group of the University of Birmingham (UOB) in initial clinical trials such as Breath research on concussed rugby players and motorway accident victims 'Golden hours sample' (6 hours) from A & E department and research on the headspace of the blood of general Neuro-Trauma victims.

I am grateful for the time spent with my Molecular Physics working colleagues Daniel Blenkhorn, Ramon Gonzalez and David Olivienza. My special thanks to Daniel Blenkhorn who was willing to help and assist me during this period. It was a great pleasure working with them. Also Joseph Bryon who helped me to proof read some part of my thesis.

This work would not have materialised without the financial support of the Ministry of Health Malaysia (MOH). My grateful acknowledgement for their funding, that made my Ph.D. work possible. The ministry has been of great help to me and through this sponsorship and allowed me to gain an extension of one year. I have been able to explore the advancement of research techniques in a range of areas and have also been able to communicate with different international scientific committees and clinical scientists. Besides that, I would like to acknowledge Mr Nik Mohammed Hazmi (Allied Health Science Division), Mrs Mahsom Pawanchek and Mr Hizwan (seniors) who supported my extension. I appreciate their time.

A deep appreciation and thanks to my parents, Mr Chellayah Arunasalam and Moganambal Govindasamy who let me go, to explore this journey and their constant

support and love throughout. I am a first generation traveller and the first person in my family to pursue international education and travel experiences. It was a huge sacrifice for them and myself to live 10588 km away from each other, especially myself being overseas for an extended period of time. Very special thanks to my family members and relatives who encouraged and supported me morally. I am taking this opportunity to thank all my good friends who helped to go through this Ph.D journey.

TABLE OF CONTENTS

ABSTRACT	i
DEDICATION	ii
TABLE OF CONTENTS	vi
LIST OF FIGURES	x
Chapter 5	xi
Chapter 6	xii
Chapter 7	xv
Chapter 8	xvii
LIST OF TABLES	xviii
LIST OF ABBREVIATIONS	xxii
CHAPTER 1	1
1 Introduction	1
1.1 Background.....	1
1.2 Thesis Outline.....	4
1.3 AREAS INVESTIGATED	5
1.3.1 VOLATILE ORGANIC COMPOUNDS ASSOCIATED WITH SHISHA PASTE AND SHISHA SMOKING	5
1.3.2 INVESTIGATION OF THE PRODUCT IONS RESULTING FROM THE REACTIONS OF H ₃ O ⁺ WITH VANILLIN, MENTHOL AND ASSOCIATED COMPOUNDS (CYCLOHEXANOL, PHENOL, ANISOLE, BENZALDEHYDE AND GUAIACOL)	6
1.3.3 PTR-TOF-MS STUDIES OF THE REACTIONS OF H ₃ O ⁺ AND O ₂ ⁺ WITH THE GENERAL ANAESTHETIC GASES HALOTHANE, ISOFLURANE, ENFLURANE, SEVOFLURANE, DESFLURANE AND METHOXYFLURANE.....	6
1.3.4 BREATH ANALYSIS TO DETERMINE HUMAN WASHOUT CHARACTERISTICS OF KEY VOLATILE ORGANIC COMPOUNDS CONTAINED IN PEPPERMINT OIL	7
1.3.5 BREATH ANALYSIS OF RUGBY PLAYERS WHO HAD A CONCUSSION (HEALTHY AND INJURED).....	8
CHAPTER 2	10
2 PRINCIPLE OF PROTON TRANSFER REACTION MASS SPECTROMETRY ...	10
2.1 Background and Development of PTR-MS Instruments.....	10
2.1.1 Advantages of PTR-MS technology.....	14
2.1.2 Principles of Proton Transfer Reaction Mass Spectrometry	15
2.1.3 Proton Affinity and protonation	21
2.1.4 Fragmentation.....	23
2.1.5 Components of a PTR-MS	25
2.1.6 The ratio of electric field and number density of buffer gas - reduced electric field (<i>E/N</i>)	29
2.1.7 Ion Mobility.....	30

2.1.8 Quantitative characteristics of PTR-MS.....	32
2.1.9 Detection system of Mass Spectrometer (MS).....	33
2.2 PTR-MS Data Analysis	40
3 Breath Sampling for Clinical Screening, Diagnosis and Monitoring.....	44
3.1 Introduction	44
3.1.1 Breath composition.....	47
3.2 Human Respiratory System.....	50
3.2.1 Gas exchange in Humans	51
3.2.2 Lung capacities and volumes.....	53
3.3 Methods of Alveolar Breath Sampling collection	55
3.4 Glass syringes and other consumables for breath sampling.....	57
3.5 Capnometry (Capnography) for alveolar breath sampling.....	60
3.6 Exhaled breath sampling protocol	63
4 VOLATILE ORGANIC COMPOUNDS ASSOCIATED WITH SHISHA PASTE AND SHISHA SMOKING	67
4.1 Introduction	67
4.2 Experimental Methods.....	72
4.2.1 Instrumentation.....	72
4.3 Samples.....	76
4.3.1 Shisha Pastes	76
4.3.2 Charcoal Briquettes	76
4.4 Results	77
4.4.1 Headspace Analyses of Shisha Pastes	77
4.5 VOCs in mainstream smoke.....	82
4.6. Discussion.....	85
4.6.1 Key Findings	85
4.6.2 VOCs from combustion of shisha paste and charcoal.....	87
4.7 Conclusion.....	89
5 INVESTIGATION OF THE PRODUCT IONS RESULTING FROM THE REACTIONS OF H_3O^+ WITH VANILLIN, MENTHOL AND ASSOCIATED COMPOUNDS (CYCLOHEXANOL, PHENOL, ANISOLE, BENZALDEHYDE AND GUAIACOL)	91
5.1 Introduction	91
5.2 Experimental Details	93
5.3 Results and Discussion	96
5.3.1 Headspace of associated compounds (Cyclohexanol, Phenol, Anisole, Benzaldehyde, Guaiacol).....	96
5.3.2 The reaction of menthol with H_3O^+	113
5.3.3 The reaction of vanillin with H_3O^+	116
5.4 Conclusion.....	119
6 PTR-TOF-MS STUDIES OF THE REACTIONS OF H_3O^+ AND O_2^+ WITH THE GENERAL ANAESTHETIC GASES HALOTHANE, ISOFLURANE, ENFLURANE, SEVOFLURANE, DESFLURANE AND METHOXYFLURANE ..	120

6.1. Introduction	120
6.2 Anaesthetics Details	123
6.3 Results and Discussion	125
6.3.1 Halothane.....	125
6.3.1.1 Reaction with H ₃ O ⁺	125
6.3.2 Isoflurane	130
6.3.3 Enflurane	143
6.3.4 Sevoflurane.....	153
6.3.5 Methoxyflurane	162
6.3.6 Desflurane.....	171
6.4 Conclusion.....	179
7 BREATH ANALYSIS TO DETERMINE HUMAN WASHOUT CHARACTERISTICS OF KEY VOLATILE ORGANIC COMPOUNDS CONTAINED IN PEPPERMINT OIL	181
7.1 Introduction	181
7.2 Experimental Details and Protocol.....	184
7.3 Peppermint Oil Capsules	187
7.4 Participant information	191
7.5 Buffered End Tidal (BET).....	193
7.6 Headspace measurements of compounds associated with peppermint oil	195
7.6.1 Headspace of α -pinene	195
7.6.2 Headspace of β -pinene	198
7.6.3 Headspace of 1,8-cineole.....	200
7.6.4 Headspace of limonene.....	202
7.6.5 Headspace of menthone.....	204
7.6.6 Headspace of menthol	206
7.6.7 Headspace of the oil contained in the Boots' Peppermint Capsule.....	209
7.6.8 VOCs in the exhaled breath after ingestion of a peppermint capsule	212
7.6.9 Washout characteristic of peppermint capsule. Personal and inter- individual variations	213
7.7 Conclusion.....	225
8 Breath analysis of Rugby Players who had concussion (controls and injured).....	228
8.1 Introduction	228
8.2 Details of analytes measured from exhaled breath of rugby players (healthy and injured players)	232
8.2.1 Isoprene	234
8.2.2 Acetone.....	235
8.2.3 Methanol.....	236
8.3 Experimental details	237
8.3.1 Details of the players who took part in this breath analysis of concussion study	239
8.3.2 Data analysis.....	240
8.4 Isoprene calibration	241

8.4.1 Materials and methods.....	242
8.5 Results	245
8.5.1 Pre and post injured samples from the same players.....	245
8.5.2 Comparison of methanol, acetone and isoprene of healthy players and injured players	249
8.6 Gravimetric calibration and the use of scaling for using different sized Tracer Cert® diffusion tubes	254
8.7 Using calibrated diffusion tubes and other Tracer Cert® diffusion tubes with scaling for calibration for of PTR-MS quadrupole.....	256
8.8 Discussion.....	258
8.9 Conclusion.....	261
9 CONCLUSIONS AND FURTHER DISCUSSION.....	262
9.1.1 Volatile Organic Compounds Associated with Shisha Paste and Shisha Smoking.....	262
9.1.2 Investigation of the product ions resulting from the reactions of H_3O^+ with menthol and vanillin and associated compounds (cyclohexanol, phenol, anisole, benzaldehyde and guaiacol).	262
9.1.3 PTR-ToF-MS studies of the reactions of H_3O^+ and O_2^+ with the anaesthetic gases halothane, isoflurane, enflurane, sevoflurane, desflurane and methoxyflurane.....	263
9.1.4 Washout Characteristics of the Peppermint capsule	264
9.1.5 Breath analysis of Rugby Players who have had concussion (control and injured)	265
9.2 Limitations of the Investigations	266
9.3 Future work related to current studies	267
9.4 Summary.....	268
REFERENCES	270
APPENDIX 1- GC-MS measurements of various shisha pastes.....	286
APPENDIX 2 - Chapter 6	289
APPENDIX 3 – Chapter 7 (Peppermint Washout Characteristics studies).....	306

LIST OF FIGURES

Chapter 2

Figure 2.1 Photograph of the a) top view and b) hollow cathode and drift tube of a PTR-QUAD-MS Ionicon Analytik GmbH apparatus	16
Figure 2.2 Photograph of the a) top view and b) hollow cathode and drift tube a PTR-ToF-MS KORE Technology Ltd	17
Figure 2.3 Schematic diagram of an Ionicon PTR-MS instrument (Quadrupole) taken from Hansel et al. 1995 [21].	18
Figure 2.4 Schematic of the KORE PTR- TOF-MS [22]	19
Figure 2.5 Hollow cathode discharge	26

Chapter 3

Figure 3.1 Human Respiratory System and the structure of the alveoli in the lungs Reprinted from Lumen Learning, The Respiratory System and Direct Diffusion with the permission of Lumen Learning copyright [48].	51
Figure 3.2 The respiration process	53
Figure 3.3 Lung volumes and their measurement. Reprinted from.....	55
Figure 3.4 Workflow of steps in a breath analysis study, Reprinted with permission form the Journal of Breath research, 2014 [66].	59
Figure 3.5 Photograph of a) Fortuna® Optima glass syringe (Sigma Aldrich) b) B-braun stopcock and c) Elbow gas sampling port (Intersurgical complete respiratory system)	60
Figure 3.6 Photograph of Capnometer a) capnograph b) airway adapter c) reference cell d) capnostat.	61
Figure 3.7 Breath profile of a volunteer using, Capnograph 1265 from Novamatrix	62
Figure 3.8 Normal breath profile	64
Figure 3.9 Schematic diagram of a breath sampling system. The diagram is reprinted.	65
Figure 3.10 A healthy volunteer giving a breath sample. The syringe is coupled	65
Figure 3.11 Photograph show the glass syringe attached to the PTR-MS inlet using Swagelok.	66
Figure 3.12 Heating blanket and plastic cover used to maintain the humidity of the breath sample	66

Chapter 4

- Figure 4.1 “Shisha” . 1) Clay pot for tobacco, 2) Pipe stem connecting to the water container, 3) Water bowl, 4) Hose which connected to the mouth piece. 69
- Figure 4.2 Show the shisha sampling in the fume hood. 73
- Figure 4.3 Schematic diagram of experimental set up. 73
- Figure 4.4 A mass spectrum illustrating the product ions (starred) resulting from the reaction of H_3O^+ whilst operating the drift tube at a reduced electric field of 120 Td. 83
- Figure 4.5 Shows VOCS from headspace of charcoal via shisha pipe. 84

Chapter 5

- Figure 5.1 Experimental set up for headspace measurement of menthol, vanillin and associated compounds for reduced electric field studies (80 Td- 220 Td). 95
- Figure 5.2 Schematic diagram of experimental set up for the associate compounds using tedlar bags. 95
- Figure 5.3 A mass spectrum illustrating the product ions from the reaction of H_3O^+ with cyclohexanol whilst operating the drift tube at reduced electric field of 120 Td for 10 second integration time. 98
- Figure 5.4 Product ion branching ratios in percentages as a function of E/N resulting from the reaction of H_3O^+ with cyclohexanol ($\text{C}_6\text{H}_{12}\text{O}$). 99
- Figure 5.5 A mass spectrum illustrating the product ions from the reaction of H_3O^+ with phenol whilst operating the drift tube at reduced electric field of a) 120 Td b) 220 Td for 10 second integration time. There are some impurities recorded from the sample. m/z 77 can be seen at 220 Td. 101
- Figure 5.6 Product ion branching ratios in percentages as a function of E/N resulting from the reaction of H_3O^+ with phenol ($\text{C}_6\text{H}_{12}\text{O}$) from 150-220 Td. 102
- Figure 5.7 A mass spectrum illustrating the product ions resulting from the reaction of H_3O^+ with anisole whilst operating the drift tube at reduced electric field of 120 Td. An ion resulting from an impurity is highlighted. 104
- Figure 5.8 Product ion branching ratios in percentages as a function of E/N resulting from the reaction of H_3O^+ with anisole ($\text{C}_7\text{H}_8\text{O}$) using PTR-ToF-MS (8000). 105
- Figure 5.9 A mass spectrum illustrating the product ions from the reaction of H_3O^+ with benzaldehyde whilst operating the drift tube at reduced electric field of 120 Td. An ion resulting from an impurity is highlighted. 107
- Figure 5.10 Product ion branching ratios in percentages as a function of E/N resulting from the reaction of H_3O^+ with benzaldehyde ($\text{C}_7\text{H}_6\text{O}$). 108

Figure 5.11 A mass spectrum illustrating the product ions from the reaction of H_3O^+ with guaiacol whilst operating the drift tube at reduced electric field of a) 120 Td b) 220 Td. Some impurities from the sample are recorded.	111
Figure 5.12 Product ion branching ratios in percentages as a function of E/N resulting	112
Figure 5.13 Product ion branching ratios in percentages as a function of E/N resulting from the reactions of menthol ($\text{C}_{10}\text{H}_{20}\text{O}$) in the reaction region of the PTR-MS as a function of E/N	114
Figure 5.14 An illustrative mass spectrum illustrating the product ions resulting reactions with menthol in the drift tube of the PTR-MS at a reduced electric field of 120 Td.	115
Figure 5.15 Product ion branching ratios in percentages as a function of E/N resulting from the reactions in the drift tube of the PTR-MS with vanillin ($\text{C}_8\text{H}_8\text{O}_3$).	117
Figure 5.16 A mass spectrum resulting from the reaction of H_3O^+ with vanillin at reduced electric field of 120 Td.	117

Chapter 6

Figure 6.1 A mass spectrum illustrating the product ions (starred) resulting from the reaction of O_2^+ with halothane ($\text{C}_2\text{HClF}_3\text{Br}$) whilst operating the drift tube at a reduced electric field of 140 Td. Other ions such as the reagent ion O_2^+ and an impurity ion (NO_2^+) coming from the ion source are also highlighted. Note that the recombination energy of NO_2^+ is 9.6 eV, and hence cannot charge transfer to halothane given that the (adiabatic) ionisation potential for halothane is 11.0 eV, and hence is not of concern to us.	127
Figure 6.2 Spectra illustrating the complete set of product ions (including isotopes) observed following the reaction of O_2^+ with halothane, and in order of increasing m/z a) m/z 67 ($\text{CHF}^{35}\text{Cl}^+$) and m/z 69 ($\text{CHF}^{37}\text{Cl}^+/\text{CF}_3^+$) b) m/z 117 ($\text{C}_2\text{HF}_3^{35}\text{Cl}^+$) and m/z 119 ($\text{C}_2\text{HF}_3^{37}\text{Cl}^+$) c) m/z 127 ($\text{CH}^{35}\text{Cl}^{79}\text{Br}^+$), m/z 129 ($\text{CH}^{35}\text{Cl}^{81}\text{Br}^+/\text{CH}^{37}\text{Cl}^{79}\text{Br}^+$) and m/z 131 ($\text{CH}^{37}\text{Cl}^{81}\text{Br}^+$) e) m/z 176 ($\text{C}_2\text{F}_2^{35}\text{Cl}^{79}\text{Br}^+$), m/z 178 ($\text{C}_2\text{F}_2^{35}\text{Cl}^{81}\text{Br}^+/\text{C}_2\text{F}_2^{37}\text{Cl}^{79}\text{Br}^+$) and m/z 180 ($\text{C}_2\text{F}_2^{37}\text{Cl}^{81}\text{Br}^+$) and f) m/z 196 ($\text{C}_2\text{HF}_3^{35}\text{Cl}^{79}\text{Br}^+$), m/z 198 ($\text{C}_2\text{HF}_3^{35}\text{Cl}^{81}\text{Br}^+/\text{C}_2\text{HF}_3^{37}\text{Cl}^{79}\text{Br}^+$) and m/z 200 ($\text{C}_2\text{HF}_3^{37}\text{Cl}^{81}\text{Br}^+$).	128
Figure 6.3 Product ion branching percentages as a function of E/N resulting from the reaction of O_2^+ with halothane ($\text{C}_2\text{HBrClF}_3$).	129
Figure 6.4 A mass spectrum illustrating the product ions (starred) resulting from the reaction of H_3O^+ with isoflurane ($\text{C}_3\text{H}_2\text{F}_5\text{ClO}$) whilst operating the drift tube at a reduced electric field of 140 Td. Other ions such as the protonated water dimer, m/z 37, and an impurity ion (NO_2^+) coming from the ion source are also highlighted. (That observation shown there is no change in the NO_2^+ signal with and without isoflurane, indicates that the ionisation energy of isoflurane is greater than that of NO_2 (9.6 eV).) The ionisation energy of isoflurane is not available in the literature, but that for an isomeric form, enflurane, is, which is at 11.7 eV.	135
Figure 6.5 Expanded figure of the product ions resulting from the reactions of H_3O^+ with isoflurane to illustrate their isotopic abundances for a) m/z 67 ($\text{CHF}^{35}\text{Cl}^+$) and m/z	

69 (CHF³⁷Cl⁺) b) m/z 99 (C₂H₂F₃O⁺), m/z 115 (C₂H₂F₂³⁵ClO⁺), m/z 117 (C₂HF₃³⁵Cl⁺/C₂H₂F₂³⁷ClO⁺) and m/z 119 (C₂HF₃³⁷Cl⁺) c) m/z 145 (C₃HF₃³⁵ClO⁺), m/z 147 (C₃HF₃³⁷ClO⁺), m/z 149 (Impurity), m/z 163 (C₃F₄³⁵ClO⁺), m/z 165 (C₃H₂F₄³⁵ClO⁺/C₃F₄³⁷ClO⁺) and m/z 167 (C₃H₂F₄³⁷ClO⁺) d) m/z 183 (C₃HF₅³⁵ClO⁺) and m/z 184 (C₃HF₅³⁷ClO⁺). 136

Figure 6.6 Product ion branching ratios in percentages as a function of reduced electric field (E/N) resulting from the reaction of H₃O⁺ with isoflurane (C₃H₂F₅ClO)..... 137

Figure 6.7 A mass spectrum illustrating the product ions (starred) resulting from the reaction of O₂⁺ with isoflurane (C₃H₂F₅ClO) whilst operating the drift tube at a reduced electric field of 140 Td. Other ions such as an impurity ion (NO₂⁺) coming from the ion source are also highlighted..... 140

Figure 6.8 Expanded figure of the product ions resulting from the reactions of O₂⁺ with isoflurane to illustrate their isotopic abundances a) m/z 51 (CHF₂⁺), m/z 67 (CHF³⁵Cl⁺) and m/z 69 (CHF³⁷Cl⁺/CF₃⁺) b) m/z 99 (C₂H₂F₃O⁺), m/z 115 (C₂H₂F₂³⁵ClO⁺), m/z 117 (C₂HF₃³⁵ClO⁺/C₂H₂F₂³⁷ClO⁺) and m/z 119 (CHF₃C³⁷Cl) c) m/z 145 (C₃HF₃³⁵ClO⁺), m/z 147 (C₃HF₃³⁷ClO⁺) and m/z 149 (C₃H₂F₅O⁺) d) m/z 163 (C₃F₄³⁵ClO⁺), m/z 165 (C₃F₄³⁷ClO⁺/C₃H₂F₄³⁵ClO⁺), m/z 167 (C₃H₂F₄³⁷ClO⁺), m/z 181 (C₃H₂F₄ClO₂⁺) m/z 183 (C₃HF₅³⁵ClO⁺) and m/z 185 (C₃HF₅³⁷ClO⁺)..... 141

Figure 6.9 Product ion branching ratios in percentages as a function of E/N resulting from the reaction of O₂⁺ with isoflurane (C₃H₂F₅ClO)..... 142

Figure 6.10 A mass spectrum illustrating the product ions (starred) resulting from the reaction of O₂⁺ with enflurane (C₃H₂F₅ClO) whilst operating the drift tube at a reduced electric field of 140 Td. Other ions present, such as an impurity ion coming from the sample is also highlighted. 145

Figure 6.11 Expanded figure of the product ions resulting from the reactions of O₂⁺ with enflurane to illustrate their isotopic abundances for a) m/z 51 (CHF₂⁺), m/z 67 (CHF³⁵Cl⁺), m/z 69 (CHF³⁷Cl⁺/CF₃⁺) and m/z 82 (Impurity) b) m/z 98 (C₂HF₂³⁵Cl⁺) and m/z 100 (C₂HF₂³⁷Cl⁺) c) m/z 113 (C₂F₂³⁵ClO⁺), m/z 115 (C₂F₂³⁷ClO⁺/C₂H₂F₂³⁵ClO⁺), m/z 117 (C₂HF₃³⁵Cl⁺/C₂H₂F₂³⁷ClO⁺) and m/z 119 (C₂HF₃³⁷Cl⁺) d) m/z 131 (C₃H₃³⁵ClF₃⁺), m/z 133 (C₃H₃³⁷ClF₃⁺/C₂H₃³⁵ClF₃O⁺), m/z 135 (C₂F₄³⁵Cl⁺/C₂H₃³⁷ClF₃O⁺) and m/z 137 (C₂F₄³⁷Cl⁺) e) m/z 145 (C₃HF₃³⁵ClO⁺), m/z 147 (C₃HF₃³⁷ClO⁺), m/z 163 (C₃F₄³⁵ClO⁺), m/z 165 (C₃H₂F₄³⁵ClO⁺/C₃F₄³⁷ClO⁺) and m/z 167 (C₃H₂F₄³⁷ClO⁺). 146

Figure 6.12 Product ion branching ratios in percentages as a function of E/N resulting from the reaction of O₂⁺ with enflurane (C₃H₂F₅ClO)..... 147

Figure 6.13 A mass spectrum illustrating the product ions (starred) resulting from the reaction of H₃O⁺ with enflurane (C₃H₂F₅ClO) whilst operating the drift tube at a reduced electric field of 140 Td. 150

Figure 6.14 Expanded figure of the product ions resulting from the reactions of H₃O⁺ with enflurane to illustrate their isotopic abundances a) m/z 67 (CHF³⁵Cl⁺) and m/z 69 (CHF³⁷Cl⁺) b) m/z 98 (C₂HF₂³⁵Cl⁺) and m/z 100 (C₂HF₂³⁷Cl⁺) c) m/z 113 (C₂F₂³⁵ClO⁺), m/z 115 (C₂F₂³⁷ClO⁺/C₂H₂F₂³⁵ClO⁺), m/z 117 (C₂H₂F₂³⁷ClO⁺/C₂HF₃³⁵Cl⁺) and m/z 119 (C₂HF₃³⁷Cl⁺) d) m/z 131 (C₃H₃F₃³⁵Cl⁺), m/z 133 (C₃H₃F₃³⁷Cl⁺/C₂HF₃³⁵ClO⁺) and m/z 135 (C₂HF₃³⁷ClO⁺) e) m/z 163

(C ₃ F ₄ ³⁵ ClO ⁺) and <i>m/z</i> 165 (C ₃ F ₄ ³⁷ ClO ⁺) f) <i>m/z</i> 183 (C ₃ HF ₅ ³⁵ ClO ⁺) and <i>m/z</i> 185 (C ₃ HF ₅ ³⁷ ClO ⁺).....	151
Figure 6.15 Product ion branching ratios in percentages as a function of <i>E/N</i> resulting from the reaction of H ₃ O ⁺ with enflurane (C ₃ H ₂ ClF ₅ O). Other ions such as the reagent ion O ₂ ⁺ and an impurity ion (NO ₂ ⁺) coming from the ion source are also highlighted.	152
Figure 6.16 A mass spectrum illustrating the product ions (starred) resulting from the reaction of O ₂ ⁺ with sevoflurane (C ₄ H ₃ F ₇ O) whilst operating the drift tube at a reduced electric field of 140 Td. Other ions, such as impurity ions are highlighted.	155
Figure 6.17 Expanded figure of the product ions resulting from the reactions of O ₂ ⁺ with sevoflurane to illustrate their isotopic abundances for a) <i>m/z</i> 79 (C ₂ F ₂ OH ⁺ /impurity), <i>m/z</i> 91(Impurity), b) <i>m/z</i> 129 (C ₃ HF ₄ O ⁺) and <i>m/z</i> 131 (C ₃ H ₃ F ₄ O ⁺) c) <i>m/z</i> 181(C ₄ H ₃ F ₆ O ⁺), <i>m/z</i> 183 (C ₄ HF ₇ ⁺) and <i>m/z</i> 199 (C ₄ H ₂ F ₇ O ⁺).	156
Figure 6.18 Product ion branching ratios in percentages as a function of <i>E/N</i> resulting from the reaction of O ₂ ⁺ with sevoflurane (C ₄ H ₃ F ₇ O).....	157
Figure 6.19 A mass spectrum illustrating the product ions resulting from the reaction of H ₃ O ⁺ with sevoflurane whilst operating the drift tube at a reduced electric field of 140 Td. Other ions such as <i>m/z</i> 49 which is produced via a secondary process and an impurity ion C ₃ H ₇ O ⁺ coming from the sample are also highlighted.....	160
Figure 6.20 A Mass spectrum illustrating product ions <i>m/z</i> 181(C ₄ H ₃ F ₆ O ⁺), <i>m/z</i> 182 C ₄ H ₄ F ₆ O ⁺ / ¹³ CC ₃ H ₃ F ₆ O ⁺ , <i>m/z</i> 183 (¹³ CC ₃ H ₄ F ₆ O ⁺) and <i>m/z</i> 199 (C ₄ H ₂ F ₇ O ⁺).	160
Figure 6.21 Product ion branching ratios in percentages as a function of <i>E/N</i> resulting from the reaction of H ₃ O ⁺ with sevoflurane (C ₄ H ₃ F ₇ O). Product ions that contribute less than 1% to the branching percentages at any given <i>E/N</i> have not been included in the figure.	161
Figure 6.22 A mass spectrum illustrating the product ions (starred) resulting from the reaction of O ₂ ⁺ with methoxyflurane (C ₃ H ₄ F ₂ Cl ₂ O) whilst operating the drift tube at a reduced electric field of 140 Td. Other ions such as impurity ion (NO ₂ ⁺) coming from the ion source are also highlighted.....	164
Figure 6.23 Mass spectrum illustrating product ions resulting from the reactions of O ₂ ⁺ to methoxyflurane with illustrate their isotopic abundances a) <i>m/z</i> 51 (CHF ₂ ⁺), <i>m/z</i> 67 (CHF ³⁵ Cl ⁺), <i>m/z</i> 69 (CHF ³⁷ Cl ⁺) b) <i>m/z</i> 81 (C ₂ H ₃ F ₂ O ⁺) c) <i>m/z</i> 129 (C ₃ H ₄ F ₂ ³⁵ ClO ⁺), <i>m/z</i> 131 (C ₃ H ₄ F ₂ ³⁷ ClO ⁺ /C ₂ H ₂ F ³⁵ ClO ⁺), <i>m/z</i> 133 (Impurity) d) <i>m/z</i> 143 (C ₃ H ₂ F ^(35,35) Cl ₂ O ⁺), <i>m/z</i> 145 (C ₃ H ₄ F ^(35,35) Cl ₂ O ⁺ / C ₃ H ₂ F ^(35,37) Cl ₂ O ⁺), <i>m/z</i> 147 (C ₃ H ₄ F ^(37,35) Cl ₂ O ⁺ / C ₃ H ₂ F ^(37,37) Cl ₂ O ⁺) and <i>m/z</i> 149 (C ₃ H ₄ F ^(37,37) Cl ₂ O ⁺).....	165
Figure 6.24 Product ion branching ratios in percentages as a function of <i>E/N</i> resulting from the reaction of O ₂ ⁺ with methoxyflurane (C ₃ H ₄ F ₂ Cl ₂ O).	166
Figure 6.25 A mass spectrum illustrating the product ions (starred) resulting from the reaction of H ₃ O ⁺ with methoxyflurane whilst operating the drift tube at a reduced electric field of 140 Td. Impurities such as the one resulting from protonated acetone.	168

Figure 6.26 Mass spectrum illustrating product ions resulting from the reactions of H_3O^+ with methoxyflurane to illustrate their isotopic abundances a) m/z 67 ($\text{CHF}^{35}\text{Cl}^+$) and m/z 69 ($\text{CHF}^{37}\text{Cl}^+$) b) m/z 79 ($\text{C}_2\text{HF}^{35}\text{Cl}^+$), m/z 81 ($\text{C}_2\text{H}_3\text{F}^{35}\text{Cl}^+/\text{C}_2\text{HF}^{37}\text{Cl}^+$) and m/z 83 ($\text{C}_2\text{H}_3\text{F}^{37}\text{Cl}^+$) and c) m/z 143 ($\text{C}_3\text{H}_2\text{F}^{(35,35)}\text{Cl}_2\text{O}^+$), m/z 145 ($\text{C}_3\text{H}_4\text{F}^{(35,35)}\text{Cl}_2\text{O}^+/\text{C}_3\text{H}_2\text{F}^{(35,37)}\text{Cl}_2\text{O}^+$), m/z 147 ($\text{C}_3\text{H}_4\text{F}^{(35,37)}\text{Cl}_2\text{O}^+/\text{C}_3\text{H}_2\text{F}^{(37,37)}\text{Cl}_2\text{O}^+$) and m/z 149 ($\text{C}_3\text{H}_4\text{F}^{(37,37)}\text{Cl}_2\text{O}^+$).....	169
Figure 6.27 Product ion branching ratios in percentages as a function of E/N resulting from the reaction of H_3O^+ with methoxyflurane ($\text{C}_3\text{H}_4\text{F}_2\text{Cl}_2\text{O}$).....	170
Figure 6.28 A mass spectrum illustrating the product ions resulting from the reaction of O_2^+ with desflurane whilst operating the drift tube at a reduced electric field of 140 Td. An impurity ion is highlighted.	172
Figure 6.29 Mass spectrum illustrating product ions resulting from the reactions of O_2^+ with desflurane to illustrate their isotopic abundances a) m/z 49 (CH_2FO^+), m/z 51(CHF_2^+), m/z 69 (CF_3^+) b) m/z 99 ($\text{C}_2\text{H}_2\text{F}_3\text{O}^+$), m/z 101($\text{C}_2\text{F}_4\text{H}^+$), m/z 117($\text{C}_2\text{HF}_4\text{O}^+$) and m/z 119 ($\text{C}_2\text{H}_3\text{F}_4\text{O}^+$) c) m/z 147 ($\text{C}_3\text{F}_5\text{O}^+$), m/z 149 ($\text{C}_3\text{H}_2\text{F}_5\text{O}^+$) and m/z 167 ($\text{C}_3\text{HF}_6\text{O}^+$)	173
Figure 6.30 Product ion branching ratios in percentages as a function of E/N resulting from the reaction of O_2^+ with desflurane ($\text{C}_3\text{H}_2\text{F}_6\text{O}$).....	174
Figure 6.31 A mass spectrum illustrating the product ions resulting from the reaction of H_3O^+ with desflurane ($\text{C}_3\text{H}_2\text{F}_6\text{O}$) whilst operating the drift tube at a reduced electric field of 140 Td. Other impurity such as protonated acetone resulting from an impurity in the sample is also highlighted.	176
Figure 6.32 Mass spectrum illustrating product ions resulting from the reactions of H_3O^+ with desflurane to illustrate their isotopic abundances a) m/z 51 (CHF_2^+), m/z 67(CHF_2O^+) b) m/z 99 ($\text{C}_2\text{H}_2\text{F}_3\text{O}^+$), m/z 101 (Impurity), m/z 117 ($\text{C}_2\text{HF}_4\text{O}^+$) and m/z 119 ($\text{C}_2\text{H}_3\text{F}_4\text{O}^+$) c) m/z 127 ($\text{CHF}_6^+/\text{Impurity}$), m/z 147 ($\text{C}_3\text{F}_5\text{O}^+$) and m/z 149 ($\text{C}_3\text{H}_2\text{F}_5\text{O}^+$) d) m/z 167 ($\text{C}_3\text{HF}_6\text{O}^+$).....	177
Figure 6.33 Product ion branching ratios in percentages as a function of E/N resulting from the reaction of H_3O^+ with desflurane ($\text{C}_3\text{H}_2\text{F}_6\text{O}$).....	178
Chapter 7	
Figure 7.1 A breath-volunteer exhaling smoothly through the BET which was coupled to a PTR-TOF 8000 (not shown). For each measurement five breaths were collected.	186
Figure 7.2 Schematic of the buffered end-tidal (BET) sampling apparatus (reproduced from Herbig <i>et al.</i> Journal of Breath Research (2008) [127].....	194
Figure 7.3 A mass spectrum illustrating the product ions (starred) resulting from the reaction of H_3O^+ with α -pinene at a reduced electric field of 130 Td.	196
Figure 7.4 A mass spectrum illustrating the product ions (starred) from the reaction of H_3O^+ with β -pinene whilst operating the drift tube at reduced electric field of 130 Td for 10 second experiment time.....	199

Figure 7.5 A mass spectrum illustrating the product ions (starred) from the reaction of H_3O^+ with 1,8-cineole ($C_{10}H_{19}O^+$) whilst operating the drift tube at reduced electric field of 130 Td. Other ion such as impurity ion coming from the drift tube is also highlighted.	201
Figure 7.6 A mass spectrum illustrating the product ions (starred) from the reaction of H_3O^+ with limonene whilst operating the drift tube at reduced electric field of 130 Td. An ion resulting from an impurity of acetone in the drift tube is highlighted. and protonated water clusters (m/z 37 and m/z 55) were observed in this measurement.	203
Figure 7.7 A mass spectrum illustrating the product ions (starred) from the reaction of H_3O^+ with menthone whilst operating the drift tube at reduced electric field of 130 Td. An ion resulting from an impurity in the drift tube is identified.	205
Figure 7.8 A mass spectrum illustrating the product ions from the reaction of H_3O^+ with menthol whilst operating the drift tube at reduced electric field of 130 Td e. Impurity ion was observed in this measurement.	208
Figure 7.9 A mass spectrum illustrating the product ions and their intensities from the reaction of H_3O^+ with peppermint oil contained capsule whilst operating the drift tube at reduced electric field of 130 Td. Some impurity ions from the sample are highlighted.	210
Figure 7.10 Shows five breath for each measuring period by monitoring <i>alveolar phase</i> of m/z 59, 81, 137 and 155.	212
Figure 7.11 Shows an example of exponential decay graph of a volunteer for a) m/z 81, b) m/z 137 and c) m/z 155 (normalised counts per second (ncps) versus time) which indicates possible to calculate pseudo excretion rate using natural Ln function. .	214
Figure 7.12 The washout characteristics of volatiles in breath recorded at m/z 81, 137, and 155 following the ingestion of a capsule containing 200 mg of peppermint oil for volunteer 1.	215
Figure 7.13 The washout characteristics of volatiles in breath recorded at m/z 81, 137, and 155 following the ingestion of a capsule containing 200 mg of peppermint oil for volunteer 2.	216
Figure 7.14 The washout characteristics of volatiles in breath recorded at m/z 81, 137, and 155 following the ingestion of a capsule containing 200 mg of peppermint oil for volunteer 3 (day 1).	217
Figure 7.15 The washout characteristics of volatiles in breath recorded at m/z 81, 137, and 155 following the ingestion of a capsule containing 200 mg of peppermint oil for volunteer 3 (day 2).	217
Figure 7.16 The washout characteristics of volatiles in breath recorded at m/z 81, 137, and 155 following the ingestion of a capsule containing 200 mg of peppermint oil for volunteer 3 (day 3)	218
Figure 7.17 The washout characteristics of volatiles in breath recorded at m/z 81, 137, and 155 following the ingestion of a capsule containing 200 mg of peppermint oil for volunteer 3 (day 4).	218

Figure 7.18 The washout characteristics of volatiles in breath recorded at m/z 81, 137, and 155 following the ingestion of a capsule containing 200 mg of peppermint oil for volunteer 4 (day 1).	219
Figure 7.19 The washout characteristics of volatiles in breath recorded at m/z 81, 137, and 155 following the ingestion of a capsule containing 200 mg of peppermint oil for volunteer 4 (day 2).	220
Figure 7.20 The washout characteristics of volatiles in breath recorded at m/z 81, 137, and 155 following the ingestion of a capsule containing 200 mg of peppermint oil for volunteer 4 (day 3).	220

Chapter 8

Figure 8.1 Different sizes of diffusion tubes. This picture was reprinted from J.Thompson , 2009, Journal of environmental monitoring [176].	243
Figure 8.2 The experimental set up of isoprene calibration for Ionicon quadrupole ...	244
Figure 8.3 An example of a mass spectrum which shows an average of three breath cycle of an injured rugby player measured using Ionicon quadrupole PTR-MS.	245
Figure 8.4 a) and b) Show the differences of obvious VOCs (starred) from the exhaled breath of healthy rugby player (RCA 23) and injured rugby players (RCP 23) which the samples are from the same player. The background measurement was included for comparison.	247
Figure 8.5 a) and b) Show the differences of obvious VOCs (starred) from the exhaled breath of healthy rugby player (RCB 13) and injured rugby players (RCB 22) which the samples are form the same player. The background measurement was included for comparison.	248
Figure 8.6 Boxplot showing lower quartile (LQ), median, mean and upper quartile (UQ) normalised counts per second for exhaled methanol from a healthy rugby player and an injured player.	251
Figure 8.7 Boxplot (acetone) showing lower quartile (LQ), median, mean and upper quartile (UQ) normalised counts per second for exhaled acetone from a healthy rugby player and an injured player.....	252
Figure 8.8 Boxplot (isoprene) showing lower quartile (LQ), median, mean and upper quartile (UQ) normalised counts per second for exhaled isoprene from healthy rugby player and injured player.....	253
Figure 8.9 Isoprene in tracer refillable (0.2 mm bore 2cm long diffusion tube using gravimetric method.	255
Figure 8.10 Isoprene calibration (normalised data) of PTR-MS (Ionicon) using 0.2 ..	257
Figure 8.11 Isoprene calibration of PTR-MS Ionicon for non-normalised data (robust rank regression) using refillable diffusion tube	257

LIST OF TABLES

Chapter 2

Table 2.1 Proton affinities of the most abundant components in clean air [24].	22
Table 2.2 Proton affinities of some common volatile organic compounds [24].	22
Table 2.3 Proton affinities of water and water clusters [23, 25].	23
Table 2.4 Proton affinities of acetone, isoprene, and limonene. For comparison the proton affinity of water is given [28, 29].	24

Chapter 3

Table 3.1 Example of classes of Volatile Organic Compounds in the Breath taken from Mazzone in Journal of Thoracic Oncology, 2008 [47].	49
---	----

Chapter 4

Table 4.1 Common VOCs emitted from burning barbecue charcoal (adapted from the work of Kabir et al, 2010 [88]).	71
Table 4.2 Type of shisha paste (brand Al-Fakher, taken from the shisha paste).	76
Table 4.3 m/z of product ions resulting from the reaction of H_3O^+ with the headspace of various shisha pastes using PTR- MS at 120 Td and possible VOC identification based on m/z of product ions and a GC-MS analysis of the shisha pastes.	80
Table 4.4 Assignments of VOCs emitted from burning charcoal after exiting a shisha water pipe.	84

Chapter 5

Table 5.1 Information on compounds in this experiment, including vapour pressure and purity.	94
Table 5.2 m/z values of the product ions and neutral species and their branching ratio percentages resulting from the reaction of cyclohexanol with H_3O^+ at a reduced electric field of 120 Td.	98
Table 5.3 m/z values of the product ions and neutral species and their branching ratio percentages resulting from the reaction of phenol with H_3O^+ at a reduced electric field of 120 Td	102
Table 5.4 m/z values of the product ions and neutral species and their branching ratio percentages resulting from the reaction of anisole with H_3O^+ at a reduced electric field of 120 Td.	105
Table 5.5 m/z values of the product ions and neutral species and their branching ratio percentages resulting from the reaction of benzaldehyde with H_3O^+ at a reduced electric field of 120 Td.	108

Table 5.6 m/z values of the product ions and neutral species and their branching ratio percentages resulting from the reaction of guaicol with H_3O^+ at a reduced electric field of 120 Td and 220 Td.	112
Table 5.7 m/z values of the product ions and their branching ratio percentages resulting from the reaction of menthol ($C_{10}H_{20}O$) with H_3O^+ at a reduced electric field of 120 Td.	115
Table 5.8 Proposed product ions, neutral products and relative intensities resulting from the reaction of vanillin with H_3O^+ at 120 Td	118
 Chapter 6	
Table 6.1 Details of the anaesthetic compounds investigated in this thesis.	124
Table 6.2 m/z values of the product ions and their branching ratio percentages resulting from the reaction of halothane with O_2^+ at a reduced electric field of 140 Td using the KORE PTR-ToF-MS in comparison to SIFT-MS results published by Wang et al.[115].	126
Table 6.3 m/z values of the product ions and neutral species and their branching percentages resulting from the reaction of isoflurane with H_3O^+ at a reduced electric field of 140 Td for a KORE PTR-ToF-MS, an IONICON PTR-Quad-MS, and an IONICON PTR-TOF 800 (Michaela Malásková, Institute of Breath research, University of Innsbruck, Austria). For comparison the results from the SIFT-MS study [117] are also provided.	134
Table 6.4 m/z values of the product ions and their branching ratio percentages resulting from the reaction of isoflurane with O_2^+ at a reduced electric field of 140 Td using the KORE PTR-ToF-MS in comparison to SIFT-MS results published by Wang et al. [72].	139
Table 6.5 m/z values of the product ions and their branching ratio percentages resulting from the reaction of enflurane with O_2^+ at a reduced electric field of 140 Td using the KORE PTR-ToF-MS.	144
Table 6.6 m/z values of the product ions and their branching ratio percentages resulting from the reaction of enflurane with H_3O^+ at a reduced electric field of 140 Td using a KORE PTR-ToF-MS. The IONICON PTR-ToF-MS results are presented for comparison (courtesy of Michaela Malásková from the Institute of Breath research, University of Innsbruck, Austria).	149
Table 6.7 m/z values of the product ions and neutral species and their branching ratio percentages resulting from the reaction sevoflurane of with O_2^+ at a reduced electric field of 140 Td using the KORE PTR-ToF-MS in comparison to SIFT-MS results published by Wang et al.[115].	154
Table 6.8 m/z values of the product ions and neutral species and their branching ratio percentages resulting from the reaction sevoflurane of with H_3O^+ at a reduced electric field of 140 Td. The IONICON PTR-ToF-MS were measured following a request to Michaela Malásková from the Institute of Breath research, University of Innsbruck, Austria. SIFT-MS results of Wang et al. are also presented.	159

Table 6.9 m/z values of the product ions and their branching ratio percentages resulting from the reaction of methoxyflurane with O_2^+ at a reduced electric field of 140 Td using the KORE PTR-ToF-MS.....	163
Table 6.10 m/z values of the product ions and their branching ratio percentages resulting from the reaction of methoxyflurane with H_3O^+ at a reduced electric field of 140 Td using the KORE PTR-ToF-MS.....	167
Table 6.11 m/z values of the product ions and their branching ratio percentages resulting from the reaction of desflurane with O_2^+ at a reduced electric field of 140 Td using the KORE PTR-ToF-MS.	171
Table 6.12 m/z values of the product ions and their branching ratio percentages resulting from the reaction of desflurane with H_3O^+ at a reduced electric field of 140 Td using the KORE PTR-ToF-MS and The IONICON PTR-ToF 8000 instruments. The IONICON measurements were made by Michaela Malásková from the Institute of Breath research, University of Innsbruck, Austria.)	176

Chapter 7

Table 7.1 The principle chemical composition of peppermint oil adapted from the GC work reported by Schmidt et al. [11].	188
Table 7.2 Details about standard compounds investigated in this study related to peppermint oil capsule in this experiment, including vapour pressure and purity.	190
Table 7.3 Details of the age, sex and number of measurements of the volunteers who participated in this peppermint oil study.....	192
Table 7.4 Table m/z values of the product ions and their relative intensities (dominant ion given an intensity of 100) resulting from the reaction of α -pinene with H_3O^+ at a reduced electric field of 130 Td.	197
Table 7.5 m/z values of the product ions and their relative intensities (dominant ion given an intensity of 100) resulting from the reaction of β -pinene with H_3O^+ at a reduced electric field of 130 Td.....	199
Table 7.6 m/z values of the product ions and their relative intensity resulting from the reaction of 1,8-cineole with H_3O^+ at a reduced electric field of 130 Td.....	201
Table 7.7 m/z values of the product ions and their relative intensities (dominant ion given an intensity of 100) resulting from the reaction of limonene with H_3O^+ at a reduced electric field of 130 Td.....	203
Table 7.8 m/z values of the product ions and their relative intensities (dominant ion given an intensity of 100) resulting from the reaction of menthone with H_3O^+ at a reduced electric field of 130 Td.....	205
Table 7.9 m/z values of the product ions and their relative intensities (dominant ion given an intensity of 100) resulting from the reaction of menthol with H_3O^+ at a reduced electric field of 130 Td.....	208

Table 7.10 <i>m/z</i> values (tentative identification) of the product ions and their relative intensities (dominant ion given an intensity of 100) resulting from the reaction of peppermint capsule with H ₃ O ⁺ at a reduced electric field of 130 Td.	211
Table 7.11 Shows the pseudo excretion rate (decrease in the product ions) of volunteers for each product ion measured from the exhaled breath after ingestion of the peppermint capsule for each of the volunteers.....	221

Chapter 8

Table 8.1 Information about in-vitro blood/gas partition coefficients of the VOCS chosen for this study [60, 164].	233
Table 8.2 Details on healthy male rugby player's (controls) and injured male rugby players'. This table includes details about age, weight, height, ID (identification code) and healthy rugby player's injured player's ID.....	239
Table 8.3 Information on isoprene in this experiment, including vapour pressure and purity.	243

LIST OF ABBREVIATIONS

BR	Branching ratio
bckg	Background
CID	Collisional induced dissociation
cps	Counts per second
DT	Drift tube
EI	Electron impact
<i>E/N</i>	Reduced electric field
GC-MS	Gas chromatography mass spectrometry
GD	Glow discharge
HV	High voltage
PTR-MS	Proton Transfer Reaction Mass Spectrometry
MCP	Micro-channel plate
MS	Mass spectrometer
NAA	N-Acetyl-L-aspartate
Ncps	Normalised Counts Per Second
PA	Proton affinity
Pa	Pascal
ppbv	Parts per billion by volume
pptv	Parts per trillion by volume
SD	Source drift
SIFT	Selected ion flow tube
STP	Standard temperature and pressure
TOF	Time of flight
Td	Townsend
VOC	Volatile organic compound

CHAPTER 1

1 Introduction

1.1 Background

Owing to the absence of phenotypic signs and symptoms during the development of many chronic diseases, they can remain unidentified and this could lead to fatality. These diseases can either be cured or in remission, a manageable state. For example, diseases like diabetes and cancer in the early stages of development can be managed and controlled well to prevent severity and recurrence if the diseases can be identified and treated quickly.

Medical diagnosis for diseases involves a complex process. Certain prognosis are time consuming and involve invasive techniques. Most of the medical diagnosis concentrates on the investigation of biological fluids such as blood, urine and tissue cultures in order to get more details about the disease for further medical observation and treatment planning by the clinician. This has encouraged the development of sophisticated instruments to facilitate medical diagnosis, treatment and therapy for better healthcare of patients. Scientists are still working on new techniques to get prompt diagnosis of diseases.

Proton Transfer Mass Spectrometry (PTR-MS) is a very sensitive analytical technique which has been developed to detect Volatile Organic Compounds (VOCs). In medical and health sciences, it is used as a potential non-invasive technique to investigate or examine VOCs from various medical conditions. This technique does not require a complex sample or no sample preparation.

Application of PTR-MS for breath analysis in the clinical field would aid to produce potential biomarkers for several diseases [1]. For example, Fernandez del Rio et al. have suggested that limonene from exhaled breath could be used as a potential biomarker for liver disease [2].

PTR-MS also has been used in the operating theatre to measure VOCs during operations for multiple reasons [3, 4]. Some studies on anaesthetics were carried out to highlight the occupational exposure in operating theatres. The most recent study on anaesthetics is about elimination of isoflurane via exhaled breath after post liver surgery [5]. It explained that isoflurane can be eliminated easily and quickly via breath, urine and sweat, which is hard to be eliminated by liver [6].

Breath and headspace analysis using PTR-MS is unique because it can provide further details about metabolic pathways and physiological mechanisms that occur in the human body. Owing to know all the advantages of PTR-MS, it still has not been utilised in any of the clinical practice [7].

The only drawback of this technique is that there is no standard protocol for breath and headspace sampling. This has led to an enormous variety of outcomes with a very low certainty level. In addition to that, breath contains an assortment of volatiles with a huge range of concentrations. There are many studies which correlate the biomarkers for diseases without proper assignments or without concrete justification to be used in the clinical practice. However, only a limited number of studies have proved that volatile compounds in breath correspond to a biomarker of a specific illness or lifestyle [2, 8].

In addition to that, this technique has also been used as a fundamental research tool in many public health fields, especially in research to interrogate harmful chemicals being emitted from any particular human or industrial activities (man-made) to protect public from unnecessary exposure from the toxic chemicals and also to consider occupational health and safety. Experts used PTR-MS for breath analysis to identify the VOCs from smoking conventional [8, 9] and e-cigarettes [10].

PTR-MS is used for preliminary studies in most Universities and Research Centres. However, research expansion using this technique is limited due to the huge amount of data generated for analysis and the cost involved to maintain the instrument.

The aim of this research work is on the application of PTR-MS in health sciences. The analytical application in health sciences focuses on VOCs associated with Shisha smoking; investigation on vanillin, menthol associate compounds; H_3O^+ and O_2^+ reactions with general anaesthetics; temporal profile breath measurements of ingested peppermint capsules to monitor liver washout characteristics; measurement of the breath of rugby players who had concussion and comparison with healthy rugby players. This technique has a high capability to be used as a non-invasive tool for screening, diagnosis and monitoring of disease and any physiological changes in the body in the future. This technique also can be used to detect VOCs in a complex chemical which has complicated characteristics such as high vapour pressure, using the headspace method to identify the VOCs being emitted from the specific chemical e.g. for Shisha and to identify products from anaesthetic compounds. The primary outcome of the work in this thesis is to confer the volatiles in the complex breath profile and VOCs emitted from complex chemicals.

1.2 Thesis Outline

This thesis contains a further nine chapters. Chapter 2 explains about the theoretical aspects of PTR-MS and ion-molecule chemistry reactions. The explanation of the breath sampling protocol and the development of alveolar breath collection is given in Chapter 3. It also explains briefly about off-line measurements by PTR-MS. Chapter 4 deals with VOCs associated with shisha smoking and includes a brief description of headspace analysis, and also explains the identification of VOCs from shisha paste with and without burning charcoal. Meanwhile, Chapter 5 is a follow-up chapter from Chapter 4 which is linked with shisha. In this chapter, the associate compounds related with two flavour compounds vanillin (vanilla shisha paste) and menthol (mint shisha paste) were investigated.

Chapter 6 describes and explains about H_3O^+ and O_2^+ reactions with general anaesthetics using headspace analysis. Product ions are identified and the product ions branching ratios of each anaesthetic compounds as a function of the reduced electric field are calculated. Chapter 6 presents work on breath analysis of rugby players who had a concussion. This chapter elaborates the comparison of VOCs concentration between healthy rugby players (control) and players who had a concussion. Chapter 7 describes about the temporal profile measurements of ingested peppermint capsules. This chapter concisely describes about how quick peppermint can be washed out by the liver using breath analysis technique.

Each experimental chapter has introduction, methodology, results and discussion.

This thesis ends with Chapter 9 which consists of further discussion. It also includes conclusion, summary of findings, limitation of the techniques and discussion of

the PTR-MS application in the health sciences and future direction of PTR-MS in medical and health sciences.

1.3 AREAS INVESTIGATED

The work presented in this report involves PTR-MS and its analytical applications in health sciences. As mentioned earlier, Chapters 4-8 are based on PTR-MS experimental measurements. The aim of the project is listed as below:

1.3.1 VOLATILE ORGANIC COMPOUNDS ASSOCIATED WITH SHISHA PASTE AND SHISHA SMOKING

Headspace analysis of shisha paste measurements was undertaken to identify

Few studies have been undertaken to ascertain how safe these forms of smoking are. The key aims of the “smoking” projects are:

- a) Identification of volatile compounds released from the headspace of vanilla, strawberry, mint and double apple flavoured shisha paste.
- b) Determining the concentration (relative intensity to 100) of harmful volatiles, such as benzene after lighting the charcoal at time intervals of approximately 3-12 minutes coming directly from the shisha pipe
- c) To prove that a shisha pipe with ‘water bubbling’ is not really functioning as a filter by measuring the VOCs being emitted from the shisha pipe.

1.3.2 INVESTIGATION OF THE PRODUCT IONS RESULTING FROM THE REACTIONS OF H_3O^+ WITH VANILLIN, MENTHOL AND ASSOCIATED COMPOUNDS (CYCLOHEXANOL, PHENOL, ANISOLE, BENZALDEHYDE AND GUAIACOL)

The objective of the study is to monitor the fragmentation pattern and identify the product ions from vanillin and menthol. In addition to that, benzene ring which associated with vanillin and menthol were investigated using different functional group such as cyclohexanol for menthol and phenol, benzaldehyde, anisole and guaicol for vanillin.

1.3.3 PTR-TOF-MS STUDIES OF THE REACTIONS OF H_3O^+ AND O_2^+ WITH THE GENERAL ANAESTHETIC GASES HALOTHANE, ISOFLURANE, ENFLURANE, SEVOFLURANE, DESFLURANE AND METHOXYFLURANE

a) The motivation of this study was to provide the necessary identification of product ions and possible reaction channel by analysing the reactions of H_3O^+ and O_2^+ with anaesthetic gases halothane, isoflurane, desflurane, sevoflurane, enflurane and methoxyflurane as a function of reduced electric field from 80 Td to 220 Td using PTR-ToF-MS.

b) This study would be useful for further studies on anaesthetics in exhaled breath for patients who have undergone surgery and for the staff who work in the operation theatres for occupational health and safety purposes. This study also could be used as a follow up study to monitor the anaesthetic isoflurane in blood and breath as the wash out characteristics for post liver transplant a few days after the operation [5].

1.3.4 BREATH ANALYSIS TO DETERMINE HUMAN WASHOUT CHARACTERISTICS OF KEY VOLATILE ORGANIC COMPOUNDS CONTAINED IN PEPPERMINT OIL

This project is an European project which coordinated by Dr. Simone Cristescu (University of Nijmegen, The Netherlands) and Professor Paul Thomas (University of Loughborough, United Kingdom). One of the aims of this work is to investigate the potential of PTR-MS for detecting and monitoring peppermint washout characteristics by the liver applying non-invasive techniques and real time measurement by using breath analysis technique. This will provide breath data of healthy volunteers which later would be used for followed-up study for liver disease patients. Also this study would aid in the benchmarking endeavour to estimate the range of results between participating laboratories.

In this study, peppermint capsule [Peppermint oil 200mg, The Boots Company PLC, Nottingham, England NG2 3AA] was used to monitor the washout characteristics. The peppermint capsule contains some series of monoterpenes such as menthol, menthone, menthofuran, isomenthone and some minor compounds such as 1,8-cineole, methylacetate, α -Pinene, β -pinene and limonene [11]. After ingestion of the peppermint oil contained capsule, it will absorbed into the bloodstream and some compounds are being released in the breath.

In this preliminary study, investigation on washout characteristic of peppermint oil contained capsule which contains the blood-born volatile compounds in breath was performed by taking breath samples before and after ingestion of the peppermint capsule for 6 hours from healthy volunteers. In addition to that, the VOCs from the exhaled breath from the peppermint oil contained capsule were identified. Also, the headspace

measurements for the associated compounds with peppermint were investigated to identify the product ions. This project has been carried out at the Institute of Breath Research, Dornbin, Austria and University of Birmingham, UK.

1.3.5 BREATH ANALYSIS OF RUGBY PLAYERS WHO HAD A CONCUSSION (HEALTHY AND INJURED)

This study was the first clinical trial using breath analysis. In this study, PTR-MS was used to measure the exhaled breath of healthy rugby players and rugby players who had suffered a concussion during a rugby match. They were initially diagnosed with various medical diagnostic tools such as MRI (Magnetic Resonance Imaging), a CT scan (Computed Tomography) or a focused orientation exam, which tests for short term memory recall, and a focused neurological exam either at the Brain Imaging Centre of Queen Elizabeth Hospital, Birmingham or in the School of Sports Science at the University of Birmingham. The objective was to observe if there is a change in the major breath volatiles especially isoprene, acetone and methanol. In addition to that, comparison of VOCs concentration from the exhaled breath was done in between pre (healthy) and post (injured) for two players who had given pre and post breath samples.

N-acetylaspartate is a common metabolite in the brain, which depletes following a brain injury. It is suggested that this decrease is a result of the compound passing across the blood-brain barrier after which it is metabolised in the body. Therefore, the investigation also was done corresponding to N-acetylaspartate (NAA) from the exhaled breath due to concussion injury. NAA plays many important roles in the physiology and metabolic processes of the brain [12].

The conclusion of these results will be discussed in terms of medical relevance and possible advancements in sampling technique and measurement. Having said this, this study is purely an exploratory study which can help us to decide whether a potentially PTR-MS can be used for further investigation.

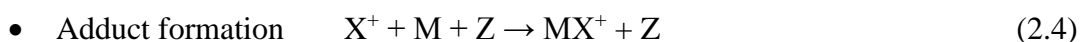
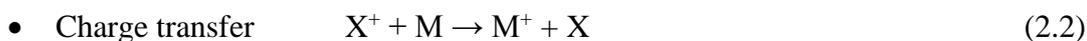
CHAPTER 2

2 PRINCIPLE OF PROTON TRANSFER REACTION MASS SPECTROMETRY

2.1 Background and Development of PTR-MS Instruments

The detection and monitoring of trace quantities of Volatile Organic Compounds (VOCs) are important in many areas of industry and science, especially involving food, the environment, homeland security and health applications [1]. For example, the atmosphere contains VOCs coming from plants and trees and anthropogenic sources such as car exhausts, biomass burning and industrial processes, which have significant impact on air quality. In human breath there are VOCs typically at parts per billion by volume (ppbv), such as acetone, isoprene and methanol, often resulting from metabolic processes in the human body which are transported via the bloodstream to the lungs where they are exhaled. In such environments, changes in VOC concentrations can occur in seconds. To detect such VOCs in low concentrations, and especially for those whose concentrations change rapidly, in the last two decades analytical chemical techniques have been developed based on soft chemical ionisation mass spectrometry [13].

The origins of soft chemical ionisation mass spectrometry date back to the 1960s through a development by Munson and Field, [14]. Chemical ionisation results in a lower energy process than the more common form of mass spectrometry which uses electron ionization, and hence results in less fragmentation resulting in a simpler spectrum which is easier to interpret. Chemical ionisation involves the production of product ions via a reaction process, the main ones of which are [1];



Where Z is a third body to stabilize the adduct MX^+ .

Reactions (2.1) and (2.2) are the major ion-molecule processes used in this study. Reaction (2.1) proceeds with unit efficiency providing the proton affinity (PA) of X is less than that of M. Reaction (2.2) is exothermic provided the ionisation energy of X is greater than that of M, with the reaction rate coefficient not necessarily being at the collisional value [1]. Although the reactions (2.1) and (2.2) are shown to be non-dissociative, the transfer of charge can lead to fragmentation.

A mass spectrometer is an instrument which produces numerous ions from the sample under examination and separates the ions according to their specific mass-charge-ratio (m/z) where,

The basic equation for sector mass spectrometers with
 c = instrument constant,
 B = magnetic field strength and
 V = acceleration voltage

$$\frac{m}{z} = c \cdot B^2 / V$$

The instrument contains three major components ion source, analyser and detector system. Ion source plays an important role in ionizing atoms or molecules by knocking one or more electrons off to give positive ions. This is followed by ion accelerations where all the ions have the same kinetic energy. These ions with the same

kinetic energy will be deflected by a magnetic field. The most deflected ion has the smallest value of m/z (lightest ions) compared to the heavier ones. The ions appearing from the final analysis will be detected by the ion detector where it produces electrical signals in proportion to their abundance and processed by an amplifier which shapes it and makes it larger for further analysis. The processed signals from the detector will be transmitted and displayed as a mass spectrum (detailed explanation in section 2.1.9). Followed by this, identification of specific compounds in a gas can be done based on the mass spectrum obtained.

A mass spectrum shows the final output of mass spectrometer by presenting a distribution of ions. A mass spectrum simply represents a “stick diagram” which shows the relative current generated by ions of varying mass/charge ratios. The vertical axis of a mass spectrum is usually labelled as either relative intensity or relative abundance. Meanwhile, the horizontal axis is labelled as mass to charge ratio (m/z).

Hence, there are several analytical methods used to analyse compounds in trace quantities. These respective techniques have their pros and cons. The common method of mass spectrometry to identify the VOCS are high-performance Liquid Chromatography-Mass Spectrometry (HPLC-MS), selected ion flow tube mass spectrometry (SIFT-MS), Ion mobility Spectrometry (IMS) and gas chromatography mass spectrometry (GC-MS). Among these, the most established technique in many laboratories is gas chromatography (GC) which has been used for more than 50 years [15, 16]. GC combined with mass spectrometry and an electron impact ionisation source, takes a longer time to get an analysis done. However, to overcome this problem, GC fast was introduced, but this technique still requires a few minutes for a complete separation [15, 16]. Therefore, it is crucial to monitor any incidents quickly where remedial action may be required, e.g.

environmental contamination, security and safety. In SIFT-MS, reagent ions are introduced into a carrier gas via a quadrupole mass filter where they are convected into a reaction region (flow tube) to react with the VOCs present. SIFT-MS is capable of achieving ppbv sensitivity and has the ability to study reaction kinetics for a series of reagent ions. The drawback of SIFT-MS is that it requires a different pressure in the reaction region (1-3 mbar) compared to the injection and detection regions ($\leq 10^{-4}$ mbar). Ion Mobility Spectrometry (IMS) is another analytical instrument which has been mainly used for homeland security and military applications, but is also finding use in medical diagnosis, food quality and environmental chemistry [17]. IMS performance depends on the mobility of the ions within the gas phase in an electric field of a drift tube at ambient pressure. Physical parameters such as size, shape and charge of ions and also type of buffer gas used in IMS are very important because they influence the collision cross section of the neutral gas molecules and the ions. The disadvantage of IMS is that it has a poor temporal resolution and selectivity which could lead to false positives. PTR-MS can overcome these problems where it has some similarities with IMS such as the drift tube, but at different pressures and no pulsing involved. However, PTR-MS has special characteristics and it has a high certainty level in chemical compound assignment due to its mass spectrometry capabilities.

PTR-MS is a robust, sensitive, analytical technique with minimal sample preparation and was developed in the mid-90s by scientists at the Institute of Ion Physics at the Leopold-Franzes University of Innsbruck (Austria) led by Werner Lindinger [13]. They developed the system based on the soft chemical ionization mass spectrometry for online and real time VOCs analysis. Lindinger and co-workers also introduced a simple and compact instrument by replacing the mass-selected H_3O^+ source with a hollow

cathode discharge which yields a $> 99.5\%$ H_3O^+ [1]. PTR-MS has been used in numerous analytical sciences such as, homeland security, food sciences, environmental sciences and health sciences [1]. In comparison to SIFT-MS, PTR-MS provides a better sensitivity and selectivity by adding two major changes to SIFT-MS. Firstly, they introduced a short drift tube instead of the flow drift tube. Secondly, they injected the analyte gas rather than inert carrier gas in SIFT [1]. These had made the technique simple by creating faster reactions using shorter drift time.

The first PTR-MS instruments used quadrupole mass spectrometers. However, in 2007, time of flight (TOF) mass spectrometric techniques were developed and introduced in 2008. TOF-MS is based on the time taken by the ions to travel a known distance and electric field strength where the different m/z hit the detector (Micro Channel Plate) at different times. It has number of advantages compared to Quad-MS, including higher selectivity owing to its higher mass resolution compared to the unit mass resolving power of a quadrupole mass spectrometer [1].

2.1.1 Advantages of PTR-MS technology

- i) The measurement can be done within a short period of time
- ii) PTR-MS can do on-line measurements using direct breath samples from a patient or volunteer. This will help in reducing the risk of sample degradation or contamination.
- iii) It does not require sample preparation unlike GC-MS which involves many protocols in preparing the samples.
- iv) Air can be used as a buffer or carrier gas with minimum reaction in the instrument except for O_2^+ and NO^+ which can be seen as a low contaminant and negligible.

- v) There will be no reaction with main constituents in air (N_2 , O_2 , Ar, CO_2 , etc.) which has proton affinity less than water.
- vi) It uses a lower energy reaction (soft CI), unlike GC-MS which requires 70 eV energy (electron impact) in order for the reaction to happen. Therefore, there will be a minimal fragmentation and easy interpretation can be done on the spectrum obtained.
- vii) It can detect low concentration of VOCs due to high sensitivity (as low as ppbv) and the instrument is transportable to different locations and areas.

2.1.2 Principles of Proton Transfer Reaction Mass Spectrometry

PTR-MS is a soft chemical ionization technique often used for on-line measurements of trace chemical compounds with detection concentrations as low as a few parts per trillion per volume (pptv) [18, 19]. The first commercial model of PTR-MS was constructed by IONICON Analytik Technology GmbH (figure 2.1) which used a quadrupole mass analyser. Later, KORE Technology Ltd designed PTR-MS with time of flight (figure 2.2).

For PTR-MS, a flow tube is not used in order to reduce the size of the instrument and the pumping requirements. Instead a drift tube is employed so that ions migrate into and through the reaction region under the influence of an electric field (E). Both instruments have their own advantages and disadvantages, but both have been successfully demonstrated for their application in the health sciences, the key area for this current report.



Figure 2.1 Photograph of the a) top view and b) hollow cathode and drift tube of a PTR-QUAD-MS Ionicon Analytik GmbH apparatus.

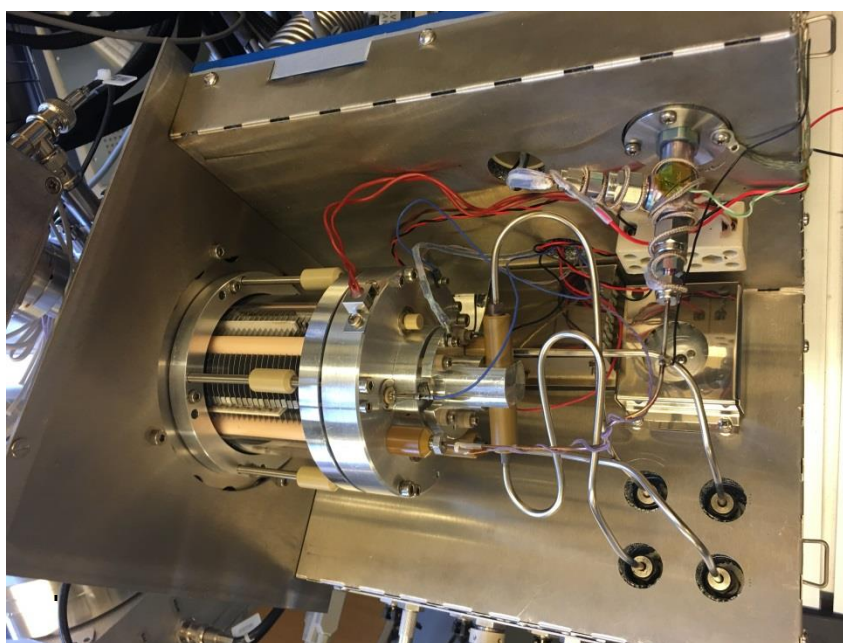
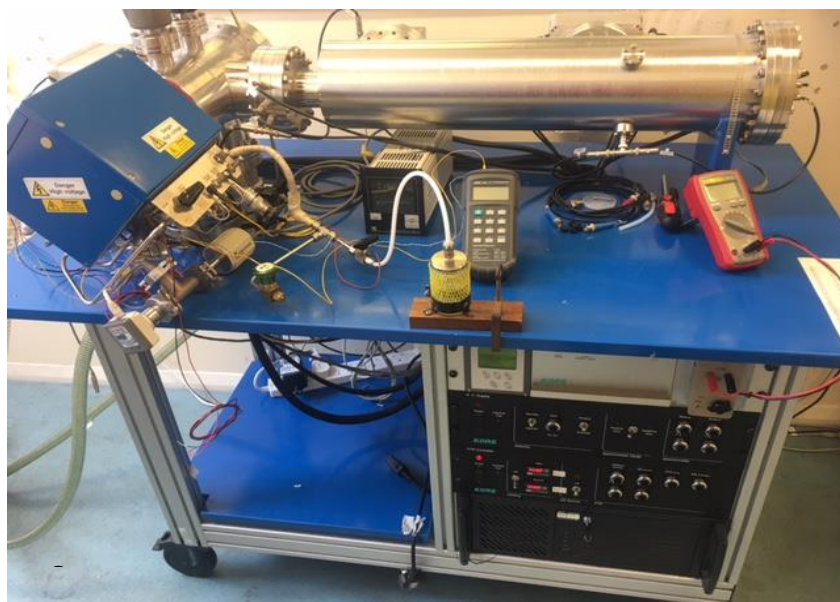


Figure 2.2 Photograph of the a) top view and b) hollow cathode and drift tube a PTR-ToF-MS KORE Technology Ltd.

Two different PTR-MS instruments have been used in this study. The one used for breath analysis, employed a quadrupole mass spectrometric filter and the other used for head space analysis a time-of-flight (ToF) mass spectrometer. The high resolution PTR-ToF-MS is required to do headspace analysis which involves complex chemical and identifying numerous product ions accurately. Meanwhile, PTR-MS quadrupole was used for breath analysis which requires high sensitivity in identifying compounds from exhaled breath. Besides that, this similar instrument has been used by other researchers in institute for breath analysis and it would be helpful to compare some of the results obtained from these studies and theirs for future research studies.

Figure 2.3 [20] shows a schematic diagram of the quadrupole PTR-MS system used in this study, which has higher sensitivity for detecting VOCs than the ToF instrument, but has lower mass resolution. This instrument was used for breath analysis of rugby players who had concussion injuries and also for the rugby players' control group. A schematic representation the KORE PTR-ToF-MS is shown in figure 2.4.

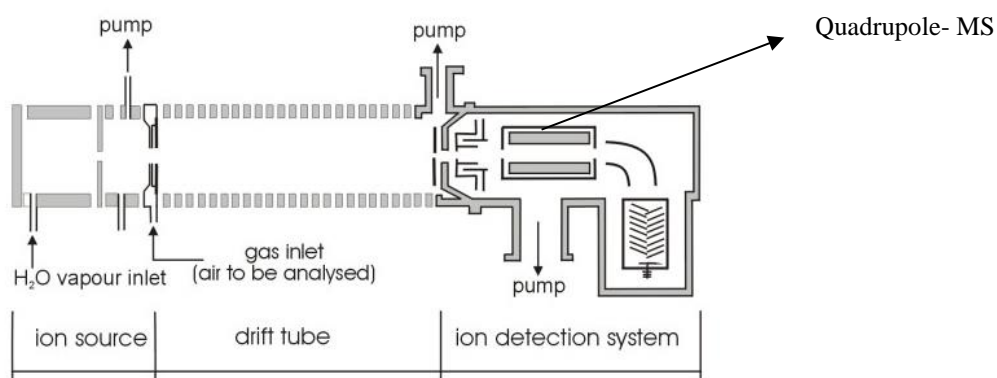


Figure 2.3 Schematic diagram of an Ionicon PTR-MS instrument (Quadrupole) taken from Hansel et al. 1995 [21].

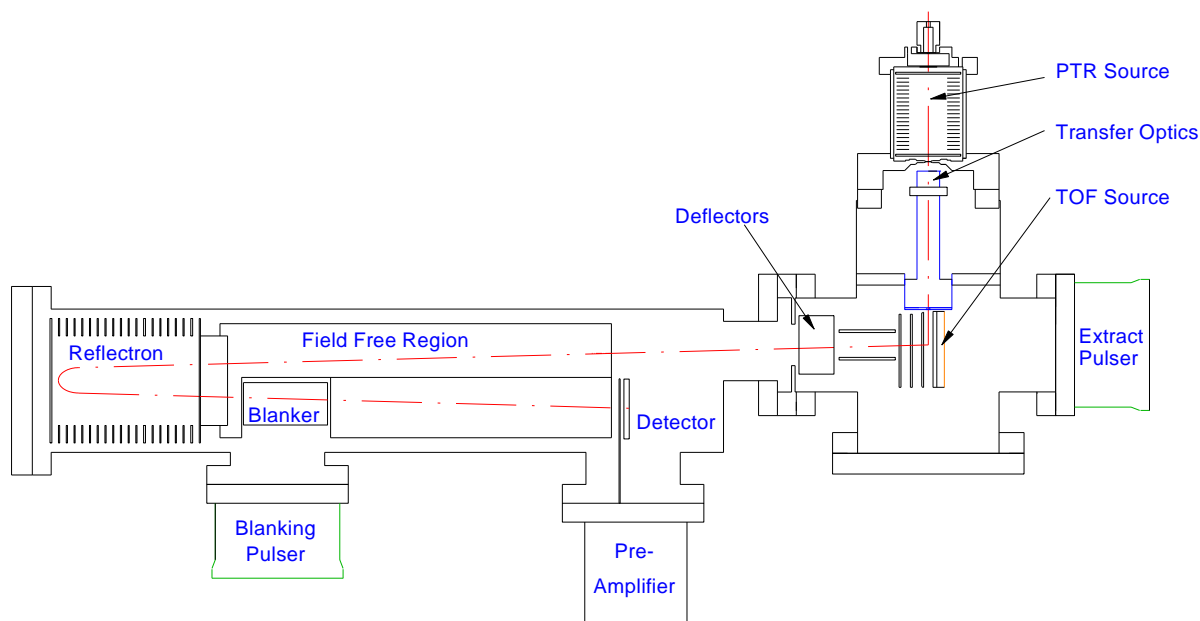


Figure 2.4 Schematic of the KORE PTR- TOF-MS [22]

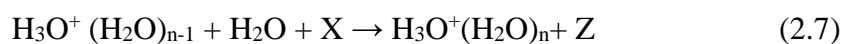
The reagent ion commonly used in PTR-MS is H_3O^+ . However, H_3O^+ and O_2^+ have been used as reagent ions for headspace of anaesthetic studies and only H_3O^+ reagent ions for breath and Shisha measurements. Reagent ions H_3O^+ reacts with VOCs via proton transfer (Reaction (2.5)). O_2^+ reagent ions react via charge transfer with VOCs.



Both processes, as mentioned earlier can be dissociative. For the reactions to proceed requires for proton transfer and charge transfer that $\text{PA}(\text{VOC}) > \text{PA}(\text{H}_2\text{O})$ and IP

(Ionization Potential) (VOC) < IP (O₂), respectively. Importantly H₃O⁺ reagent ions cannot react with the major constituents in air because they all have much lower proton affinities than water (691 kJ mol⁻¹) (A detailed explanation about proton affinity is in section 2.1.3). This makes H₃O⁺ an ideal reagent ion for detecting VOCS in breath and the atmosphere.

In addition to H₃O⁺ reagent ions being present in the reaction region, there are protonated water clusters, formed via a 3rd body reaction (2.7) the intensities of which are dependent on instrumental operating conditions and humidity [19].



Where, Z is a 3rd body.

Water clusters possess higher proton affinities than H₂O, and the more water molecules the greater is the proton affinity of the water cluster up to a certain limit. This means that some proton transfer reactions that occur with H₃O⁺ do not occur with H₃O⁺ (H₂O)_n.

2.1.3 Proton Affinity and protonation



Reaction (2.8) shows gas phase proton transfer to an analyte molecule M which will be detected by PTR-MS.

Proton affinity (PA) is the negative enthalpy change of the reaction in equation (2.8). It always has been used to check whether a proton transfer reaction is likely to be thermodynamically spontaneous. This process which is better known as an exothermic reaction in gas by releasing energy. This process is well explained by the change in the standard Gibbs free energy at certain temperature T, ΔG_T^0 where a negative of the enthalpy change of the reaction (2.8) happens by proton donation to the compound of interest which has PA more than H_2O (691 kJ mol^{-1}). Table 2.1 shows the PA of the most abundant components in clean air. The majority of common VOCs have higher proton affinities (table 2.2), allowing for spontaneous protonation. However, the predominant inorganic gases in the environment such as N_2 , O_2 and CO_2 have lower proton affinity than the H_2O . Ideally, H_3O^+ is the only ion that should react with the analyte gas and it is an ideal reagent ion in our studies to measure and identify VOCs in gas phase samples. However, hydronium water clusters of the form $\text{H}_3\text{O}^+ \cdot n\text{H}_2\text{O}$, ($n \geq 1$) are formed in most of the experiments especially using a lower energy and temperatures. Generally, these water clusters have a higher proton affinity (table 2.3). For example $\text{H}_2\text{O} \cdot \text{H}_2\text{O}$ has a proton affinity of 833 kJ mol^{-1} [23]. As the PA of the water clusters increases with growing n, the reaction become more selective.

Table 2.1 Proton affinities of the most abundant components in clean air [24].

Molecule	Proton affinity (kJ/mol)
Oxygen (O ₂)	421
Nitrogen (N ₂)	494
Carbon dioxide (CO ₂)	541
Water (H ₂ O)	691

Table 2.2 Proton affinities of some common volatile organic compounds [24].

Molecule	Proton Affinity (kJ/mol)
Propane	626
Methanol	754
Acetaldehyde	770
Pyridine	948
Limonene	875

Table 2.3 Proton affinities of water and water clusters [23, 25].

Neutral Molecule	Proton Affinity (kJ/mol)
H ₂ O	691
(H ₂ O) ₂	833
(H ₂ O) ₃	889
(H ₂ O) ₄	920

2.1.4 Fragmentation

Although proton transfer is considered soft ionization, it does not mean that there will be no fragmentation. Fragmentation results from dissociative proton transfer, which can be instantaneous owing to the chemistry involved or can be a result of collisional induced dissociation occurring through energy gained by the reagent and/or protonated parent in the electric field of the drift tube. Non-dissociative proton process results in the protonated parent being observed. Often both the protonated parent and fragment ions are observed. For example, for limonene and using reduced electric fields in the range of 80-200 Td, proton transfer from H₃O⁺ results in product ions being observed at m/z 137, which corresponds to the protonated parent C₁₀H₁₇⁺ and m/z 81, which is a fragment ion (C₆H₉⁺). The fragmentation pattern in a mass spectrum can be useful to determine structural information of an unknown molecule. In comparison, acetone, whose proton affinity is high (table 2.4), shows no fragmentation resulting from reactions with H₃O⁺,

and only the protonated parent is observed for all reduced electric fields investigated to date, whereas the reaction of H_3O^+ with isoprene, whose proton affinity is similar to acetone, results in the protonated parent m/z 69 and product ions at m/z 41 [25] and m/z 39 [26]. Table 2.4 shows the proton affinities of various chemical compounds e.g. acetone, isoprene, methanol and other relevant molecules which have been used to make a comparative study between the healthy rugby players and players who had a concussion injury. On the other hand, some claimed that isoprene can fragment but some claimed it does not fragment [20, 26, 27].

Table 2.4 Proton affinities of acetone, isoprene, and limonene. For comparison the proton affinity of water is given [28, 29].

Molecule	Proton affinity kJ mol^{-1}	Formula
acetone	812	$(\text{CH}_3)_2\text{CO}$
isoprene	826	$\text{CH}_2=\text{C}(\text{CH}_3)\text{CH}=\text{CH}_2$
limonene	875	$\text{C}_{10}\text{H}_{16}$
water	691	H_2O

2.1.5 Components of a PTR-MS

The proton transfer reactions mass spectrometer consists of four different sections.

1. An ion source is the region where the H_3O^+ ions are produced by a hollow cathode discharge (HC) in water vapour.
2. Drift tube. This is the reaction region. The air which contains traces of volatile organic compounds enters into the drift tube where the proton transfer reaction takes place.
3. Mass spectrometer (analyser). In this region the ions are separated according to mass/charge ratio.
4. An ion detector

The ions are detected by a secondary electron multiplier (SEM) for the PTR-Quad-MS instrument and by microchannel plates (MCP) for PTR-ToF-MS.

2.1.5.1 Hollow Cathode

A detailed description of the operation of the hollow cathode is to be found in Chapter 3 of the book “Proton Transfer Mass Spectrometry by Ellis and Mayhew [1]. The details in that book have been adapted for this section. Basically, a reservoir of distilled water provides the water vapour that enters the hollow cathode (HC) ion source via a mass flow controller, bringing the pressure inside to about 2 mbar. An electrical discharge results in ionisation and dissociation of the water, leading to ions such as H_2O^+ , OH^+ , O^+ , and H^+ , all of which react with water, which through a series of ion-molecule reactions leads to the formation of H_3O^+ . This is the terminal ion, because it does not bimolecularly react with water – it can only associate via a three body process, leading to protonated water clusters. In addition to H_3O^+ , back diffusion of the air into the HC, leads to the discharge

forming N_2^+ , O_2^+ and NO^+ . N_2^+ reacts with water via charge transfer, so those reagent ions are ultimately converted to H_3O^+ . O_2^+ and NO^+ cannot react with H_2O and hence are considered impurity ions in the HC which enter the drift tube. These are usually about 3% of the intensity that is found for H_3O^+ .

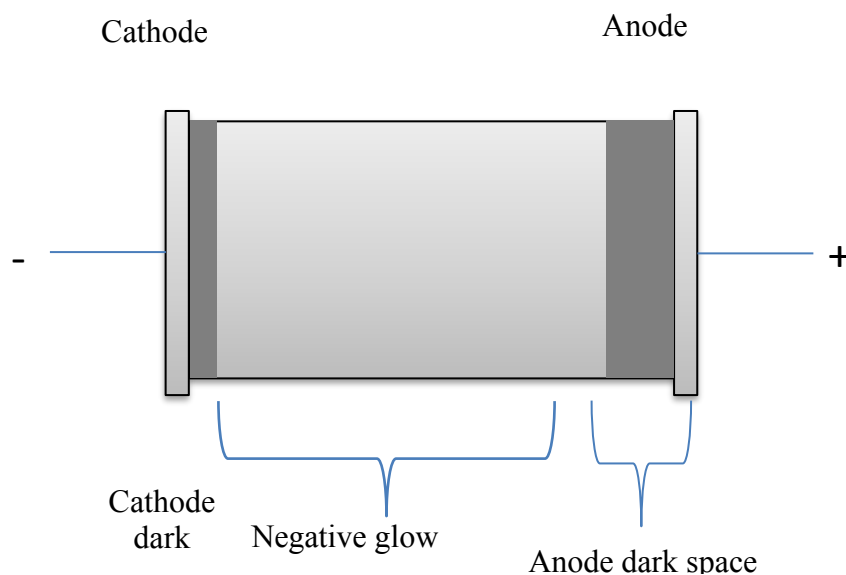


Figure 2.5 Hollow cathode discharge

H_3O^+ is a terminal ion produced through a series of ion-molecule processes following the electron impact ionization of molecules in the hollow cathode, reactions (equations (2.9-2.15) [30]). All of these reactions are fast in order of magnitude $10^{-9} \text{ cm}^3 \text{ s}^{-1}$ [1] with a measured reaction rate coefficient, k , being at or close to the collisional value.



As pointed out earlier, some air entering into the discharge region of the PTR-MS instrument is unavoidable. This results in the generation of other ions such as N_2^+ and O_2^+ . N_2^+ is rapidly removed by a charge exchange reaction with H_2O [1].



Therefore, the presence of N_2^+ leads to formation of H_3O^+ via a reaction of H_2O^+ with H_2O (reaction 2.9).

The ionization energy of O_2 (12.06 eV) is less than H_2O (12.6 eV). Thus, O_2^+ cannot react with H_2O by charge transfer. Hence, O_2^+ will be seen as a low level contaminant reagent ion in PTR-MS experiments. Besides that, NO^+ is another impurity reagent ion owing to the recombination energy of NO . NO^+ is formed via reaction (2.15).



However, the concentrations of O_2^+ and NO^+ can be reduced to negligible levels by selecting appropriate experimental conditions and by altering gas flow conditions. Typically, the ion intensities of these ions are below 3% of the total reagent ion signal.

2.1.5.2 Drift Tube

The drift tube is where the soft chemical ionisation occurs. The drift tube is formed of a series of equally spaced electrodes, separated by insulating spacers which control the voltages applied to each electrode. The important role of the drift tube is to produce a uniform electric field which will cause the ions to migrate along the length of the drift tube. The drift tube in the PTR-MS is operated using a set reduced electric field, which is the ratio of the electric field strength E to the number density of gas, N , units of V cm^2 . E/N (Td) where Td is the unit for E/N also known as the townsend. It can be defined as $1 \text{ Td} = 10^{-17} \text{ V cm}^2$. E/N provides a measure of the ions' kinetic energy in the drift tube (E/N will be discussed in more detail in section 2.1.6). A typical length for a drift tube in PTR-MS is approximately 10 cm. The electric field is important because it gives energy to the ion-molecule collisions limiting clustering of neutral molecules, especially H_2O to ions. The usual drift tube pressure for sufficient reactive collisions to happen is approximately 1-2 mbar and operating temperatures used is between 50-200°C. With suitably applied drift tube voltages this results in operating E/N values of between 120 to 140 Td ($1 \text{ Td} = 1 \text{ Townsend} = 10^{-17} \text{ V cm}^2$).

A source drift tube region is added between the HC and the Drift tube to enhance the yield of H_3O^+ through additional ion-molecule reactions away from the hollow cathode source. It also aids fragmenting protonated water clusters to the monomer.

2.1.6 The ratio of electric field and number density of buffer gas - reduced electric field (E/N)

The average ion energy in a PTR-MS is determined by the reduced electric field E/N . The electric field, E in the PTR-MS provides the driving force for the ions to migrate down the drift tube. It also provides sufficient energy to ions to prevent excessive clustering with water molecules. The electric field E is given by $E = V/d$ where V is the potential difference across the drift tube and d is the length of the drift tube (typically 10 cm in a PTR-MS). However, E alone is not the important parameter, because ions lose energy in collisions, which depends on the neutral number density N . Hence it is the ratio of E/N which is important in determining the mean drift velocity and hence mean kinetic energy of the reagent and product ions. This can be calculated from:

$$N = \frac{N_A}{V_M} \frac{273.15}{T_d} \frac{P_d}{101.325} \quad (2.17)$$

Where, N_A is Avogadro's number ($6.022 \times 10^{23} \text{ mol}^{-1}$), V_M ($22414 \text{ cm}^3 \text{ mol}^{-1}$) is the molar volume of an ideal gas at 1 atmosphere of pressure (101.325 kPa) at a temperature of 273.15 K. T_d is the operational temperature of the drift tube (in Kelvin), and P_d is the gas pressure in the drift tube (in kPa).

2.1.7 Ion Mobility

The ions which enter the potential gradient inside the reactor will be accelerated towards the most negative potential. The ions collide with the neutral buffer gas due to relatively high pressure and the swarm reaches a constant drift velocity, V_d [1].

V_d is the ion drift velocity, which is linearly dependent on the electric field (E) at low electric fields. The following equation explained about the ion drift velocity,

$$V_d = KE \quad (2.18)$$

where, K is the coefficient known as the ion mobility. The equation describes the mean drift velocity of the ion swarm and not the velocity of the individual ions. The ion mobility coefficient is a function of temperature and pressure of the ions [1]:

$$K = \frac{760}{P} \frac{T}{273} K_0 \quad (2.19)$$

In the above equation, T is temperature (Kelvin) in the drift tube and P is the pressure (Torr) in the drift tube and K_0 is the reduced mobility.

$$v_d = \frac{760}{P} \frac{T}{273} K_0 E \quad (2.20)$$

If L = drift tube length and the t_d is the drift time in the drift tube.

$$t_d = \frac{L}{v_d}$$

$N_0 = 2.687 \times 10^{19} \text{ cm}^{-3}$ gas number density under standard temperature and pressure (equation 2.19 and 2.20) (i.e. $T = 273.15 \text{ K}$ and $P = 101.325 \text{ k Pa}$) and K_0 is known as the reduced mobility of the ion for a given analyte molecule. The drift tube v_d is proportional to the electric field. Following equation expressed about v_d :

$$v_d = K_0 N_0 \frac{E}{N} \quad (2.21)$$

The drift velocity is inversely proportional to the pressure. Therefore, the drift velocity decreases as the drift tube pressure increases. The above equation (2.21) shows that, the effect of the gas is expressed here in terms of number density (N) rather than pressure. As a consequence, it can be seen that by varying the electric field strength, one can vary the drift velocities of the ions which leads to a change in the collisional energies within the drift tube. Owing to the low bond energies associated with the protonated water clusters, increasing collision energies will lead to lower concentrations in the drift tube of these ions. If the E/N is sufficiently low that the collisional energies are insufficient to limit clustering then protonated water clusters dominate formed through the reaction: $(H_3O^+ + (H_2O)_n$ ($n = 0$), via the following general process [19];



With the knowledge of ion mobilities, it is possible to calculate the transit time for (H_3O^+) through a drift tube by considering ion mobilities in air and nitrogen are similar. We also assume the conditions for H_3O^+ are far more abundant than hydrated hydronium cluster ions [1].

$$t_d = \frac{L}{K_0 N_0} \frac{N}{E} \quad (2.23)$$

For example, by using a drift tube length of 10 cm and using $N_0 = 2.687 \times 10^{19} \text{ cm}^{-3}$, $K_0 = 2.81 \text{ cm}^2 \text{ V}^{-1} \text{ s}^{-1}$ and $E/N = 120 \text{ Td}$ ($1.2 \times 10^{-15} \text{ V cm}^2$) results in a drift time of $t_d = 110 \text{ } \mu\text{s}$ and 906 ms^{-1} as a mean drift time velocity [1].

2.1.8 Quantitative characteristics of PTR-MS

The description for this section and the equations were adapted from Ellis and Mayhew's book on 'Proton Transfer Mass Spectrometry' [1]. The PTR-MS can be used to measure the absolute concentration of a specific constituent of a gas mixture by using a measurement of the ion signals. Taking into account that H_3O^+ is the proton source, an assumption can be made by considering that this reaction only occurs with a single organic gas. For example, in this case M is assigned as the organic gas. The proton reaction is shown as in equation (2.24).

$$\frac{d[\text{H}_3\text{O}^+]}{dt} = -k[\text{H}_3\text{O}^+][\text{M}] \quad (2.24)$$

By assuming that $[\text{M}] \gg [\text{H}_3\text{O}^+]$ even at trace levels, we can assume that $[\text{M}]$ remains constant, and hence the reaction is pseudo first order and this explains in equation (2.25) where concentration of protonated reagent ions as a function of time t ,

$$[\text{H}_3\text{O}^+]_t = [\text{H}_3\text{O}^+]_0 e^{-k[\text{M}]t} \quad (2.25)$$

The reaction time t is the time taken by the reagent ion where the concentration of protonated reagent ions H_3O^+ lost in time t , in this scenario,

$$[\text{MH}^+]_t = [\text{H}_3\text{O}^+]_0 - [\text{H}_3\text{O}^+]_t \quad (2.26)$$

provides substituting into Equation 2.27,

$$[\text{MH}^+]_t = [\text{H}_3\text{O}^+]_0 [1 - e^{-k[\text{M}]t}] \quad (2.27)$$

According to description by Ellis et al [1], assumption is made according to the condition and usually the condition is chosen. For instance, only a small proportion of H_3O^+ is consumed by the reaction in order to obtain the following conditions, $[\text{H}_3\text{O}^+]_0 \approx [\text{H}_3\text{O}^+]_t$, or equivalently $[\text{MH}^+] \ll [\text{H}_3\text{O}^+]$ where $k[\text{M}]t \ll 1$. This provides that M presents lower than the parts per million level. Equation 2.28 explains about the concentration of M.

$$\frac{[\text{MH}^+]}{[\text{H}_3\text{O}^+]} = \frac{i(\text{MH}^+)}{i(\text{H}_3\text{O}^+)} = k[\text{M}]t \quad (2.28)$$

$\frac{[\text{MH}^+]}{[\text{H}_3\text{O}^+]}$ is the concentration at the end of the drift tube. i is the ratio of currents for the measured count rates of these two ions at the detector of the mass spectrometer. It is possible to calculate the concentration of gas M in the drift tube by having measured the ratio of $i(\text{MH}^+)/i(\text{H}_3\text{O}^+)$ (Equation 2.28).

2.1.9 Detection system of Mass Spectrometer (MS)

2.1.9.1 TOF MS Analyser

The following description has been adapted from Ellis et al [1].

The time-of-flight mass analyser was used to separate out the ions according to their flight times where the heavier ions have a longer flight time than the lighter ions. The ions exit the drift tube and enter into a short acceleration region (referred as the x direction). This acceleration region (figure 2.4) has two electrodes (repeller and extractor electrodes,). The extractor allows most of the ions to enter into the flight tube via a high transmission grid using a differential pumping stage. There is no electrical field inside the flight tube before they hit the detector. Therefore, the velocities of the ions as they leave the acceleration region are maintained through the flight tube.

In order to prevent the deflection of the incoming ions, initially the electrical potential is kept the same for both the repeller and extractor. The voltage state is adjusted continuously such that the repeller has a higher voltage compared to the extractor in order to obtain a mass spectrum. A pulse of ions is sent into the flight tube using this potential gradient. Collisions with the background gases should be avoided in order to get an effective collision between reagent ions and analytes by providing a good vacuum system preferably $< 10^{-5}$ mbar pressure. Ions with positive charges q near to the repeller surface will have the same kinetic energy when they enter the flight tube, E , which is governed by the following equation:

$$E = qV = \frac{1}{2}mv^2 = \frac{1}{2}m\left(\frac{l}{t}\right)^2 \quad (2.29)$$

Where; V is the potential different between the extractor and repeller electrodes, m is mass of the ion, v is the velocity of the ions in the drift tube, l is the length of the flight tube and t is the time taken by the ions to reach the detector.

The ions fly into a 'field free region' (FFR) before reaching the reflectron. All the ions are reflected and returned back through the field free region to strike the detector. The FFR is divided longitudinally to ensure that the blanking plates (figure 2.4) do not affect ions travelling towards the reflectron. Aperture plates are mounted in the flight path before and after the blanking plates to reduce the influence of any ions except those passing through between them.

ToF-MS made by KORE Technology Ltd., has another important part known as the reflectron. This consists of a piece of apparatus which is made up of a series of electrodes known as a reflector array. The same m/z ions can move at different velocities depending on the distribution of energy that ions have within the flight tube. Therefore,

the faster moving ions for a given m/z will penetrate deeper into the reflectron than the slower ones. The reflector voltages can be adjusted so that the ions with the same m/z with have different speeds reach the detector at a similar time. This improvement in temporal resolution results in an improved mass resolution.

A Microchannel Plate (MCP) Detector is used in the PTR-TOF-MS as the detector. It consists of a resistive glass plate with numerous narrow channels organised in a honeycomb structure. Each channel acts as a miniature electron multiplier. A MCP has a larger surface area for incoming ions compared to the discrete dynode and channeltron detectors. This allows a systematic ion collection from a spatially broad source while achieving a high gain. The transit distance via MCP is short (0.5-2.0 mm) compared to other detectors such as channeltron and discrete detector. This results in a MCP detector to have a high time resolution (< 1 ns). These have had made MCP a suitable detector for use in TOF-MS [1].

Two plates have been used in the MCP detector we have used, with a Chevron configuration (pair of microchannel plates) in order to achieve a high gain (figure 2.6) and to minimise ion feedback. Every individual channel has an entrance diameter in the region of $10\ \mu\text{m}$ and the channel walls are aligned at an angle to the surface of the plate to maximise the incoming charged particles to strike the wall. Positive ions enter the MCP detector via a conducting mesh. This is usually maintained at Earth potential after which the ions are accelerated through a voltage of ~ 2 kV whereupon they strike the channel walls to generate one or more secondary electrons. Consequently, this initiates a cascade process as the newly generated electrons are accelerated to the back of the second plate by the increasingly positive electrical potential.

The signal (electron) is pre-processed by using an amplifier and then converted to a digital signal using time to digital converter (TDC). The final signal will be recorded as a pulse representing the arrival of one ion.

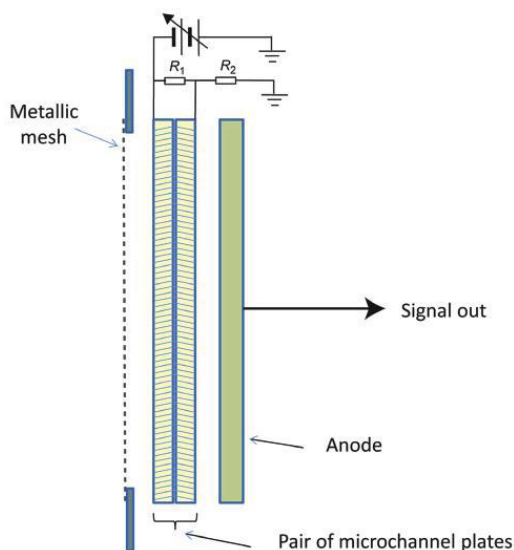
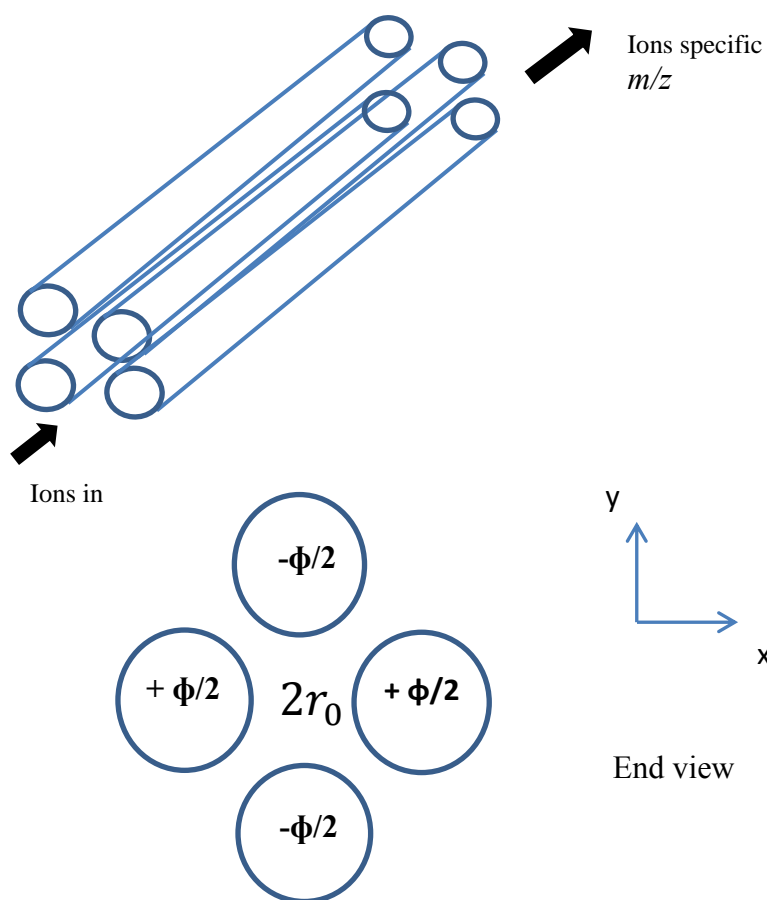


Figure 2.6 Schematic diagram of a microchannel plate (MCP) detector. Reproduced with permission from reference [1]. Copyright © 2014 Wiley.

2.1.9.2 QMS

The quadrupole mass selector (QMS) usually uses a secondary electron multiplier (SEM) to detect ions. The quadrupole mass filter sequentially scans over m/z range by applying a superposition of AC and DC voltages to four parallel rods (figure 2.7). An oscillating electric field is generated in the x-y plane when an electrical voltage is applied to the four parallel electrodes. The ions with positive charge will enter the region between the electrodes. The repulsion increases from the nearest rod and will drive the ion to opposite electrode. As the repulsion increases the ions oscillate from one side to other side. For particular AC and DC fields only ions with a given m/z ratio can pass through, all other ions are lost on the surfaces of the rods. The selected ions are deflected by 90° where they are incident on a secondary electron multiplier (SEM).

The quadrupole mass spectrometer has a limited m/z range, usually not much more than 1000 amu, and a not much better than unit mass resolution (low mass resolving power) allowing only nominal m/z detection. It is therefore difficult to discriminate different compounds which have the same nominal mass (isobaric). For example, the protonated nominal mass of furan is 69 but the exact mass is 69.03349. Whilst, protonated isoprene's exact mass is m/z 69.06988. In this case, if both compounds are present only a single signal on the mass spectra will be seen.



$$\phi = U + V \cos 2\pi vt$$

where applied electrical potentials (ϕ) of equal magnitude applied to the four electrodes and $r = 1.148 r_0$ where r_0 is the field radius in a square array.

Figure 2.7 Side view of Quadrupole mass analyser [1].

The advantage of a quadrupole system is its low cost compared to TOF and it has the ability to perform both qualitative and quantitative analysis. In addition to that, it can increase the sensitivity by MID (multiple ion detection mode).

The SEM gives an electrical pulse for each incident ion. As the SEM lifetime decreases, it drops sensitivity and this has to be checked regularly. The ideal operating voltage for a

SEM can be determined from where its response plateaus. If there is no characteristic signal maximum visible (“Plateau”) while the operating voltage is increased then SEM has to be replaced. If the voltage is too high the signal to noise ratio declines and causes a dark current which produces a poor quality signal. More than one million CPS incidents on the SEM leads to losses in linearity of the output signal. Figure 2.8 shows the SEM used in a PTR-MS Quadrupole instrument.

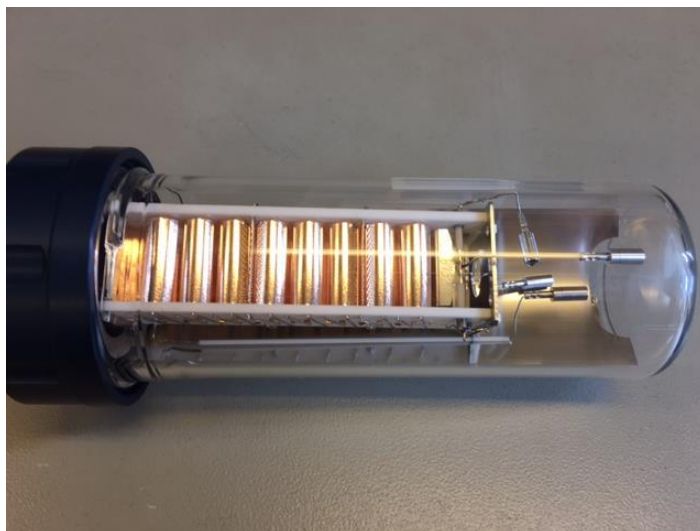


Figure 2.8 Photograph of a new secondary electron multiplier. The dynodes are visible between the white ceramic layers.

2.2 PTR-MS Data Analysis

The PTR-MS quadrupole is operated using the software for data collection provided by Balzers QMS-422. The software contains a different set of controller programs to operate the PTR-MS system. Workplace is a program which aids control and handling of the PTR-MS to make measurements and analysis much easier and also used to optimize the ion source. For example, it also allows us to control different settings such as controlling water flows, inlet flows, and voltages in the drift tube. Besides that, the online concentration analyser gives an immediate preview of measured data with all the detailed parameters for further analysis.

There are two ways to generate a mass spectrum in the PTR-MS Quadrupole. Firstly, a mass spectrum can be generated by using ion count rates versus mass m/z (molecular mass). This mass spectrum generation is also known as mass scan mode from m/z 30-300. Figure 2.9 shows a typical mass spectrum of alveolar breath which used mass scan mode. Prior to running the sample, in the software settings, a specific dwell time was set in the mass scan mode for the complete cycle because the software does not allow setting an individual mass. In the mass scan mode, the dwell time can be set between 0.5 ms up to 60 s per channel as displayed on the settings. In this study, 0.5 s was used to get an optimal data acquisition. A complete scan cycle is considered finished when the set range of m/z has been scanned over a stated dwell time for each point. The dwell time also plays an important role to improve signal to noise ratio. For example, shorter integration time was used for the volatiles with higher concentration e.g. higher than 100s of ppbv. However, for volatiles with lower concentration, typically for several ppbv, a longer integration time is needed.

A mass spectrum also can be obtained by using ‘multiple ion detection’ (MID). MID is the the mass scan mode where only selected m/z of interest will be chosen for any measurements over a time period of scanning (dual time). Generally, for the unknown VOCs samples, mass scan mode has been used. It also can be employed to monitor the change in concentration over time. The data extraction and analysis for PTR-MS Quadrupole (QMS 422, Balzers) instrument which was used for the breath analysis investigation was not an instant and automated process. In order to get the data, every obtained cycle during the measurement was converted to an ASCII file using the Balzers Quadstar 422 software package and then copied to Excel spreadsheets.

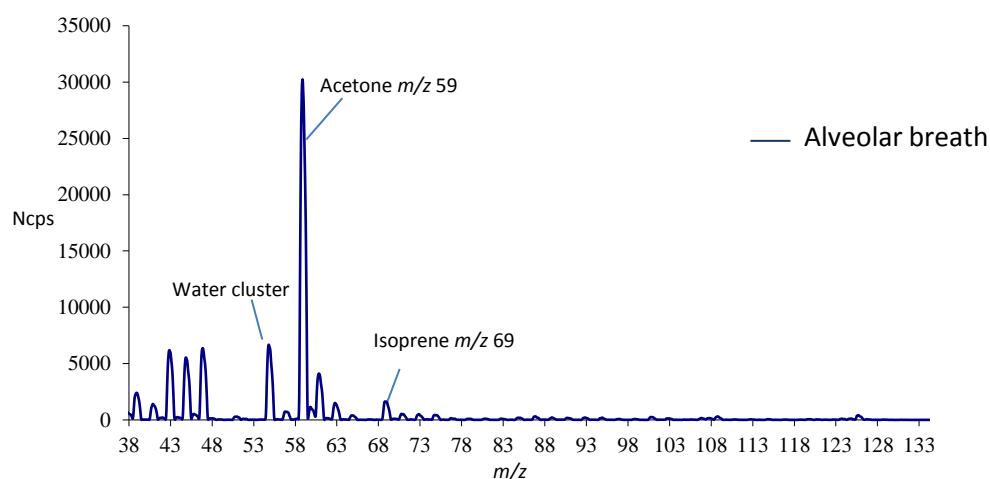


Figure 2.9 Example of PTR-MS alveolar breath spectrum of a healthy rugby player (Quadrupole, Ionicon Analytik G.m.b.H).

In PTR-TOF-MS, GRAMS/AI TOF-MS software is used to collect the data. The KORE Workbook program contains interface, customisation of the toolbar and menus. There are normally four pages in the workbook where the first page is related to set parameters to collect spectra, load spectra and perform the actual collection. The other three pages are related to calibration tools, printing facilities and provides an interface for chromatography collection. In PTR TOF-MS, mass spectra (figure 2.10) can be acquired using theoretical mass/charge (m/z) values versus measured time of flights. The spectrum acquisition parameters adjusted based on length of experiments (sec), length of cycle (cycle time) and the width of each time bin in nanoseconds. All spectra are collected as time spectra and stored to disk format. Conversion of time data to mass is achieved as the spectrum is loaded. The mass conversion for PTR-TOF-MS (KORE) is based on t_0 , Cb and t (equation 2.30).

$$m = \left(\frac{t-t_0}{Cb} \right) \quad 2.30$$

where t_0 and Cb are unknown, in this case, these parameters will be determined by the software provided by the manufacturer and t is measured flight time. The data are then extracted from GRAMS software and copied into an excel worksheet for further analysis.

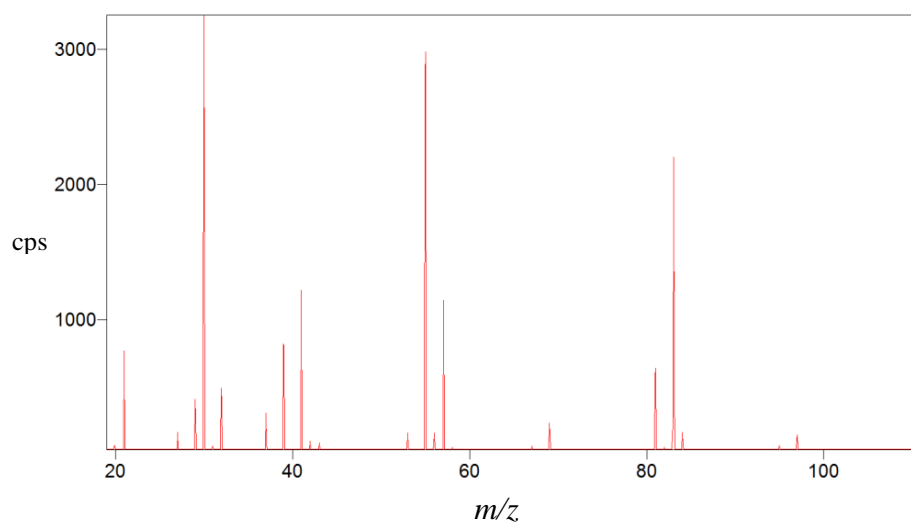


Figure 2.10 Example of PTR-TOF-MS spectrum (KORE Technology Ltd)

CHAPTER 3

3 Breath Sampling for Clinical Screening, Diagnosis and Monitoring

3.1 Introduction

Breath consists of mixture of a number of dominant gases, such as nitrogen, oxygen and carbon dioxide, and also some water vapour. A typical concentration of normal human inhaled air contains 79% of nitrogen, 21% oxygen and a small percentage of argon, carbon dioxide, neon, hydrogen, helium and water vapour. However, exhaled breath typically contains 78 % nitrogen, 18 % oxygen and 4% carbon dioxide.

Besides that, it also has some inert gases and trace amounts (from parts per million to parts per trillion by volume) of volatile organic compounds (VOCs). Although, these gases are in low concentrations, they are the result of metabolic processes in the body [2, 31]. Endogenous VOCs produced in the body are products of normal activities based on normal metabolism and metabolic pathways. Some VOCs are produced due to modified metabolisms because of a certain disease or illness. Exogenous VOCs are transported to the lungs via the bloodstream where they contribute to exhaled breath. Breath analysis can be applicable to people of all ages and certain medical conditions. It also involves a harmless and no risk procedure to the patients. Breath sampling gives a possible way to identify a dangerous disease, screening and monitoring disease growth, behaviour and the reaction towards the treatment.

The possibilities of breath analysis have been proven by clinicians ‘smelling’ some kind of odours in their patients’ exhaled breath. As a consequence, the adjectives of uremic, hepatic and acetone in the breath corresponding to several diseases have been used for many years [32]. However, the limitation of this approach towards some diseases

was only noticed at chronic stage of the respective disease when the systemic metabolism was fully adjusted [32].

Rather than smelling breath, which has been done since the ancient Greeks, a new analytical age of breath analysis started approximately 40 years when Linus Pauling and co-workers found 250 VOCs in an ordinary breath sample [33], using breath analysis technique. The results were that some of these VOCs were associated with certain systemic disorders and pathological conditions [33]. A more recent pioneer of breath analysis is Michael Philips at the New York Medical College, US who is the founder and chief executive officer of Mensanna Research. He has claimed that breath test can be the least invasive compared to the all diagnostic tests and technical advances encouraged his research group to introduce a new role for breath testing in detecting early stage of disease [34]. His research team also have developed a portable breath collection device where breath samples can be collected anywhere. This remarkable advancement in the identification capability of breath analysis has stimulated the exploration of airway diseases by interpretation of biomarkers deriving from the airways and lung structures.

As mentioned earlier, odour from the breath may be used to detect certain diseases in their advanced stages. For example, the breath of diabetic patients has a fruity odour which is linked to the high concentration of acetone in the body and hence in the breath due to the lack of insulin produce by the pancreas. Therefore, the level of glucose in the body goes extremely high and is unused. This leads to the body using the stored fat as a substitute source for energy. As a consequence, acidic ketones build up in the body and are detectable via the breath.

Some researchers used breath analysis to detect VOCs from critically ill patients, such as oxidative stress, lung, liver, and kidney diseases, and organ dysfunction or tissue rejection where they found unusual VOCs via exhaled breath due to change in pathophysiology and metabolism [35]. For example, Scott et al., claimed to have found biomarkers in the breath of patients suffering from cystic fibrosis lung and tuberculosis [36, 37].

Besides that, Micheal Philips evaluated a breath test for VOCs from breast cancer patients to prevent unnecessary mammogram screening which involves radiation exposure and potentially introduces a painless screening test [38]. Recently in 2016, Fernandez et al. used breath analysis without involving any painful procedure and found three VOCs (limonene, methanol, and 2-pentanone) associated with liver cirrhosis patients from a study involving pre and post liver transplant patients [2]. In addition to this, O'Hara et al. have linked limonene in exhaled breath to No-HCC (Hepatocellular) and/or hepatic encephalopathy (HE) [31].

On the other hand, there are a few challenges involved in breath sampling to have reproducible results. The breath sample is humid and transitory. No one has done any studies on how long the breath sample can be kept under certain conditions to obtain good results. In addition to that, the exhaled breath sample is not homogenous a sample. Therefore, the challenge of segregation and collection of alveolar from dead space (a portion of breath volume contained in the upper airways) has to be tackled. The 'alveolar' air can be defined as the air from the deeper expiration where the equilibrium happens between lungs and blood. This produces a maximum concentration of endogenous VOCs in the exhaled breath. In order to achieve the alveolar phase for clinical purposes such as

monitoring, diagnosis, and screening, a standard breath protocol is needed. For this purpose, CO₂ levels can be monitored during breath sampling.

Therefore, to meet the challenges, PTR-MS has been used as an analytical instrument to detect VOCs from breath for the last 20 years. Recently, most of the universities and research centres have used PTR-MS for their breath analysis research work.

3.1.1 Breath composition

The volatile compounds in the exhaled breath can be categorized into two groups, exogenous and endogenous. The human body naturally produces some VOCs in breath based on common metabolism and daily activities and also food intake. Some of the VOCs in the exhaled breath originate from current or previous environmental exposure (exogenous compounds).

Diet and drug intake can be considered as exogenous compounds. Benzene and acetonitrile are also considered as exogenous compounds which have been found in higher concentrations in the exhaled breath from smokers compared to non-smokers. Allicin (an odourless compound in garlic) can be turned into organosulphides by crushed or cutting the garlic [39]. Some obvious compounds were found in the breath of people after ingesting garlic e.g. allyl methyl sulphide, diallyl sulphide, diallyl disulphide, diallyl trisulfide and dimethyl sulphide. In particular, concentrations of diallyl sulphide and allyl methyl sulphide are markedly increased as a result of metabolic processes in the body [13]. This early work demonstrated how volatiles in breath resulting from a metabolic process can be monitored as a function of time using PTR-MS, with a resolution of hundreds of millisecond.

Endogenous compounds are produced in the body by internal metabolic activities (anabolic and catabolic). For example, the most abundant VOCs from the normal breath are isoprene, acetone, methanol, ethanol, and propanol [13, 40-42]. Deficiency or excess of isoprene and acetone can be linked to certain conditions or diseases. Isoprene production is related to the isoprenoid biosynthetic pathway. Isoprene which believed to be produced from cholesterol metabolism, considered as the most abundant product of isoprenoid and found in the exhaled breath [43] [44]. Acetone is produced via ketogenesis metabolism. People who are suffering from diabetes and also people who are starving produce a high level of acetone in the breath [45]. In addition to that, there are other endogenous compounds produced due to different pathologies and diseases [44] [46]. Table 3.1 shows the class of VOCs and the example in the breath.

Table 3.1 Example of classes of Volatile Organic Compounds in the Breath taken from Mazzone in Journal of Thoracic Oncology, 2008 [47].

Class of VOC	Example	Example of Mechanisms of Production
Saturated hydrocarbons	Ethane, pentane, aldehydes	Lipid peroxidation of fatty acid components of cell membranes—triggered by reactive oxygen species
Unsaturated hydrocarbons	Isoprene	Mevalonic pathway of cholesterol synthesis
Oxygen-containing	Acetone	Decarboxilation of acetoacetate from lipolysis or lipid peroxidation
Sulphur-containing	Ethylmercaptane, dimethylsulfide	Incomplete metabolism of methionine
Nitrogen-containing	Dimethylamine, ammonia	Elevated in liver impairment and uraemia

3.2 Human Respiratory System

The primary goal of the respiratory system is the exchange of gases especially between the circulatory system and the outside atmosphere. The respiratory system is located in the upper part of body known as the thorax. It consists of the organs of the mouth, pharynx, larynx, trachea, bronchi and bronchioles, lungs, and the muscles of the respiration system (figure 3.1). Air always goes through in the upper airways (the nasal cavity, pharynx and larynx) and then to the lower airways (trachea, primary bronchi and bronchial tree). The air then goes into the small bronchioles and alveoli within the lungs.

Every branch of the bronchial is divided to terminal bronchioles which end with alveoli. There are millions of alveoli in both lungs where normally the exchange of gases take place. There are two types of gas respiration involved in a respiratory system. The first is known as an external respiration where the gas exchange process happens between the air filling the alveoli and blood in the capillaries surrounding the alveoli walls. Internal respiration occurs in the distal respiratory tree and it includes gaseous exchange from higher concentration to a lower concentration where O_2 containing blood is transported to the peripheral tissue of the body. Thereafter, the O_2 will be absorbed by the tissues and produce CO_2 as a waste product where it will be diffused back into blood and transported out via lungs through exhalation.

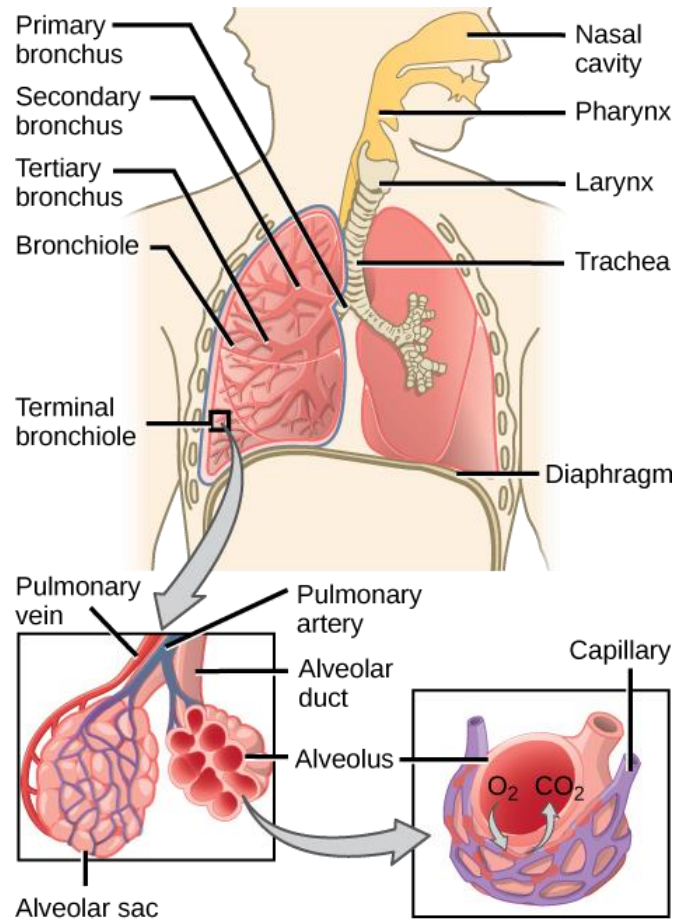


Figure 3.1 Human Respiratory System and the structure of the alveoli in the lungs Reprinted from Lumen Learning, The Respiratory System and Direct Diffusion with the permission of Lumen Learning copyright [48].

3.2.1 Gas exchange in Humans

Gas exchange is an important process in the lungs of a human body. There are two types of respiratory gases involved in a respiration system. The distribution of oxygen from the alveoli into the blood and carbon dioxide from the blood into alveoli is performed by the exhalation process. The carbon dioxide is removed via air sacs (alveoli) at the end of the bronchial tubes from exhalation and is considered as a waste metabolic product from

respiration. For example, during a person's breath in (inhalation), oxygen shifts from the alveoli to the surrounding capillaries and into the bloodstream. Meanwhile, during breath out (exhalation), carbon dioxide shifts from the bloodstream to the capillaries and into alveoli. Figure 3.2 summarizes a respiratory event. There are several processes involved for the transfer of oxygen from outside air to body by the blood flow to the lung:

1) Breathing is a process of moving the air into and out of the lungs also known as 'Ventilation'

Ventilation in breathing:

- Inhalation- air inspires into the lungs
 - Exchange of gases happen between the blood and body cells
- Exhalation- air is forced out of the lungs
 - Exchange of gases happen between the lungs and blood

Ventilation is the process where the air in and out of the lung occurs due to differences in pressure brought by the variation in the thorax volume e.g. when the air goes into the lungs, the pressure inside must be lower than the atmospheric pressure.

2) Gas transport by blood – This process happens when the oxygen is transported to the body cells and carbon dioxide will be returned as a waste product. The oxygen (98 %) will be carried in the blood by attaching to the haemoglobin which is also known as a type of protein in the red blood cells to form oxyhaemoglobin with each haemoglobin molecule binds up to four oxygen molecules.

3) Cellular Respiration- This is a process where the oxygen in the cells goes through a few processes and the final production is carbon dioxide.



Figure 3.2 The respiration process

3.2.2 Lung capacities and volumes

The total lung capacity of a normal human being is usually 6-7 litres. Figure 3.3 shows the lung volumes and their measurement. The lung capacities can be categorized to several volumes:

- i) Tidal volume (TV or V_T)
- ii) Expiratory volume (ERV)
- iii) Residual volume (RV)
- iv) Inspiratory volume (IRV)

During normal respiration, about 0.5 L of air is taken in and it is defined as the resting tidal volume (TV or V_T). Meanwhile, the inspiration volume can be expanded by an additional 3 L which is known as an inspiratory reserve volume (IRV). Furthermore,

expiration can be expanded by approximately 1.7 L more on forced (maximum) expiration. This volume is defined as the expiratory reserve volume (ERV) [49]. Normally, this reserve volume will be used during physical exercise or when normal tidal volume is insufficient. Residual volume (RV) is the volume (1.3 L) which remains in the lungs after the forced expiration. Lung capacity can be defined as the sum of the individual lung volumes. Besides that, the vital capacity (VC) is the maximum volume of air which can be carried in and out in a single breath. Consequently, the $VC = V_T + IRV + ERV$ [49]. The VC decreases as the RV increases with age (1.5 L to 3L). Therefore, the total lung capacity is 6 to 7 L (VC and RV) and the functional residual capacity is the total of ERV and RV (figure 3.3). A Spirometer is used to measure the total ventilation per unit time, O_2 consumption and dynamic function tests. For a normal variation, the normal range of lung volumes and capacities depend on age, height, physical condition and sex. For example, the range of normal variation of VC is 2.5 to 7 L.

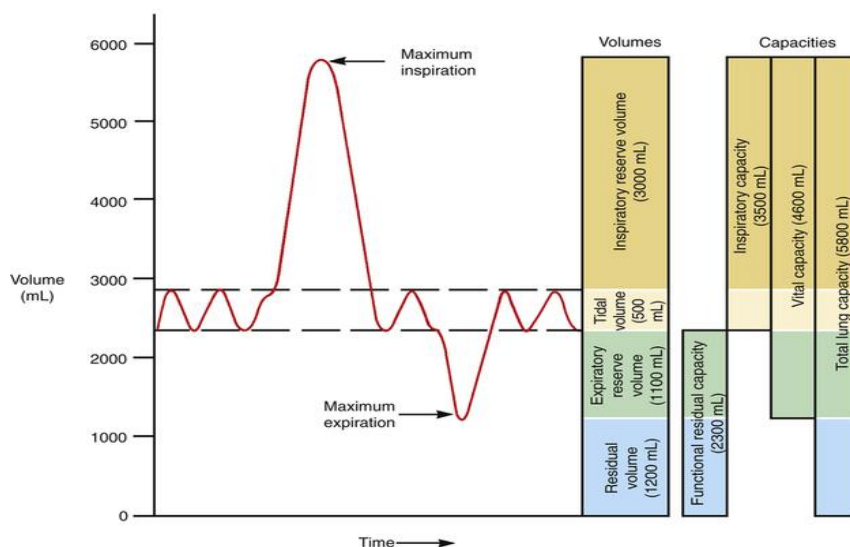


Figure 3.3 Lung volumes and their measurement. Reprinted from <https://clinicalgate.com/mechanics-of-ventilation> [50].

3.3 Methods of Alveolar Breath Sampling collection

Mixed expiratory breath samples were collected either by using Tedlar bags, Tenax Tubes or Polypropylene by some research groups [51-53]. One of the most obvious problems faced by researchers involves mixed expired air in the breath which includes the dead space air. It is complex to control a portion of the dead space air, especially when it varies from individual to individual. It also varies within individuals and depends on how strong and deep the inhalation is before giving the sample.

A number of studies were done using various breath sampling procedures to measure VOCs from breath which have been exhaled [54]. Some groups collected late expiratory breath samples using Tedlar bags for their studies [54-56]. This method has improved the breath sampling protocol by discarding the first portion of dead space and maximizes the contribution of endogenous compounds [54, 57]. In this work, only the end of breath sample is used to avoid a mixed air sample.

Meanwhile, other research groups have used end tidal or alveolar breath using either Tenax tubes or Tedlar bags [58, 59]. Alveolar breath contains high concentrations of endogenous VOCs and least contamination. However, it could mislead the result by giving an incorrect alveolar concentration because the VOCs exchange may be happening with the airways as mentioned by Anderson et al., [60, 61].

O'Hara et al., have developed a simple breath sampling protocol using a rebreathing method which enables mixed air breath to be measured that is reliable and reproducible [62]. Besides that, this method would provide equilibrium between any bag or canister (container), the airways and bloodstream [54].

Anyhow, there will be condensation which would affect the stability of VOCs and this approach is not applicable for clinical studies. Despite the large number of studies, no standardised protocol for breath sample collection has been adopted [63].

3.4 Glass syringes and other consumables for breath sampling

O'Hara et al., used Tedlar bags (5 L), with 22 mm outer diameter, 10 mm inner diameter and polypropylene EAF fitting (SKC, USA) to develop their initial rebreathing protocol to determine the dependence of concentration of VOCs in the breath with the number of re-breaths and also to compare isoprene, acetone and methanol concentration in single mixed expired breaths [62]. However, Tedlar bags are costly (approx. £55 each), they are difficult to sterilize, they are not reusable and long-time storage of VOCs is not possible, and there is contribution contaminant to the end result [62, 64]. In order to avoid all these problems, Teflon bags were used (5 L, Welch Fluorocarbon, NH, USA) for her measurement on endogenous VOCs in breath of healthy volunteers which does not emit any contaminants [65].

The main reasons for an optimization of the protocol are: i) there is a great difference in breath sampling because of the widespread of breath analysis techniques ii) potentially there are extensive variety of compounds presents in the breath iii) to avoid the big discrepancy in breath patterns in the analytical instrument, iv) to minimize the confounding factors [66]. A few groups have suggested a number of techniques to improve the method of breath sampling [66-68]. Figure 3.4 shows the standard work flow of breath analysis which summarizes breath sampling protocols.

For a standardized breath protocol especially for sampling, Fortuna® Optima glass syringe (100 ml, Sigma Aldrich) is recommended to use because it is easy to clean and decontaminate (sterilization) via autoclave and it is also re-usable (figure 3.5). Fernandez del Rio et al., have introduced an improved breath collection technique based on Rostock group's work, which uses 100 ml glass syringes to take breath samples by monitoring the alveolar breath using a capnography equipment (CO₂ controlled) to

maximise VOC concentrations. The syringe is connected to the capnograph before breath sample collection. By using this improved method, biomarkers have been found for liver associated diseases from comparisons to pre- and post-liver transplant breath samples [2]. These studies have proved that using CO₂ controlled end exhaled sampling using capnography can be practiced as a standard protocol in Breath Research [69].

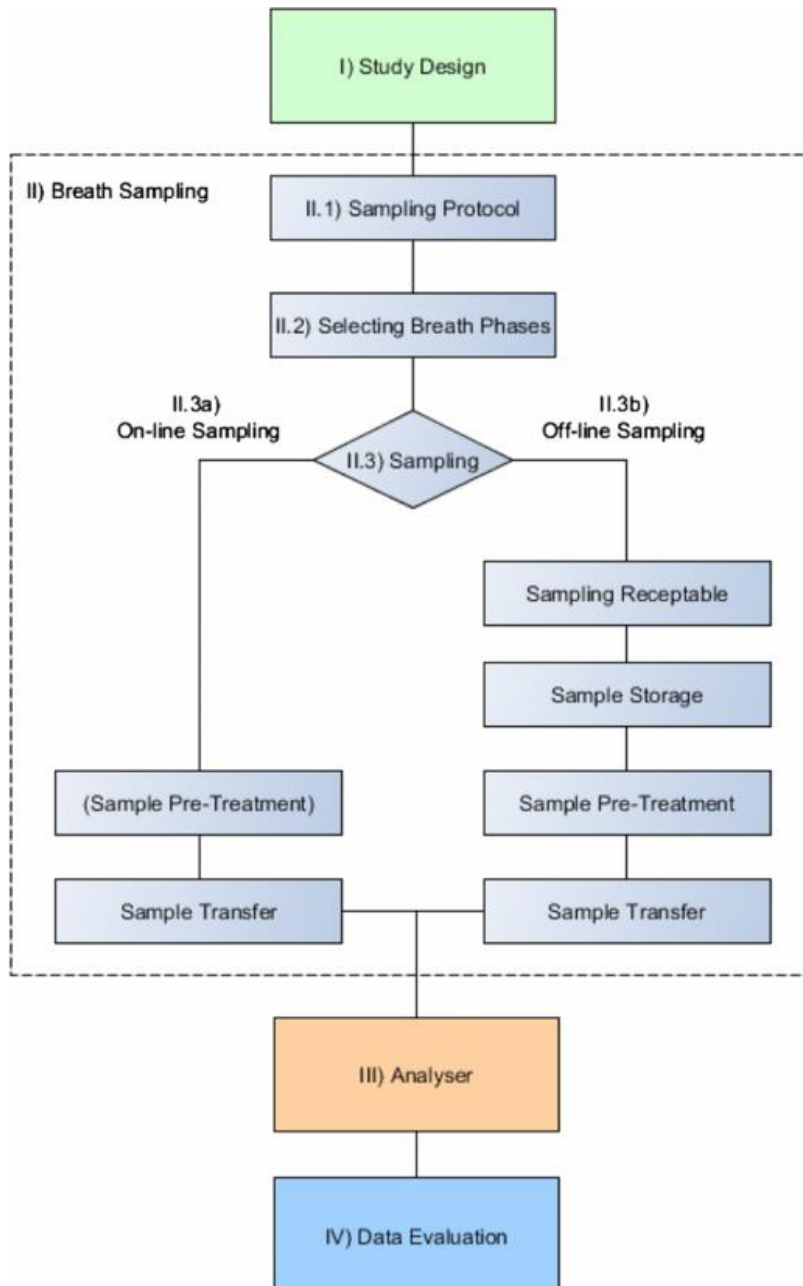


Figure 3.4 Workflow of steps in a breath analysis study, Reprinted with permission from the Journal of Breath research, 2014 [66].

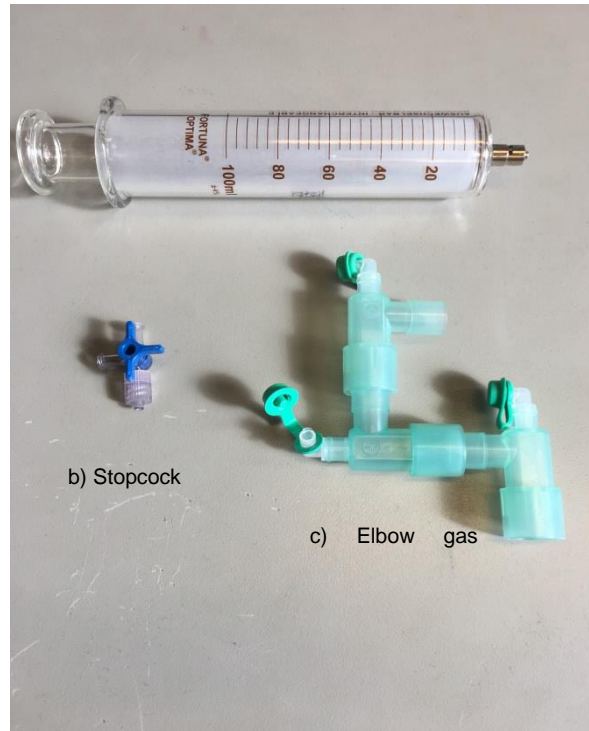


Figure 3.5 Photograph of a) Fortuna® Optima glass syringe (Sigma Aldrich) b) B-braun stopcock and c) Elbow gas sampling port (Intersurgical complete respiratory system)

3.5 Capnometry (Capnography) for alveolar breath sampling

In breath sampling, there is a portion of the exhaled breath which is not involved in gas exchange known as dead space. In a standardized breath analysis protocol, a capnograph is used to monitor the exhaled breath non-invasively. The display and waveform of CO₂ on a capnometer monitor is defined as capnography [70]. In order to establish alveolar breath sampling, a capnometer, equipped with an airway adapter, reference cell and capnostat (figure 3.6), is used to determine when end tidal breathing has been reached. Capnography provides information about CO₂ production, pulmonary perfusion, alveolar ventilation, respiratory patterns, and elimination of CO₂. Capnography also measures partial pressure (unit as a percentage or in units of mmHg) of carbon dioxide in exhaled breath. It is usually used in the clinical field especially in ITU (Intensive care unit) and in

the operating theatre by the anaesthetist to monitor the patient's breathing. This practise has been adopted to standardize the breathing protocol to measure the CO₂ end tidal by using a capnometer. It is easy to monitor the CO₂ concentration via a capnogram during the respiratory cycle. The measured CO₂ at the airway either can be presented as a function of time (concentration over time) or exhaled tidal volume (CO₂ concentration over volume).



Figure 3.6 Photograph of Capnometer a) capnograph b) airway adapter c) reference cell d) capnostat.

The basic principle of the capnometer is based on absorption of infrared (IR) radiation at a very specific wavelength (4.26 μm) which matches a vibrational mode of the infra-red active CO₂ molecule [70]. This occurs when the CO₂ breath concentration has reached the plateau where there is maximum CO₂ concentration [71]. The Beer Lambert Law (equation 2.30) [72] is used:

$$I = I_0 e^{-\epsilon bc} \quad 2.30$$

where I is the infrared intensity, b is the path length of the sample region and c is the concentration of the compound, and ϵ is the molar absorptivity. The average EtCO₂ (End tidal capnography) is approximately from 35 to 42 mm Hg or 5 % to 6 % CO₂ [70].

A Reference cell is used to calibrate the capnometer before sampling the breath to set up the sampling operation and error threshold. Figure 3.7 shows an example of capnogram (breath profile) recorded during the breath sampling from a volunteer.



Figure 3.7 Breath profile of a volunteer using a Capnograph 1265 from Novametric Medical Systems, INC (Wallingford, USA) CO₂ plateau.

3.6 Exhaled breath sampling protocol

Breath samples from the volunteers were sampled using a portable capnometer as described in the protocol of section 3.6. Figure 3.7 represents a breath sampling system where a syringe is connected to the respiratory apparatus tubing using a 3-way luer-lock stopcock (Braun Medical Limited) with a respiratory collection system. Breath samples were only collected using syringes when the capnograph showed that the alveolar phase of the exhaled breath had been achieved (figure 3.8). Usually, for the breath analysis, typically 3-4 breath samples (replicates) were collected using separate 100 ml syringes to increase the accuracy and decrease the statistical error. Besides that, the extra samples were useful to check the repeatability. Prior to measurements, the breath samples from the volunteer were placed in an incubator for 10-15 min at 37 - 40°C to reduce condensation.

The capnograph of a volunteer can be observed on the screen on the capnometer (figure 3.8). Figure 3.10 shows a volunteer giving his breath sample sitting down in a relaxed state. The volunteer was requested to breathe normally without any extra force using a gas tight respiratory system. The respiratory system which has an inline CO₂ mainstream sensor was connected to a fast-time response capnometer.

As described earlier, a capnometer is used to determine when the end tidal part of the breath has been reached. For each 100 ml glass syringe, 3 to 4 end tidal breaths were taken. The withdrawal of the breath samples from the volunteer are done manually into the syringe.

The background air of the specific location (e.g. the School of Sports Science and Exercise or Brain Imaging Centre, University Hospital Birmingham) of the breath sampling was also taken to check for background contamination. The collected breath samples were placed on an adjustable table located near to PTR-MS. The breath sample which were sealed with a 3-way stopcock connector (2 female luer locks) were connected to the PTR-MS inlet using a 4 inch Swagelok adapter (figure 3.10 and figure 3.11). The samples were covered with a heated blanket maintained at 45 °C to maintain the humidity during the measurement (figure 3.12).

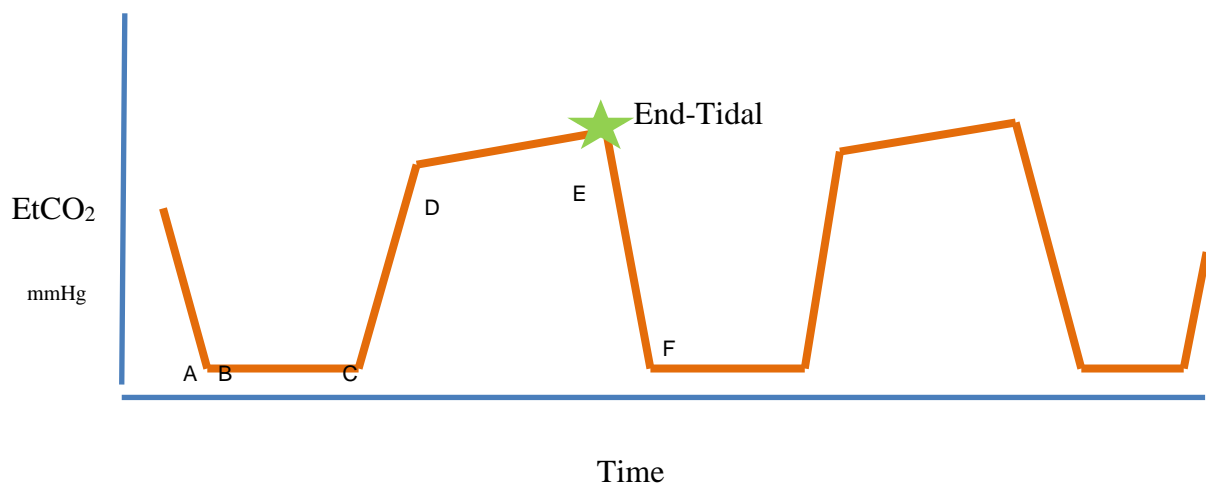


Figure 3.8 Normal breath profile.

- 1) A–B demonstrates the exhalation of the dead space
- 2) B–C represents lower airway exhalation
- 3) C–D represents alveolar exhalation, as measured from the lips or nostril
- 4) D–E represents expiration
- 5) ★ End Tidal
- 6) E–F inspiration

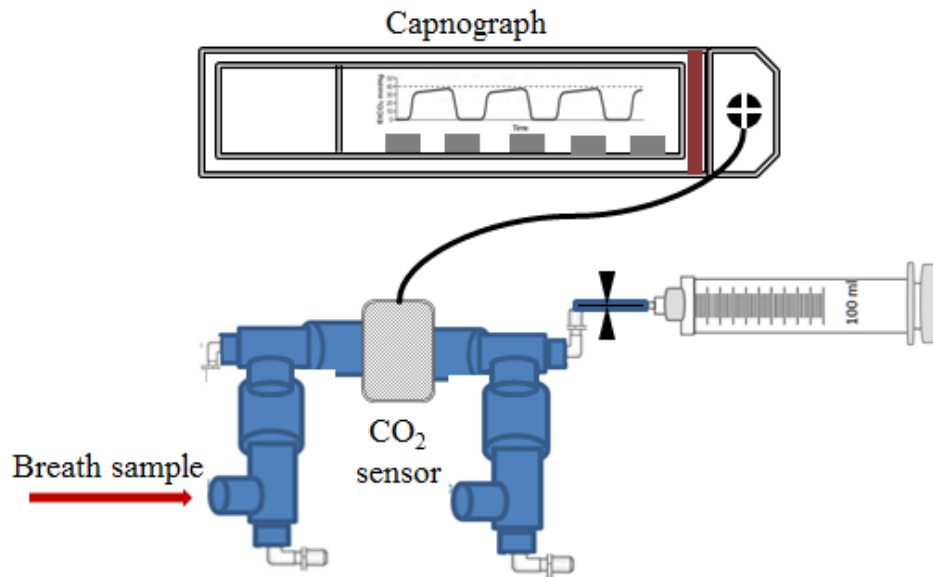


Figure 3.9 Schematic diagram of a breath sampling system. The diagram is reprinted from a figure given by Fernández del Río et al. in the Journal of EBioMedicine [2].

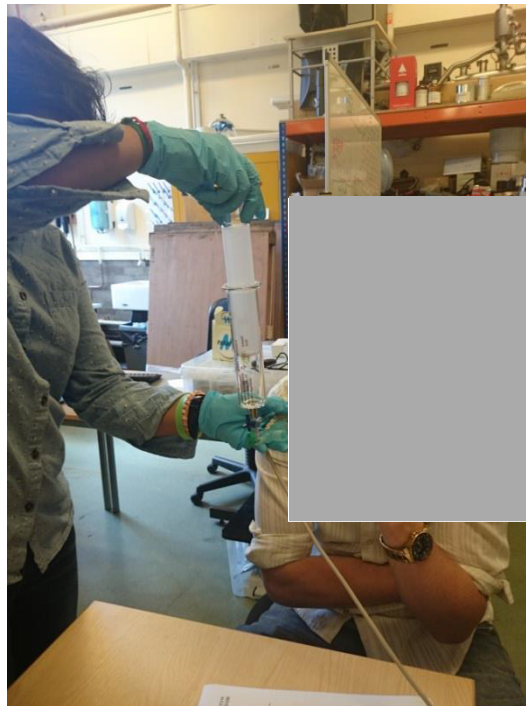


Figure 3.10 A healthy volunteer giving a breath sample. The syringe is coupled with a luer lock and elbow sampling gas port.



Figure 3.11 Photograph show the glass syringe attached to the PTR-MS inlet using Swagelok.



Figure 3.12 Heating blanket and plastic cover used to maintain the humidity of the breath sample.

CHAPTER 4

4 VOLATILE ORGANIC COMPOUNDS ASSOCIATED WITH SHISHA PASTE AND SHISHA SMOKING

4.1 Introduction

Chapter 4 provides details on the first PTR-MS study of shisha smoking, which won the best poster award at the Breath Research Conference in Zürich 2016.

Shisha smoking, also known as hookah, narghile, water pipe, hubble bubble, or ghoza social activity, has increased sharply in the Middle East and Asia [73-77], and has spread rapidly to Europe and the United States, becoming either an alternative or an addition to conventional cigarette smoking. For an example, in a 2008 cross sectional study among the student population at the University of Birmingham in the UK, 37.9% had tried Shisha smoking. Among them, 8.0% claimed to be regular shisha smokers, comparable to the 9.4% of students who claimed to be regular cigarette smokers [77]. This perhaps suggests that young adults are being influenced by the fashionable and social Shisha water pipe smoking. Certainly many more Shisha bars have opened in the UK since 2008 to supply the demand for shisha smoking.

It is well accepted that tobacco smoking causes many serious diseases resulting in significant health problems. It is therefore troubling that shisha smoking is considered to be socially acceptable. Disturbingly there is evidence to suggest that many smokers perceive that smoking shisha is less harmful to health compared with conventional cigarettes [78]. In a study by Jackson et al. [77], it was found that nearly all regular waterpipe smokers considered it to be less harmful than smoking cigarettes. It is possibly this erroneous belief that has given rise to the recent surge in the use of water pipe. This

is of concern owing to the major health effects associated with any form of tobacco smoking. Importantly, given the social nature of shisha smoking, participants are exposed to smoke for longer periods than they would be for cigarette smoking, and inhale larger quantities of smoke and hence harmful compounds than they would in comparison to smoking a cigarette.

A typical Shisha water pipe consists of a clay head, metal body, a glass bottle filled with liquid (such as water), and a flexible connecting hose with a mouthpiece (figure 4.1). Shisha smoking involves burning tobacco and molasses (Shisha paste) with the aid of charcoal. Typically 10-20 grams is encased in aluminium foil within which a few small holes has been made. The encased Shisha paste is placed in the head and burnt in a session of smoking [79]. A few pellets of charcoal are placed on top of the foil [80]. In the Shisha water pipe, tobacco undergoes a process of volatilization as it burns. Some researchers have claimed that using aluminium foil leads to less smoke with no odours, no ash fumes and a smoother smoke [81]. The burning produces tar, nicotine and carbon monoxide amongst other combustion products and two times more nicotine than that from smoking a single cigarette [82].

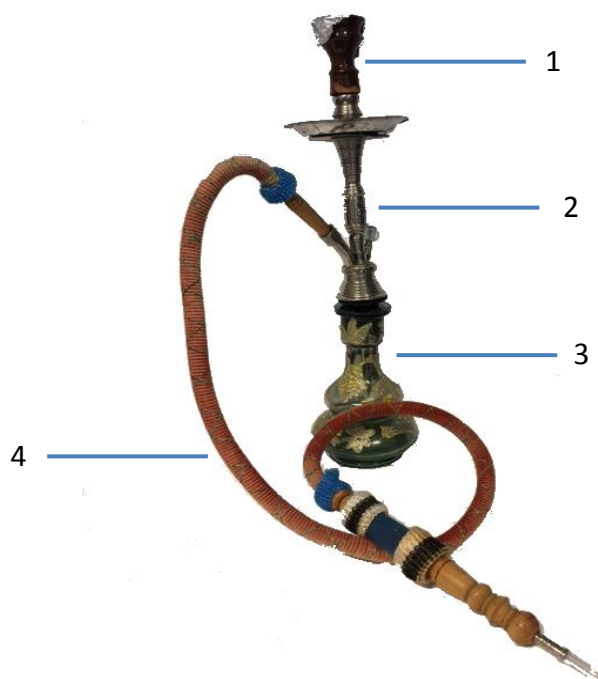


Figure 4.1 “Shisha” . 1) Clay pot for tobacco, 2) Pipe stem connecting to the water container, 3) Water bowl, 4) Hose which connected to the mouth piece.

It has been calculated that during a smoking session, a smoker inhales shisha smoke for periods of approximately anywhere between 20 and 80 minutes [75, 83] with a typical shisha smoking session involving approximately 200 puff inhalations compared to typically 20 puffs occurring during the smoking of a conventional cigarette [84]. This translates to a water pipe smoker inhaling about 90 L [85] or even more, whereas in comparison a conventional cigarette smoker inhales between 500-600 mL of smoke per cigarette [85]. Given the amount inhaled it is estimated that smoke from a smoking session of 45 minutes results in approximately 40 times more tar, 30 times more carcinogenic polycyclic aromatic hydrocarbons, 10 times more carbon monoxide and two

times more nicotine than received from smoking a single cigarette [78]. However, it is not just these compounds that are toxic. Studies using chromatography techniques have identified toxic volatiles including NO [86], formaldehyde [73], acetaldehyde [73, 86], acetone [73, 86], propionaldehyde [73, 86], benzene [87], toluene and isoprene [87].

All of these previous studies of volatiles associated with shisha have used labour intensive and time consuming offline analytical techniques. Also there are no previous studies done using PTR-MS to measure VOCs from any type of charcoal. However, there has been one study by Kabir et al., using GC-MS to investigate barbecue charcoal combustion as a potential source of aromatic volatile organic compounds and carbonyls [88]. They focused on a number of VOCs associated with the combustion, which are summarized in table 4.1, and for which concentrations in the surrounding air can be extremely high (hundreds of ppbv). The results from that investigation are used here to aid in the analysis of the volatiles resulting from the combustion of charcoal briquettes used in shisha smoking.

Table 4.1 Common VOCs emitted from burning barbecue charcoal (adapted from the work of Kabir et al, 2010 [88]).

No	Compound	Molecular weight (g mole ⁻¹)
1	Benzene	78.1
2	Toluene	92.1
3	Ethyl benzene	106
4	Meta para xylene/Ortho xylene	106
5	Styrene	104
7	Formaldehyde	30
8	Acetaldehyde	44.1
9	Acrolein	56.1
10	Acetone	58.1
11	Propionaldehyde	58.1
12	Crotonaldehyde	70.1
13	Butylaldehyde	72.1
14	Benzaldehyde	106
15	Valeraldehyde	86.1

The advantage of the instantaneous analytical capabilities of PTR-MS analytical technique described in detail in section 2.1.11.1 of Chapter 2 has been put to good use in studies of e-cigarettes by Blair *et al.* [9] and Breiev *et al* [89]. In our study, we have gone beyond e-cigarettes and present the first PTR-MS investigations of shisha. This study involves not only analyzing the volatiles coming from the combustion of the shisha paste and charcoal and through the pipe, but also for comparison an analysis of the head space of shisha paste. This can be used, for example, to check the quality and constituents of the paste, but it is used here to ascertain any differences in volatile organic compounds (VOCs) resulting from combustion to those present in the paste. The key aim of this study is to identify the VOCs, and in particular toxic ones, that would be inhaled by a smoker. This highlights the advantages of real-time measurements, namely that PTR-MS can be used for puff-by-puff shisha measurements. A weakness of the PTR-MS method is its

ambiguity in the identification of compounds in a complex chemical environment, because assignment is based solely on using m/z values of the mass spectral peaks observed. To aid in the VOC assignment, we have undertaken GC-MS measurements of the head space of shisha paste. Importantly, this study adds to the growing body of evidence showing that water pipe smoking is not a safe alternative to cigarette smoking.

4.2 Experimental Methods

4.2.1 Instrumentation

4.2.1.1 Proton Transfer Reaction – Time of Flight - Mass Spectrometry (PTR-ToF-MS)

The principles and operation of a PTR-ToF-MS have been extensively covered in this thesis in Chapter 2 and also in an in-depth review by Ellis and Mayhew [1], and hence only salient points of the instrument used for this study will be provided. For the measurements a KORE Technology Ltd. first generation instrument was used [90, 91].

The smoke coming from burning charcoal without paste using the shisha water pipe was first investigated in order to separate VOC compounds coming from the charcoal alone, but of course it is the combined VOCs in the smoke that is relevant for smokers in terms of the toxic intake. Figure 4.2 shows the Shisha smoking measurement using the fume hood and figure 4.3 shows the schematic diagram of experimental set up for sampling the headspace of shisha paste.



Figure 4.2 Shisha sampling in the fume hood.

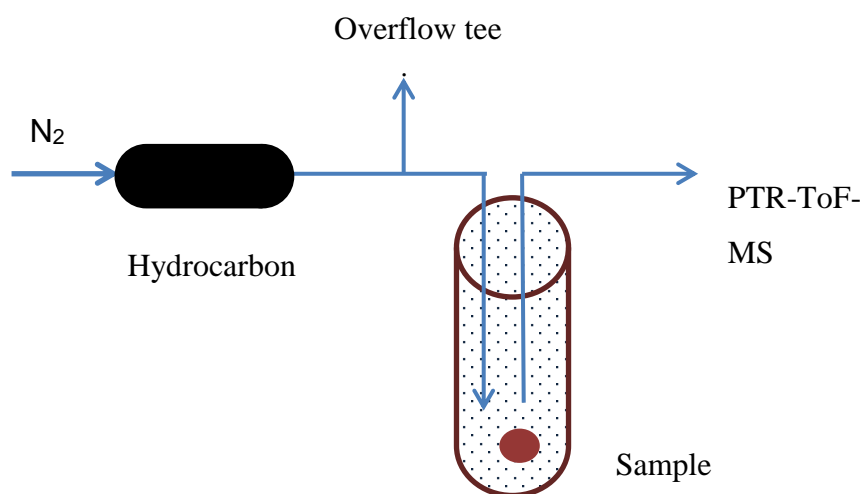


Figure 4.3 Schematic diagram of experimental set up.

To investigate the smoke coming from the water pipe we used a procedure we have used effectively for taking breath samples [2]. Smoke from the pipe was drawn into 100 ml glass syringes (Sigma Aldrich) using a 3-way luer-lock stopcock (Braun Medical Limited) at 3 minutes after the start of the burning. We noted that often ion signals were saturated when analysing the smoke directly. This indicates that the concentrations of VOCs were extremely high, and therefore to ensure we can give relative intensity values of the VOCs, it was necessary to dilute the smoke sample. In our studies, we diluted the smoke sample with clean air by a factor of ten. The luer stopcock was coupled to a Swagelok fitting and connected directly to the inlet of the PTR-ToF-MS. The syringes are gas tight and have minimal friction such that atmospheric pressure is sufficient to push the plunger in smoothly so that the smoke sample was drawn into the PTR-MS instrument with a constant flow rate. The syringes have a sufficient volume to ensure that a 60 second integration time was possible [2]. Identical but different headspace bottles and syringes were used for each flavoured paste to avoid contamination. Background mass spectral measurements of empty bottles and syringes were taken before each measurement.

4.2.1.2 GC-MS

Shortly before analysis approximately 40-70 mg ($\pm 10\%$) of a shisha sample was moved into a headspace vial (20 mL, Gerstel, Germany), which was subsequently sealed with a 1.3 mm butyl/PTFE septum (Macherey-Nagel, Germany). Next, the samples were incubated at 40°C for 30 minutes. Solid phase microextraction procedure was carried out automatically using a multipurpose sampler MPS (Gerstel, Germany) by inserting the SPME fibre coated with 75 μm CAR-PDMS (Supelco, Canada) into the vials and exposing the fibre to the sample head-space for 10 minutes. The sample temperature during the extraction was kept at 40 °C. Following the extraction, the fibre was introduced into the inlet of the gas chromatograph where VOCs were thermally desorbed at 290 °C. The fibre was conditioned at 290 °C for 5 minutes prior to each analysis.

Chromatographic analyses were performed using an Agilent 7890A/5975C GC-MS instrument (Agilent, USA). Separation of the volatiles was accomplished by using an Rt-Q-BOND column (30 m \times 0.25 mm, film thickness 8 μm , 100% divinylbenzene phase, Restek, USA) using a constant throughput of helium at a rate of 1 mL \times min⁻¹. The procedure for column temperature was as follows: increase the temperature from 60 °C to 260 °C at a rate of 5 °C minute⁻¹, and then keep the temperature constant at 260 °C for 20 minutes. The mass spectrometer worked in a SCAN mode with an associated range set from m/z 20 to m/z 200. The quadrupole mass spectrometer, ion source, and transfer line temperatures were kept at 150 °C, 230 °C, and 280 °C, respectively. The identification of compounds relied on the NIST mass spectral library matching.

4.3 Samples

4.3.1 Shisha Pastes

Commercially available flavoured shisha pastes, claimed to have been made from different types of fruits that were mixed with molasses, were purchased from shisha bars in Birmingham, UK. We restricted our investigations to some of the more popular flavoured pastes (table 4.2), namely strawberry, double apple, vanilla, and mint flavoured shisha pastes.

Table 4.2 Type of shisha paste (brand Al-Fakher, taken from the shisha paste)
A packet 5 gram.

Shisha paste	Nicotine (%)	Tar (%)
Strawberry Flavour	0.05	0.0
Double Apple Flavour	0.5	0.0
Vanilla Flavour	0.05	0.0
Mint Flavour	0.05	0.0

4.3.2 Charcoal Briquettes

The charcoal briquettes were purchased from a shisha shop in Birmingham. The make of the briquettes is Al-Fakher (a United Arab Emirates manufacturer, <http://www.alfakher.com/>). The briquettes are cylindrical with a diameter of 33 mm, a depth of 10 mm and a mass of 6.6 g. The typical burning time for these briquettes is approximately 15 minutes. Hence, during a Shisha smoking session, the charcoal is replaced several times. For the investigation of the smoke only coming from the Shisha pipe, we have recorded the intensities of the volatiles every 3 minutes for 9 minutes to ascertain changes in concentration as the charcoal is used up.

4.4 Results

4.4.1 Headspace Analyses of Shisha Pastes

Table 5.3 provides a summary of the PTR-MS analysis of the headspace of the various shisha pastes. In the following, the most intense peaks are defined as those with a relative intensity of 20 or higher.

4.4.1.1 Double Apple Shisha Paste

The most intense spectral peaks were observed at m/z 43, 61, 83, 85, 91 and 149. m/z 149 has the largest intensity (100) and, based on the GC-MS analysis, is assigned to predominantly result from protonated p-propenyl anisole with a contribution from protonated methyl chavicol (estragol). The next most intense peak is found at m/z 91 (relative intensity 40) is unassigned, m/z 83 (relative intensity of 27) results from protonated 2-methyl furan and a fragment ion from 1-hexanol. m/z 85 (relative intensity of 20) is also a product ion resulting from 1-hexanol. m/z 61 (relative intensity of 27) is from protonated acetic acid.

Other product ions observed with lower relative intensities are at m/z 33 (protonated methanol), m/z 41 (a fragment of 1-hexanol), m/z 45 (protonated acetaldehyde), m/z 57 (protonated acrolein with contribution from 1-hexanol), m/z 59 (protonated 2-methyl furan and propanal), m/z 61 (protonated acetic acid), m/z 69 (protonated isoprene and 1,3-pentadiene), m/z 75 (protonated 1-hydroxy-2-propanone), m/z 79 (unassigned, because no benzene was found in the GC-MS measurements), m/z 81 and 137 (from limonene), m/z 101 (protonated 3-Hexen-1-ol, (Z)) and from a product ion from 1-hexanol, and m/z 107 (protonated benzaldehyde).

4.4.1.2 Mint Shisha Paste

The most abundant mass spectral peaks identified from the head space of mint shisha paste are found to be at m/z 33 (protonated methanol), m/z 61 (protonated acetic acid), m/z 81 (product ions coming from limonene, menthol and menthone), m/z 83 (protonated 2-methyl furan), m/z 137 (protonated limonene and a product ion from menthone) and m/z 155 (predominantly protonated menthone). Besides these, mass spectral peaks with reasonable intensities were observed at m/z 41 and 43 (product ions from 1-hexanol), m/z 45 (protonated acetaldehyde), m/z 55 (product ion from menthol), m/z 57 (contributions from protonated acrolein, and product ions from 1-hexanol and menthol), m/z 59 (protonated acetone and propanal), m/z 69 (product ion from menthol), m/z 95 (product ion from menthone), m/z 97 and 139 (product ions from menthol), m/z 101 (protonated 3-Hexen-1-ol, (Z)-), m/z 107 (protonated benzaldehyde), m/z 129 (protonated 3-octanone), m/z 135 (protonated o-cymene) and m/z 153 (protonated 2-cyclohexen-1-one, 3 methyl-6(1-methylethyl)-).

4.4.1.3 Strawberry Shisha paste

The most intense product ions for strawberry shisha paste were observed at m/z 43 (unassigned), m/z 45 (acetaldehyde and a product ion from ethanol), m/z 47 (protonated ethanol), m/z 59 (protonated acetone, propanal and oxirane, methyl-, (S)), m/z 83 (protonated 2,4-hexadiene) and m/z 89 (protonated butanoic acid and ethyl acetate). Other product ions are observed at m/z 33 (protonated methanol), m/z 41 (unassigned), m/z 57 (protonated acrolein), m/z 61 (protonated acetic acid), m/z 71 (product ion from butanoic acid), m/z 75 (protonated hydroxy-2-propanone (acetol)), m/z 79 (protonated benzene), m/z 87 (protonated 2,3-butanedione), m/z 91 (unassigned), m/z 99 (unassigned), m/z 101

(protonated 3-Hexen-1-ol, (Z)-), m/z 103 (protonated methyl isobutyrate), m/z 107 (protonated benzaldehyde) and m/z 117 (protonated 1,3-dioxolane, 2,2,4-trimethyl-).

4.4.1.4 Vanilla Shisha Paste

From the vanilla flavoured Shisha paste, the most dominant peak is at m/z 59, which is predominantly protonated propanal with a contribution from oxirane, methyl-, (S). The second most intense mass spectral peak is at m/z 89 which is assigned to be protonated ethyl acetate. Other dominant peaks are at m/z 43 (unassigned), m/z 45 (protonated acetaldehyde with a contribution from a product ion associated with ethanol), m/z 71 (unassigned), and m/z 87 (protonated 2, 3-butanedione with a contribution from protonated butyrolactone). Less intense peaks were found at m/z 33 (protonated methanol), m/z 41 (unassigned), m/z 47 (protonated ethanol), m/z 57 (protonated acrolein), m/z 61 (protonated acetic acid), m/z 73 (unassigned), m/z 75 (protonated 2-Propanone, 1-hydroxy-), m/z 77 (protonated propylene glycol) and m/z 107 (protonated benzaldehyde). We found no evidence of the use of vanillin as a flavour compound in the shisha paste.

Table 4.3 m/z of product ions resulting from the reaction of H_3O^+ with the headspace of various shisha pastes using PTR- MS at 120 Td and possible VOC identification based on m/z of product ions and a GC-MS analysis of the shisha pastes.

m/z (product ion)	VOC Compound	Relative intensity (%)
Double apple flavour		
33	methanol	10
41	1-hexanol (fragment)	12
43	1-hexanol (fragment)	43
45	acetaldehyde	3
57	acrolein or 1-hexenol (fragment)	11
59	oxirane, methyl-, (S)-/propanal	19
61	acetic acid	27
69	isoprene/1,3-pentadiene, (E)-/1,3-pentadiene, (Z)-	2
75	2-Propanone, 1-hydroxy-	5
79	unassigned	10
81	limonene	2
83	furan, 2-methyl-/1-hexanol fragments	27
85	1-hexanol	20
91	unassigned	40
101	3-Hexen-1-ol, (Z)-	1
107	benzaldehyde	3
137	limonene	3
149	anisole, p-propenyl	100
Mint flavour		
33	methanol	55
41	1-hexanol (fragment)	3
43	1-hexanol (fragment)	18
45	acetaldehyde	3
55	menthol (fragment)	15
57	acrolein and menthol (fragment)	13
59	acetone/propanal	11
61	acetic acid	24
69	menthol (fragment)	5
81	limonene, and menthol and menthone (fragments)	47
83	furan, 2-methyl-	36
95	menthone (fragment)	10
97	menthol (fragment)	5
101	3-Hexen-1-ol, (Z)-	1
107	benzaldehyde	1
129	3-octanone	1
135	o-Cymene	1
137	limonene and menthone (fragment)	37
139	menthol (fragment)	12
151	menthofuran	3
153	2-Cyclohexen-1-one, 3-methyl-6-(1-methylethyl)-	13
155	menthone	100
Strawberry flavour		
33	methanol	19
41	unassigned	17
43	unassigned	28
45	acetaldehyde and product ion from ethanol	59
47	ethanol	87
57	acrolein	3
59	propanal/acetone/oxirane, methyl-, (S)-	100
61	acetic acid	8
71	butanoic acid fragment	15
75	2-propanone, 1-hydroxy-	4
79	benzene	2
83	2,4-hexadiene	25
87	2,3-butanedione	3
89	ethyl acetate/butanoic acid	51
91	unassigned	7
99	unassigned	4
101	3-Hexen-1-ol, (Z)-	2
103	methyl isobutyrate	3
107	benzaldehyde	1

117	1,3-dioxolane, 2,2,4-trimethyl-	18
Vanilla Flavour		
33	methanol	8
41	unassigned	7
43	unassigned	52
45	acetaldehyde and product ion from ethanol	32
47	ethanol	13
57	acrolein (2-Propenal)	1
59	propanal/oxirane, methyl-, (S)-	100
61	acetic acid	1
71	unassigned	49
73	unassigned	1
75	2-Propanone, 1-hydroxy-	3
77	propylene glycol	3
87	butyrolactone/2,3-butanedione	53
89	ethyl acetate	90
107	benzaldehyde	1

4.5 VOCs in mainstream smoke

Figure 4.4 presents the mass spectrum of the VOCs from headspace of charcoal recorded whilst operating the drift tube at 120 Td. Figure 4.5 shows VOCS coming from the charcoal after exiting the shisha pipe after 3, 6 and 9 minutes of combustion. There appears to be no direct correlation of intensities with time. This could be the result of the shisha charcoal being not fully or evenly burned during the headspace sampling.

Table 4.4 summarises the VOCs that were found in the smoke from a water pipe using a single pellet of charcoal without shisha being present. Assignment of the compounds is based on the m/z values of the product ions and using the results of a GC-FID study of the volatiles emitted from burning barbecue charcoal by Kabir *et al.* [88]. The most intense mass spectral peaks associated with the smoke from just burning charcoal using the water pipe are at m/z 43, 57, 79 and 93, assigned to be protonated propene, acrolein, benzene and toluene, respectively, with that associated with benzene being the most dominant. Less intense spectral peaks are observed at m/z 31 (protonated formaldehyde), 33 (protonated methanol), 42 (protonated acetonitrile), 45 (protonated acetaldehyde), 59 (protonated acetone and propionaldehyde), 61 (protonated acetic acid), 69 (protonated isoprene or furan), 71 (protonated crotonaldehyde), 73 (protonated butylaldehyde), 85 (protonated pentanal), 87 (protonated valeraldehyde), 97 (protonated furfural), 101 (protonated 2,3-pentadione), 107 (protonated benzaldehyde).

With the shisha paste the volatiles observed are identical to those obtained from the head space analysis and from the burning charcoal, with benzene being the most dominant compound, with the exception of strawberry, for which the most intense peak is observed at m/z 59. There are however some differences. For double apple additional peaks are observed at m/z 47 (protonated formic acid), 95 (protonated phenol), 103

(unassigned). For mint additional peaks were observed at m/z 47, 75 (protonated 2-Propanone, 1-hydroxy-), and 149 (protonated benzene, 1-methoxy-4-(1-)). For strawberry, two additional peaks are observed at m/z 47 and 77 (protonated propanoic acid).

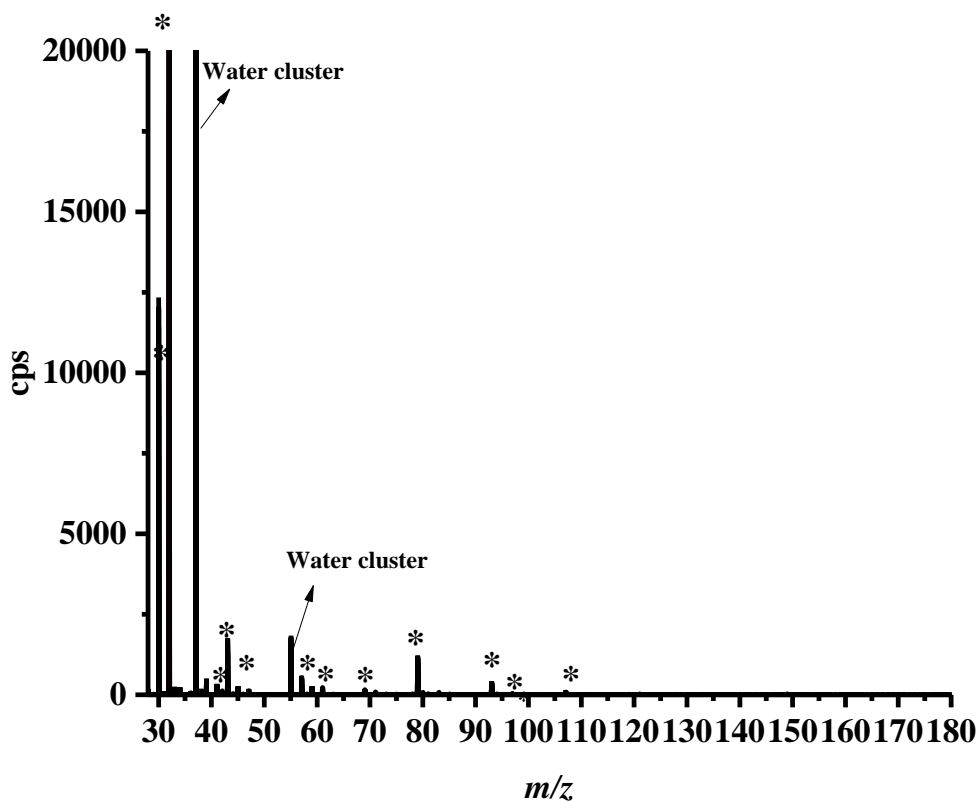


Figure 4.4 A mass spectrum illustrating the product ions (starred) resulting from the reaction of H_3O^+ whilst operating the drift tube at a reduced electric field of 120 Td.

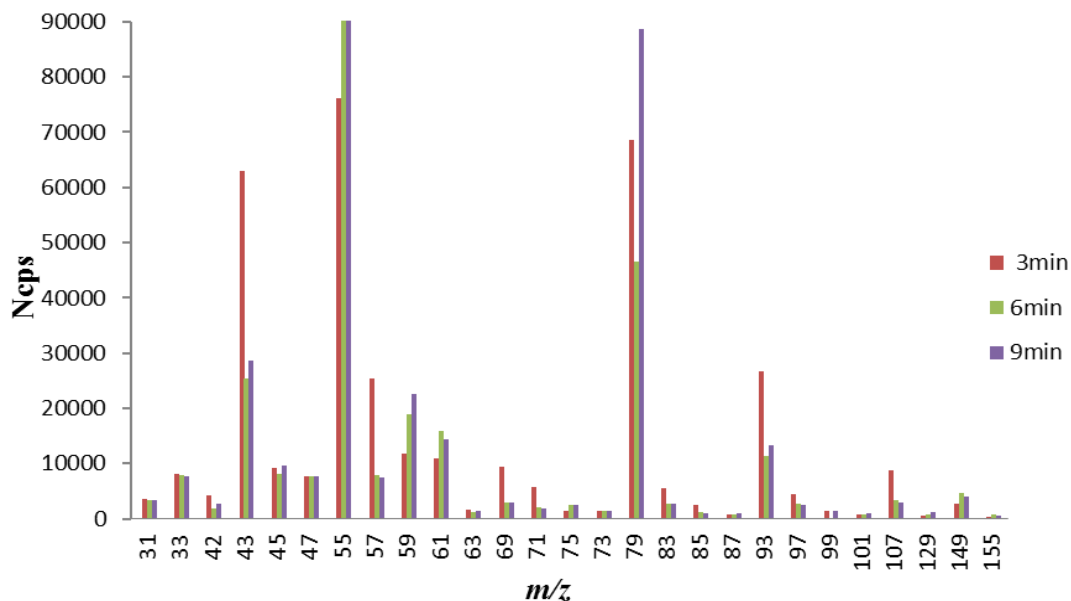


Figure 4.5 Shows VOCS from headspace of charcoal via shisha pipe.

Table 4.4 Assignments of VOCs emitted from burning charcoal after exiting a shisha water pipe.

<i>m/z</i> (protonated ion)	Assignments (based on <i>m/z</i> values and GC-MS)	Relative intensity (%)
Charcoal only		
31	formaldehyde	5
33	methanol	12
42	acetonitrile	6
43	propene	92
45	acetaldehyde	14
57	acrolein/hexenal fragments	37
59	acetone/ propionaldehyde	17
61	acetic acid	16
69	isoprene /furan	14
71	crotonaldehyde	8
73	butylaldehyde	2
79	benzene	100
85	pentanal	4
87	valeraldehyde	1
93	toluene	39
97	furfural	6
101	2,3-pentadione	1
107	benzaldehyde/meta para xylene/ortho xylene/Ethyl benzene	13

4.6. Discussion

4.6.1 Key Findings

In our study with double apple, a key compound identified anisole, p-propenyl also known as anethole. This is obviously used because it is an aromatic compound which is related to unsaturated ether and it is strongly linked with lignols. It has been used as flavouring substance to give a sweet flavour, because it is 13 times sweeter than sugar [92].

Among these compounds, 1-hexenol is one of the alcohol compounds which have given a significant contribution to double apple shisha paste. 1-hexenol has an odour of fresh grass and is widely used in the perfume industry. It can cause irritation of the eyes and respiratory tract and possible [95].

Acrolein (m/z 57) is another toxic compound found in this study. It is an unsaturated aldehyde and this has been used widely as a biocide and also as a building blocker for other chemicals. It is a well known toxin which is strongly associated with skin, eyes, nasal passages [93] and has an impact on increasing the risk of cancer [94]. Another toxic compound is acetic acid. The concentrated acetic compound would potentially cause eye, nose and throat irritation if exposed to a prolong inhalation.

For mint shisha paste, there were compounds corresponded to mint flavour detected. There were similar compounds as Saint et al., detected in our study too. For example, m/z 55, m/z 81, m/z 83, m/z 137, m/z 139 and m/z 155 were found as menthol fragments. Besides that, there were some menthone fragment ions found such as m/z 81, m/z 95, m/z 137 and m/z 155. Also there was some contribution from monoterpenes (m/z 137 and m/z 81) which are related to limonene. We are uncertain about the type of mint used to prepare mint shisha paste and it is very difficult to confirm this because it indicated only an overall mint note intensity.

Some of the compounds are not really harmful if they are used carefully and safely. However, some “safe” compounds can still be toxic if exposed to them for too long or too frequently. For instance, one main compound in this study menthone has significant human health effects if exposed to large concentrations, according to Toxicology Data Network report [28], According to the report, over exposure to menthone causes ataxia, confusion, coma, nausea, and vomiting [95].

Methanol is also one of the significant compounds found in the mint shisha paste which is far more toxic than menthone and can cause blindness if more than 10 mL is taken. 30 mL, can lead to death [96]. Another “safe” compound found in mint shisha is 1-hexenol which has a reasonable contribution to mint shisha paste where the possible side effects already have been explained.

This study confirms that mint shisha paste is associated with menthol and menthone. Hence, this study also shows that there were additional chemicals used to prepare the mint shisha paste.

The key compounds from the strawberry are propanal, acetone and oxirane, methyl-, (S)-. Propanal also known as propionaldehyde and it has a fruity odour. It is widely used in manufacturing of plastics [97]. There is no evidence on acute effects and chronic effects. However, it has some health effects such as eye, nose, skin and throat irritation and also pulmonary edema if overexposed [97]. Meanwhile, acetone is a ketone compound and mainly use for laboratory purposes. There is no strong evidence on chronic health effects of acetone if safety precautions are taken [98]. Generally, exposure to acetone could cause skin and eye irritation, while severe exposure could cause unconsciousness and potentially can be harmful to the nervous system [98]. Acetone also could lead to hepatotoxic effects which can damage the liver [97]. Oxirane, methyl-, (S)-

, also another source of toxicity and the level of health effect depends on the concentration and period of exposure and it may cause cancer (Carcinogenic) [97].

Also, the contribution from ethanol is also relatively high from strawberry shisha paste. High concentration of ethanol is a risk for health and eventually long term usage would cause liver damage [99]. Strawberry shisha paste also has high concentration of acetaldehyde. It is toxic and carcinogenic in humans [100].

There was no vanillin (protonated m/z 153) compound or any fragment ions of vanillin compound found from the headspace of vanilla flavour Shisha paste in our studies [101].

The most obvious compounds from vanilla shisha paste were propanal and oxirane, methyl-, (S)-, where the possible health effects have already been discussed in earlier discussion. In addition to that, we also already discussed about toxicity of methanol, acetaldehyde, propanal, ethanol and acrolein in the previous shisha paste discussion which can be associated with similar compounds found from the vanilla shisha paste.

4.6.2 VOCs from combustion of shisha paste and charcoal

There were many VOCs produced from the combustion of the combination of shisha paste and charcoal. The main contributions were from the burning of charcoal.

Shockingly, there were a lot of VOCs produced just from the burning charcoal itself. Kabir reported that, the main contribution from barbecue charcoal was toluene and then benzene [88]. In our study, the main contribution was from benzene, and then followed by propene and toluene. Benzene is the main source of carcinogenic which [97]. Exposure to benzene is also known as factor for leukaemia. Propene (m/z 43) is another main

compound from the burning charcoal and excess exposure and intentional inhalation of propene could damage the central nervous system which sometimes can be life threatening via asphyxiation [97]. Inhalation of toluene in the modest levels can cause lethargy, memory loss, confusion, nausea and loss of appetite [97]. The extreme inhalation level could cause a lot of side effects such as nausea and headache, and in the case of high inhalation would cause death [97]. The other intense VOCs emitted by charcoal are acrolein and hexenal. In addition to that, there were some carbonyl emissions especially formaldehyde, acetaldehyde, propionaldehyde and acetone. These carbonyl compounds potentially cause a threat to health [88] because it is an electrophilic compound which is highly toxic and which can cause skin, eye and nasal passages irritation and also possibly increase the risk of cancer [97].

The other toxic compounds coming from the combustion of charcoal are methanol, acetonitrile, acetic acid, isoprene and furan, fragments of C_{6/8} compounds benzaldehyde, meta para xylene, ortho xylene and ethyl benzene. Acetonitrile can cause acute toxicity such as cyanosis, cardiac and respiratory arrest if exposed for some period.

Another important finding for some shisha samples was that, certain VOCs were only being produced during combustion because some compounds only become volatile when a high temperature is applied.

4.7 Conclusion

The aim of the study was to analyse which VOCs are resulting from Shisha smoking. There were many VOCs from the head paste of shisha paste, conclusively identified using GC-MS and which could be identified by the mass spectral peaks observed in our PTR-MS measurements. However, a number of spectral peaks could not be assigned to any compound detected with GC-MS.

This work, as the first PTR-MS study of Shisha, has shown that many VOCs are inhaled when smoking Shisha including aldehydes, esters, ketones, acids, alcohols, C_{6/8} aromatic compounds, and esters. We also found that harmful chemicals come directly from the combustion of charcoal e.g., methanol, acetonitrile, acrolein, acetic acid or propionaldehyde, furan, propene, acetonitrile, benzene and toluene.

It is important to highlight that our samples were diluted as compared to the real shisha smoke particularly to measure the VOCs from charcoal burning and combination of shisha paste with charcoal burning in order to avoid signal saturation in the PTR-MS system, and hence no quantitative measurements of concentrations are given here. The main focus was to identify the compounds in shisha smoke.

Based on the available evidence, in a real scenario, the health effects would be expected to be more severe for shisha especially when inhaling shisha smoke directly from a shisha water pipe. A session of shisha involves many hours and it could ultimately result in a huge intake of harmful VOCs. In addition to exposure to toxicants and carcinogens, which are to be found in the smoke, by shisha smokers, non-smokers who socialize with the smokers will also inhale large quantities of these harmful volatiles through passive smoking.

Further work on shisha is needed to monitor public and occupational exposure in Shisha bars under the COSHH Regulations (Control of Substances hazardous to health regulations). This may indicate a need for guidelines to improve the ventilation in local Shisha bars. Such guidelines and regulations must be implemented to inform workers and customers of shisha bars of the effects that are potentially hazardous to human health. Nakkest et al., report that a detailed labelling system is required on the shisha paste or related accessories for health awareness of the potential risk of Shisha smoking [102].

This study suggests that, future epidemiological studies on potential diseases associated with VOCs produced by shisha smoking are required to investigate the damage caused by shisha smoking. In addition to that, investigations of shisha smokers' breath could be done using pre and post hookah smoke session to investigate the uptake of VOCs.

In summary, our research has shown that shisha pipe smoking results in the exposure to a large variety of VOCs some of which are toxic and/or carcinogenic. The findings of this study have a number of important implications to the health of shisha smokers. At the very least we have shown that shisha smoking is not risk free.

CHAPTER 5

5 INVESTIGATION OF THE PRODUCT IONS RESULTING FROM THE REACTIONS OF H_3O^+ WITH VANILLIN, MENTHOL AND ASSOCIATED COMPOUNDS (CYCLOHEXANOL, PHENOL, ANISOLE, BENZALDEHYDE AND GUAIACOL)

5.1 Introduction

This chapter is a direct follow-up from the previous one dealing with shisha. Flavour compounds are often used in shisha paste and this chapter deals with two expected flavour compounds (vanillin and menthol) in the vanilla and mint flavoured shishas. Originally this work was intended to be part of Chapter 4 to identify the product ions resulting from the reactions of H_3O^+ with vanillin ($\text{C}_8\text{H}_8\text{O}_3$) and menthol ($\text{C}_{10}\text{H}_{20}\text{O}$) and then to compare those to the shisha results. However, owing to the interesting product ions found for the two flavour compounds, we expanded the original study to include an investigation as to what happens to related compounds in the PTR-MS, namely cyclohexanol for comparison with menthol, and phenol, anisole, benzaldehyde and guaiacol for comparison with vanillin. Basically, we are systematically investigating how the proton transfer reaction changes as functional groups are changed.

Although the shisha study was undertaken at 120 Td, for completeness, we investigated the intensity of the product ions as a function of the reduced electric field (E/N) from 80 to 220 Td.

The two compounds being investigated are also of interest to food sciences owing to their common use as food flavouring. Vanillin (4-hydroxy-3 methoxybenzaldehyde) is an organic natural compound which is widely used as a common flavouring compound

in foods, drinks and fragrances [103]. It is the key compound of vanilla flavour with 1-2% in cured vanilla pods [104]. Vanillin can be extracted from vanilla beans, but the process is labour intensive and hence expensive. To reduce production costs there are a number of different biotechnical synthesis routes to produce vanillin flavoured products, which have been on the market for more than a decade. The synthesis involves different types of chemical and microorganisms' processes to produce the familiar vanilla flavour.

Menthol is also commonly used to flavour foods, but it also finds use as an active decongestant in drugs. Menthol is readily available as an extract from peppermint, mint oils and corn mint. Cigarette companies use menthol flavouring to attract young adults to smoking, in part because of the misconception by young people that smoking menthol cigarettes reduces the tar consumed and is less harmful [105], and we can assume that this follows for shisha.

To our knowledge this is the first PTR-MS study of vanillin. In comparison there have been two PTR-MS studies investigating menthol [106, 107]. The first by Saint-Eve et al. reported product ions at a fixed E/N of 140 Td. The second, by Gordon et al. present an E/N study over the range of approximately 90-140 Td involving L-menthol powder. This study goes much further in the E/N range used.

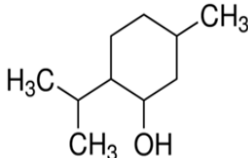
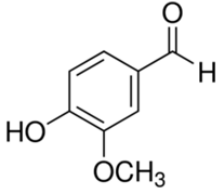
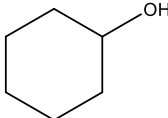
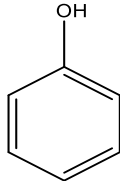
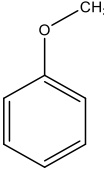
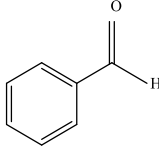
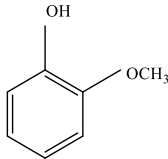
5.2 Experimental Details

Table 5.1 shows the details (Chemical formula, CAS number, vapour pressure and chemical structure) for menthol, vanillin and the associated compounds. With the exception of benzaldehyde and guaiacol, the chemicals used in this study were purchased from Sigma Aldrich (UK). Benzaldehyde and guaiacol were purchased from Alfa Aesar. All chemicals were used without further purifying.

For each compound (menthol and vanillin), 1 mg samples were placed into 20 ml glass vials. The motive of using vials is because the samples were in crystal form. The inlet of a vial containing the compound was connected to a hydrocarbon filter via a 1/8th inch peek tube and nitrogen gas was then flowed through the trap. (Nitrogen was used rather than laboratory air to avoid any possible background contamination from the environment that is not trapped by the filter.) The outlet of the vial was connected to the PTR-ToF-MS (Kore Technology, Ltd) inlet using peek and Teflon tubes (see figure 5.1). A tee piece was used to exhaust any excess gas in order to maintain a constant drift tube pressure. For the vanillin sample, the vials were wrapped with a heating tape to increase their temperature to 80 °C. This was needed because vanillin has a low vapour pressure at room temperature. The concentrations of menthol and vanillin in the drift tube were sufficiently low to ensure that there was no depletion of the reagent ion signal or pulse counting saturation. For the associate compounds, tedlar bags were filled with nitrogen gas flow using a teflon tube with similar settings.

A background mass spectrum for each reduced electric field was taken before the measurements with any compound were done, which was then subtracted from that obtained from the vial containing the sample.

Table 5.1 Information on compounds in this experiment, including vapour pressure and purity.

Molecular weight of the lightest isotopomer m/z	CAS Number, purity and company	Vapour pressure (mmHg)	Molecular structure
Menthol $C_{10}H_{20}O$ 156	89-78-1, 99 %, Sigma Aldrich	0.8 at 20 °C	
Vanillin $C_8H_8O_3$ 152	121-33-5, 99%, Sigma Aldrich	> 0.01 at 25 °C	
Cyclohexanol $C_6H_{12}O$ 100	108-93-0, 99 % Sigma Aldrich	0.657 at 25 °C	
Phenol C_6H_5OH 94	108-95-2, 99% Sigma Aldrich	0.4 at 20 °C	
Anisole C_7H_8O 108	100-66-3, 99 % Sigma Aldrich	0.47 at 25 °C	
Benzaldehyde C_7H_6O 106	100-52-7, 99 % Alfa Aesar	1 at 26 °C	
Guaiacol $C_7H_8O_2$ 124	90-05-1, 98 % Alfa Aesar	0.103 at 20 °C	

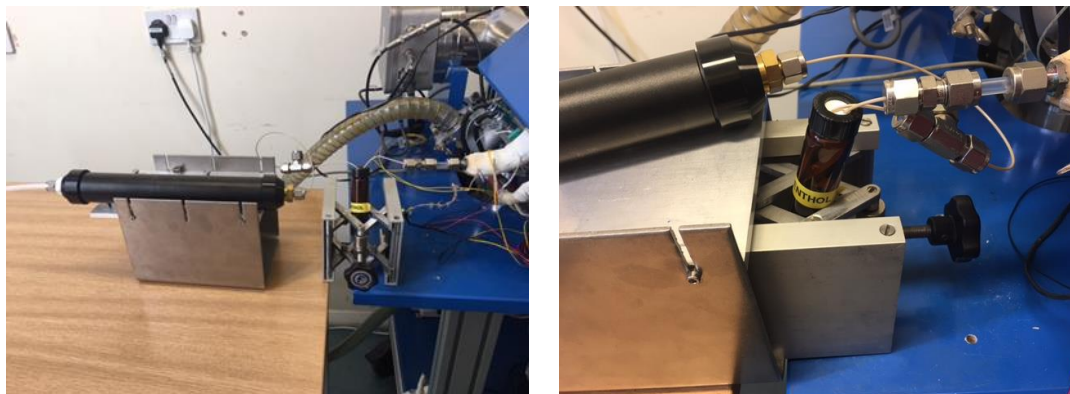


Figure 5.1 Experimental set up for headspace measurement of menthol, vanillin and associated compounds for reduced electric field studies (80 Td- 220 Td).

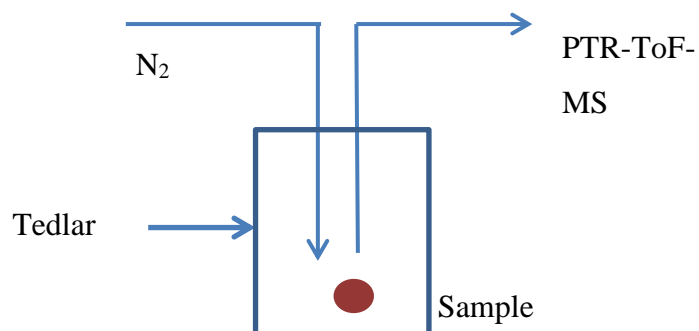


Figure 5.2 Schematic diagram of experimental set up for the associate compounds using tedlar bags.

5.3 Results and Discussion

5.3.1 Headspace of associated compounds (Cyclohexanol, Phenol, Anisole, Benzaldehyde, Guaiacol)

5.3.1.1 The reaction of cyclohexanol with H_3O^+

The proton affinity of cyclohexanol is unknown. However, in this investigation we have not only observed the protonated parent, indicating that the proton affinity of cyclohexanol is greater than water, but that the proton transfer can be non-dissociative and dissociative. This is illustrated in figure 5.3 which shows a mass spectrum resulting from the reaction of H_3O^+ with cyclohexanol at 120 Td. Table 5.2 provides the details of product ion branching ratio as a percentage for cyclohexanol also at 120 Td. Seven product ions are identified as C_4H_7^+ (m/z 55), $\text{C}_3\text{H}_5\text{O}^+$ (m/z 57), C_5H_7 (m/z 67), C_6H_9^+ (m/z 81), $\text{C}_6\text{H}_{11}^+$ (m/z 83), $\text{C}_6\text{H}_{11}\text{O}^+$ (m/z 99) and $\text{C}_6\text{H}_{13}\text{O}^+$ (m/z 101). At 120 Td, $\text{C}_6\text{H}_{11}^+$ (m/z 83) is found to be the major product ion resulting from the loss of a water molecule (H_2O) from the protonated parent. Hence, using high resolution KORE PTR-ToF-MS, it could be resulting from $\text{C}_5\text{H}_7\text{O}^+$ with loss of CH_4 and H_2 but the measured peak position was 83.086 which is close to $\text{C}_6\text{H}_{11}^+$. This agrees with a PTR-Quad-MS study reported by Brown [72]. In agreement with this Jürschik et al., observed m/z 83 as a main product ion at 130 Td [108]. At 115 Td he reported that the product ion branching ratio is 76%. In addition to this product ion, he reports $\text{C}_6\text{H}_{11}\text{O}^+$ (m/z 99) (corresponding to a loss of H_2 from the protonated parent), where we found the similar measured value of 99.08, thus no ambiguity in that assignment and C_4H_7^+ (3%) (resulting from a sequential loss of H_2O and C_2H_4 from the protonated parent) [109], where it can be also assigned as $\text{C}_3\text{H}_3\text{O}^+$ (55.02). However, the measured value was close to C_4H_7^+ . m/z 57 can be assigned as $\text{C}_3\text{H}_5\text{O}^+$ (57.034) or C_4H_9^+ (57.070) but we found that the measured mass was close to

$C_3H_5O^+$ (57.03). Meanwhile for m/z 67 ($C_5H_7^+$, 67.05), 81 (81.070) and 101 (101.096), there is no uncertainty on that assignments because their exact masses are close to the measured value.

Figure 5.4 illustrates how the product ion distributions vary as a function of the reduced electric field. m/z 83 ($C_6H_{11}^+$) is the dominant ion from 80-150 Td. Meanwhile, m/z 55 ($C_4H_7^+$) is the dominant ion from 160-220 Td. m/z 81 is only observed from 130 Td–220 Td.

In our study we observed the protonated parent (m/z 101) for all of E/N (180-220 Td), but with a low intensity. Brown reported no protonated monomer [109].

Winterhalter has mentioned that the protonated parent at m/z 101 is unstable and decays to protonated cyclohexene [C_6H_{11}] $^+$ measured at m/z 83 [110].

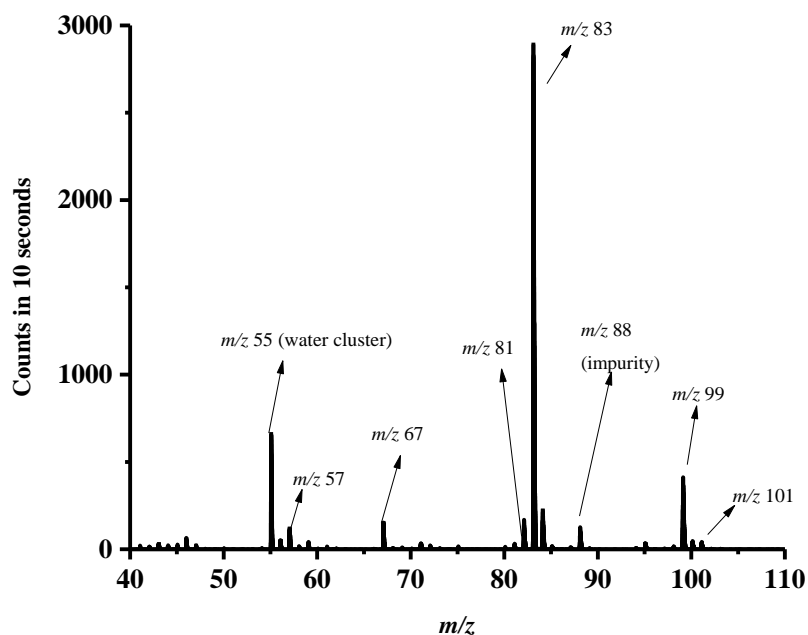


Figure 5.3 A mass spectrum illustrating the product ions from the reaction of H_3O^+ with cyclohexanol whilst operating the drift tube at reduced electric field of 120 Td for 10 second integration time.

Table 5.2 m/z values of the product ions and neutral species and their branching ratio percentages resulting from the reaction of cyclohexanol with H_3O^+ at a reduced electric field of 120 Td.

Name/ Formula	Product ion m/z	Product ion molecular formula m/z	Neutral Products	Branching ratio at 120 Td
Cyclohexanol	55	C_4H_7^+	$\text{C}_2\text{H}_4 + \text{H}_2\text{O}$	7
$\text{C}_6\text{H}_{13}\text{O}$	57	$\text{C}_3\text{H}_5\text{O}^+$	$\text{C}_2\text{H}_4 + \text{CH}_4$	3
	67	C_5H_7^+	$\text{CH}_4 + \text{H}_2\text{O}$	3
	81	C_6H_9^+	$\text{H}_2 + \text{H}_2\text{O}$	1
	83	$\text{C}_6\text{H}_{11}^+$	H_2O	74
	99	$\text{C}_6\text{H}_{11}\text{O}^+$	H_2	10
	101	$\text{C}_6\text{H}_{13}\text{O}^+$	-	2

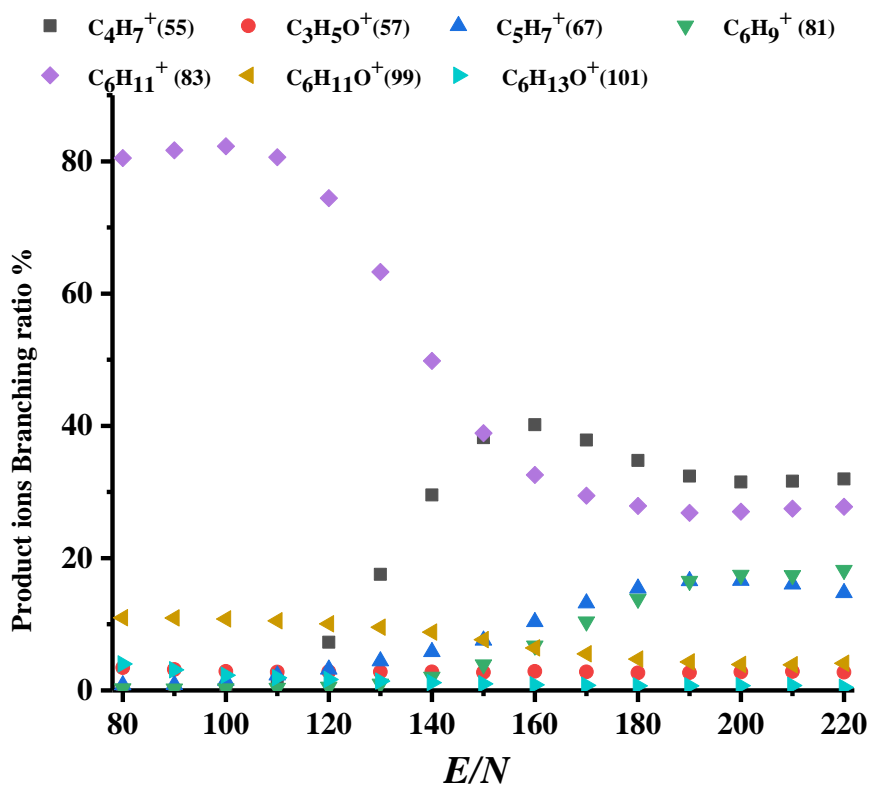


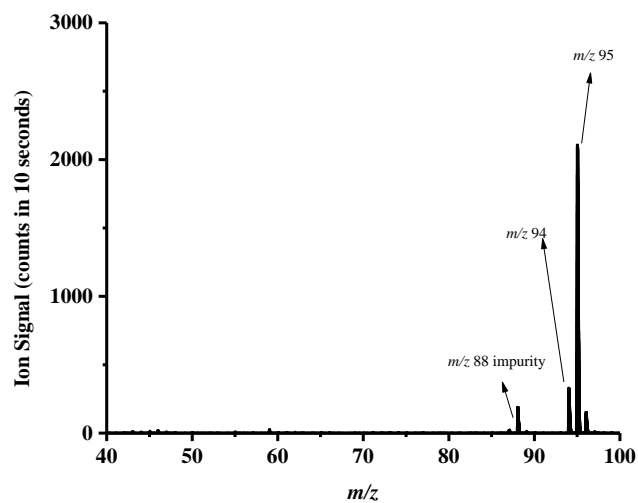
Figure 5.4 Product ion branching ratios in percentages as a function of E/N resulting from the reaction of H_3O^+ with cyclohexanol ($C_6H_{12}O$).

5.3.1.2 The reaction of phenol with H_3O^+

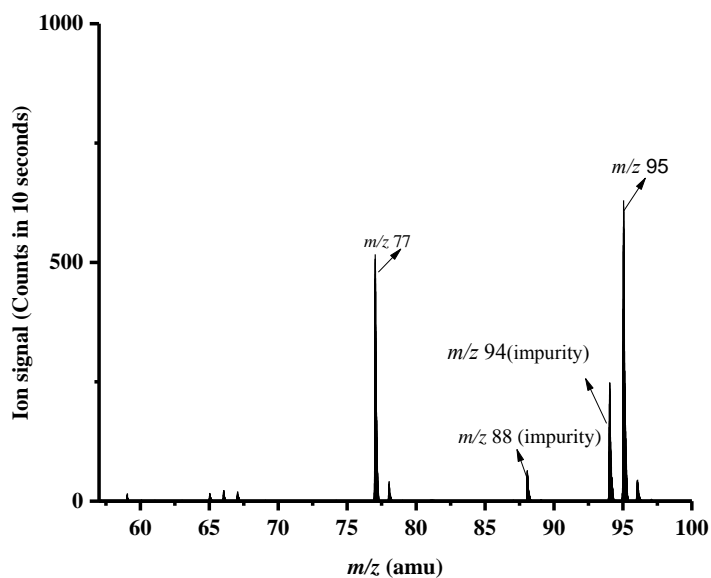
The proton affinity of phenol is high, at 817 kJ mol^{-1} [24]. Therefore, we could expect substantial dissociative transfer resulting from the reaction with H_3O^+ . However, that is not the case. Instead the dominant product ion is the protonated parent, as illustrated in figure 5.5, which shows the mass spectrum taken at 120 Td. Figure 5.6 presents the product ion branching ratio in percentages as a function of the reduced electric field and Table 5.3 provides the information about the branching ratio contribution for each of the product ions at 120 Td. Only two product ions were observed. In addition to the protonated parent, an ion at m/z 77 (C_6H_5^+) corresponding to the loss of H_2O from the protonated parent, but only is observed for reduced electric fields above 160 Td. m/z 77 could be assigned as C_6H_5^+ (77.04) or C_5HO^+ (77.003). However, using high resolution KORE-ToF-MS, the measured value was close to the exact mass of C_6H_5^+ .

In agreement with our study, in a previous study looking at phenol by Feilberg et al., they reported only the protonated parent ion m/z 95 at 138 Td [111], . In another more recent PTR-MS study covering the range 48-144 Td, Romano et al., also only observed the protonated parent at all reduced electric field values except at 48 Td where association of the protonated parent with water was observed [112]. This agrees with our observations.

Figure 5.6 shows how the product ion distributions vary as a function of the reduced electric field. m/z 95 ($\text{C}_6\text{H}_7\text{O}^+$) is the dominant ion from 80-220 Td. Its branching ratio decreases as the channel resulting from the loss of water opens.



a)



b)

Figure 5.5 A mass spectrum illustrating the product ions from the reaction of H_3O^+ with phenol whilst operating the drift tube at reduced electric field of a) 120 Td b) 220 Td for 10 second integration time. There are some impurities recorded from the sample. m/z 77 can be seen at 220 Td.

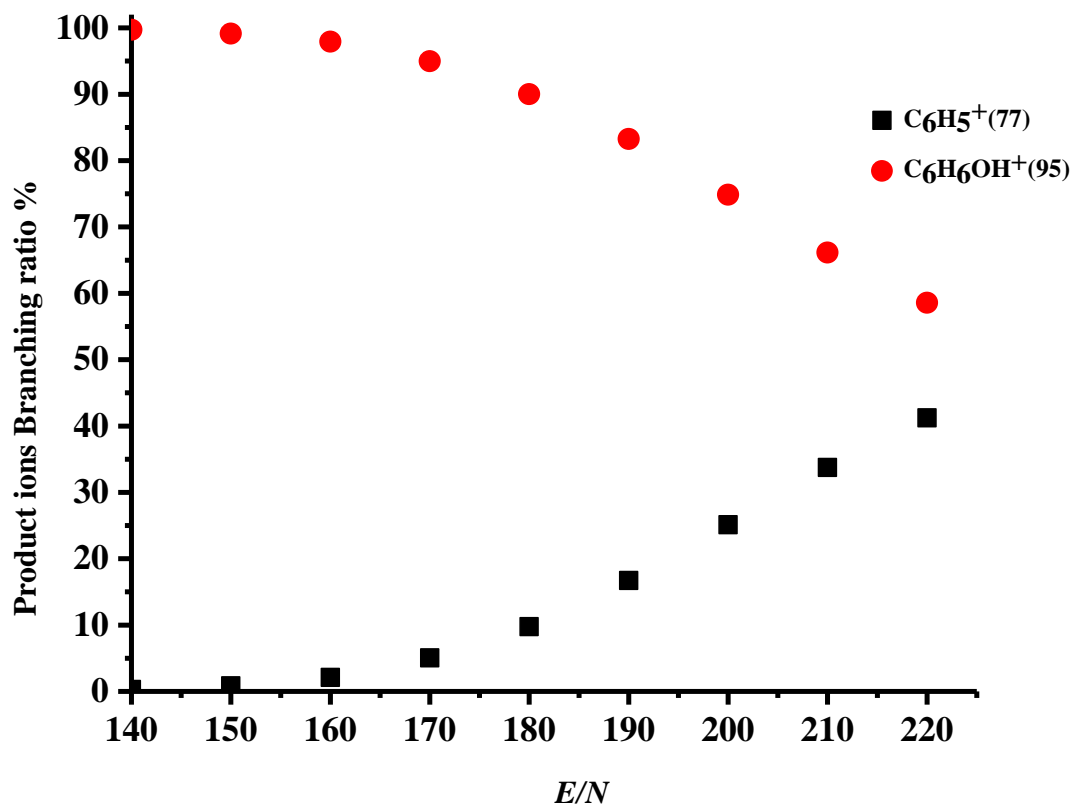


Figure 5.6 Product ion branching ratios in percentages as a function of E/N resulting from the reaction of H_3O^+ with phenol ($\text{C}_6\text{H}_{12}\text{O}$) from 150-220 Td.

Table 5.3 m/z values of the product ions and neutral species and their branching ratio percentages resulting from the reaction of phenol with H_3O^+ at a reduced electric field of 120 Td

Name/ Formula	Product ion m/z	Product ion molecular formula m/z	Neutral Products	Branching ratio at 120 Td	Branching ratio at 220 Td
Phenol	77	C_6H_5^+	H_2O	-	41
$\text{C}_6\text{H}_6\text{O}$	95	$\text{C}_6\text{H}_7\text{O}^+$	-	100	59

5.3.1.3 The reaction of anisole with H_3O^+

To our knowledge, this is the first PTR-MS study of anisole. As for phenol, anisole has a large proton affinity. Its value is 840 kJ mol^{-1} [24]. This means that proton transfer is not only efficient, but it is highly exothermic. So again we could expect dissociative proton transfer to dominate. But in fact that again is not the case.

Figure 5.7 shows the overview of the whole spectrum reaction of anisole with H_3O^+ . Figure 5.8 shows the branching ratio in percentages as the function of reduced electric field (80-200Td). Only two product ions are found. One of them is the protonated parent at m/z 109 ($\text{C}_7\text{H}_9\text{O}^+$). The other is at m/z 94 and is assigned to be $\text{C}_6\text{H}_6\text{O}^+$. Unusually this means a loss of a radical, CH_3 from the protonated parent. The branching ratios for m/z 109 ($\text{C}_7\text{H}_9\text{O}^+$) and m/z 94 ($\text{C}_6\text{H}_6\text{O}^+$) at 120 Td are 97 % and 3%, respectively (table 5.4). There is no uncertainty on assigning the product ion.

Figure 5.8 illustrates how the product ions distributions vary as a function of the reduced electric field. For all values of E/N the dominant ion is $\text{C}_7\text{H}_9\text{O}^+$. Its branching ratio decreases owing to more fragmentation as the collisional energies of both the reagent ions and product ions increase with increasing E/N .

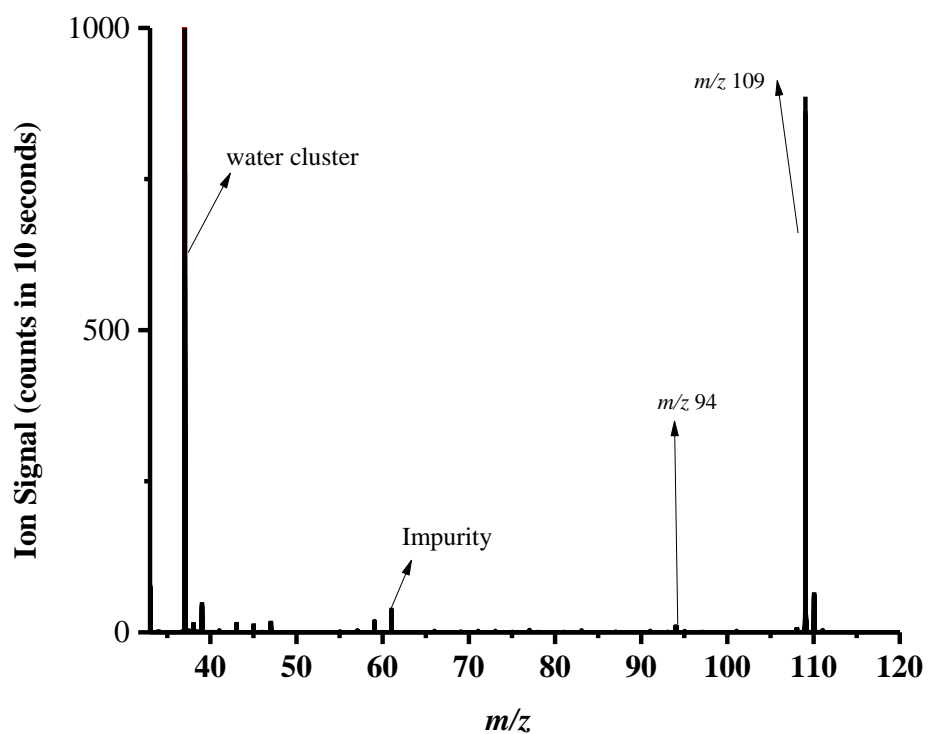


Figure 5.7 A mass spectrum illustrating the product ions resulting from the reaction of H_3O^+ with anisole whilst operating the drift tube at reduced electric field of 120 Td. An ion resulting from an impurity is highlighted.

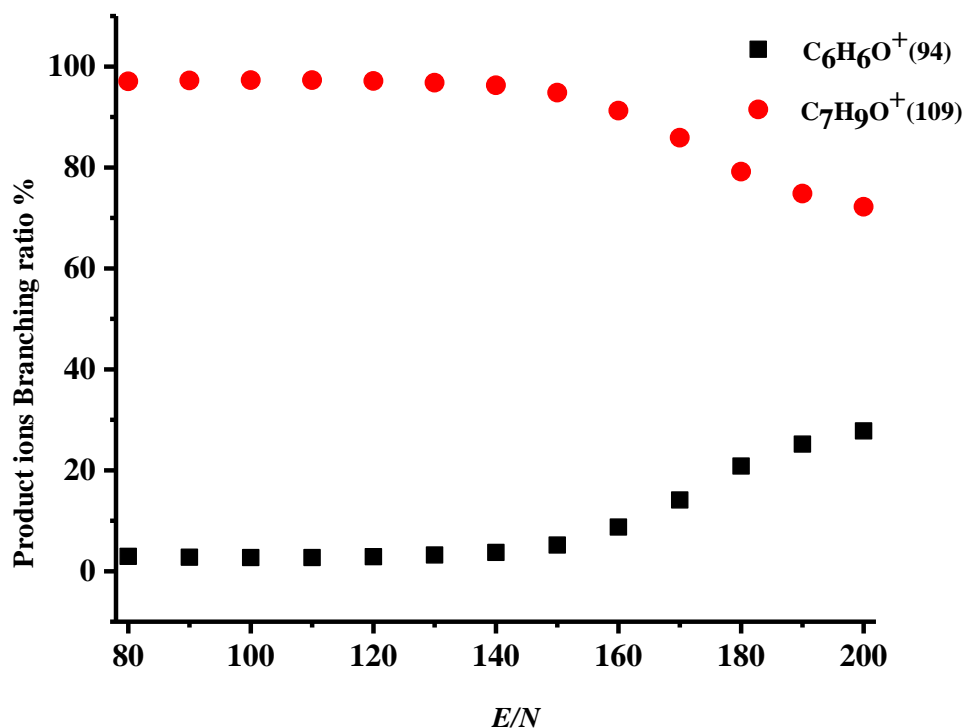


Figure 5.8 Product ion branching ratios in percentages as a function of E/N resulting from the reaction of H_3O^+ with anisole (C_7H_8O) using PTR-ToF-MS (8000).

Table 5.4 m/z values of the product ions and neutral species and their branching ratio percentages resulting from the reaction of anisole with H_3O^+ at a reduced electric field of 120 Td.

Name/ Formula	Product ion m/z	Product ion molecular formula m/z	Neutral Products	Branching ratio at 120 Td
Anisole C_7H_8O	94	$C_6H_6O^+$	CH_3	3
	109	$C_7H_9O^+$	-	97

5.3.1.4 The reaction of benzaldehyde with H_3O^+

The proton affinity of benzaldehyde is 834 kJ mol^{-1} [24]]. Like the previous two molecules the protonated parent is a prominent product ion. However, unlike the previous two molecules, it does not dominate for all of the reduced electric fields investigated. Instead after about 170 Td, dissociative proton transfer processes dominate. Figure 5.9 represents the mass spectrum of benzaldehyde at 120 Td. Figure 5.10 shows the branching ratio of benzaldehyde as a function of reduced electric field from 80 Td - 220 Td and table 5.5 provides the details of product ions and their branching ratios at 120 Td.

Four product ions are observed at m/z 77 (C_6H_5^+), m/z 79 (C_6H_7^+), m/z 105 ($\text{C}_7\text{H}_5\text{O}^+$), m/z 107 ($\text{C}_7\text{H}_7\text{O}^+$). With the high resolution KORE-ToF-MS, m/z 77 could be assigned either as C_6H_5^+ (77.04) or C_5HO^+ (77.003). In this study, m/z 77 was close to (C_6H_5^+) with loss of CO and H_2 . Similarly, the ion at a nominal m/z 79 could be assigned to be C_6H_7^+ (79.06) which was close to the exact mass of 79.06 with loss of CO and H_2O . There was no other ambiguity in the assignment of other product ions.

Among these ions, m/z 107 is the dominant ion at 120 Td where it contributes 91 % to the branching ratio. The second most abundant ion at 120 Td is m/z 105 (6 %) followed by m/z 79 (3 %). m/z 77 only is significant above 180 Td.

There has only been one other PTR-MS study of benzaldehyde by Maleknia et al. [12] who reports the product ions at an unspecified reduced electric field. They reported the protonated parent as the dominant ion, but also observed a product ion at m/z 79 (C_6H_7^+).

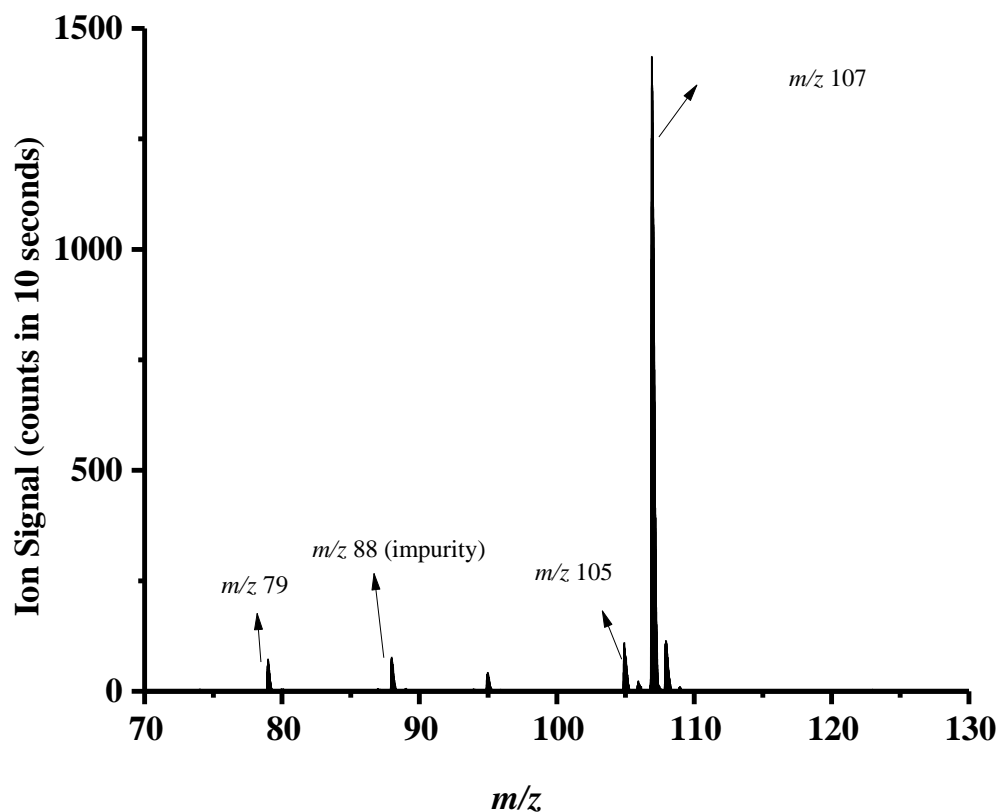


Figure 5.9 A mass spectrum illustrating the product ions from the reaction of H_3O^+ with benzaldehyde whilst operating the drift tube at reduced electric field of 120 Td. An ion resulting from an impurity is highlighted.

Figure 5.10 shows how the product ion distributions vary as a function of the reduced electric field. m/z 107 ($\text{C}_7\text{H}_7\text{O}^+$) is the dominant ion from 80-160 Td. Its branching ratio decreases as more fragmentation occurs as the collisional energies of both the reagent ions and product ions increase with increasing E/N . For example m/z 79 (C_6H_7^+) and m/z 77 (C_6H_5^+) branching ratios start to increase from 140 Td and 180 Td respectively.

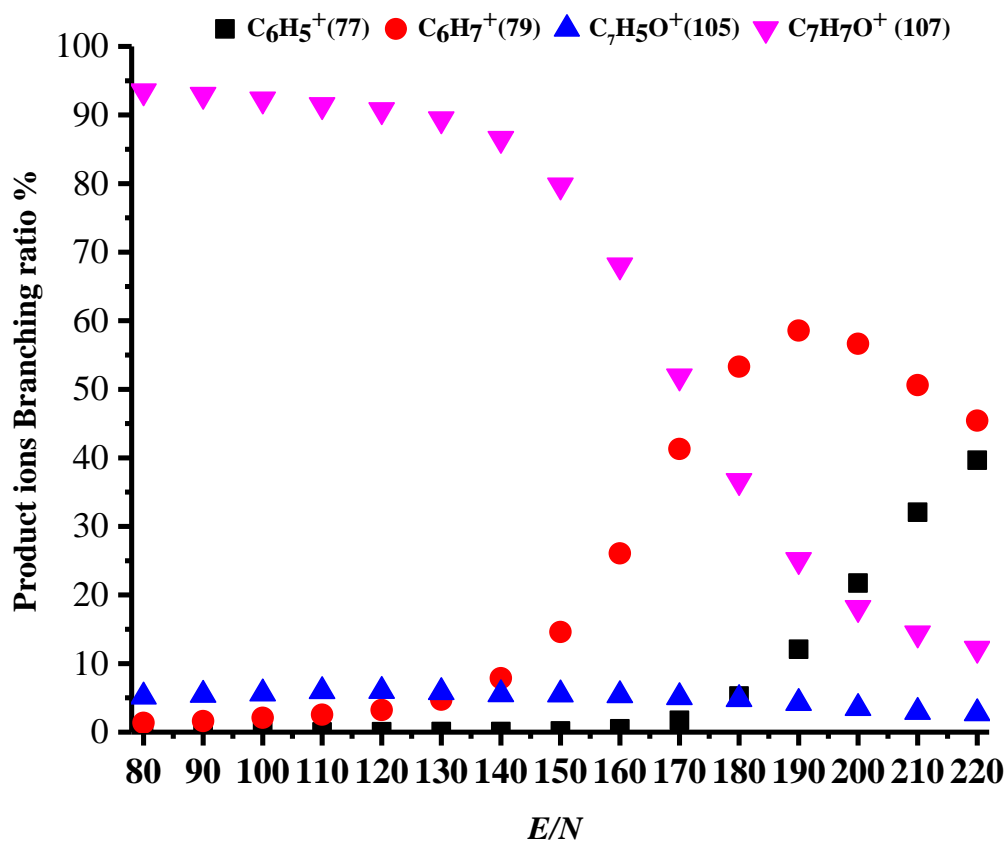


Figure 5.10 Product ion branching ratios in percentages as a function of E/N resulting from the reaction of H_3O^+ with benzaldehyde (C_7H_6O).

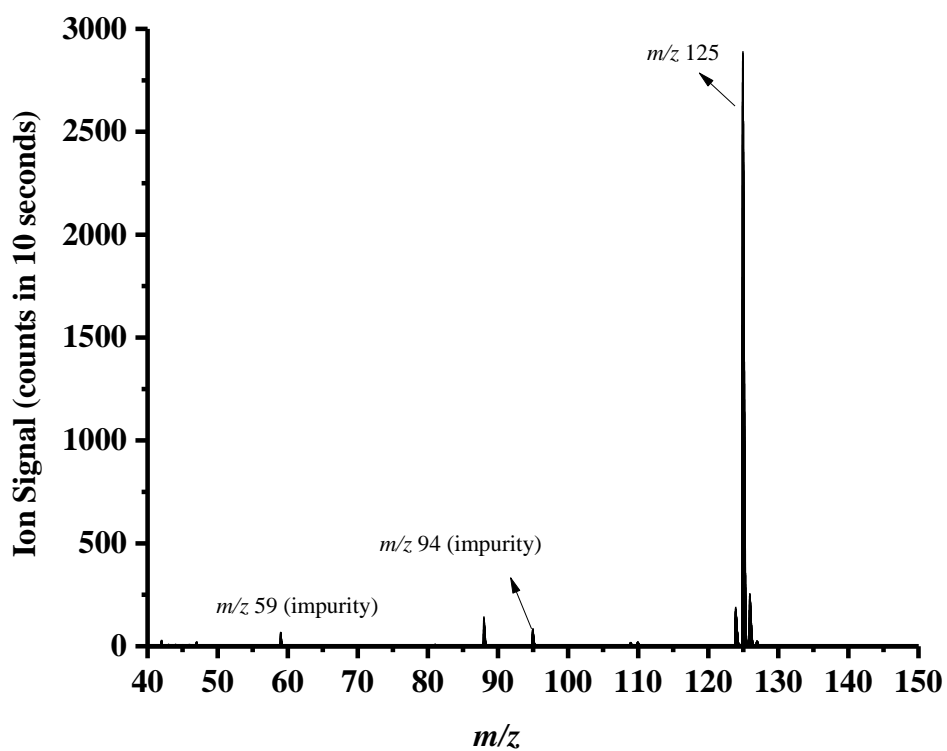
Table 5.5 m/z values of the product ions and neutral species and their branching ratio percentages resulting from the reaction of benzaldehyde with H_3O^+ at a reduced electric field of 120 Td.

Name/ Formula	Product ion m/z	Product ion molecular formula m/z	Neutral Products	Branching ratio at 120 Td
Benzaldehyde C_7H_6O	77	$C_6H_5^+$	$CO+H_2$	0
	79	$C_6H_7^+$	CO	3
	105	$C_7H_5O^+$	H_2	6
	107	$C_7H_7O^+$	-	91

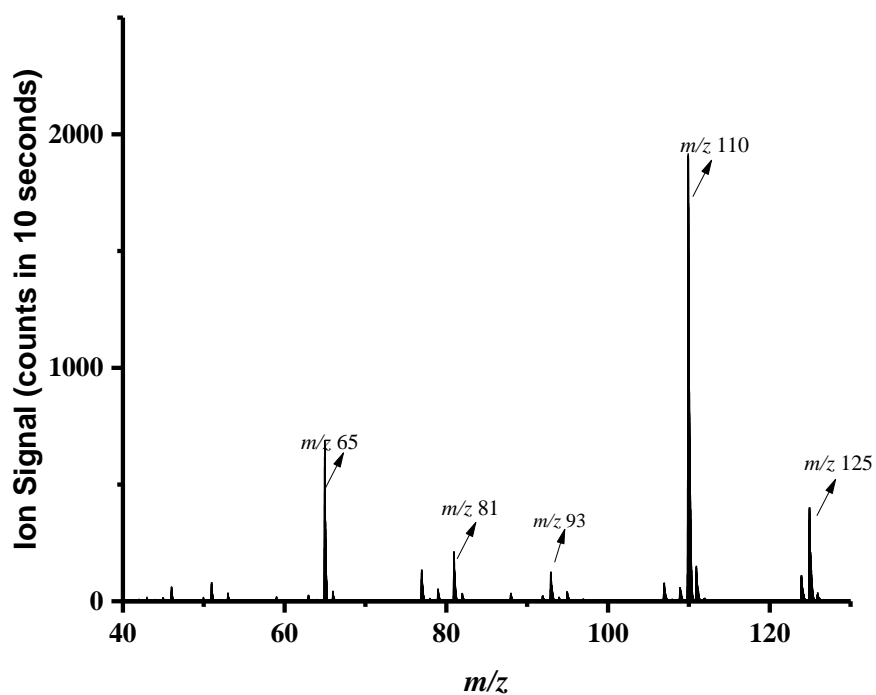
5.3.1.5 Guaiacol reaction with H_3O^+

This study represents the first PTR-MS study of guaiacol. The proton affinity of guaiacol is unknown. However, it must be higher than water, given the observed efficiency of the reaction and the formation of various product ions. Figure 5.11 shows the mass spectrum of guaiacol at 120 Td and figure 5.12 shows the product ion branching ratios in percentages as a function of reduced electric field. There are eight product ions observed resulting from the reaction of guaiacol with H_3O^+ at m/z 65 (C_5H_5^+), m/z 77 (C_6H_5^+), m/z 79 (C_6H_7^+), m/z 81 ($\text{C}_5\text{H}_5\text{O}^+$), m/z 93 ($\text{C}_6\text{H}_5\text{O}^+$), m/z 107 ($\text{C}_6\text{H}_3\text{O}_2^+$), m/z 110 ($\text{C}_6\text{H}_6\text{O}_2^+$) and m/z 125 ($\text{C}_7\text{H}_9\text{O}_2^+$) (table 5.6). m/z 110 represents a loss of CH_3 from the protonated parent. The loss of a free radical is unusual in proton transfer reactions. This will have to be investigated with quantum mechanical calculations to help in the interpretation as to how that can occur. The ion at a nominal m/z 107 could result from a loss of H_2O or CH_4 and H_2 . However, using the high resolution capabilities of the KORE PTR-ToF-MS, the peak position can be measured accurately, and that comes to m/z 107.012. $\text{C}_7\text{H}_7\text{O}^+$ has an exact m/z of 107.050, whereas that for $\text{C}_6\text{H}_3\text{O}_2^+$ is at the exact value of 107.013. Thus we can assign the product ion at a measured m/z of 107.012 as $\text{C}_6\text{H}_3\text{O}_2^+$. There is thus no ambiguity in that assignment. Similarly the ion at the nominal m/z 93 has a measured value of 93.03, which means it is $\text{C}_6\text{H}_5\text{O}^+$ and not C_7H_9^+ , which has an exact m/z of 93.070. Similarly, the ion at a nominal m/z 79 could be assigned to be $\text{C}_5\text{H}_5\text{O}^+$, but that would lead to an exact m/z of 79.02, whereas the measured value is 79.05 in good agreement with the exact m/z for C_6H_7^+ . The ion at nominally m/z 65 could either C_5H_5^+ or $\text{C}_2\text{H}_9\text{O}_2^+$, but the measured value is closer to the exact m/z for C_5H_5^+ .

The most abundant product ion at 120 Td is m/z 125 (99 %), which is the protonated parent). The branching ratio of the protonated parent decreases gradually when the reduced electric field is greater than 130 Td.



a)



b)

Figure 5.11 A mass spectrum illustrating the product ions from the reaction of H_3O^+ with guaiacol whilst operating the drift tube at reduced electric field of a) 120 Td b) 220 Td. Some impurities from the sample are recorded.

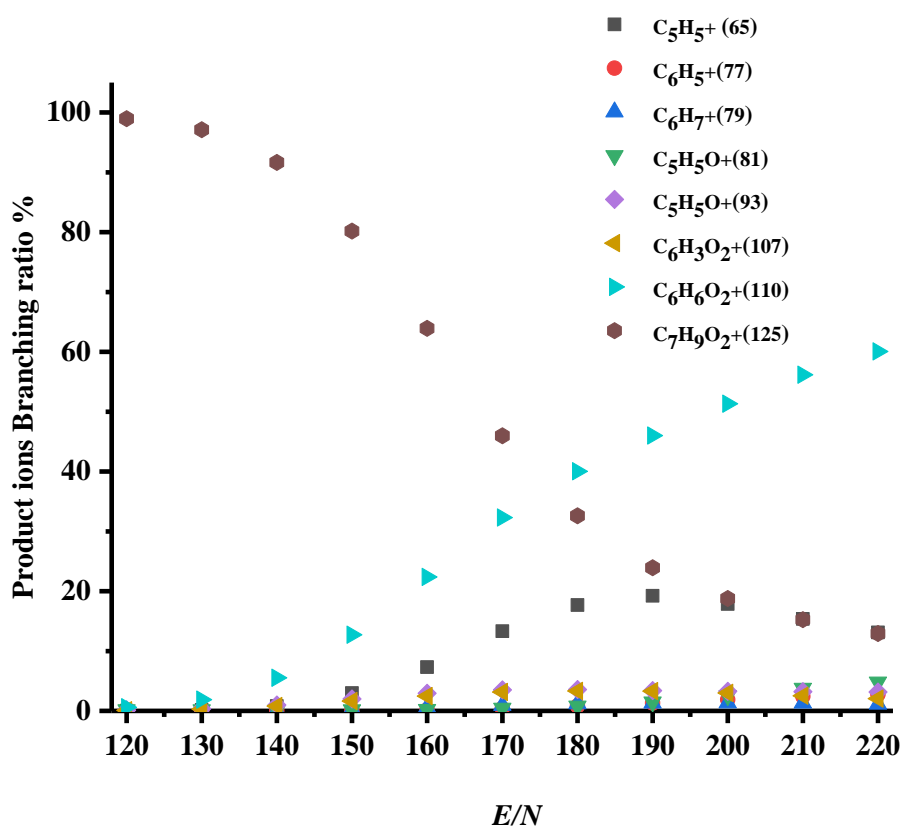


Figure 5.12 Product ion branching ratios in percentages as a function of E/N resulting from the reaction of H_3O^+ with guaiacol ($\text{C}_7\text{H}_8\text{O}_2$).

Table 5. 6 m/z values of the product ions and neutral species and their branching ratio percentages resulting from the reaction of guaiacol with H_3O^+ at a reduced electric field of 120 Td and 220 Td.

Name/ Formula	Product ion m/z	Product ion molecular formula m/z	Neutral Products	Branching ratio at 120 Td	Branching ratio at 220 Td
Guaiacol	65	C_5H_5^+	$\text{C}_2\text{H}_4+\text{O}_2$	0	13
$\text{C}_7\text{H}_8\text{O}_2$	77	C_6H_5^+	CH_4+O_2	0	3
	79	C_6H_7^+	$\text{H}_2\text{O}+\text{CO}$	0	10
	81	$\text{C}_5\text{H}_5\text{O}^+$	CH_4+CO	0	5
	93	$\text{C}_6\text{H}_5\text{O}^+$	$\text{CO}+\text{H}_2\text{O}+\text{H}_2$	0	3
	107	$\text{C}_6\text{H}_3\text{O}_2^+$	$\text{CH}_4 + \text{H}_2$	0	2
	110	$\text{C}_6\text{H}_6\text{O}_2^+$	CH_3	1	60
	125	$\text{C}_7\text{H}_9\text{O}_2^+$	-	99	13

5.3.2 The reaction of menthol with H_3O^+

For the E/N range investigated, no protonated parent was observed. Instead extensive fragmentation occurs following proton transfer from H_3O^+ to menthol, as summarised in table 5.7, which presents the relative branching ratios for the product ions at 120 Td. Figure 6.13 presents the product ion branching percentages as a function of E/N . Meanwhile, figure 6.14 represents the mass spectrum of menthol at 120 Td.

At 120 Td $\text{C}_5\text{H}_7\text{O}^+$ is found to be the major product ion observed. In comparison, a SIFT-MS study only observed one product ion, $\text{C}_{10}\text{H}_{19}^+$, which results from the elimination of H_2O from the protonated parent [113]. That considerable fragmentation observed with the PTR-MS is a result of the increased collisional energies associated with reactions in the drift tube compared to the thermal collisional energies that occur in a SIFT. Substantial fragmentation in the drift tube of a PTR-MS was also observed in two previous PTR-MS studies of pure menthol [106, 107]. The first by Saint-Eve *et al.* used a PTR-Quad-MS system at a fixed E/N of 140 Td and reported product ions at m/z 81 (100), 55 (62), 83 (42), 137 (22), and 139 (4) (relative intensities given in brackets, which are considerably different from those we recorded). The second investigation, by Gordon *et al.* presented E/N measurements over the range of approximately 90-140 Td identifying four product ions at m/z values of 55, 81, 83 and 139, with m/z 83 being the dominant one at 120 Td. The relative abundance of the product ions identified by Gordon *et al.* are in reasonable agreement with our values. However, we mention here that direct comparisons of relative intensities between different PTR-MS instruments have to be done with care owing to differences in the operating conditions for fixed E/N (e.g. temperature and humidity) and the differences in the transmission of ions from the drift tube to the transfer optics and then through the mass spectrometer, followed by any m/z detection efficiency

of the detector [114]. The key point of branching percentages is that they inform the user what should be detected for their own instrument under given operating conditions.

From figure 5.13 it can be seen that at reduced electric fields higher than 120 Td, additional product ions are observed at nominal m/z values of 41, 53 and 79 corresponding to the product ions $C_3H_5^+$, $C_4H_5^+$ and $C_6H_7^+$, respectively. As the reduced electric field is reduced below about 100 Td, the dominant product ion is $C_{10}H_{19}^+$, which agrees with the thermal SIFT-MS observation.

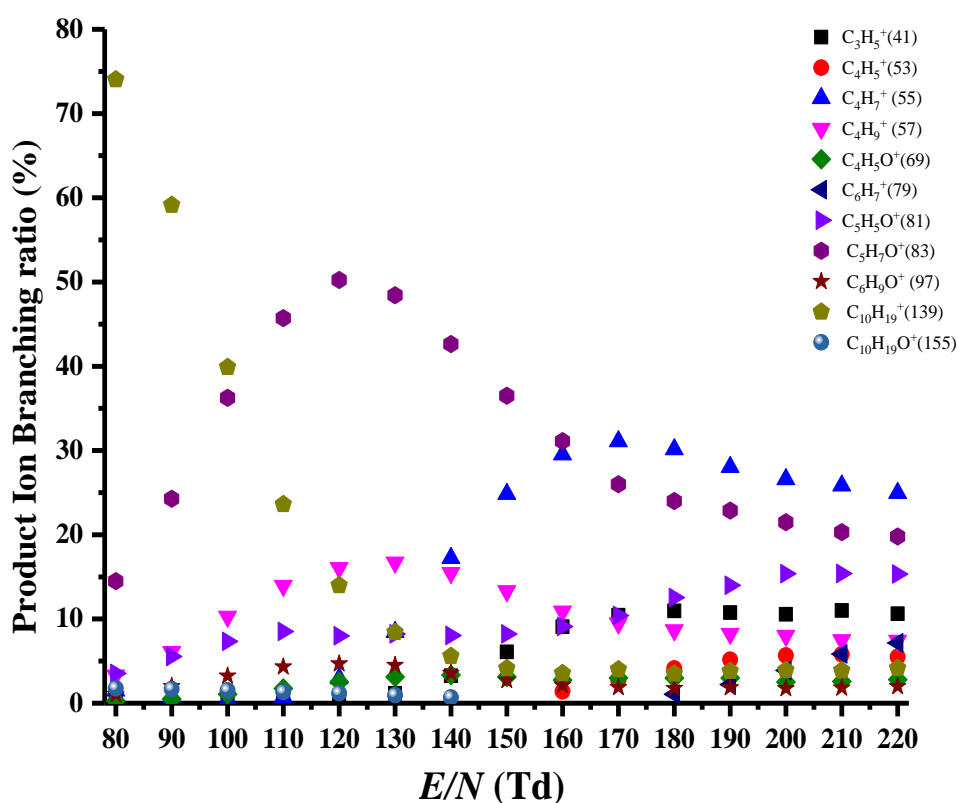


Figure 5.13 Product ion branching ratios in percentages as a function of E/N resulting from the reactions of menthol ($C_{10}H_{20}O$) in the reaction region of the PTR-MS as a function of E/N .

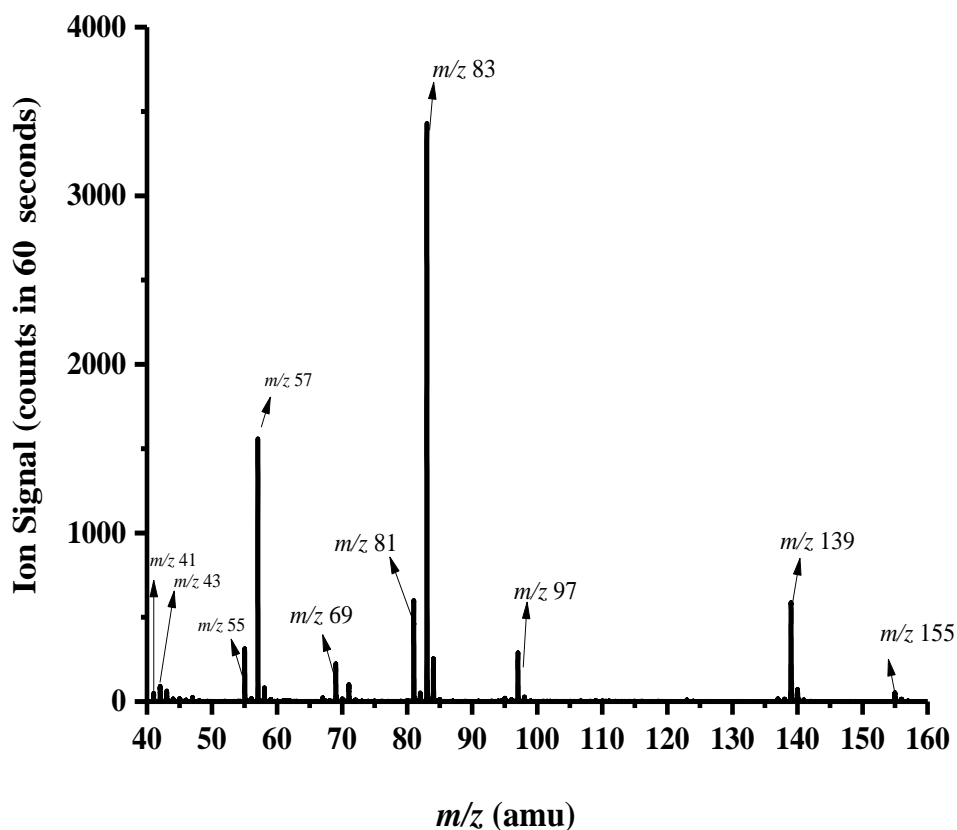


Figure 5.14 An illustrative mass spectrum illustrating the product ions resulting reactions with menthol in the drift tube of the PTR-MS at a reduced electric field of 120 Td.

Table 5.7 m/z values of the product ions and their branching ratio percentages resulting from the reaction of menthol ($C_{10}H_{20}O$) with H_3O^+ at a reduced electric field of 120 Td.

Product ion nominal m/z	Product ion molecular formula	Neutral product	Branching ratio % at 120 Td
55	$C_4H_7^+$	$C_6H_{14}O$	3
57	$C_4H_9^+$	$C_6H_{12}O$	16
69	$C_4H_5O^+$	C_6H_{16}	3
81	$C_5H_5O^+$	C_5H_{16}	8
83	$C_5H_7O^+$	C_5H_{14}	50
97	$C_6H_9O^+$	C_4H_{12}	5
139	$C_{10}H_{19}^+$	H_2O	14
155	$C_{10}H_{19}O^+$	H_2	1

5.3.3 The reaction of vanillin with H_3O^+

Figure 5.15 represents the branching ratio of the product ions of vanillin at 120 Td and figure 5.16 represents the mass spectrum of vanillin at 120 Td. In comparison to menthol, vanillin shows little fragmentation from reactions in the drift tube of the PTR-MS. The protonated parent at the nominal m/z of 153 dominates throughout the E/N range investigated, as illustrated in figure 5.15 which provides the product ion branching percentages as a function of E/N . For all values of the reduced electric field another product ion is observed at m/z 125, the measured peak position of which indicates it to be $\text{C}_7\text{H}_9\text{O}_2^+$, which results from the loss of CO from the protonated parent. Only for E/N values greater than about 160 Td is a third product ion observed, which is assigned to be C_5H_5^+ . That the protonated parent is the dominant product ion agrees with an earlier study by Heenan et al., who report m/z 153 as the only product ion resulting from the reaction of H_3O^+ with vanillin in their vanilla food flavour studies [101].

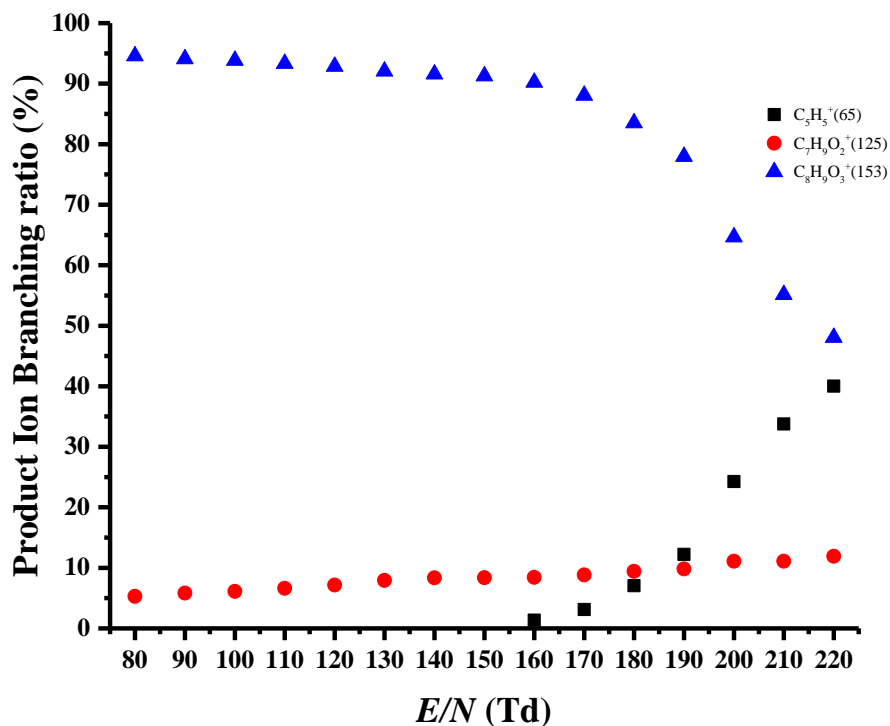


Figure 5.15 Product ion branching ratios in percentages as a function of E/N resulting from the reactions in the drift tube of the PTR-MS with vanillin ($C_8H_8O_3$).

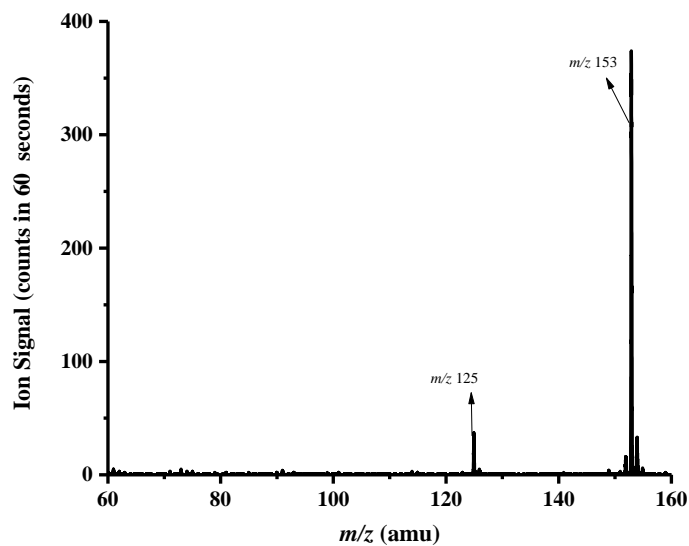


Figure 5.16 A mass spectrum resulting from the reaction of H_3O^+ with vanillin at reduced electric field of 120 Td.

Table 5.8 Proposed product ions, neutral products and relative intensities resulting from the reaction of vanillin with H_3O^+ at 120 Td.

<i>Product ion</i> <i>m/z</i>	Product ion molecular formula	Neutral product	Relative intensity at 120 Td (%)
65	C_5H_5^+	$\text{C}_3\text{H}_4\text{O}_3$	-
125	$\text{C}_7\text{H}_9\text{O}_2^+$	CO	7
153	$\text{C}_8\text{H}_9\text{O}_3^+$		93

5.3.4 Comparisons of vanillin and menthol with other compounds – similarities

An aim of the studies associated with vanillin and menthol was to see if these compounds are used in the shisha paste for vanilla and mint flavours, respectively.

5.3.4.1 Menthol with cyclohexanol

All of the product ions identified with menthol have been observed in the shisha paste such as m/z 55, m/z 57, m/z 69, m/z 81, m/z 83, m/z 139, m/z 97, m/z 155.

5.3.4.2 Vanillin with phenol, anisole, benzaldehyde and guaiacol

However, for vanillin no product ions associated with this compound were observed.

These results agree with the GC-MS studies, which were undertaken after that of the headspace analysis of the shisha pastes and compounds.

5.4 Conclusion

One of the more significant findings to emerge from this study is that of identifying the product ions from menthol and vanillin. For mint shisha paste, we found some similar product ions which were associated with menthol such as m/z 57, 69, 83, and 139 and suggested that menthol was used in mint shisha paste. Whereas, for vanilla shisha paste, there were no associated product ions monitored from vanillin. In addition to that, also some associate compounds to menthol and vanillin were measured using a different functional group such as cyclohexanol, phenol, anisole, benzaldehyde and guaiacol which have a benzene ring. The finding from the headspace of cyclohexanol has shown that it has a very strong link with menthol. Meanwhile for vanillin, guaiacol was the only compound which produced associate ions. Guaiacol is an artificial vanillin. However, guaiacol was not found from the GC-MS measurement. This needs further investigation.

CHAPTER 6

6 PTR-TOF-MS STUDIES OF THE REACTIONS OF H_3O^+ AND O_2^+ WITH THE GENERAL ANAESTHETIC GASES HALOTHANE, ISOFLURANE, ENFLURANE, SEVOFLURANE, DESFLURANE AND METHOXYFLURANE

6.1. Introduction

Halogenated anaesthetics have been used in surgical procedures for decades so that patients do not feel pain. But interestingly, there is little information as to how long these anaesthetics stay in the body post-surgery.

To our knowledge there are only two studies associated with the retention of general anaesthetics in the body. The first by Yasuda et al. investigated the kinetics of isoflurane and sevoflurane administered to healthy young men. According to their investigation, there was a fast elimination of isoflurane from the body of the volunteers [6]. A later study by Fernández del Río et. al. (2015), but actually dealing with severely ill patients undergoing liver transplants, showed that the anaesthetic being used during surgery, isoflurane, remained in their bodies for weeks after this major operation [5].

If correct, the study by Fernández del Río et. al. [5] could have consequences in terms of when cognitive function is fully restored to a patient, and hence further studies are required to investigate elimination characteristics.

Studies are therefore currently being planned in the Molecular Physics Group, University of Birmingham, and at the Breath Research Institute in Austria to continue the work of Fernández del Río et al. by undertaking longitudinal studies to determine the loss

of inhaled anaesthetics from the body following surgery. Concentrations of the anaesthetics and their metabolites in exhaled in breath will be determined as a function of time. The objective of those studies is to determine the factors which affect washout, such as the health, sex and age of the patient, the ASA (American Society of Anaesthesiologists) classification of the patient (1-4), the timing and dose of anaesthetics, and the type and length of the surgery.

Previously published studies by Wang et al. have used a selected ion flow tube (SIFT) to analyse the reactions of H_3O^+ , NO^+ and O_2^+ with anaesthetic gases e.g. halothane, isoflurane and sevoflurane by observing these gases via on-line breath monitoring [115]. In this study, the PTR-MS was used in all the experiments. Comparisons between the SIFT-MS and PTR-MS results will be presented here. IMS and PTR-MS analytical instruments are being proposed to measure the concentrations of these compounds in the breath. However, before any of those studies can be undertaken, specific knowledge of reduced ion mobilities (IMS) and product ions (PTR-MS) are required. Furthermore, for applications of PTR-MS, it is important to determine what is the best operational reduced electric field to use to maximise sensitivity and specificity.

A key aim of the study presented in this chapter is to determine the product ions resulting from the reactions of H_3O^+ and O_2^+ with a number of volatile halogenated anaesthetics, namely halothane, isoflurane, enflurane, sevoflurane, desflurane and methoxyflurane, with a major focus on the most commonly used ones, isoflurane and sevoflurane, as a function of reduced electric field for use in the later studies being planned.

In Birmingham the key apparatus used was a KORE PTR-ToF-MS and in Austria an IONICON PTR-TOF 8000. It is important to ascertain the product ions separately,

because studies undertaken within the Molecular Physics Group have shown that the product ion branching ratios are very much instrument dependent. A full investigation as to why these differences occur is outside the goals of this PhD, but they are related to differences in ion production (e.g. internal energy of the reagent ion) and ion transmission properties, in the drift tube, the transfer optics to the mass spectrometer, and mass spectrometer.

Here, the results from these investigations were reported and hence provided a library of product ions that can be used to determine the concentrations of inhaled anaesthetics in the breath of patients for two types of PTR-MS systems (the most commonly used ones).

We will also show that the isomeric compounds isoflurane and enflurane can be distinguished.

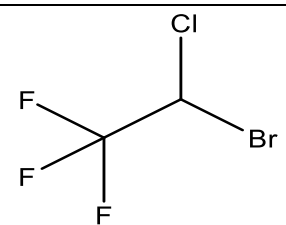
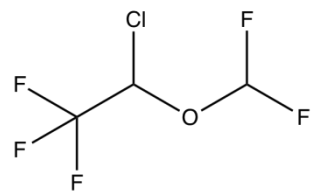
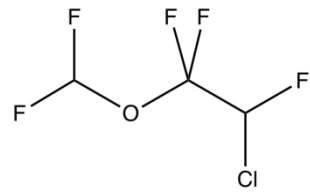
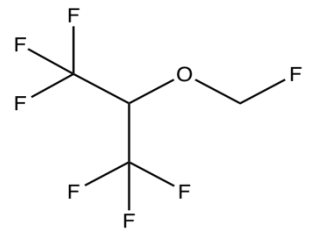
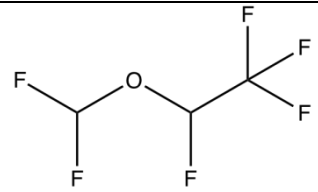
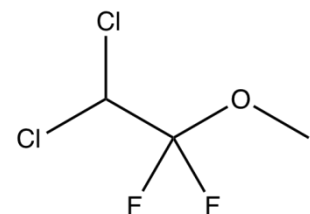
Finally, density function calculations for isoflurane and enflurane, undertaken by Dr Peter Watts of the Molecular Physics Group as part of this study, are also included to aid in the interpretation of results.

6.2 Anaesthetics Details

The details about the anaesthetic compounds purchased from Sigma Aldrich (UK) and for one compound (Methoxyflurane), from Alfa Aesar are listed in table 6.1 and used without further purification.

1 μl samples were taken and placed into a 100 ml glass bottle. A sample of the headspaces was then taken (10 ml) using a 100 ml glass syringe which was coupled to the top part of the bottle using a luer-lock stopcock. The withdrawn samples were then diluted with 90 ml of clean air. The concentration of the anaesthetics was monitored closely to avoid depletion of H_3O^+ and O_2^+ . Background spectra for each reduced electric field were obtained which were subtracted from the compound spectra. The drift tube pressure was set at 1 mbar and the glow discharge pressure set at 1.3 mbar. The drift tube and hollow cathode temperature were maintained at 100 °C.

Table 6.1 Details of the anaesthetic compounds investigated in this thesis.

Anaesthetic Molecular weight in Daltons of the lightest isotopomer is given	CAS Number/ purity/company name	Vapour pressure 20 degree C (mmHg)	Molecular structure
Halothane $C_2HBrClF_3$ 196	151-67-7, 99 % Sigma Alridch	243	
Isoflurane $C_3H_2ClF_5O$ 184	26675-46-7, 99 % Sigma Alridch	238	
Enflurane $C_3H_2ClF_5O$ 184	13838-16-9, 99 % Sigma Alridch	172	
Sevoflurane $C_4H_3F_7O$ 200	28523-86-6, 99 % Sigma Alridch	157	
Desflurane $C_3H_2F_6O$ 168	57041-67-5, 99 % Sigma Alridch	672	
Methoxyflurane $C_3H_4Cl_2F_2O$ 164	76-38-0, 99 % Alfa Aesar	224	

6.3 Results and Discussion

6.3.1 Halothane

6.3.1.1 Reaction with H_3O^+

An early SIFT-MS study by Wang et al. [115] has shown that there is no bimolecular reaction of H_3O^+ with halothane. Hence the proton affinity of halothane must be less than that of water and when proton transfer does occur the protonated species does not fragment within the lifetime between collisions with the water molecules. Instead these authors observed that the reaction proceeds through a three body process leading to $\text{H}_3\text{O}^+\cdot\text{CFCHClBr}$ as the product ion. With PTR-MS, endothermic bimolecular processes may be driven by the electric field. However, there were no such interactions with halothane observed, nor association processes observed owing to the collisional effects in the PTR-MS.

6.3.1.2 Reaction with O_2^+

The ionization energies of O_2 and halothane are 12.07 eV and 11.2 eV, respectively [116]. Therefore, charge transfer is exothermic by about 0.9 eV. Table 6.2 summaries the results of the charge transfer reactions of halothane with O_2^+ at 140 Td for measurements taken on the KORE PTR-ToF-MS in comparison to those obtained in the SIFT-MS studies by Wang et al. [115].

Table 6.2 m/z values of the product ions and their branching ratio percentages resulting from the reaction of halothane with O_2^+ at a reduced electric field of 140 Td using the KORE PTR-ToF-MS in comparison to SIFT-MS results published by Wang et al.[115].

Name/ Formula	Product ion <i>Nominal m/z</i>	Product ion	Neutral Products	PTR-ToF-MS (KORE) %	SIFT-MS % [115]
Halothane C_2HClF_3Br 196	51	CHF_2^+	CFCIBr	4	-
	67+69	$CHFCl^+$	CF_2Br	18	-
	69	CF_3^+	CHClBr	5	-
	117+119	$C_2HF_3Cl^+$	Br	9	20
	127+129+131	$CHClBr^+$	CF_3	3	5
	161+163	$C_2HF_3Br^+$	Cl	-	5
	176+178+180	$C_2F_2ClBr^+$	HF	58	10
196+198+200	$C_2HF_3ClBr^+$	-	3	60	

The O_2^+ reactions occur via charge (electron) transfer producing an excited parent cation, $(M^+)^*$. The majority of these fragments produce seven product ions, and only a small signal is observed for the non-dissociative charge transfer channel, even at the lowest E/N . These seven product ions were observed in order of increasing m/z (using the lightest isotopomer) at m/z 51 (CHF_2^+), 67 ($CHFCl^+$), 69 (CF_3^+), 117 ($C_2HF_3Cl^+$), 127 ($CHClBr^+$), 176 ($C_2F_2ClBr^+$) and 196 ($C_2HF_3ClBr^+$). The most abundant product ion at 140 Td was found to be at m/z 176 (58%). Figure 6.1 provides an overview of the complete spectrum recorded, including the product ions and other ions present in the drift tube and figure 6.2 (a)-(e) shows the product ions in more detail.

Unsurprisingly, our product ion distributions and types of ions differ from those reported by Wang et al. They reported five product ions at m/z 117 ($C_2HF_3Cl^+$), 127 ($CHClBr^+$), 161 ($C_2HF_3Br^+$), 176 ($C_2F_2ClBr^+$), and 196 ($C_2HF_3ClBr^+$). According to them, the most abundant ion is the protonated parent ion m/z 196 ($C_2HF_3ClBr^+$). In PTR-MS at 140 Td, m/z 176 is the dominant ion corresponding to the loss of HF from $C_2HF_3ClBr^+$.

With the exception of m/z 161, the same ions were observed as the SIFT, but some additional ones too, and with different branching percentages. These differences are simply a result of the differences in the techniques; namely, because SIFT-MS reactions are at thermal energies, whereas the PTR-MS reactions are not. Some other ions also were observed in low intensities less than 1% such as m/z 79 (Impurity), m/z 85 (Unknown), m/z 95 (Unknown), m/z 97 (Unknown) and m/z 99 (Unknown) after the sample was introduced, but that they could not be associated to halothane, and hence are considered to result from an impurity. Also, the intensities of the peaks were not overlapping with the expected isotope peaks and agree with the isotope ratios.

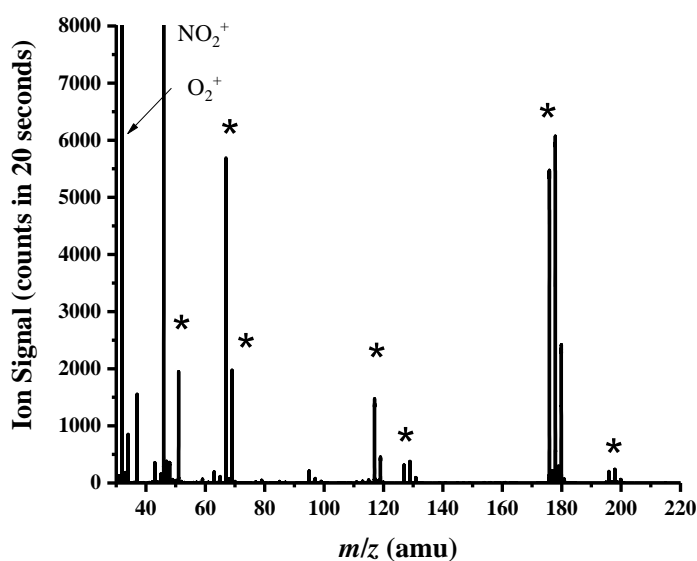


Figure 6.1 A mass spectrum illustrating the product ions (starred) resulting from the reaction of O_2^+ with halothane (C_2HClF_3Br) whilst operating the drift tube at a reduced electric field of 140 Td. Other ions such as the reagent ion O_2^+ and an impurity ion (NO_2^+) coming from the ion source are also highlighted. Note that the recombination energy of NO_2^+ is 9.6 eV, and hence cannot charge transfer to halothane given that the (adiabatic) ionisation potential for halothane is 11.0 eV, and hence is not of concern to us.

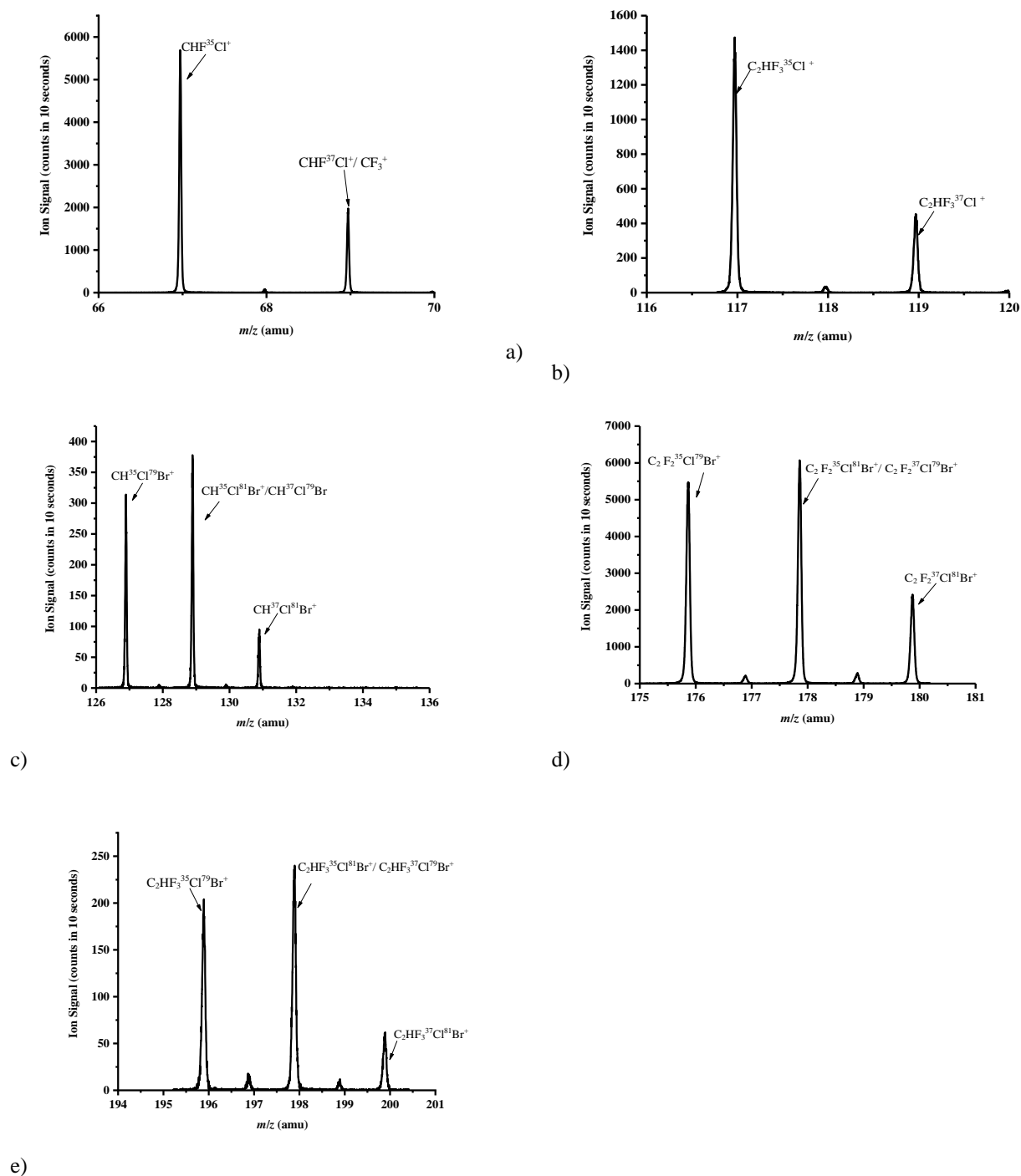


Figure 6.2 Spectra illustrating the complete set of product ions (including isotopes) observed following the reaction of O_2^+ with halothane, and in order of increasing m/z a) m/z 67($CHF^{35}Cl^+$) and m/z 69 ($CHF^{37}Cl^+/CF_3^+$) b) m/z 117 ($C_2HF_3^{35}Cl^+$) and m/z 119 ($C_2HF_3^{37}Cl^+$) c) m/z 127($CH^{35}Cl^{79}Br^+$), m/z 129 ($CH^{35}Cl^{81}Br^+/CH^{37}Cl^{79}Br$) and m/z 131($CH^{37}Cl^{81}Br^+$) e) m/z 176 ($C_2F_2^{35}Cl^{79}Br^+$), m/z 178 ($C_2F_2^{35}Cl^{81}Br^+/C_2F_2^{37}Cl^{79}Br^+$) and m/z 180 ($C_2F_2^{37}Cl^{81}Br^+$) and f) m/z 196 ($C_2HF_3^{35}Cl^{79}Br^+$), m/z 198 ($C_2HF_3^{35}Cl^{81}Br^+/C_2HF_3^{37}Cl^{79}Br^+$) and m/z 200 ($C_2HF_3^{37}Cl^{81}Br^+$).

Figure 6.3 illustrates how the product ion distributions vary as a function of the reduced electric field. For all values of E/N the dominant ion is $C_2F_2ClBr^+$, but its branching ratio decreases owing to more fragmentation as the collisional energies of both the reagent ions and product ions increase with increasing E/N .

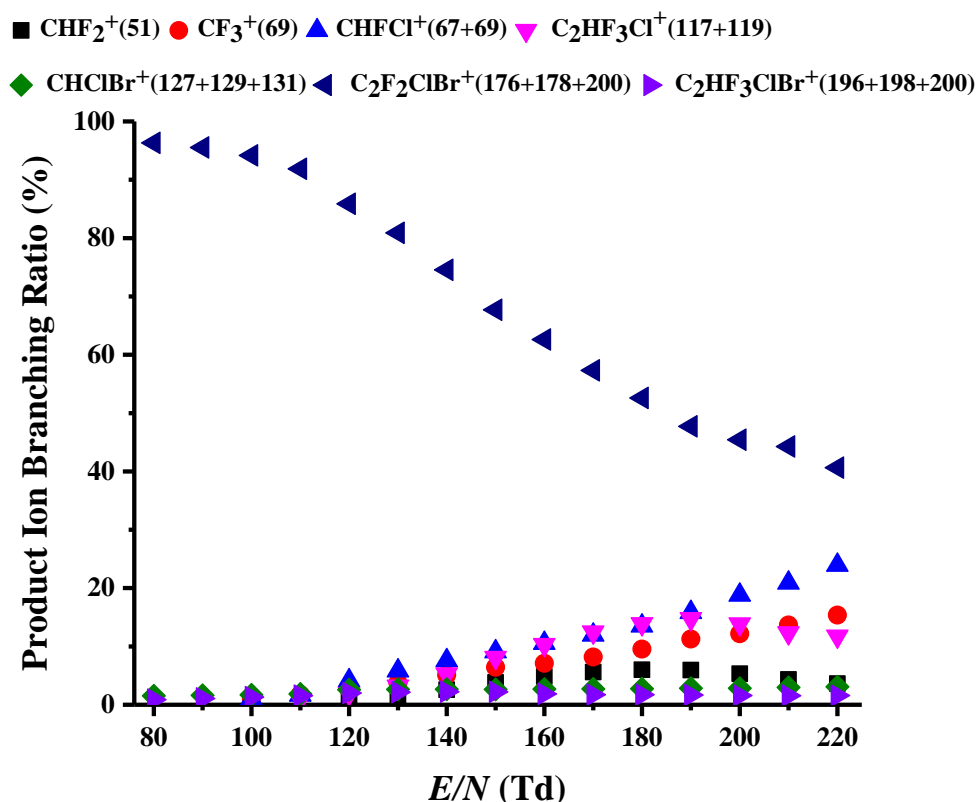


Figure 6.3 Product ion branching percentages as a function of E/N resulting from the reaction of O_2^+ with halothane ($C_2HBrClF_3$).

6.3.2 Isoflurane

6.3.2.1 Reaction with H_3O^+

Figure 6.4 shows the full mass spectrum of isoflurane and figure 6.5 shows the mass spectrum of each product ion in more detail at 140 Td. The product ion branching percentages at 140 Td are presented in table 6.3 for measurements undertaken on the Birmingham KORE PTR-ToF-MS and an IONICON PTR-TOF 8000. The values displayed took into account isotopic abundances. Also presented in table 6.3 are published values of product ion percentages recorded using an IONICON PTR-Quad-MS (Fernandez del Rio et al. [2]), unpublished results from a PTR-TOF 8000 (kindly recorded by Michaela Malásková from the Institute of Breath research, University of Innsbruck, Austria, for reasons given below) and results from a SIFT-MS study [117].

Seven product ions resulting from the reaction of isoflurane with H_3O^+ ; namely (using the lightest isotopomer) m/z 51 (CHF_2^+), m/z 67 (CHFCl^+), m/z 115 ($\text{C}_2\text{H}_2\text{F}_2\text{ClO}^+$), m/z 117 ($\text{C}_2\text{HF}_3\text{Cl}^+$), m/z 145 ($\text{C}_3\text{HF}_3\text{ClO}^+$), m/z 163 ($\text{C}_3\text{F}_4\text{ClO}^+$) and m/z 165 ($\text{C}_3\text{H}_2\text{F}_4\text{ClO}^+$). The most intense product ion observed at 140 Td is m/z 67 (40 %) and this is followed by m/z 51 (31%) and m/z 117 (16%). The full product ion branching percentages over an E/N range of 80 to 220 Td are provided in figure 6.6. The product ion branching ratios for CHF_2^+ and CHFCl^+ increase as the reduced electric field increases. However, the branching ratios for other product ions decrease as the reduced electric field increases as the result of more fragmentation occurring as the collisional energies of both the reagent ions and product ions increase with increasing E/N .

The only other published PTR-MS study is by Fernandez del Rio et al. [72], who used an Ionicon PTR-Quad-MS, and covered the range of reduced electric fields from 95 to 140 Td, finding identical ions to ours, other than $\text{C}_3\text{HF}_3\text{ClO}^+$ which was not observed

by them. This is surprising given its relatively good branching percentage at low E/N . However, at an E/N of 140 Td the branching percentage associated with this channel is small, and hence the branching percentages of the ions measured by the PTR-Quad-MS and KORE PTR-ToF-MS at 140 Td should be similar. Certainly, there are some similarities. For example, the most abundant ion at 140 Td in Fernandez del Rio et al. study is at m/z 67 (CHFCl^+) (50%), which is consistent with our results, although with a lower percentage at 40%. The rest of the ion branching percentages are, however, significantly different. This is illustrated at 140 Td in table 6.3, which compares the results of our measurements with those of Fernandez del Rio et al. These disparities in the branching percentages between the two studies must result from differences in the transmission properties of the mass spectrometers (quadrupole versus ToF), the efficiency of the detectors and the transfer optics of the two instruments as a function of m/z .

This significant difference in product ions between PTR-MS instruments is an important issue and has only recently been raised as an issue in the literature [118]. To ascertain whether there is a difference between different PTR-ToF-MS instruments, isoflurane measurements at 140 Td on an IONICON PTR-ToF-8000 was undertaken. The results are presented in table 6.3. From that table, it can be seen that the branching percentages qualitatively agree with each other, but quantitatively they are different. This must be a result again of differences in transmission and detection efficiencies between the two instruments. Another issue to consider is that little is known about the internal energy of the reagent ion. Owing to differences in its formation in the hollow cathode, it could enter the drift tube with different internal energies. Only one study so far has tried to investigate this [109] and in that study, it was found that product ion distributions change according to hollow cathode

current. The key message here is that the product ion branching percentages must be measured for individual instruments in order to determine their sensitivities for analytical purposes.

No protonated parent ion was detected in this study or the earlier PTR-MS study for any value of the reduced electric field. That no protonated parent was observed is in agreement with that found in the SIFT-MS studies by Wang et al., in which they found six product fragment ions at m/z 67 (CHF_2O^+), m/z 99 ($\text{C}_2\text{H}_2\text{F}_3\text{O}^+$), m/z 117 ($\text{C}_2\text{HF}_3\text{Cl}^+$) and m/z 119 ($\text{C}_2\text{H}_3\text{F}_4\text{O}^+$), m/z 147 ($\text{C}_3\text{H}_3\text{F}_3\text{ClO}^+$) and m/z 165 ($\text{C}_3\text{H}_2\text{F}_4\text{ClO}^+$) [115]. That no protonated parent is observed is important, because our DFT (Density functional theory) calculations show that the proton affinity of isoflurane is close to that of water (Appendix 2). According to Dr Peter Watts', DFT calculation (please see appendix 2), there are three sites for protonation on the isoflurane molecule. He also has shown the possible formation and fragmentation.

These calculations are in agreement with the measurements of Wang et al.[115] who obtained a reaction rate coefficient ($3.4 \times 10^{-9} \text{ cm}^3 \text{ s}^{-1}$) which is only slightly less than the collisional value ($3.5 \times 10^{-9} \text{ cm}^3 \text{ s}^{-1}$). The difference implies that the reaction of H_3O^+ with isoflurane is marginally endothermic, meaning that the proton affinity of isoflurane must be slightly less than that of water (by a few kJ/mol). Thus if the protonated parent did not fragment instantaneously then it would back react with the high concentrations of water in the PTR-MS drift tube, resulting in a lower observed signal (as found for example with protonated formaldehyde in a PTR-MS [1]), resulting in less sensitivity for its detection.

In this study, there were no product ions associated with CHF_2O^+ (nominal m/z 67), m/z 99, m/z 119 and m/z 147 ($\text{C}_3\text{H}_3\text{F}_3\text{ClO}^+$) observed, with the latter confirmed from

the lack of any m/z 149 and the correct isotope abundance of our m/z 147 relative to m/z 145 in our measurements. For m/z 67 (nominally) is not assigned to CHF_2O^+ because m/z 69 is seen in the correct isotope ratio expected for chlorine. Differences between SIFT-MS and PTR-MS results can again be explained by the nature of the collisional energies involved in the two techniques and the types of detection mass spectrometers used (SIFT-MS used a quadrupole mass filter).

Table 6.3 m/z values of the product ions and neutral species and their branching percentages resulting from the reaction of isoflurane with H_3O^+ at a reduced electric field of 140 Td for a KORE PTR-ToF-MS, an IONICON PTR-Quad-MS, and an IONICON PTR-TOF 800 (Michaela Malásková, Institute of Breath research, University of Innsbruck, Austria). For comparison the results from the SIFT-MS study [117] are also provided.

Name/ Formula	Product ion m/z	Product ion molecular formula	Neutral Products	PTR-ToF- MS(KORE) %	PTR- Quad- MS %	SIFT- MS % [115]	PTR-ToF- MS IONICON %
Isoflurane $\text{C}_3\text{H}_2\text{F}_5\text{ClO}$	51	CHF_2^+	$\text{C}_2\text{H}_2\text{F}_3\text{ClO}$	31	12	-	16
	67	CHF_2O^+	$\text{C}_2\text{H}_2\text{F}_3\text{Cl}$	-	-	15	-
184	67+69	CHFCl^+	$\text{C}_2\text{H}_2\text{F}_4\text{O}$	40	50	-	47
	99	$\text{C}_2\text{H}_2\text{F}_3\text{O}^+$	CHF_2Cl	-	-	10	-
	115+117	$\text{C}_2\text{H}_2\text{F}_2\text{ClO}^+$	CF_3	2	-	-	-
	117+119	$\text{C}_2\text{HF}_3\text{Cl}^+$	$\text{CH}_2\text{F}_2\text{O}$	16	6	30	28
	119	$\text{C}_2\text{H}_3\text{F}_4\text{O}^+$	CClF	-	-	25	-
	145+147	$\text{C}_3\text{HF}_3\text{ClO}^+$	$\text{C}_2\text{F}_2\text{Cl}$	1	-	-	-
	147+149	$\text{C}_3\text{H}_3\text{F}_3\text{ClO}^+$	F_2	-	-	10	-
	163+165	$\text{C}_3\text{F}_4\text{ClO}^+$	$\text{HF} + \text{H}_2$	2	24	-	7
	165+167	$\text{C}_3\text{H}_2\text{F}_4\text{ClO}^+$	HF	8	8	10	2

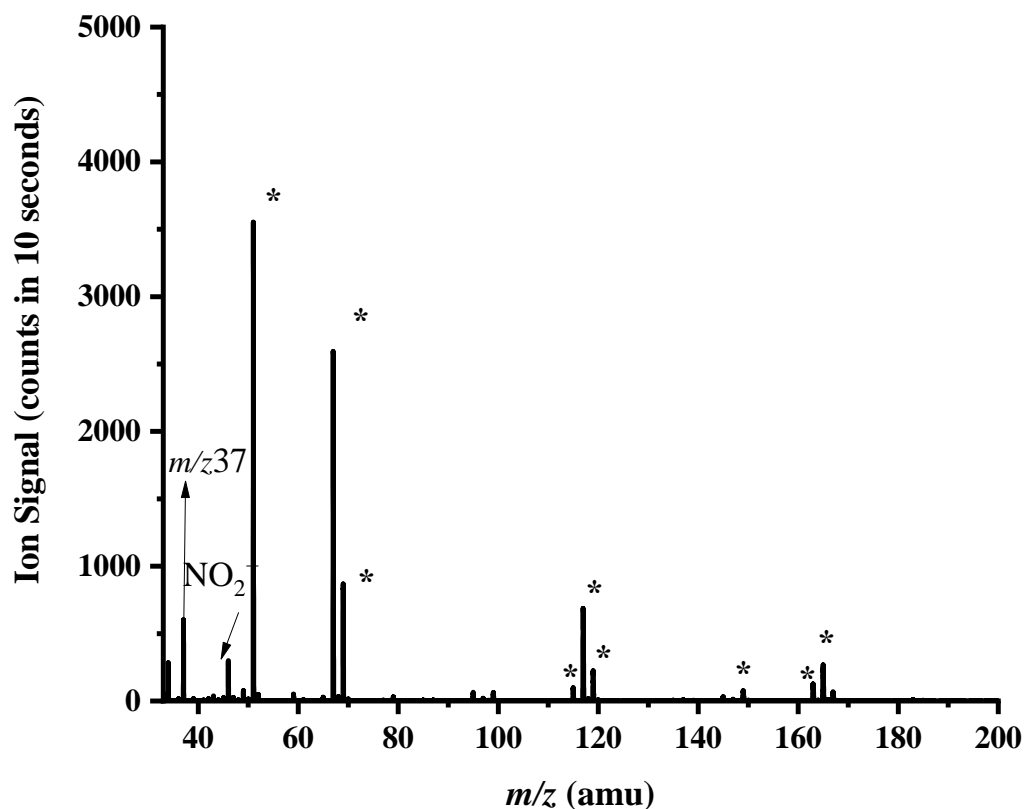
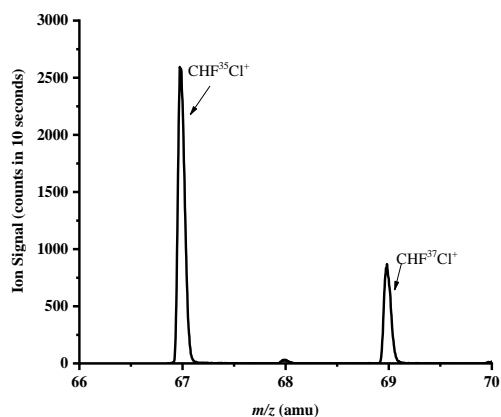
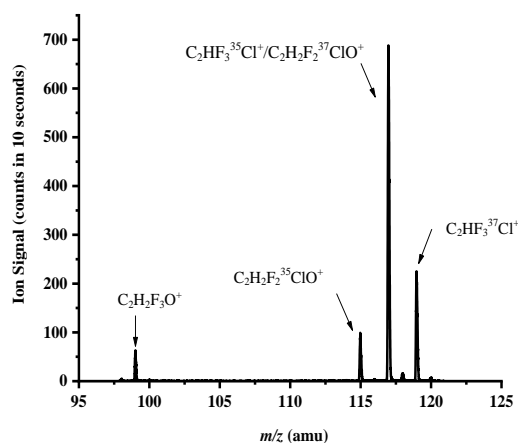


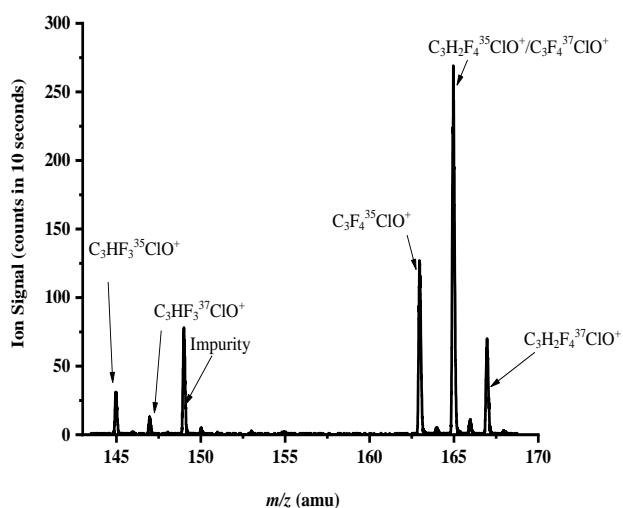
Figure 6.4 A mass spectrum illustrating the product ions (starred) resulting from the reaction of H_3O^+ with isoflurane ($\text{C}_3\text{H}_2\text{F}_5\text{ClO}$) whilst operating the drift tube at a reduced electric field of 140 Td. Other ions such as the protonated water dimer, m/z 37, and an impurity ion (NO_2^+) coming from the ion source are also highlighted. (That observation shown there is no change in the NO_2^+ signal with and without isoflurane, indicates that the ionisation energy of isoflurane is greater than that of NO_2 (9.6 eV).) The ionisation energy of isoflurane is not available in the literature, but that for an isomeric form, enflurane, is, which is at 11.7 eV.



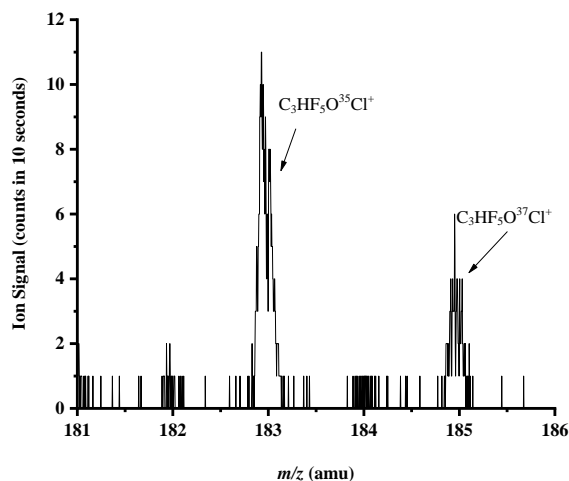
a)



b)



c)



d)

Figure 6.5 Expanded figure of the product ions resulting from the reactions of H_3O^+ with isoflurane to illustrate their isotopic abundances for a) m/z 67 ($\text{CHF}^{35}\text{Cl}^+$) and m/z 69 ($\text{CHF}^{37}\text{Cl}^+$) b) m/z 99 ($\text{C}_2\text{H}_2\text{F}_3\text{O}^+$), m/z 115 ($\text{C}_2\text{H}_2\text{F}_2^{35}\text{ClO}^+$), m/z 117 ($\text{C}_2\text{HF}_3^{35}\text{Cl}^+/\text{C}_2\text{H}_2\text{F}_2^{37}\text{ClO}^+$) and m/z 119 ($\text{C}_2\text{HF}_3^{37}\text{Cl}^+$) c) m/z 145 ($\text{C}_3\text{HF}_3^{35}\text{ClO}^+$), m/z 147 ($\text{C}_3\text{HF}_3^{37}\text{ClO}^+$), m/z 149 (Impurity), m/z 163 ($\text{C}_3\text{F}_4^{35}\text{ClO}^+$), m/z 165 ($\text{C}_3\text{H}_2\text{F}_4^{35}\text{ClO}^+/\text{C}_3\text{F}_4^{37}\text{ClO}^+$) and m/z 167 ($\text{C}_3\text{H}_2\text{F}_4^{37}\text{ClO}^+$) d) m/z 183 ($\text{C}_3\text{HF}_5^{35}\text{ClO}^+$) and m/z 185 ($\text{C}_3\text{HF}_5^{37}\text{ClO}^+$).

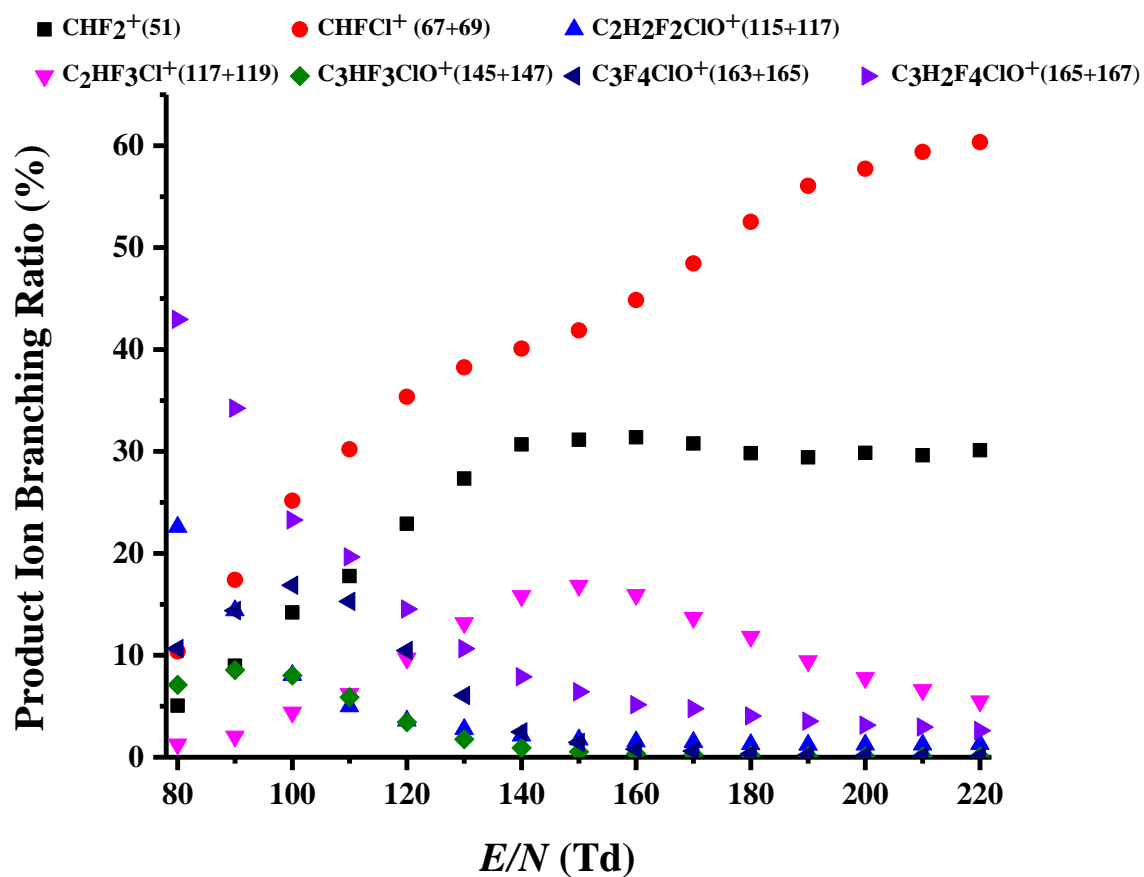


Figure 6.6 Product ion branching ratios in percentages as a function of reduced electric field (E/N) resulting from the reaction of H_3O^+ with isoflurane ($\text{C}_3\text{H}_2\text{F}_5\text{ClO}$).

6.3.2.2 Reaction with O_2^+

Figure 6.7 presents the mass spectrum resulting from the reaction isoflurane with O_2^+ . The details of the product ions branching percentages at a reduced electric field of 140 Td are presented in table 6.4. All the results take into account isotopic abundance. For comparison the results from the (Thermal) SIFT-MS study are also provided [117].

Eleven product ions were observed resulting from charge transfer; namely (and using the lightest isotopomer) m/z 51 (CHF_2^+), m/z 67 ($CHFCI^+$), m/z 99 ($C_2F_3H_2O^+$), m/z 115 ($C_2H_2F_2ClO^+$), m/z 117 ($C_2HF_3Cl^+$), m/z 145 ($C_3HF_3ClO^+$), m/z 149 ($C_3H_2F_5O^+$), m/z 163 ($C_3F_4ClO^+$), m/z 165 ($C_3H_2F_4ClO^+$), m/z 181 ($C_3H_2F_4ClO_2^+$) and m/z 183 ($C_3HF_5ClO^+$). All of these ions can be seen at 140 Td except $C_3H_2F_4ClO_2^+$. That is only observed at low E/N with a relatively low intensity. The most abundant product ions from this study at 140 Td are m/z 67 ($CHFCI^+$) (36%), m/z 51 (CHF_2^+) (23%) followed by m/z 117 ($C_2HF_3Cl^+$) (11%). The details of the complete spectrum of isoflurane reaction with O_2^+ is presented in figure 6.8 (a)-(d).

In comparison to our observations, Wang et al. only report four product ions using SIFT. Their product ions are m/z 69 (CF_3^+), m/z 99 ($C_2F_3H_2O^+$), m/z 115 ($C_2H_2F_2ClO^+$) and m/z 149 ($C_3H_2F_5O^+$). The common ions found between Wang's study and ours are at m/z 99 ($C_2F_3H_2O^+$), m/z 115 ($C_2H_2F_2ClO^+$) and m/z 149 ($C_3H_2F_5O^+$), however with significantly different branching percentages. This is because ion-molecule reactions in the flow tube of a SIFT-MS are at thermal energies as has been mentioned in section 6.3.1.2 (reaction with O_2^+).

Table 6.4 m/z values of the product ions and their branching ratio percentages resulting from the reaction of isoflurane with O_2^+ at a reduced electric field of 140 Td using the KORE PTR-ToF-MS in comparison to SIFT-MS results published by Wang et al. [72].

Name/ Formula	Product ion m/z	Product ion molecular formula	Neutral Products	PTR- ToF- MS %	SIFT- MS %
Isoflurane	51	CHF_2^+	C_2HF_3ClO	23	-
$C_3H_2F_5ClO$	67+69	$CHFCl^+$	C_2HF_4O	36	-
m/z 184	69	CF_3^+	$C_2H_2F_2ClO$	-	10
	99	$C_2F_3H_2O^+$	CF_2Cl	2	20
	115+117	$C_2H_2F_2ClO^+$	CF_3	7	45
	117+119	$C_2HF_3Cl^+$	CHF_2	11	-
	145+147	$C_3HF_3ClO^+$	HF_2	2	-
	149	$C_3H_2F_5O^+$	Cl	6	25
	163+165	$C_3F_4ClO^+$	H_2F	6	-
	165+167	$C_3H_2F_4ClO^+$	F	6	-
	181+183	$C_3H_2F_4ClO_2^+$	FO	0	-
	183+185	$C_3HF_5ClO^+$	H	1	-

Also, in the study by Wang et al., the dominant ion was found to be $C_2H_2F_2ClO^+$ (45 %) corresponding to a loss of CF_3 from the charged parent, whereby in this study this product ion only has a branching percentage of 7 %.

According to PubChem Chemistry database [119], the most dominant peak from 70 eV electron impact (EI) technique is m/z 51 (CHF_2^+) (100), followed by m/z 149 ($C_3H_2F_5O^+$) (~25) and m/z 117 ($C_2HF_3Cl^+$) (~20). Similar product ions were found from this study for isoflurane but the abundance of each ion are different. Then there are a large number of fragment ions (intensities less than 20) in the EI mass spectrum, which are not observed in our PTR-MS study owing to its softer ionisation process. EI which has been used in mass spectrometry leads to excess energy and extensive fragmentation. However, excessive fragmentation will cause difficulty in finding a peak which can be associated to the molecule especially for the parent ion.

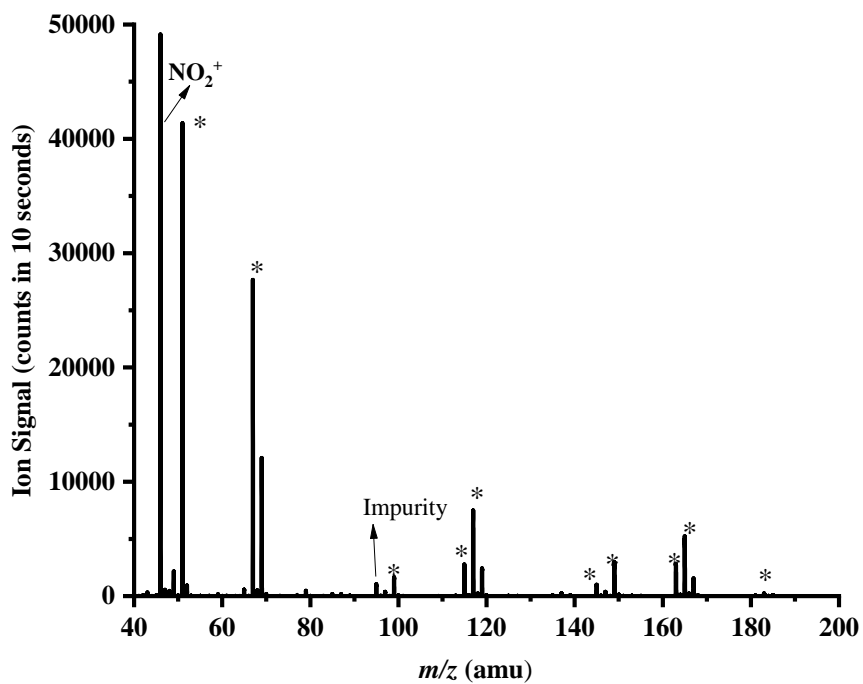


Figure 6.7 A mass spectrum illustrating the product ions (starred) resulting from the reaction of O_2^+ with isoflurane ($\text{C}_3\text{H}_2\text{F}_5\text{ClO}$) whilst operating the drift tube at a reduced electric field of 140 Td. Other ions such as an impurity ion (NO_2^+) coming from the ion source are also highlighted.

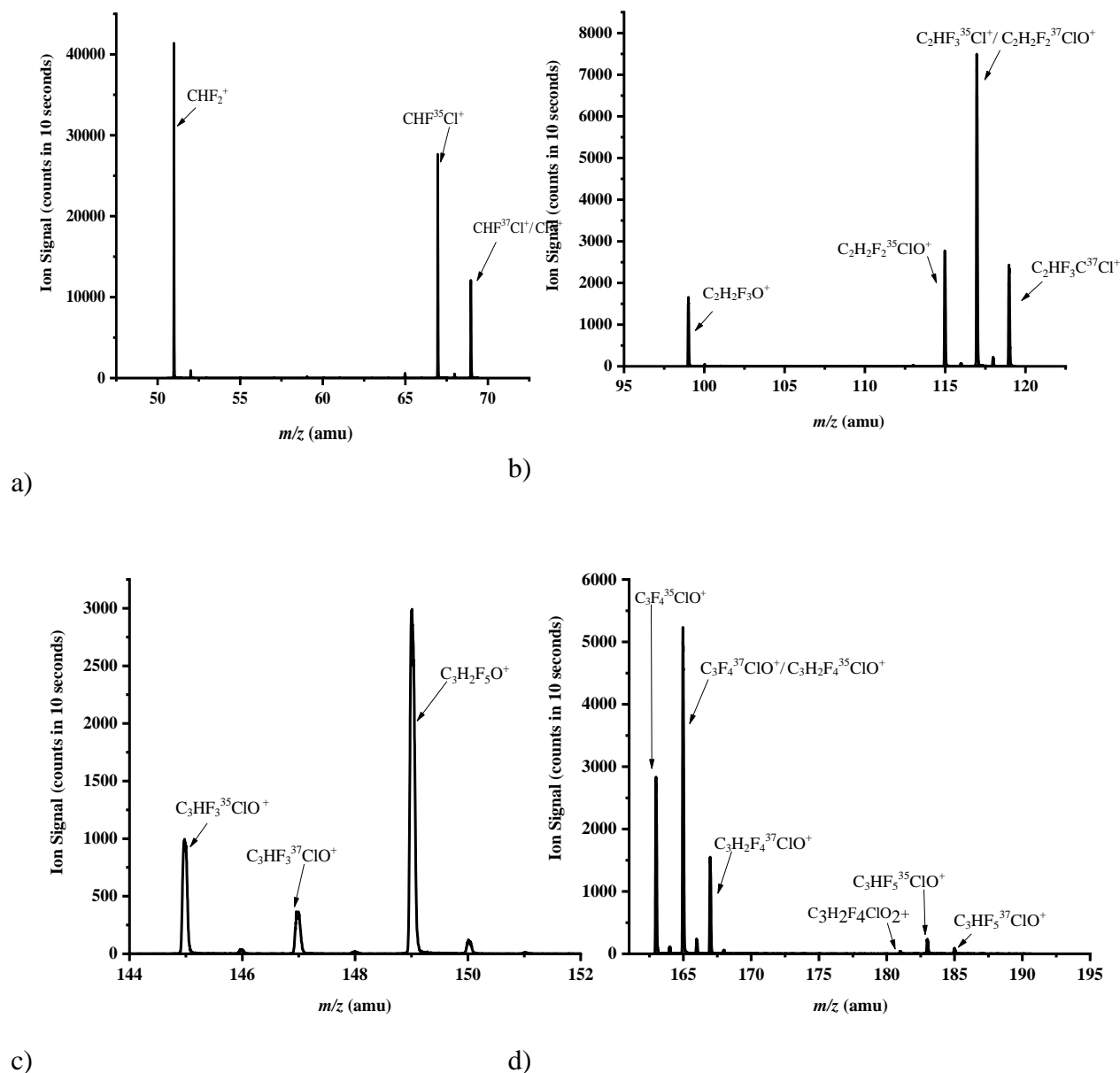


Figure 6.8 Expanded figure of the product ions resulting from the reactions of O_2^+ with isoflurane to illustrate their isotopic abundances a) m/z 51 (CHF_2^+), m/z 67 ($\text{CHF}^{35}\text{Cl}^+$) and m/z 69 ($\text{CHF}^{37}\text{Cl}^+/\text{CF}_3^+$) b) m/z 99 ($\text{C}_2\text{H}_2\text{F}_3\text{O}^+$), m/z 115 ($\text{C}_2\text{H}_2\text{F}_2^{35}\text{ClO}^+/\text{C}_2\text{H}_2\text{F}_2^{37}\text{ClO}^+$) and m/z 119 ($\text{CHF}_3\text{C}^{37}\text{Cl}$) c) m/z 145 ($\text{C}_3\text{HF}_3^{35}\text{ClO}^+$), m/z 147 ($\text{C}_3\text{HF}_3^{37}\text{ClO}^+$) and m/z 149 ($\text{C}_3\text{H}_2\text{F}_5\text{O}^+$) d) m/z 163 ($\text{C}_3\text{F}_4^{35}\text{ClO}^+$), m/z 165 ($\text{C}_3\text{F}_4^{37}\text{ClO}^+/\text{C}_3\text{H}_2\text{F}_4^{35}\text{ClO}^+$), m/z 167 ($\text{C}_3\text{H}_2\text{F}_4^{37}\text{ClO}^+$), m/z 181 ($\text{C}_3\text{H}_2\text{F}_4\text{ClO}_2^+$) m/z 183 ($\text{C}_3\text{HF}_5^{35}\text{ClO}^+$) and m/z 185 ($\text{C}_3\text{HF}_5^{37}\text{ClO}^+$).

Figure 6.9 represents how the product ion distributions vary as a function of the reduced electric field. CHF_2^+ is the dominant ion from 110 Td-220 Td. The branching ratios for CHF_2^+ and CHFCI^+ increase as the reduced electric field increase. But the branching for $\text{C}_2\text{F}_3\text{H}_2\text{O}^+$, $\text{C}_2\text{H}_2\text{F}_2\text{ClO}^+$ and $\text{C}_3\text{F}_4\text{ClO}^+$ decrease owing to increased fragmentation as the collisional energies of both the reagent ions and product ions increase with increasing E/N .

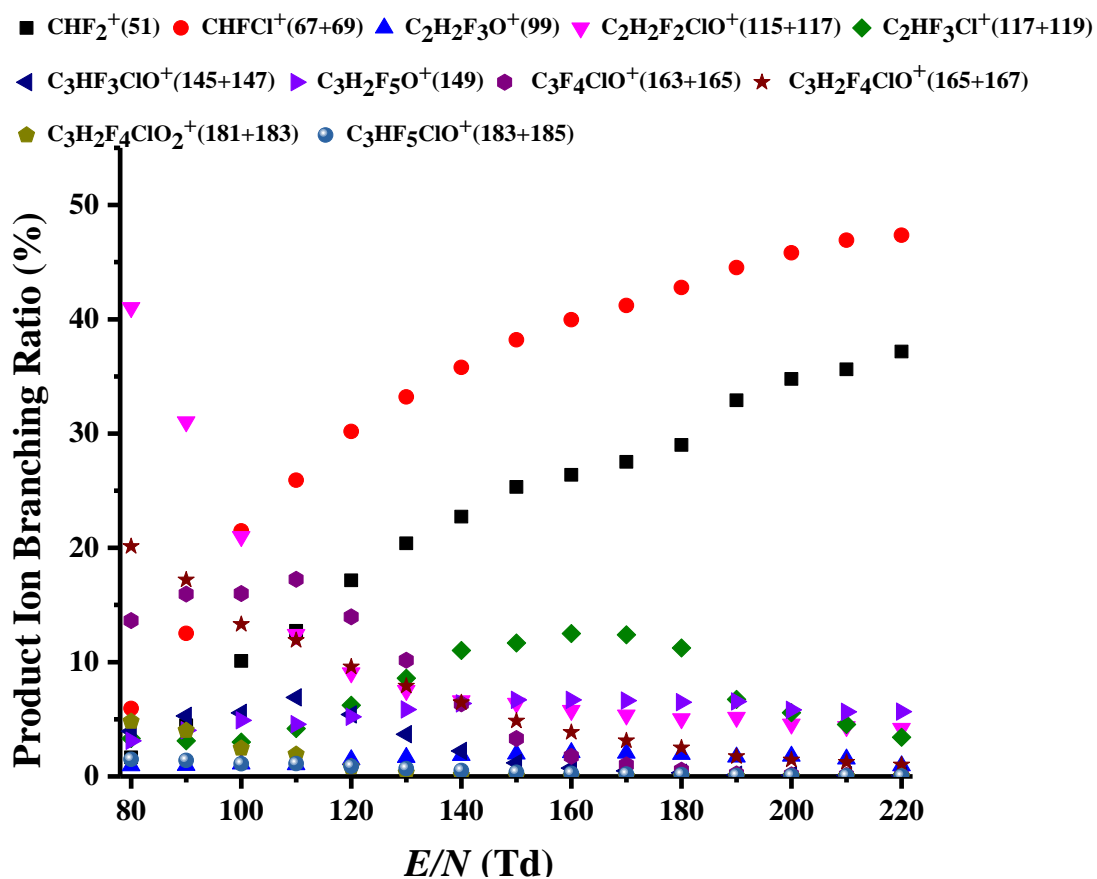


Figure 6.9 Product ion branching ratios in percentages as a function of E/N resulting from the reaction of O_2^+ with isoflurane ($\text{C}_3\text{H}_2\text{F}_5\text{ClO}$).

6.3.3 Enflurane

Enflurane is a structural isomer of isoflurane, and therefore it is of interest to investigate if there are any changes in the ion-chemistry as a result of this, that could provide a method to distinguish one isomer from another.

6.3.3.1 Reaction with O_2^+

This is the first reported PTR-MS study of the reactions of enflurane, an isomer of isoflurane, with O_2^+ . The ionization energy of enflurane is 11.7 eV [4] whereas the recombination energy of O_2^+ is 12.07 eV. Therefore, charge transfer is exothermic by only about 0.37 eV. In our study no parent ion was observed, instead there is enough energy in the reaction for dissociative charge transfer to occur. Figure 6.10 presents the mass spectrum resulting from the reaction of enflurane with O_2^+ at 140 Td. Figure 6.11 (a)-(e) shows the product ions at this reduced electric field in more detail.

Table 6.5 summarizes the results of the enflurane reactions with O_2^+ at 140 Td for measurements taken on the KORE PTR-ToF-MS. Nevertheless, substantial dissociative charge transfer is observed, as highlighted in the table below (table 6.5). Seven product ions were observed, namely (and using the lightest isotopomer) m/z 51 (CHF_2^+), m/z 67 ($CHFCl^+$), m/z 69 (CF_3^+), m/z 98 ($C_2HF_2Cl^+$), m/z 113 ($C_2F_2ClO^+$), m/z 115 ($C_2H_2F_2ClO^+$) and m/z 117 ($C_2HF_3Cl^+$). The most abundant ion at 140 Td is m/z 67 ($CHFCl^+$) (table 6.5 and figure 6.11) which contributes 32 % to the branching ratio. This is followed by CHF_2^+ (27 %), $C_2HF_2Cl^+$ (26 %), and then the rest of the product ions contribute less than 5 %.

Isoflurane reactions with O_2^+ produced eleven product ions. Some identical ions from both measurement are m/z 51 CHF_2^+ , m/z 67 $CHFCl^+$, m/z 115 $C_2H_2F_2ClO^+$ and m/z 117 $C_2HF_3Cl^+$. Also, some additional ions were found from isoflurane reactions with O_2^+ compared to enflurane such as m/z 99 ($C_2F_3H_2O^+$), m/z 145 ($C_3HF_3ClO^+$), m/z 149

$C_3H_2F_5O^+$, m/z 163 ($C_3F_4ClO^+$), m/z 165 $C_3H_2F_4ClO^+$, m/z 181 $C_3H_2F_4ClO_2^+$, and m/z 183 ($C_3HF_5ClO^+$).

Table 6.5 m/z values of the product ions and their branching ratio percentages resulting from the reaction of enflurane with O_2^+ at a reduced electric field of 140 Td using the KORE PTR-ToF-MS.

Name/ Formula	Product ion m/z	Product ion Molecular formula	Neutral Products	PTR-ToF- MS (KORE) %
Enflurane	51	CHF_2^+	C_2HF_3ClO	27
$C_3H_2F_5ClO$	67+69	$CHFCl^+$	C_2HF_4O	32
184	69	CF_3^+	C_2F_2OCl	4
	98+100	$C_2HF_2Cl^+$	CHF_3O	26
	113+115	$C_2F_2ClO^+$	CH_2F_3	4
	115+117	$C_2H_2F_2ClO^+$	CF_3	3
	117+119	$C_2HF_3Cl^+$	CHF_2O	4

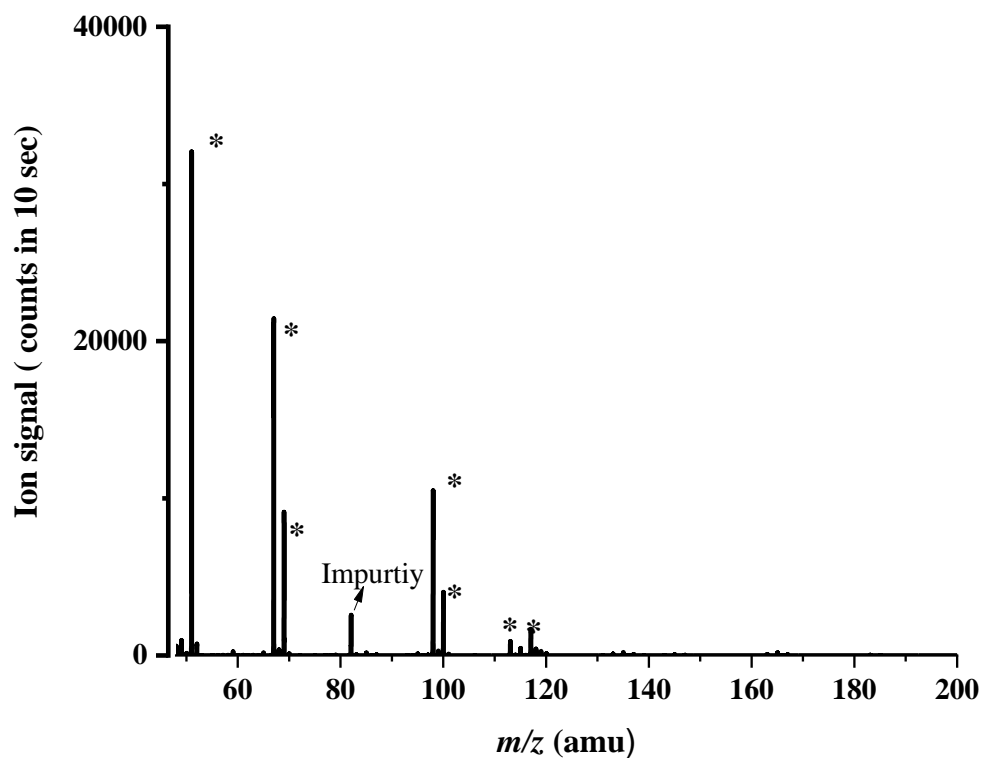


Figure 6.10 A mass spectrum illustrating the product ions (starred) resulting from the reaction of O_2^+ with enflurane ($C_3H_2F_5ClO$) whilst operating the drift tube at a reduced electric field of 140 Td. Other ions present, such as an impurity ion coming from the sample are also highlighted.

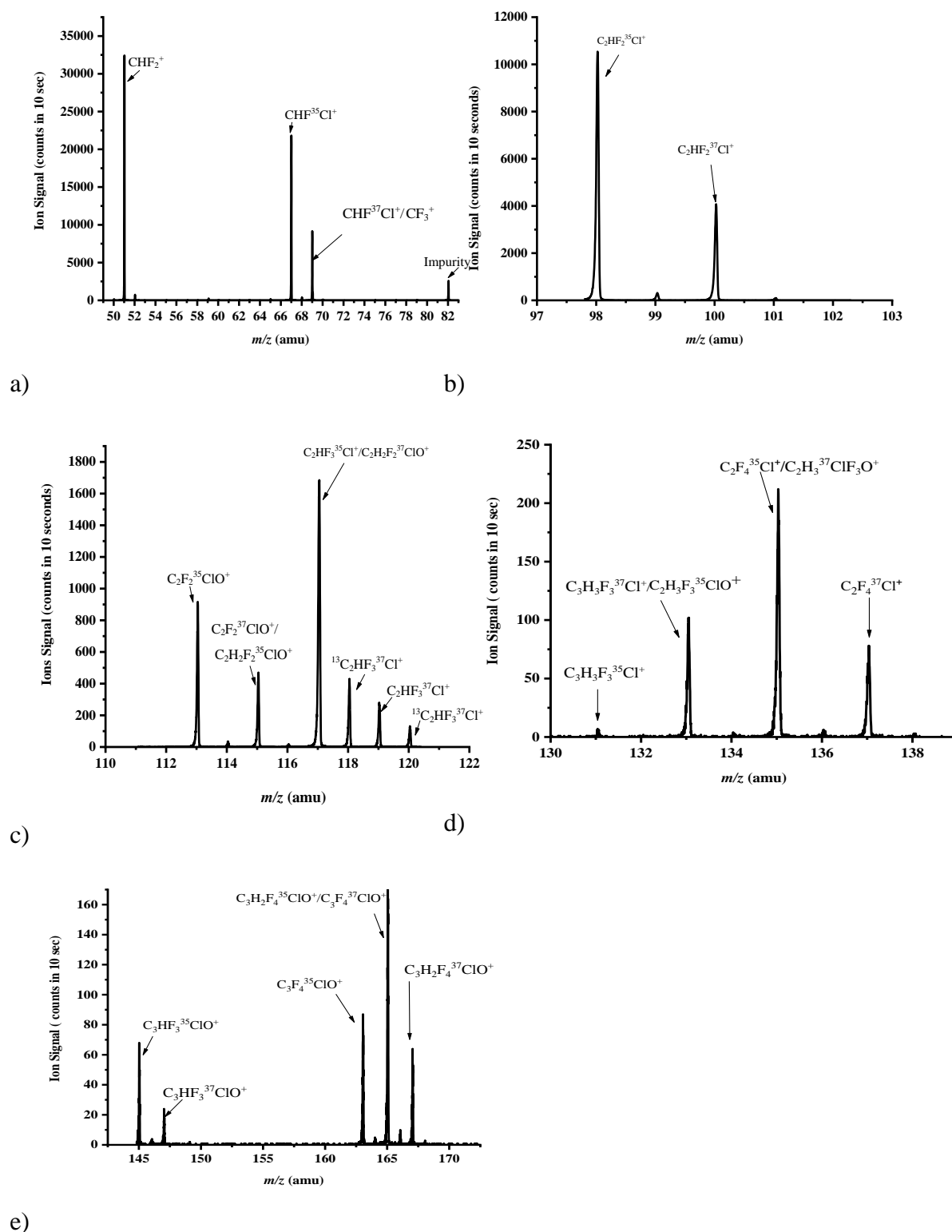


Figure 6.11 Expanded figure of the product ions resulting from the reactions of O_2^+ with enflurane to illustrate their isotopic abundances for a) m/z 51 (CHF_2^+), m/z 67 ($CHF^{35}Cl^+$), m/z 69 ($CHF^{37}Cl^+/CF_3^+$) and m/z 82 (Impurity) b) m/z 98 ($C_2HF_2^{35}Cl^+$) and m/z 100 ($C_2HF_2^{37}Cl^+$) c) m/z 113 ($C_2F_2^{35}ClO^+$), m/z 115 ($C_2F_2^{37}ClO^+/C_2H_2F_2^{35}ClO^+$), m/z 117 ($C_2HF_3^{35}Cl^+/C_2H_2F_2^{37}ClO^+$) and m/z 119 ($C_2HF_3^{37}Cl^+$) d) m/z 131 ($C_3H_3F_3^{37}Cl^+/C_2H_3F_3^{35}ClO^+$), m/z 133 ($C_3H_3F_3^{35}Cl^+$) and m/z 137 ($C_2F_4^{37}Cl^+$) e) m/z 145 ($C_3HF_3^{35}ClO^+$), m/z 147 ($C_3HF_3^{37}ClO^+$), m/z 163 ($C_3F_4^{35}ClO^+$), m/z 165 ($C_3H_2F_4^{35}ClO^+/C_3F_4^{37}ClO^+$) and m/z 167 ($C_3H_2F_4^{37}ClO^+$).

Figure 6.12 illustrates how the product ion distributions vary as a function of the reduced electric field. m/z 51 (CHF_2^+) and m/z 67 (CHFCl^+) are dominant ions from 150 Td to 220 Td and their branching ratio increase owing to more fragmentation as the collisional energies of both the reagent ions and product ions increase with increasing E/N .

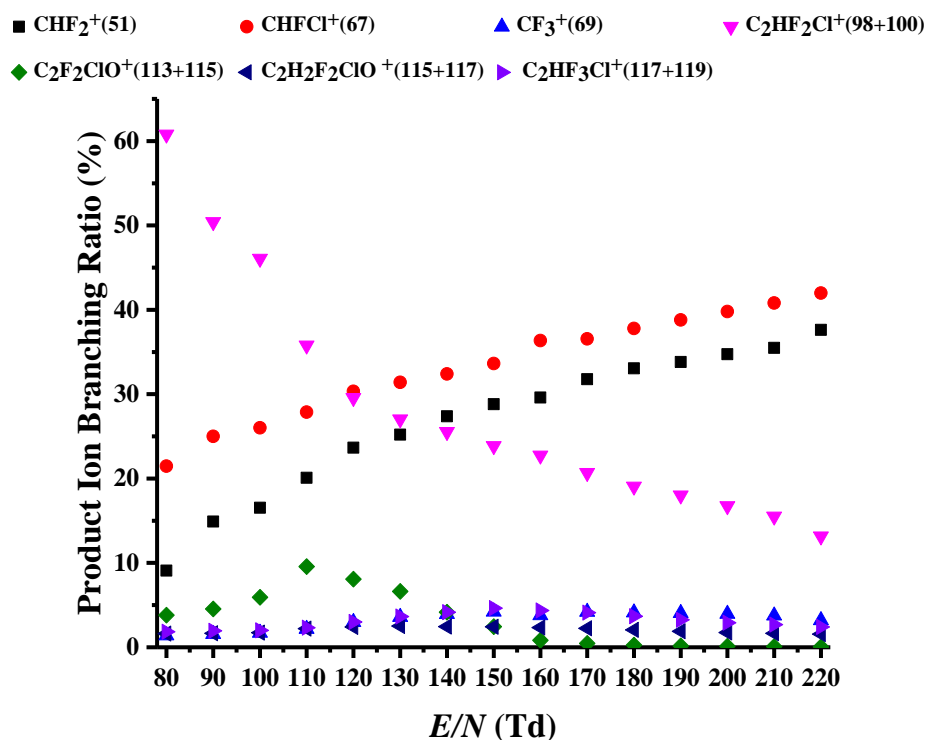


Figure 6.12 Product ion branching ratios in percentages as a function of E/N resulting from the reaction of O_2^+ with enflurane ($\text{C}_3\text{H}_2\text{F}_5\text{ClO}$).

6.3.3.2 Reaction with of H_3O^+

This is the first reported PTR-MS study of the reactions of enflurane with H_3O^+ . Figure 6.13 presents an overview of the mass spectrum resulting from the reaction of enflurane with H_3O^+ at 140 Td including other ions present in the drift tube. Figure 6.14 shows the details of product ions. Figure 6.15 represents the product ion branching ratios in percentages as a function of E/N resulting from the reaction of H_3O^+ with enflurane ($\text{C}_3\text{H}_2\text{ClF}_5\text{O}$).

Table 6.6 illustrates the main product ions of enflurane reactions with H_3O^+ . The results of this study show that there were nine product ions. The observed product ions are identified as (using the lightest isotopomer), m/z 51 (CHF_2^+), m/z 67 (CHFCl^+), m/z 98 ($\text{C}_2\text{HF}_2\text{Cl}^+$), m/z 113 ($\text{C}_2\text{F}_2\text{ClO}^+$), m/z 115 ($\text{C}_2\text{H}_2\text{F}_2\text{ClO}^+$), m/z 117 ($\text{C}_2\text{HF}_3\text{Cl}^+$), m/z 131 ($\text{C}_3\text{H}_3\text{F}_3\text{Cl}^+$), m/z 133 ($\text{C}_2\text{HF}_3\text{ClO}^+$) and m/z 163 ($\text{C}_3\text{F}_4\text{ClO}^+$) at 140 Td. The most intense product ion which has contributed 61 % at 140 Td is m/z 113. This is followed by m/z 131 (12 %) and m/z 115 (11 %). The other product ions contributed less than 10 % of the branching ratios are m/z 67 and 163. The m/z 51(CHF_2^+) branching ratio increased with the reduced electric field strength as the collisional energy increased. No protonated parent was observed.

Table 6.6 m/z values of the product ions and their branching ratio percentages resulting from the reaction of enflurane with H_3O^+ at a reduced electric field of 140 Td using a KORE PTR-ToF-MS. The IONICON PTR-ToF-MS results are presented for comparison (courtesy of Michaela Malásková from the Institute of Breath research, University of Innsbruck, Austria).

Name/ Formula	Product ion m/z	Product ion	Neutral Products	PTR- ToF-MS (KORE) (%)	PTR-ToF- MS (Innsbruck)
Enflurane	51	CHF_2^+	$\text{C}_2\text{H}_2\text{F}_3\text{ClO}$	1	8
$\text{C}_3\text{H}_2\text{ClF}_5\text{O}$	67+69	CHFCl^+	$\text{C}_2\text{H}_2\text{F}_4\text{O}$	7	66
184	98+100	$\text{C}_2\text{HF}_2\text{Cl}^+$	$\text{CH}_2\text{F}_3\text{O}$	<1	-
	113+115	$\text{C}_2\text{F}_2\text{ClO}^+$	CH_3F_3	61	11
	115+117	$\text{C}_2\text{H}_2\text{F}_2\text{ClO}^+$	CHF_3	11	1
	117+119	$\text{C}_2\text{HF}_3\text{Cl}^+$	$\text{CH}_2\text{F}_2\text{O}$	1	12
	131+133	$\text{C}_3\text{H}_3\text{F}_3\text{Cl}^+$	F_2O	12	-
	133+135	$\text{C}_2\text{HF}_3\text{ClO}^+$	CH_2F_2	2	-
	163+165	$\text{C}_3\text{F}_4\text{ClO}^+$	$\text{H}_2 + \text{HF}$	5	1

In comparison to the KORE PTR-ToF-MS results, enflurane measurements with an IONICON PTR_TOF 8000 resulted in completely different branching ratios. Furthermore, no product ions were detected on the IONICON instrument at m/z 98 ($\text{C}_2\text{HF}_2\text{Cl}^+$) m/z 131 ($\text{C}_3\text{H}_3\text{F}_3\text{Cl}^+$), and m/z 133 ($\text{C}_2\text{HF}_3\text{ClO}^+$) for any reduced electric field.

However, it did not produce identical product ions. The similarities between these two compounds are m/z 51 (CHF_2^+), m/z 67 (CHFCl^+), m/z 115 ($\text{C}_2\text{H}_2\text{F}_2\text{ClO}$), m/z 117 ($\text{C}_2\text{H}_2\text{F}_2\text{ClO}$) and m/z 163 ($\text{C}_3\text{F}_4\text{ClO}^+$). In comparison to isoflurane, enflurane has two additional product ions which are $\text{C}_2\text{HF}_2\text{Cl}^+$ and $\text{C}_2\text{F}_2\text{ClO}^+$.

The density molecular calculation by Dr Peter Watts has given as some details about the possible four protonation sites for enflurane (please see Appendix 2 chapter 6).

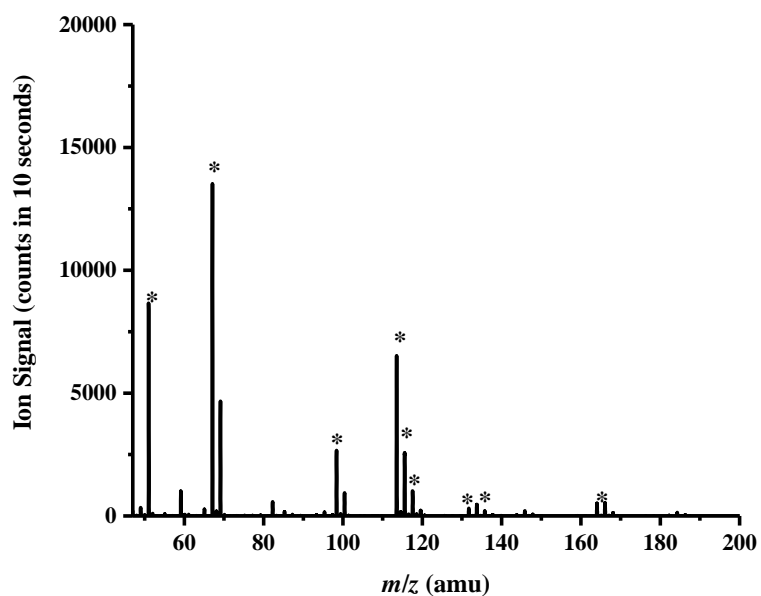


Figure 6.13 A mass spectrum illustrating the product ions (starred) resulting from the reaction of H_3O^+ with enflurane ($\text{C}_3\text{H}_2\text{F}_5\text{ClO}$) whilst operating the drift tube at a reduced electric field of 140 Td.

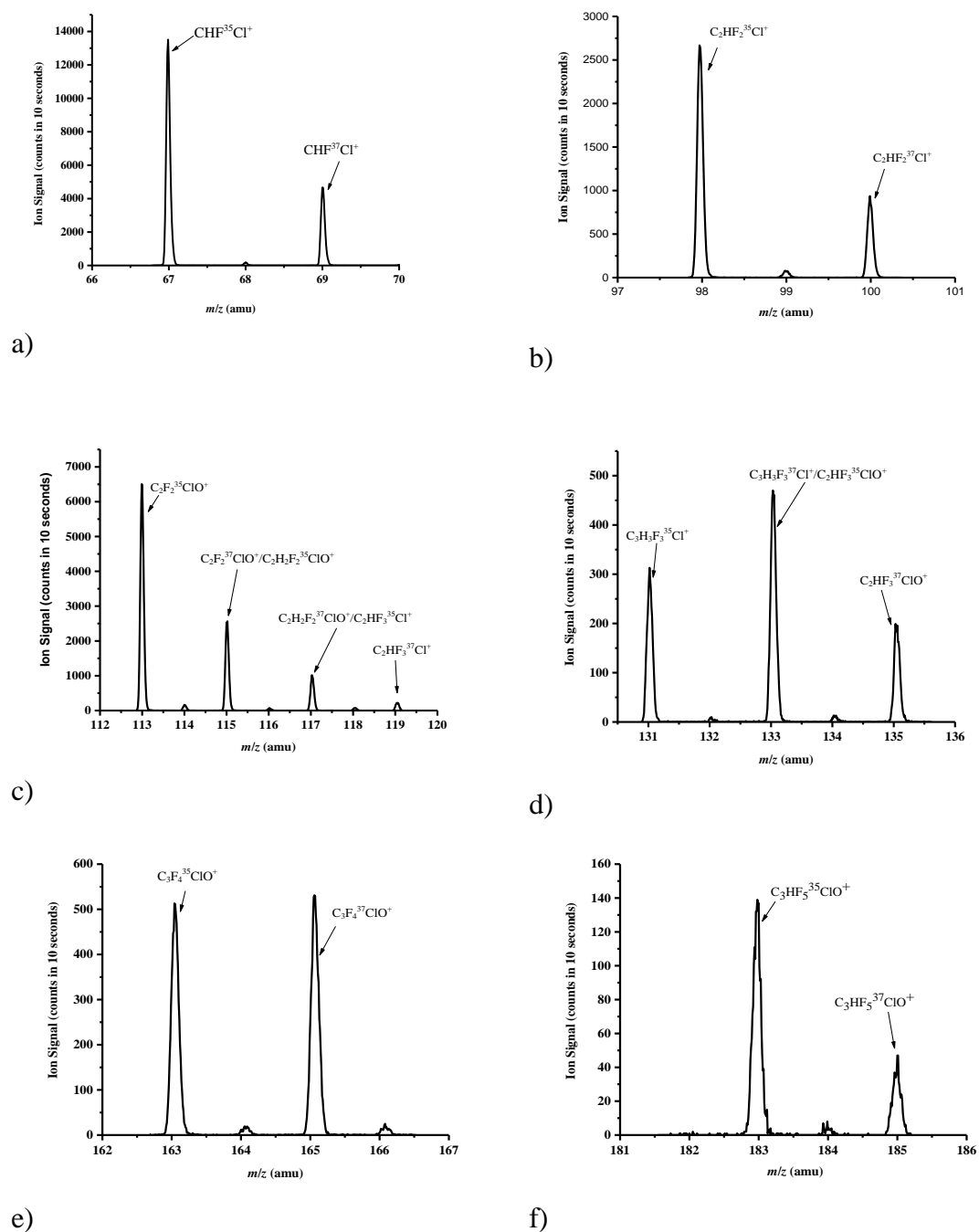


Figure 6.14 Expanded figure of the product ions resulting from the reactions of H_3O^+ with enflurane to illustrate their isotopic abundances a) m/z 67 ($\text{CHF}^{35}\text{Cl}^+$) and m/z 69 ($\text{CHF}^{37}\text{Cl}^+$) b) m/z 98 ($\text{C}_2\text{HF}_2^{35}\text{Cl}^+$) and m/z 100 ($\text{C}_2\text{HF}_2^{37}\text{Cl}^+$) c) m/z 113 ($\text{C}_2\text{F}_2^{35}\text{ClO}^+$), m/z 115 ($\text{C}_2\text{F}_2^{37}\text{ClO}^+/\text{C}_2\text{H}_2\text{F}_2^{35}\text{ClO}^+$), m/z 117 ($\text{C}_2\text{H}_2\text{F}_2^{37}\text{ClO}^+/\text{C}_2\text{HF}_3^{35}\text{Cl}^+$) and m/z 119 ($\text{C}_2\text{HF}_3^{37}\text{Cl}^+$) d) m/z 131 ($\text{C}_3\text{H}_3\text{F}_3^{35}\text{Cl}^+$), m/z 133 ($\text{C}_3\text{H}_3\text{F}_3^{37}\text{Cl}^+/\text{C}_2\text{HF}_3^{35}\text{ClO}^+$) and m/z 135 ($\text{C}_2\text{HF}_3^{37}\text{ClO}^+$) e) m/z 163 ($\text{C}_3\text{F}_4^{35}\text{ClO}^+$) and m/z 165 ($\text{C}_3\text{F}_4^{37}\text{ClO}^+$) f) m/z 183 ($\text{C}_3\text{HF}_5^{35}\text{ClO}^+$) and m/z 185 ($\text{C}_3\text{HF}_5^{37}\text{ClO}^+$).

Figure 6.15 illustrates how the product ion distributions vary as a function of the reduced electric field. m/z 113 ($C_2F_2ClO^+$) is the prominent ion from 110-180 Td but its branching ratio decreases owing to more fragmentation as the collisional energies of both the reagent ions and product ions increase with increasing E/N .

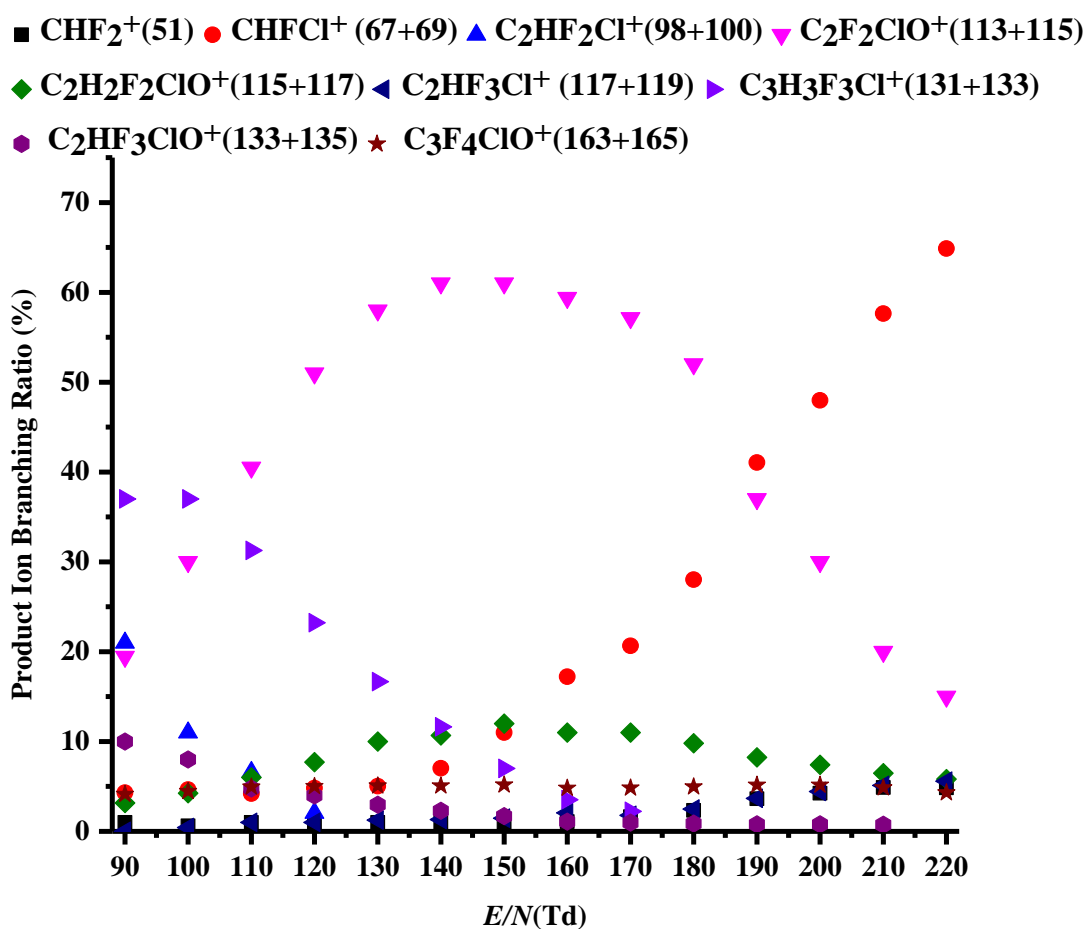


Figure 6.15 Product ion branching ratios in percentages as a function of E/N resulting from the reaction of H_3O^+ with enflurane ($C_3H_2ClF_5O$).

6.3.4 Sevoflurane

6.3.4.1 Reaction with O_2^+

Figure 6.16 shows the mass spectrum resulting from the reaction of sevoflurane with O_2^+ at 140 Td, and figures 6.17 (a)-(c) shows product ions in more detail to illustrate the isotopes.

Table 6.7 gives the m/z values of the product ions, molecular formula and their branching ratio percentages at a reduced electric field of 140 Td. Four product ions were observed which are assigned (using the lightest isotopomer) to be m/z 51 (CHF_2^+), m/z 131 ($C_3H_3F_4O^+$), m/z 181 ($C_4H_3F_6O^+$) and m/z 199 ($C_4H_2F_7O^+$). Among these ions, the dominant product ion at 140 Td, which contributes 35 % to the branching ratio, is m/z 131. The m/z 199, m/z 181 and m/z 51 contribute 28 %, 27 % and 10 %, respectively. m/z 51(CHF_2^+) branching ratio increases as the collisional energy increases. However, for m/z 131 ($C_3H_3F_4O^+$), m/z 181 ($C_4H_3F_6O^+$) and m/z 199 the branching ratios decrease as the collisional energy increase. The branching ratio for CF_3^+ increases after 170 Td.

To our knowledge there has been no other PTR-MS study of sevoflurane with using O_2^+ as the reagent ion. However, Wang et al. report the reactions of sevoflurane with O_2^+ using a SIFT-MS [117]. They observed five product ions. The assignments of ions are; m/z 49 (CH_2FO^+), m/z 129 ($C_3HF_4O^+$), m/z 131 ($C_3H_3F_4O^+$), m/z 181 ($C_4H_3F_6O^+$) and m/z 199 ($C_4H_2F_7O^+$) (table 6.7). The most dominant product ion in their study is m/z 131, the branching percentage of which varies by 70-50 % (the first number indicates shortest reaction length of 3 cm and the second one indicates long reaction length, 40 cm). This was followed by m/z 49 (5-30 %), m/z 181 (15-2 %), m/z 199 (11-4 %) and m/z 129 (5-10 %) [115]. Also, m/z 131 is the dominant product ion in our study. m/z 69 is only observed at high E/N in this study (180 Td).

There are similarities between our PTR-MS and the SIFT-MS studies. However, m/z 49 was not detected in the PTR-MS study. Hence, Wang et al. claimed that m/z 49 is relatively abundant when the reaction length is increased in the SIFT-MS but the dominant product ion remains as $\text{CH}_2\text{FOCH}(\text{CF}_3)^+$ (m/z 131) [115].

The ionization energy of sevoflurane (11 eV) is less than the recombination energy of O_2^+ (12.07 eV). The difference in the energies is 1.07 eV [120]. Probably, this could be the reason for lesser fragmentation being observed.

Table 6.7 m/z values of the product ions and neutral species and their branching ratio percentages resulting from the reaction sevoflurane with O_2^+ at a reduced electric field of 140 Td using the KORE PTR-ToF-MS in comparison to SIFT-MS results published by Wang et al.,[115].

Name/ Formula	Product ion m/z	Product ion	Neutral Product	PTR-ToF- MS (KORE) %	SIFT- MS[115] %
Sevoflurane $\text{C}_4\text{H}_3\text{F}_7\text{O}$ 200	49	CH_2FO^+	C_3HF_6	-	5-30
	51	CHF_2^+	$\text{C}_3\text{H}_2\text{F}_5\text{O}$	10	-
	69	CF_3^+	$\text{C}_3\text{H}_3\text{F}_4\text{O}$	-	-
	129	$\text{C}_3\text{HF}_4\text{O}^+$	CH_2F_3	-	5-10
	131	$\text{C}_3\text{H}_3\text{F}_4\text{O}^+$	CF_3	35	70-55
	181	$\text{C}_4\text{H}_3\text{F}_6\text{O}^+$	F	27	15-2
	199	$\text{C}_4\text{H}_2\text{F}_7\text{O}^+$	H	28	11-4

The reason for the difference in branching ratio and product ions between PTR-MS and SIFT technology has already been explained in the earlier discussion stressing the differences in the collisional energies.

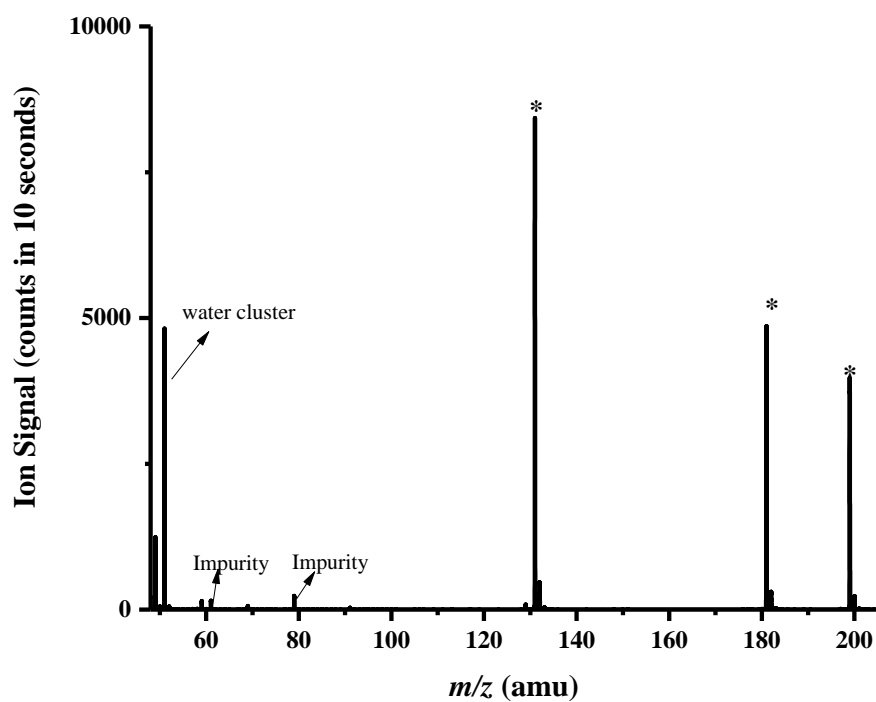


Figure 6.16 A mass spectrum illustrating the product ions (starred) resulting from the reaction of O_2^+ with sevoflurane ($C_4H_3F_7O$) whilst operating the drift tube at a reduced electric field of 140 Td. Other ions, such as impurity ions are highlighted.

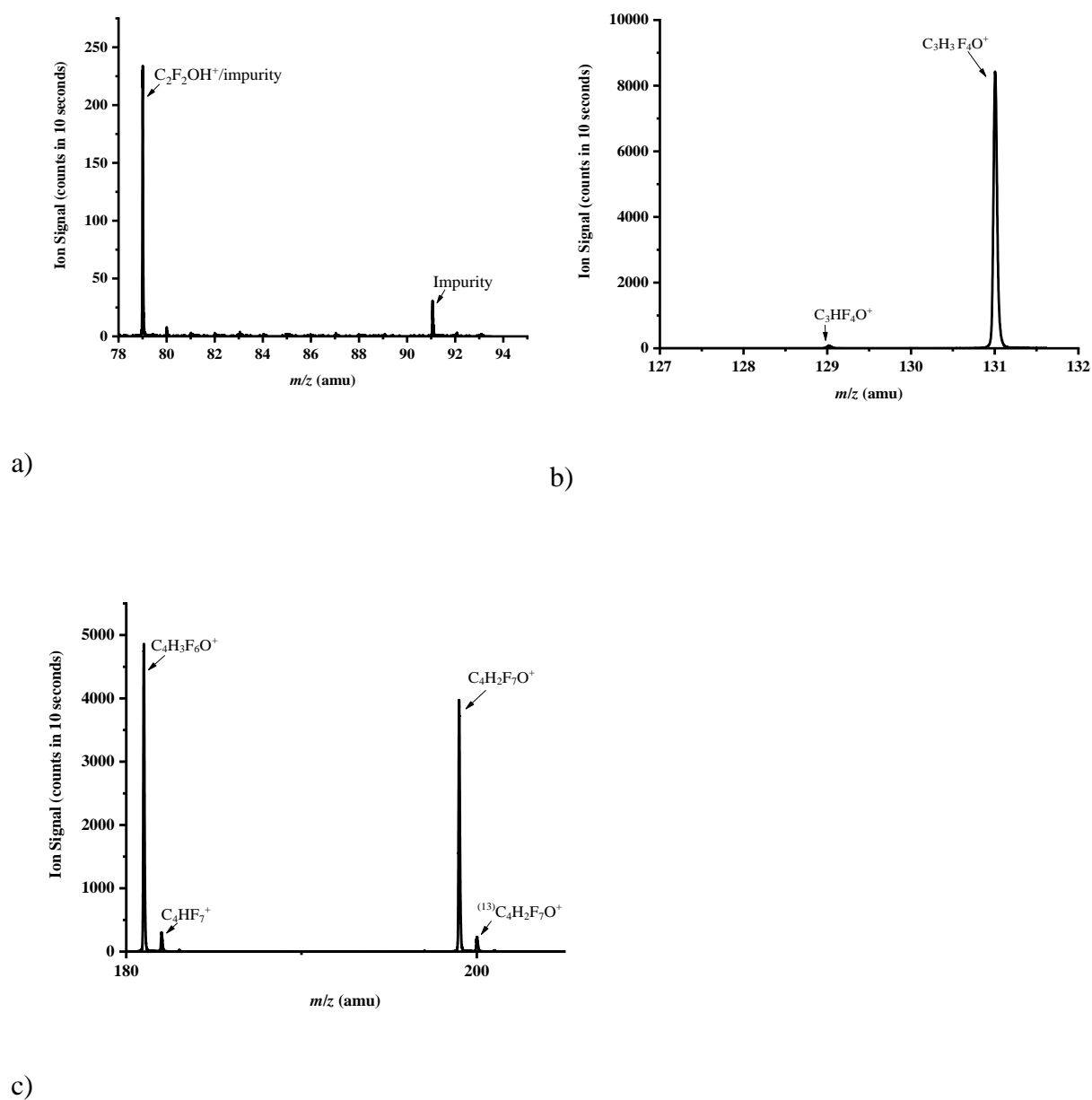


Figure 6.17 Expanded figure of the product ions resulting from the reactions of O_2^+ with sevoflurane to illustrate their isotopic abundances for a) m/z 79 ($C_2F_2OH^+$ /impurity), m/z 91 (Impurity), b) m/z 129 ($C_3HF_4O^+$) and m/z 131 ($C_3H_3F_4O^+$) c) m/z 181 ($C_4H_3F_6O^+$), m/z 183 ($C_4HF_7^+$) and m/z 199 ($C_4H_2F_7O^+$).

Figure 6.18 illustrates how the product ion distributions vary as a function of the reduced electric field. The prominent ions for all values for E/N are $C_3H_3F_4O^+$, $C_4H_3F_6O^+$ and $C_4H_2F_7O^+$ but their branching ratios decrease owing to more fragmentation as the collisional energies of both the reagent ions and product ions increase with increasing E/N .

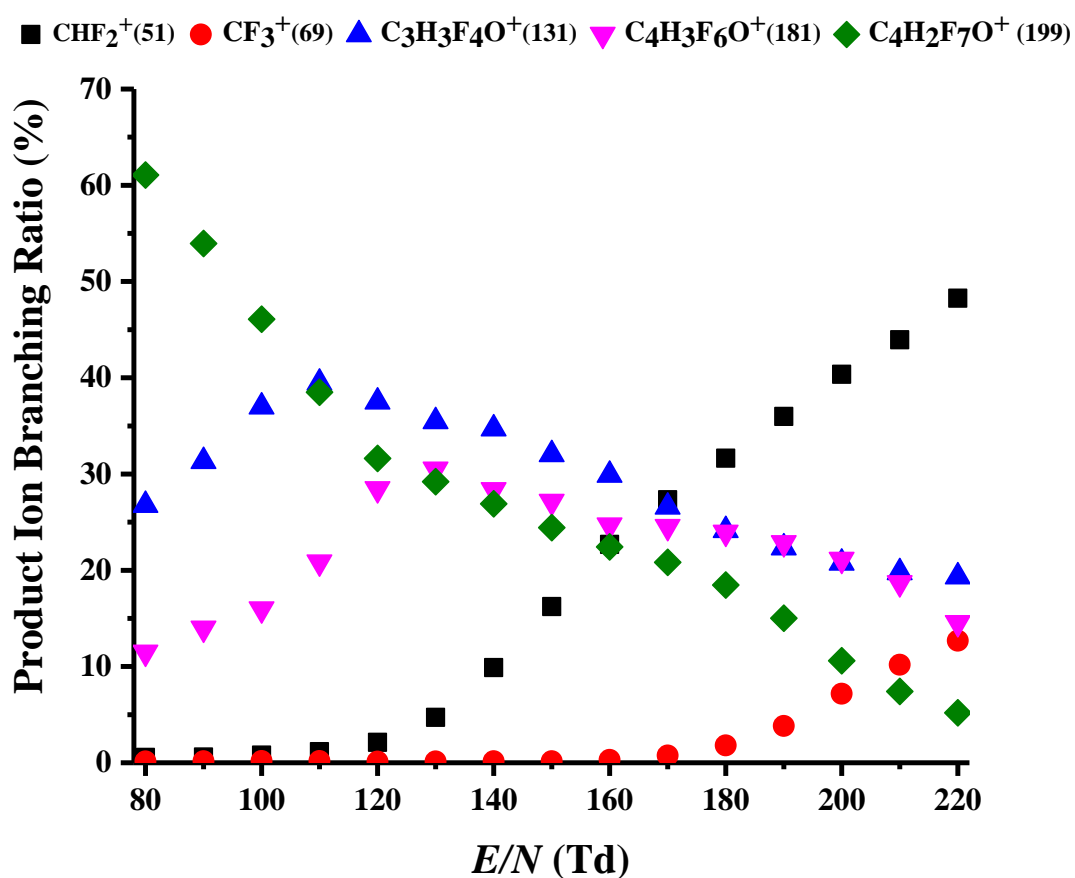


Figure 6.18 Product ion branching ratios in percentages as a function of E/N resulting from the reaction of O_2^+ with sevoflurane ($C_4H_3F_7O$).

6.3.4.2 Reaction with H_3O^+

Figure 6.19 shows the mass spectrum of sevoflurane reaction with H_3O^+ at 140 Td. The details of the product ions and the branching ratio as a function of reduced electric field are presented in the table 6.8. In this study, there were six product ions observed as a result of reaction with H_3O^+ . The corresponding ions (using the lightest isotopomer) are at m/z 51 (CHF_2^+), m/z 69 (CF_3^+), m/z 181 ($\text{C}_4\text{H}_3\text{F}_6\text{O}^+$), m/z 182 ($\text{C}_4\text{H}_4\text{F}_6\text{O}^+$) and m/z 199 ($\text{C}_4\text{H}_2\text{F}_7\text{O}^+$). It is apparent from table 6.6 (also figure 6.19 and figure 6.20) that the most intense product ion at 140 Td is m/z 181 ($\text{C}_3\text{H}_3\text{F}_4\text{O}^+$) with 69% of the branching ratio. The next most intense ion is at m/z 182 ($\text{C}_4\text{H}_4\text{F}_6\text{O}^+$) (18 %). Measurements using the PTR-TOF-8000 (Ionicon Analytik GmbH) in Innsbruck, show similar product ions, with branching ratios in good agreement (table 6.8).

In their SIFT-MS study, Wang et al. found four product ions [115]: with the dominant ion being m/z 49 (CH_2FO^+) (20-80 %) (the first number indicates shortest reaction length of 3 cm where sevoflurane is introduced into the carrier gas, close to the mass spectrometer sampling orifice and the second one indicates the longer reaction length of 40 cm, where the sample is introduced much further upstream). This is followed by m/z 199 (80-20%) and m/z 181 (15-2 %). Apparently, they claimed that the branching ratio increases with increasing humidity [115]. m/z 49 (CH_2FO^+) was in our studies, but by changing sevoflurane and water concentrations in the drift tube, our results indicate that it is a result of a secondary process.

Table 6.8 m/z values of the product ions and neutral species and their branching ratio percentages resulting from the reaction sevoflurane with H_3O^+ at a reduced electric field of 140 Td. The IONICON PTR-ToF-MS were measured following a request to Michaela Malásková from the Institute of Breath research, University of Innsbruck, Austria. SIFT-MS results of Wang et al. are also presented.

Name/ Formula	Product ion ¹ m/z	Product ion Molecular formula	Neutral Products	PTR-ToF- MS(KORE) %	SIFT- MS % [115]	PTR-ToF- MS (IONICON)
Sevoflurane	49	CH_2FO^+	$\text{C}_3\text{H}_2\text{F}_6$	-	80-20	-
$\text{C}_4\text{H}_3\text{F}_7\text{O}$	51	CHF_2^+	$\text{C}_3\text{H}_3\text{F}_5\text{O}$	<1	-	<1
200	69	CF_3^+	$\text{C}_3\text{H}_4\text{F}_4\text{O}$	<1	-	<1
	131	$\text{C}_3\text{H}_3\text{F}_4\text{O}^+$	CHF_3	<1	70-55	-
	181	$\text{C}_4\text{H}_3\text{F}_6\text{O}^+$	HF	77	15-2	98
	182	$\text{C}_4\text{H}_4\text{F}_6\text{O}^+$	FO	20	-	2
	199	$\text{C}_4\text{H}_2\text{F}_7\text{O}^+$	H_2	2	80-20	-

There have been a couple of other PTR-MS studies investigating sevoflurane. Summer et al. investigated sevoflurane in the exhaled breath of operating room personnel and they used m/z 181 (unassigned) to determine the sevoflurane concentration [121].

Critchley et al. reported the headspace spectrum of sevoflurane using an IONICON PTR-Quad-MS [122]. According to them, there were three product ions using H_3O^+ (140 Td) observed. They identified the ions as m/z 199 ($\text{C}_4\text{H}_2\text{F}_7\text{O}^+$), m/z 181 ($\text{C}_4\text{H}_3\text{F}_6\text{O}^+$), m/z 49 (CH_2FO^+) [122]. In comparison to our findings, their studies confirm that these three ions are the dominant product ions from sevoflurane. However, they did not report any observation of $\text{C}_4\text{H}_4\text{F}_6\text{O}^+$ (m/z 182) in their investigation. They also mentioned that the dissociative proton transfer leading to m/z 199 ($\text{C}_4\text{H}_2\text{F}_7\text{O}^+$) is the dominant reaction channel [122]. The dissociative reaction/channels result in H_2 and/or CH_4 loss especially in small hydrocarbons [123]. In our study, the dominant ions are m/z 181 and m/z 182, and not m/z 199 as mentioned by Critchley.

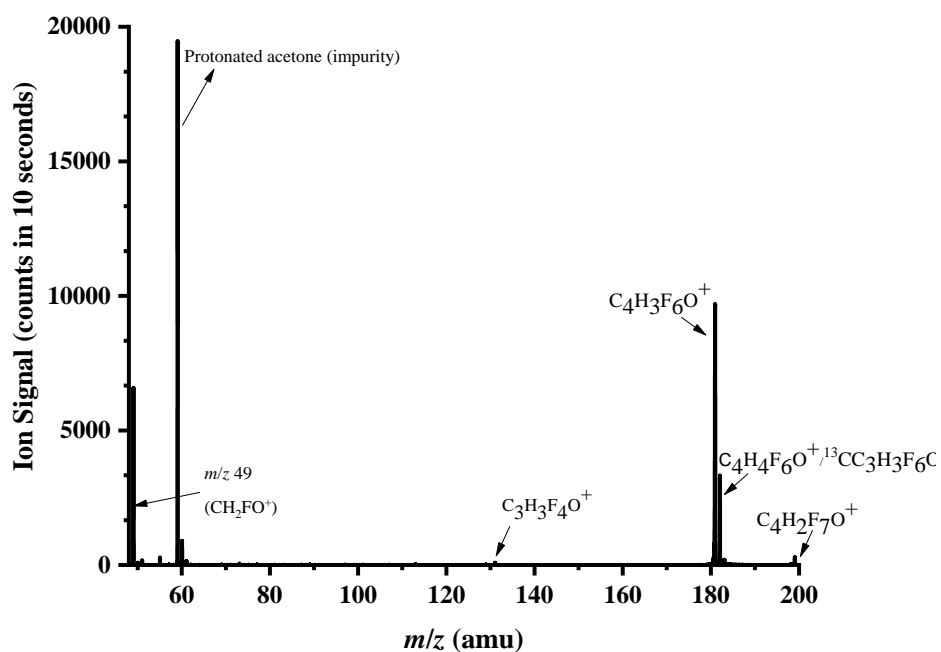


Figure 6.19 A mass spectrum illustrating the product ions resulting from the reaction of H_3O^+ with sevoflurane whilst operating the drift tube at a reduced electric field of 140 Td. Other ions such as m/z 49 which is produced via a secondary process and an impurity ion $\text{C}_3\text{H}_7\text{O}^+$ coming from the sample are also highlighted.

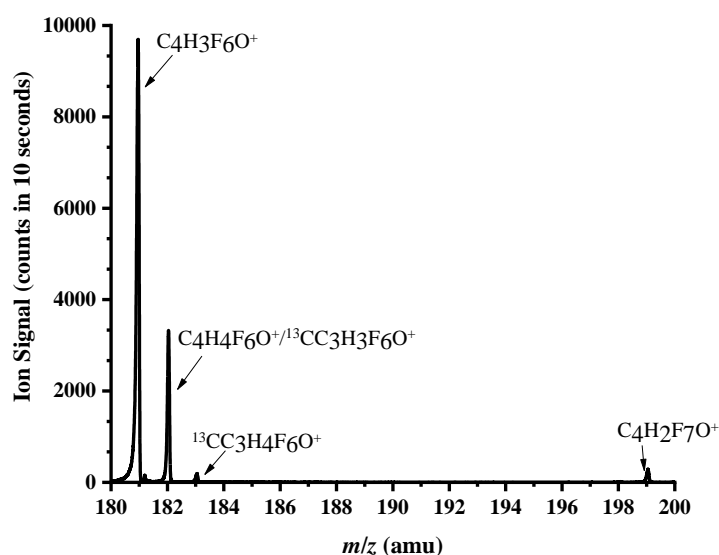


Figure 6.20 A Mass spectrum illustrating product ions m/z 181 ($\text{C}_4\text{H}_3\text{F}_6\text{O}^+$), m/z 182 $\text{C}_4\text{H}_4\text{F}_6\text{O}^+ / ^{13}\text{CC}_3\text{H}_3\text{F}_6\text{O}^+$, m/z 183 ($^{13}\text{CC}_3\text{H}_4\text{F}_6\text{O}^+$) and m/z 199 ($\text{C}_4\text{H}_2\text{F}_7\text{O}^+$).

Figure 6.21 illustrates how the product ion distributions vary as a function of the reduced electric field. For all values of E/N the dominant ion is $C_4H_3F_6O^+$, but its branching ratio decreases with increasing E/N owing to increased fragmentation as the collisional energies of both the reagent ions and product ions increase with increasing E/N . $C_4H_2F_7O^+$ was less than 3 % for all values of E/N .

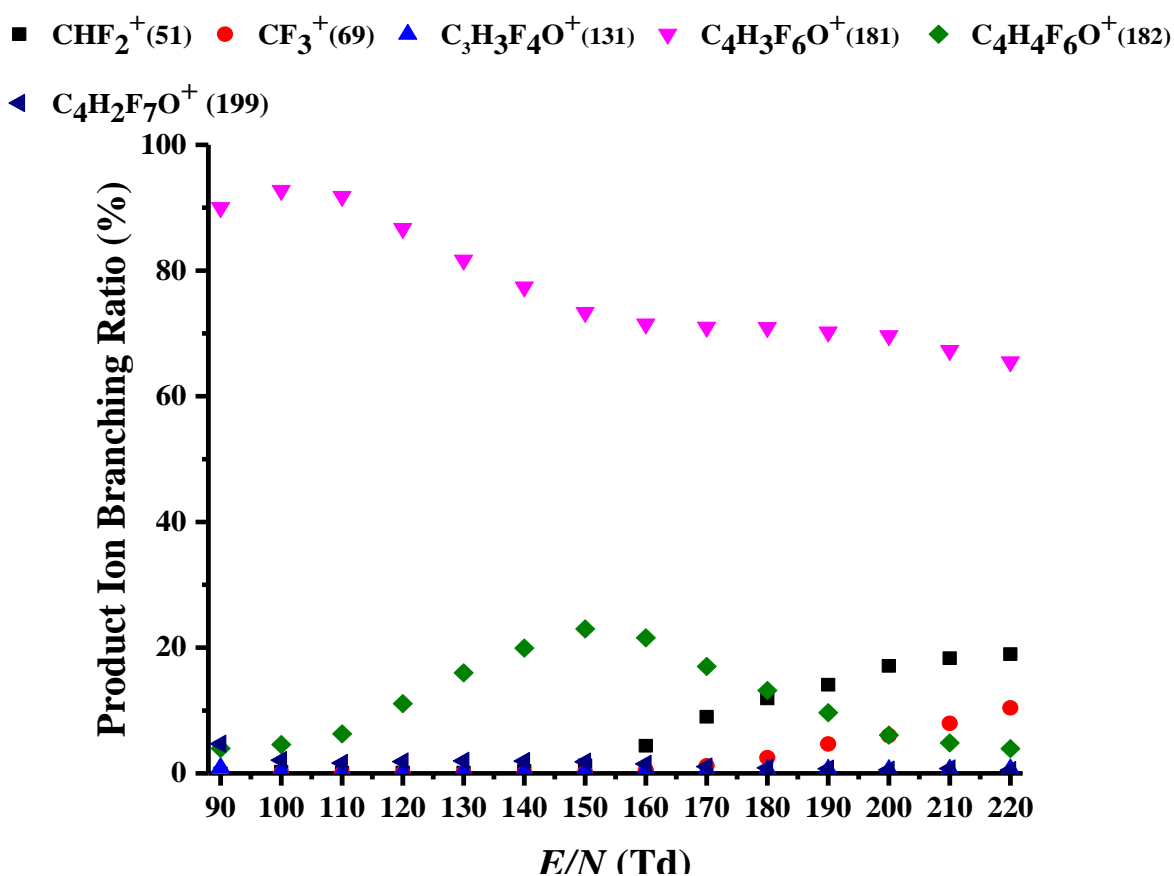


Figure 6.21 Product ion branching ratios in percentages as a function of E/N resulting from the reaction of H_3O^+ with sevoflurane ($C_4H_3F_7O$). Product ions that contribute less than 1% to the branching percentages at any given E/N have not been included in the figure.

6.3.5 Methoxyflurane

There has been no previous PTR-MS study of methoxyflurane.

6.3.5.1 Reaction with O_2^+

The ionisation potential of methoxyflurane is 11.0 eV [116]. Hence O_2^+ can energetically charge transfer, with an exothermicity of about 1.1 eV. Figure 6.22 shows the mass spectrum of methoxyflurane reaction with O_2^+ at 140 Td for which the product ions resulting from dissociative charge transfer are highlighted. Figure 6.23 (a)-(e) shows these product ions in more detail. Figure 6.24 presents the product ion branching ratio percentages resulting from the reaction of methoxyflurane with O_2^+ as a function of the reduced electric field.

Six product ions were observed from the reaction of methoxyflurane with O_2^+ . Following are the ions obtained via charge transfer (electron) process (using the lightest isotopomer); m/z 51 (CHF_2^+), m/z 67 ($CHFCl^+$), m/z 81 $C_2H_3F_2O^+$, m/z 129 ($C_3H_4F_2ClO^+$), m/z 143 ($C_3H_2FCl_2O^+$) and m/z 145 ($C_3H_4FCl_2O^+$). Among these, the most dominant product ion at 140 Td was m/z 81 which has contributed 58 % of the branching ratio. The next intense ion was m/z 145. The other product ions contributed less than 6% of the branching ratio. There was no parent ion detected in the measurement and therefore non-dissociative charge transfer dominates the reaction of methoxyflurane with O_2^+ . There were some impurities from the sample which are not associated with methoxyflurane product ions.

Table 6.9 m/z values of the product ions and their branching ratio percentages resulting from the reaction of methoxyflurane with O_2^+ at a reduced electric field of 140 Td using the KORE PTR-ToF-MS.

Name/ Formula	Product ion m/z	Product ion molecular formula	Neutral Products	PTR- ToF- MS (KORE) %
Methoxyflurane $C_3H_4F_2Cl_2O$ m/z 164	51	CHF_2^+	$C_2H_3Cl_2O$	2
	67+69	$CHFCl^+$	C_2H_3FCIO	5
	81	$C_2H_3F_2O^+$	$CHCl_2$	58
	129+131	$C_3H_4F_2ClO^+$	Cl	3
	143+145+147	$C_3H_2FCl_2O^+$	H_2F	<1
	145+147+149	$C_3H_4FCl_2O^+$	F	32

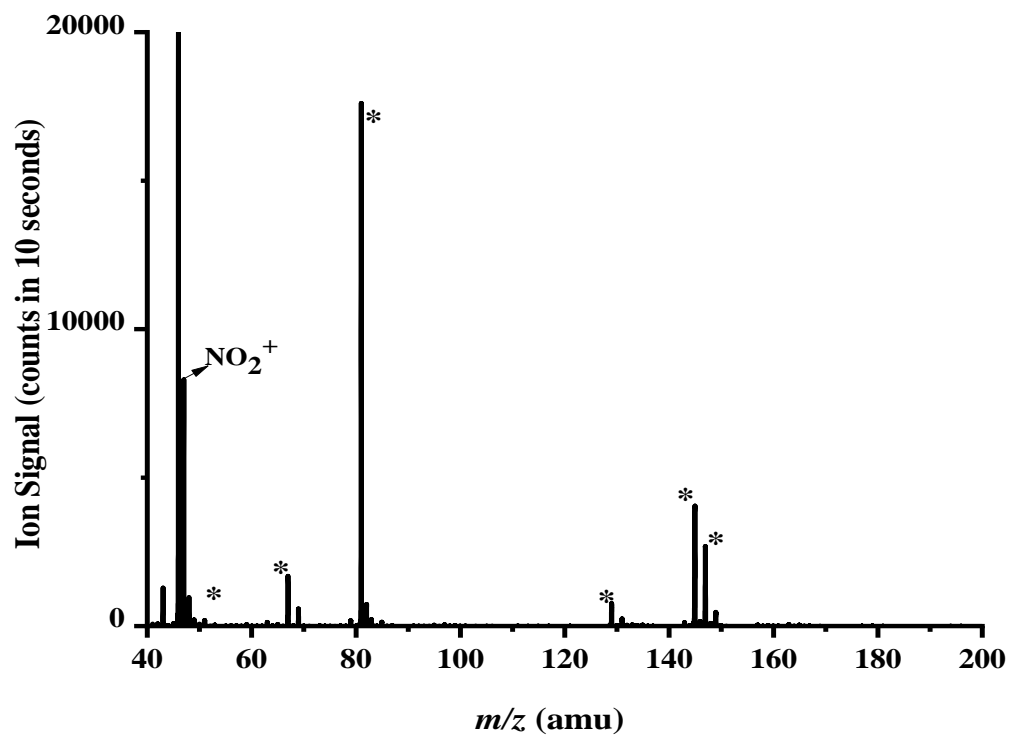


Figure 6.22 A mass spectrum illustrating the product ions (starred) resulting from the reaction of O_2^+ with methoxyflurane ($\text{C}_3\text{H}_4\text{F}_2\text{Cl}_2\text{O}$) whilst operating the drift tube at a reduced electric field of 140 Td. Other ions such as impurity ion (NO_2^+) coming from the ion source are also highlighted.

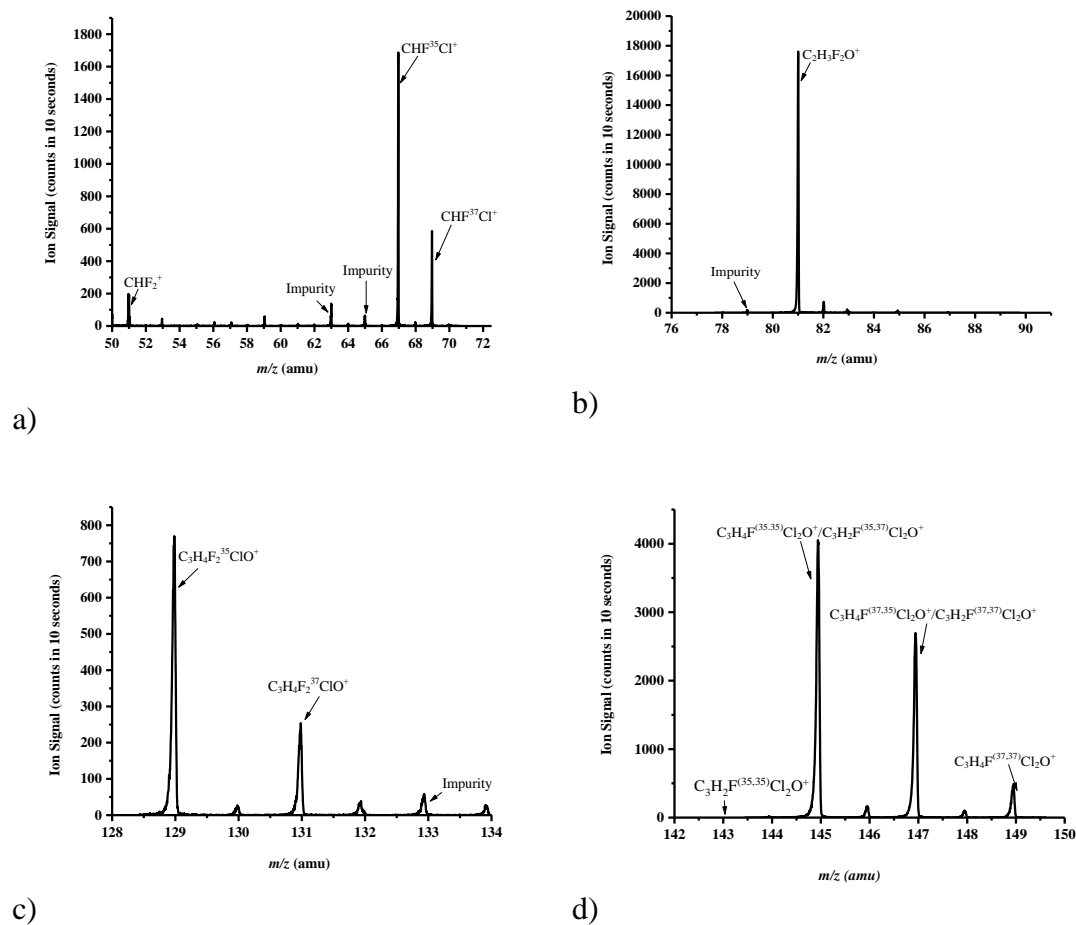


Figure 6.23 Mass spectrum illustrating product ions resulting from the reactions of O_2^+ to methoxyflurane with illustrate their isotopic abundances a) m/z 51 (CHF_2^+), m/z 67 ($CHF^{35}Cl^+$), m/z 69 ($CHF^{37}Cl^+$) b) m/z 81 ($C_2H_3F_2O^+$) c) m/z 129 ($C_3H_4F_2^{35}ClO^+$), m/z 131 ($C_3H_4F_2^{37}ClO^+$ / $C_2H_2F^{35}ClO^+$), m/z 133 (Impurity) d) m/z 143 ($C_3H_2F^{(35,35)}Cl_2O^+$), m/z 145 ($C_3H_4F^{(35,35)}Cl_2O^+$ / $C_3H_2F^{(35,37)}Cl_2O^+$), m/z 147 ($C_3H_4F^{(37,35)}Cl_2O^+$ / $C_3H_2F^{(37,37)}Cl_2O^+$) and m/z 149 ($C_3H_4F^{(37,37)}Cl_2O^+$).

Figure 6.24 illustrates how the product ion distributions vary as a function of the reduced electric field. The dominant ions from 80 Td-160 Td are m/z 81 ($C_2H_3F_2Cl^+$) and m/z 145 ($C_3H_4FCl_2O^+$) but their branching ratios decrease with increasing E/N owing to more fragmentation as the collisional energies of both the reagent ions and product ions increase with increasing E/N .

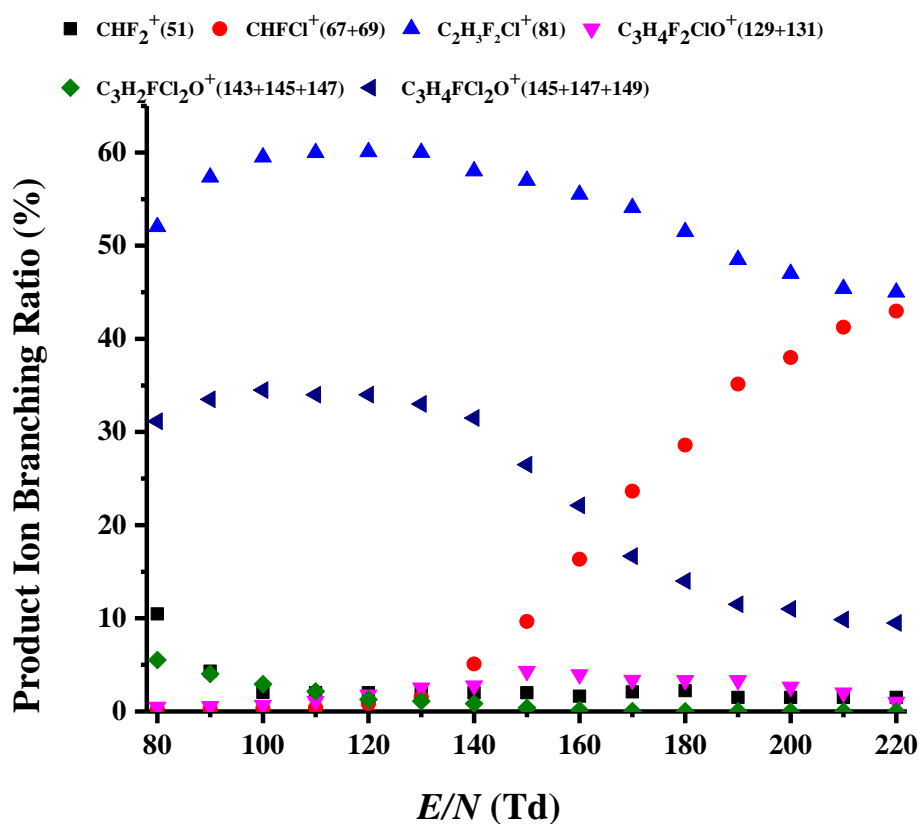


Figure 6.24 Product ion branching ratios in percentages as a function of E/N resulting from the reaction of O_2^+ with methoxyflurane ($C_3H_4F_2Cl_2O$).

6.3.5.2 Reaction with H₃O⁺

The proton affinity of methoxyflurane is unknown. However, H₃O⁺ does react with methoxyflurane via dissociative proton transfer.

Figure 6.25 presents a mass spectrum resulting from the reaction of methoxyflurane with H₃O⁺ at 140 Td, and figure 6.26 presents a mass spectrum of each product ion in detail. Figure 6.27 provides the product ion branching ratios in percentages as a function of *E/N*.

Table 6.10 provides details of product ions together with their branching ratios. There were six product ions observed. The product ions assigned (using the lightest isotopomer) are at *m/z* 51 (CHF₂⁺), *m/z* 67 (CHFCI⁺), *m/z* 79 (C₂HFCI⁺), *m/z* 81 (C₂H₃FCI⁺), *m/z* 143 (C₃H₂FCI₂O⁺) and *m/z* 145 (C₃H₄FCI₂O⁺). The most abundant product ion at 140 Td was *m/z* 145 (66 %) resulting from the loss of HF from the protonated parent, followed by *m/z* 143 (25 %), resulting from loss H₂ and HF from the protonated parent.

Table 6.10 *m/z* values of the product ions and their branching ratio percentages resulting from the reaction of methoxyflurane with H₃O⁺ at a reduced electric field of 140 Td using the KORE PTR-ToF-MS.

Name/ Formula	Product ion <i>m/z</i>	Product ion	Neutral Products	PTR-ToF-MS (KORE) %
Methoxyflurane	51	CHF ₂ ⁺	C ₂ H ₄ Cl ₂ O	1
C ₃ H ₄ F ₂ Cl ₂ O	67+69	CHFCI ⁺	C ₂ H ₄ FCIO	2
<i>m/z</i> 164	79+81	C ₂ HFCI ⁺	CH ₄ FCIO	1
	81+83	C ₂ H ₃ FCI ⁺	CH ₂ FCIO	5
	143+145+147	C ₃ H ₂ FCI ₂ O ⁺	HF+H ₂	25
	145+147+149	C ₃ H ₄ FCI ₂ O ⁺	HF	66

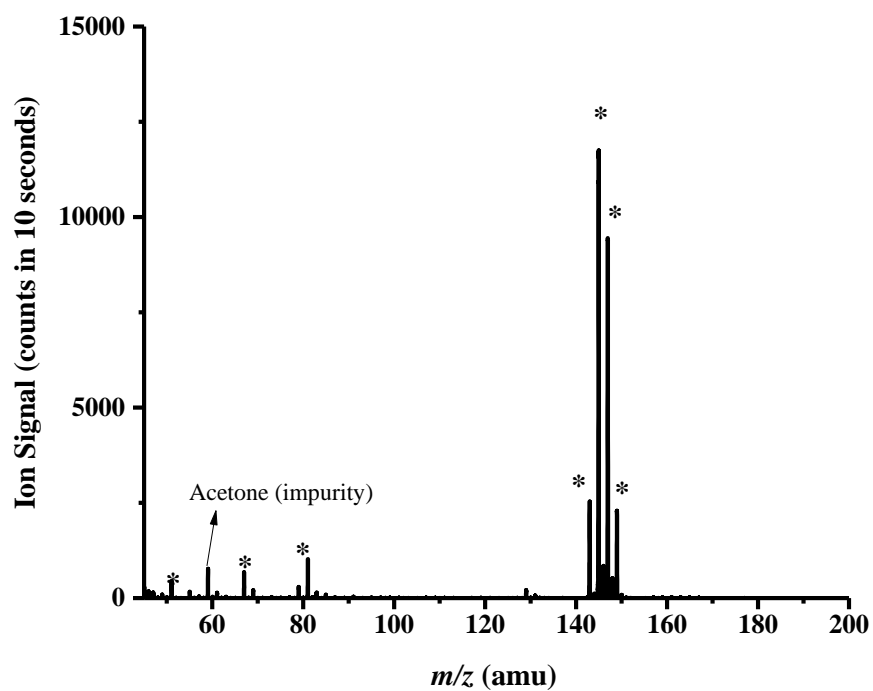


Figure 6.25 A mass spectrum illustrating the product ions (starred) resulting from the reaction of H_3O^+ with methoxyflurane whilst operating the drift tube at a reduced electric field of 140 Td. Impurities such as the one resulting from protonated acetone.

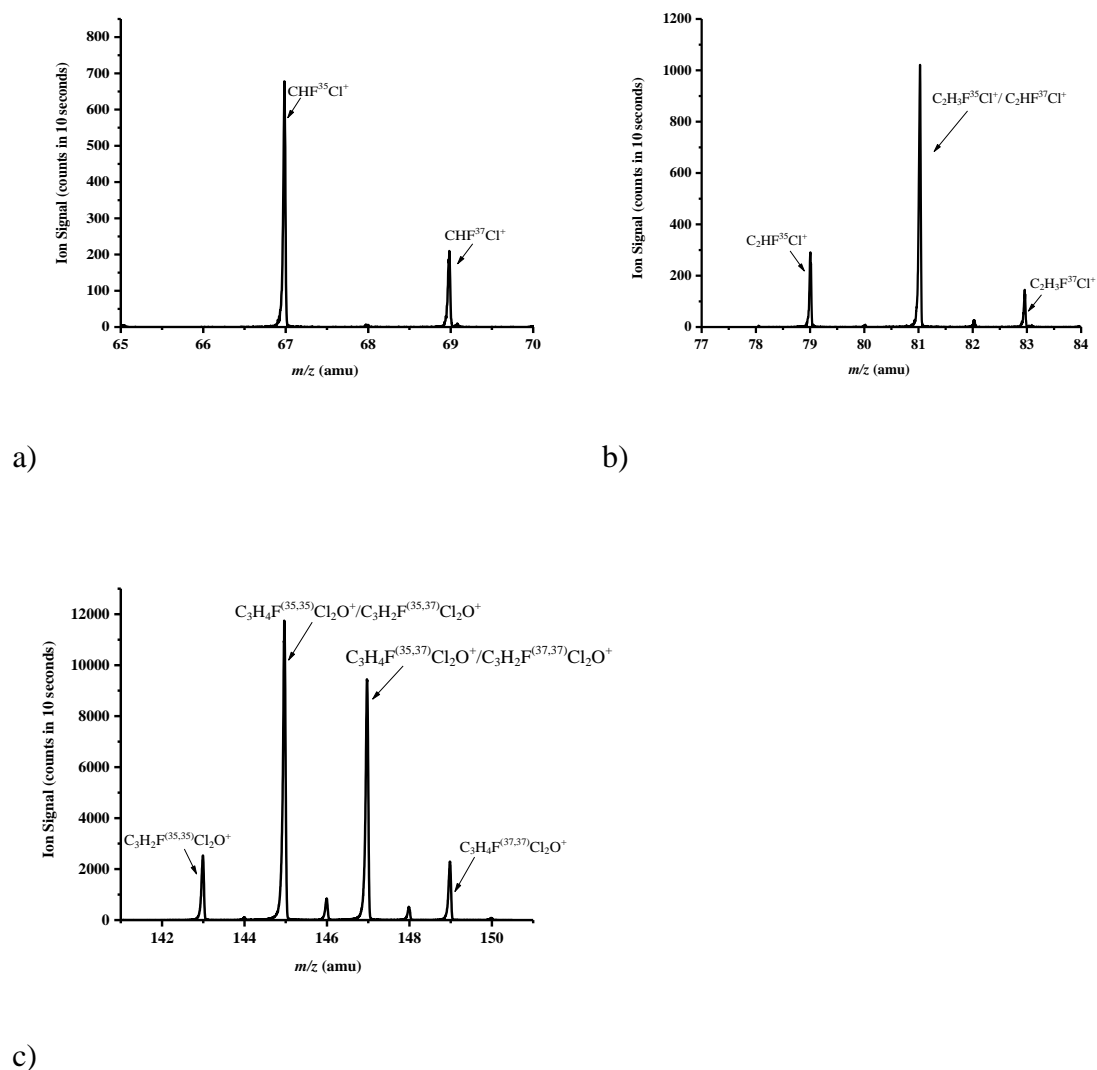


Figure 6.26 Mass spectrum illustrating product ions resulting from the reactions of H_3O^+ with methoxyflurane to illustrate their isotopic abundances a) m/z 67 ($\text{CHF}^{35}\text{Cl}^+$) and m/z 69 ($\text{CHF}^{37}\text{Cl}^+$) b) m/z 79 ($\text{C}_2\text{HF}^{35}\text{Cl}^+$), m/z 81 ($\text{C}_2\text{H}_3\text{F}^{35}\text{Cl}^+$ / $\text{C}_2\text{HF}^{37}\text{Cl}^+$) and m/z 83 ($\text{C}_2\text{H}_3\text{F}^{37}\text{Cl}^+$) and c) m/z 143 ($\text{C}_3\text{H}_2\text{F}^{(35,35)}\text{Cl}_2\text{O}^+$), m/z 145 ($\text{C}_3\text{H}_4\text{F}^{(35,35)}\text{Cl}_2\text{O}^+$ / $\text{C}_3\text{H}_2\text{F}^{(35,37)}\text{Cl}_2\text{O}^+$), m/z 147 ($\text{C}_3\text{H}_4\text{F}^{(35,37)}\text{Cl}_2\text{O}^+$ / $\text{C}_3\text{H}_2\text{F}^{(37,37)}\text{Cl}_2\text{O}^+$) and m/z 149 ($\text{C}_3\text{H}_4\text{F}^{(37,37)}\text{Cl}_2\text{O}^+$).

Figure 6.27 illustrates how the product ion distributions vary as a function of the reduced electric field. The dominant ion from 120 Td-180 Td is m/z 145 ($C_3H_4FC_2O^+$). The m/z 67 branching ratio increases when the electric field increases. At the same time, m/z 143 branching ratio decreases when the electric field increases. m/z 81 only shows low intensity throughout the E/N from 80 Td – 220 Td.

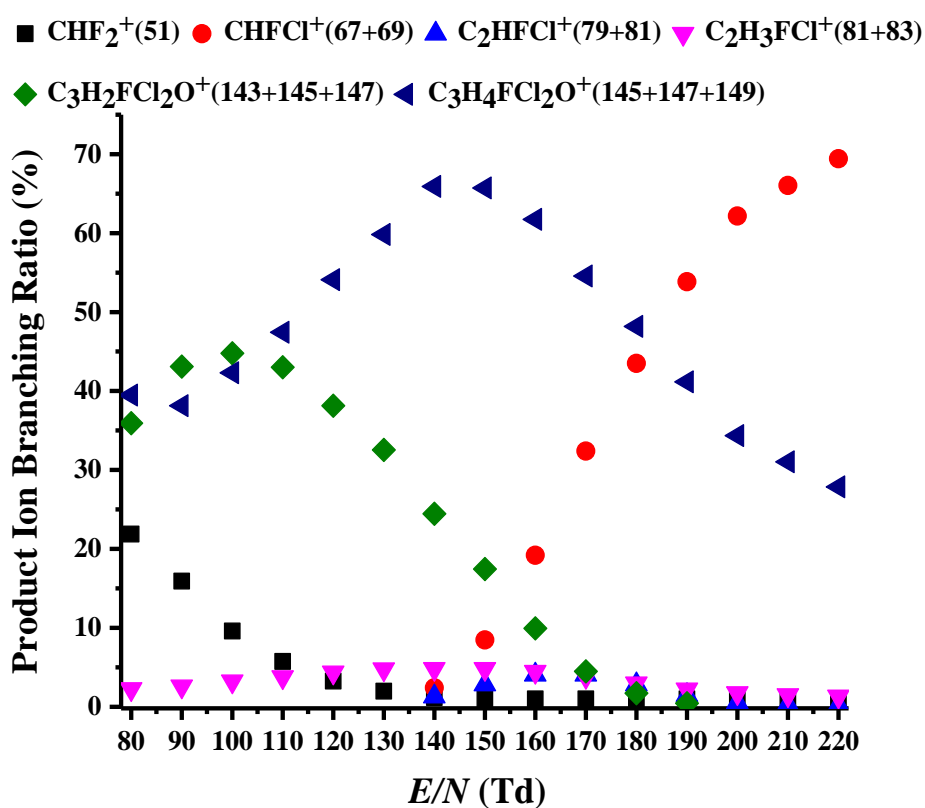


Figure 6.27 Product ion branching ratios in percentages as a function of E/N resulting from the reaction of H_3O^+ with methoxyflurane ($C_3H_4F_2Cl_2O$).

6.3.6 Desflurane

No previous PTR-MS study of desflurane has been reported.

6.3.6.1 Reaction with O_2^+

Figure 6.28 shows the mass spectrum resulting from the reaction of desflurane ($C_3H_2F_6O$) with O_2^+ at 140 Td, and figure 6.29 illustrates the product ions in more detail at 140 Td.

Figure 6.30 represents product ion branching ratios in percentages as a function of E/N .

Table 6.11 m/z values of the product ions and their branching ratio percentages resulting from the reaction of desflurane with O_2^+ at a reduced electric field of 140 Td using the KORE PTR-ToF-MS.

Name/ Formula	Product ion m/z	Product Ion	Neutral Products	PTR-ToF- MS (KORE) %
Desflurane	51	CHF_2^+	C_2HF_4O	29
$C_3H_2F_6O$	69	CF_3^+	$C_2H_2F_3O$	8
m/z 168	99	$C_2H_2F_3O^+$	CF_3	4
	101	$C_2F_4H^+$	CHF_2O	2
	147	$C_3F_5O^+$	FH_2	21
	149	$C_3H_2F_5O^+$	F	34
	167	$C_3HF_6O^+$	H	2

Table 6.11 provides the detail of m/z values of the product ions, their molecular structure, and their branching ratio percentages resulting from the reaction of desflurane with O_2^+ at a reduced electric field of 140 Td. There are seven product ions observed. The product ions (using the lightest isotopomer) are at m/z 51 (CHF_2^+), m/z 69 (CF_3^+), m/z 99 ($C_2H_2F_3O^+$), m/z 101 ($C_2F_4H^+$), m/z 147 ($C_3F_5O^+$), m/z 149 ($C_3H_2F_5O^+$) and m/z 167 ($C_3HF_6O^+$).

It can be seen from table 6.11 that the most abundant product ion at 140 Td is m/z 149 ($C_3H_2F_5O^+$), followed by m/z 51 (29 %), m/z 147 (21 %) and m/z 69 (8 %). The

branching ratios from other product ions were less than 8 %. There was no protonated ion observed.

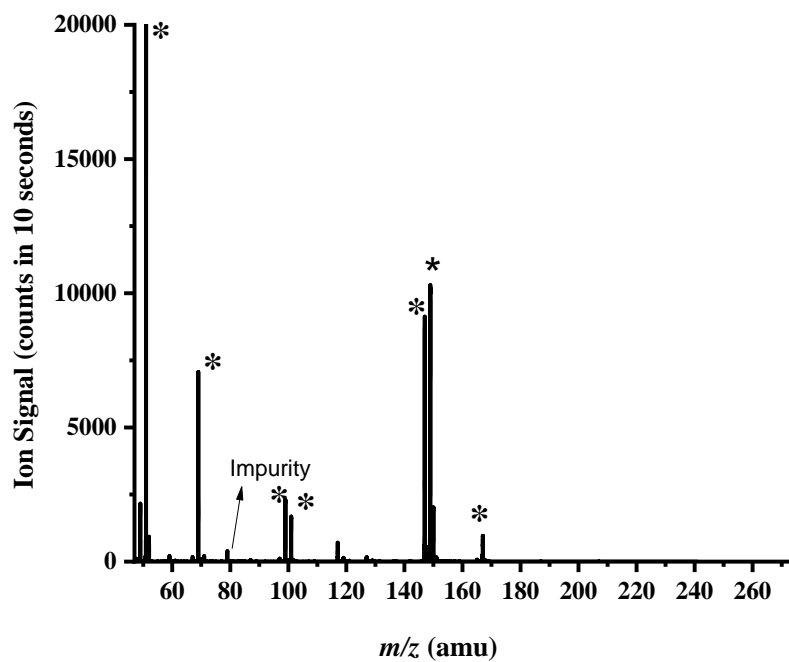


Figure 6.28 A mass spectrum illustrating the product ions resulting from the reaction of O_2^+ with desflurane whilst operating the drift tube at a reduced electric field of 140 Td. An impurity ion is highlighted.

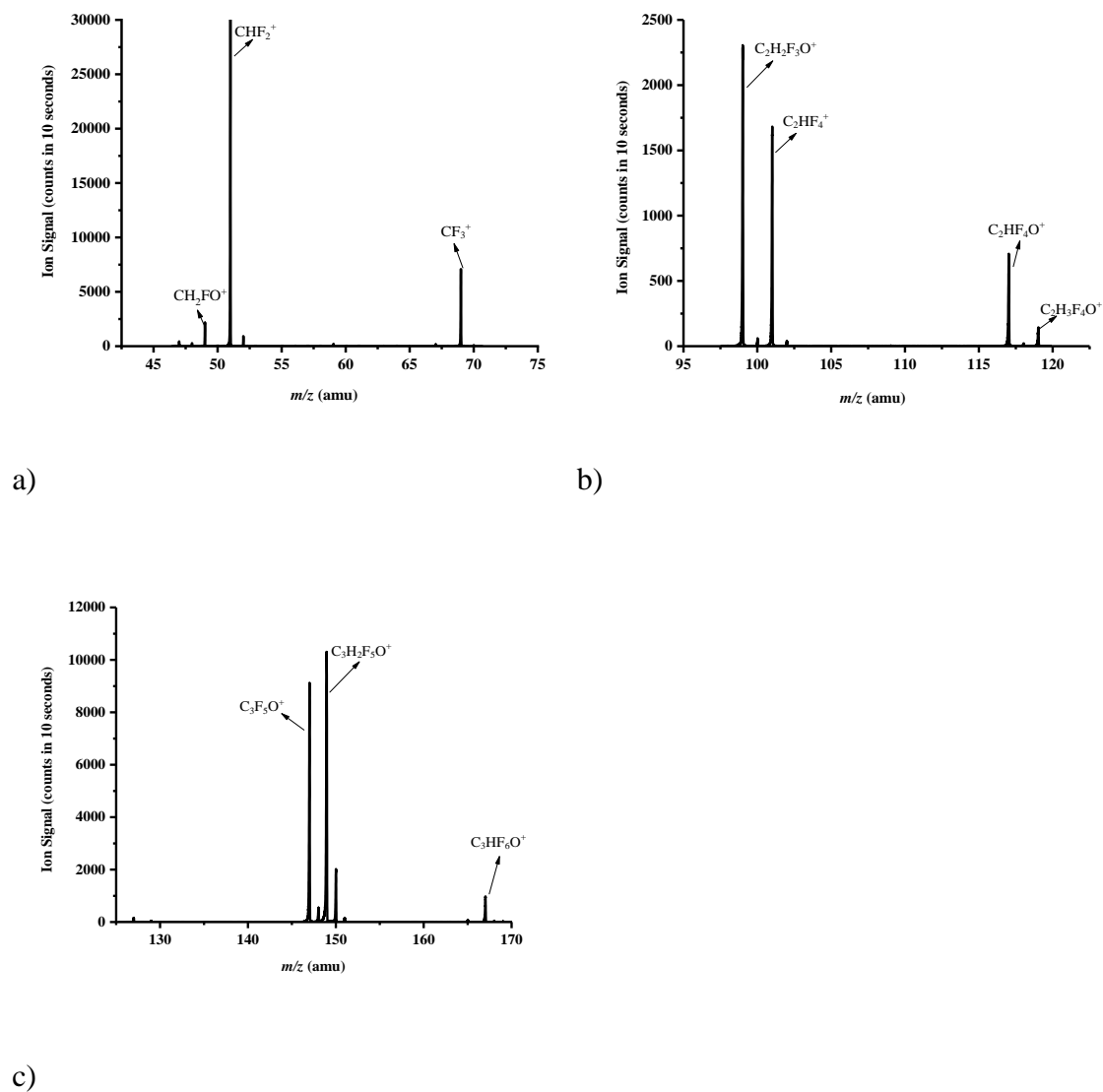


Figure 6.29 Mass spectrum illustrating product ions resulting from the reactions of O_2^+ with desflurane to illustrate their isotopic abundances a) m/z 49 (CH_2FO^+), m/z 51 (CHF_2^+), m/z 69 (CF_3^+) b) m/z 99 ($C_2H_2F_3O^+$), m/z 101 ($C_2HF_4^+$), m/z 117 ($C_2HF_4O^+$) and m/z 119 ($C_2H_3F_4O^+$) c) m/z 147 ($C_3F_5O^+$), m/z 149 ($C_3H_2F_5O^+$) and m/z 167 ($C_3HF_6O^+$).

Figure 6.30 illustrates how the branching ratio changes with as a function of reduced electric field. The m/z 51 (CHF_2^+) branching ratio increases as the reduced electric field increases, and the m/z 149 ($\text{C}_3\text{H}_2\text{F}_5\text{O}^+$) branching ratio decreases owing to more fragmentation as the collisional energies of both the reagent ions and product ions increase with increasing E/N .

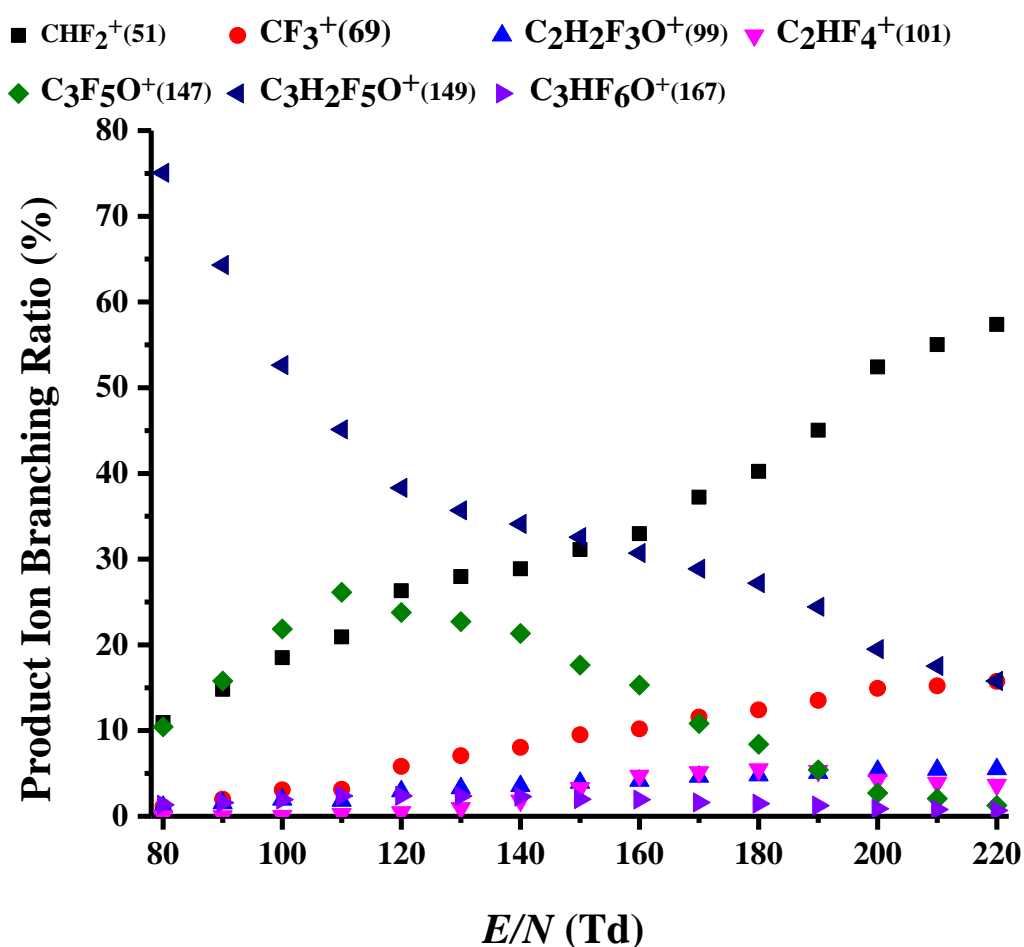


Figure 6.30 Product ion branching ratios in percentages as a function of E/N resulting from the reaction of O_2^+ with desflurane ($\text{C}_3\text{H}_2\text{F}_6\text{O}$).

6.3.6.2 Desflurane reaction of with H_3O^+

Figure 6.31 shows the mass spectrum resulting from the reaction of desflurane ($\text{C}_3\text{H}_2\text{F}_6\text{O}$) with O_2^+ at 140 Td, and figure 6.32 provides more detail of these product ions. Figure 6.33 presents the product ion branching ratios in percentages as a function of E/N resulting from the reaction of with desflurane H_3O^+ .

There are four product ions observed at 140 Td (table 6.12). They are assigned (using the lightest isotopomer) as m/z 51 (CHF_2^+), m/z 147 ($\text{C}_3\text{F}_5\text{O}^+$), m/z 149 ($\text{C}_3\text{H}_2\text{F}_5\text{O}^+$) and m/z 167 ($\text{C}_3\text{HF}_6\text{O}^+$). Among these, the most abundant product ion at 140 Td is at m/z 149, which contributes approximately 61 % to the branching ratio. The other obvious product ion is at m/z 147 which contributes 34 % to the branching ratio. The other product ions contributed less than 2 %.

Measurements using the IONICON PTR-TOF 8000 revealed four product ions. There are some similarities between our finding such as m/z 51 (CHF_2^+), m/z 147 ($\text{C}_3\text{F}_5\text{O}^+$) and m/z 149 ($\text{C}_3\text{H}_2\text{F}_5\text{O}^+$). However, an additional ion at m/z 101 (6 %) was also observed. No ions were detected at m/z 167 in the IONICON measurement.

Table 6.12 m/z values of the product ions and their branching ratio percentages resulting from the reaction of desflurane with H_3O^+ at a reduced electric field of 140 Td using the KORE PTR-ToF-MS and The IONICON PTR-ToF 8000 instruments. The IONICON measurements were made by Michaela Malásková from the Institute of Breath research, University of Innsbruck, Austria.)

Name/ Formula	Product ion m/z	Product ion Molecular formula	Neutral Product	PTR- ToF-MS (KORE) %	PTR-TOF- MS(Innsbruck) %
Desflurane	51	CHF_2^+	$\text{C}_2\text{H}_2\text{F}_4\text{O}$	2	18
	101	$\text{C}_2\text{F}_4\text{H}^+$	CHF_2O	-	6
$\text{C}_3\text{H}_2\text{F}_6\text{O}$	147	$\text{C}_3\text{F}_5\text{O}^+$	$\text{HF}+\text{H}_2$	34	23
	168	$\text{C}_3\text{H}_2\text{F}_5\text{O}^+$	HF	61	53
	167	$\text{C}_3\text{HF}_6\text{O}^+$	H_2	3	-

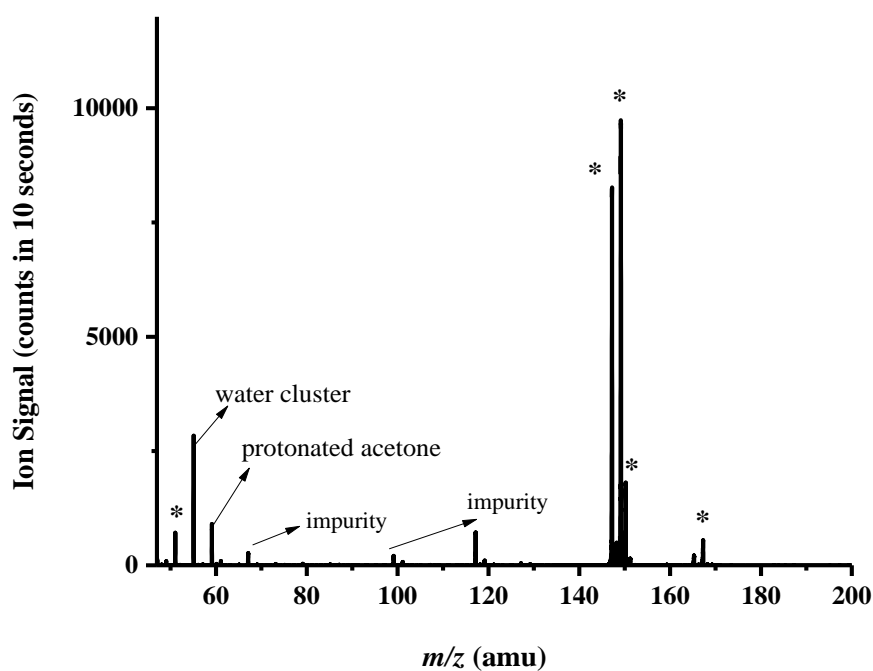
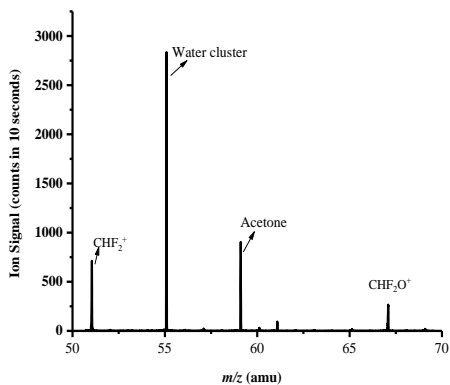
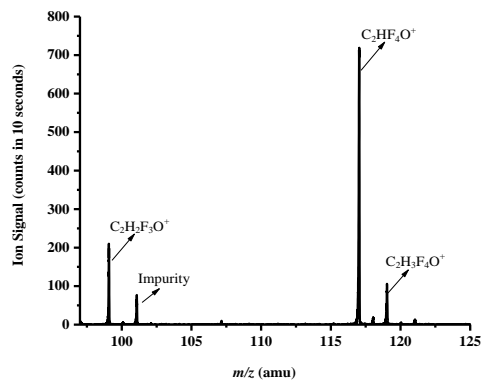


Figure 6.31 A mass spectrum illustrating the product ions resulting from the reaction of H_3O^+ with desflurane ($\text{C}_3\text{H}_2\text{F}_6\text{O}$) whilst operating the drift tube at a reduced electric field of 140 Td. Other impurities such as protonated acetone resulting from an impurity in the sample are also highlighted.

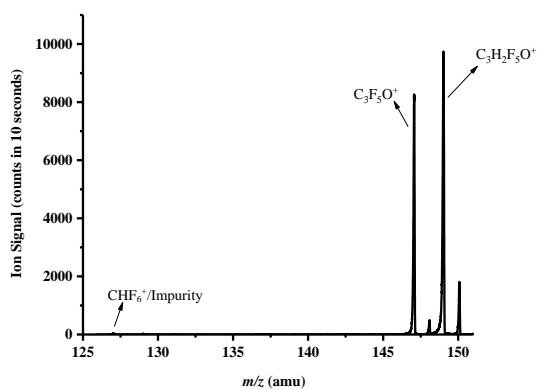
c)



d)



a)



b)

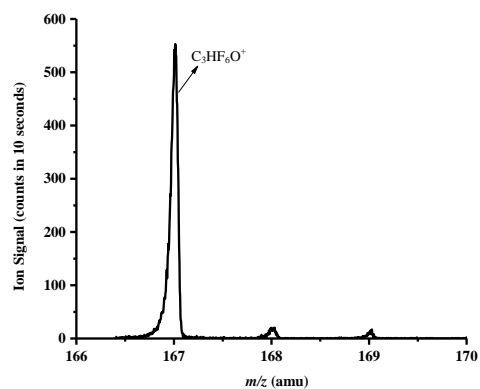


Figure 6.32 Mass spectrum illustrating product ions resulting from the reactions of H_3O^+ with desflurane to illustrate their isotopic abundances a) m/z 51 (CHF_2^+), m/z 67 (CHF_2O^+) b) m/z 99 ($\text{C}_2\text{H}_2\text{F}_3\text{O}^+$), m/z 101 (Impurity), m/z 117 ($\text{C}_2\text{HF}_4\text{O}^+$) and m/z 119 ($\text{C}_2\text{H}_3\text{F}_4\text{O}^+$) c) m/z 127 (CHF_6^+ /Impurity), m/z 147 ($\text{C}_3\text{F}_3\text{O}^+$) and m/z 149 ($\text{C}_3\text{H}_2\text{F}_5\text{O}^+$) d) m/z 167 ($\text{C}_3\text{HF}_6\text{O}^+$).

Figure 6.33 illustrates how the product ion distributions vary as a function of the reduced electric field. For all nearly all values of E/N the dominant ions are m/z 149 ($C_3H_2F_5O^+$) and m/z 147 ($C_3F_5O^+$). Only at above about 210 Td, does the branching ratio for CHF_2^+ become larger than that for $C_3F_5O^+$. The branching ratio for m/z 149 ($C_3H_2F_5O^+$) (80 Td-220 Td) and m/z 147 ($C_3F_5O^+$) (160 Td-220 Td) decreases owing to more fragmentation as the collisional energies of both the reagent ions and product ions increase with increasing E/N . Meanwhile, m/z 147 ($C_3F_5O^+$) branching ratio decreases as the reduced electric field decreases.

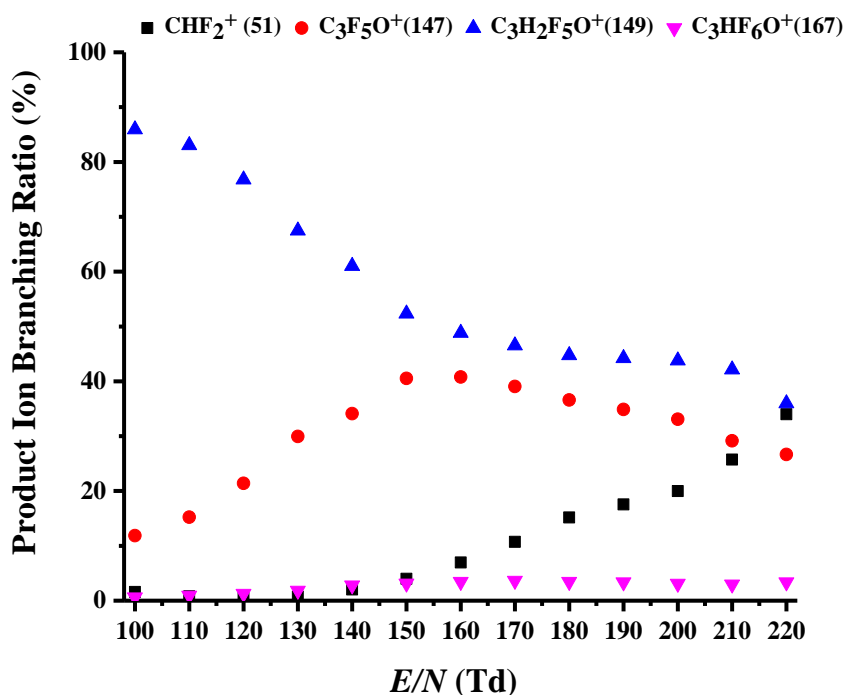


Figure 6.33 Product ion branching ratios in percentages as a function of E/N resulting from the reaction of H_3O^+ with desflurane ($C_3H_2F_6O$).

6.4 Conclusion

Although previous studies were based on a small number of studies and samples, the findings suggest that there is high potential of using exhaled breath to monitor and investigate the elimination characteristics of anaesthetics in the near future via PTR-MS biomonitoring of specific exhaled anaesthetics. A few studies performed by researchers have proved that it is possible to measure VOCs concentrations from common clinical specimens such as urine, blood and exhaled breath and they proposed to have more investigations via implementing longitudinal studies to have a better understanding.

In this study, the PTR-MS headspace analysis of various general anaesthetics, halothane, isoflurane, enflurane, sevoflurane, methoxyflurane and desflurane, was presented for two reagent ions, H_3O^+ and O_2^+ . The major aim of this study was to provide a database of the product ions that need to be recorded if these anaesthetics are going to be monitored for washout studies.

Reported for the first time are PTR-MS studies of enflurane, methoxyflurane and desflurane. The Density Functional calculation by Dr Peter Watts has given us some clues about the possible formation and fragmentation of isoflurane and enflurane. However, there were some disparities on different branching ratios produced by different instruments. These need further investigation.

The ion chemistry for H_3O^+ and O_2^+ with these compounds is very complex, because of the many product ions observed in each reaction. The detailed information of ion chemistry of each anaesthetic compound and specific monitored ion channels are identified and discussed. In most of the studies, the protonated parent (H_3O^+ as reagent ion) and parent ion by charge transfer (for O_2^+ as reagent ions) were not observed.

Certainly, most of these anaesthetic compounds react via non-collisional dissociation. However, the protonated parent ion using H_3O^+ reagent ions, quickly dissociates into other product ions. This study will be useful for diagnostics purpose in future washout characteristics studies.

Now, there is some concrete data of the potential ions provided from the anaesthetics gas either using H_3O^+ or O_2^+ as reagent ions to aid the investigation on washout characteristics of anaesthetics gases for patients who have undergone surgery and also possibly for staff who were exposed to these highly volatile anaesthetics, mainly for occupational health and safety in the operating theatres.

CHAPTER 7

7 BREATH ANALYSIS TO DETERMINE HUMAN WASHOUT CHARACTERISTICS OF KEY VOLATILE ORGANIC COMPOUNDS CONTAINED IN PEPPERMINT OIL

7.1 Introduction

In general, pharmacokinetic (and hence washout) characteristics of ingested drugs and health supplements are usually determined using an analysis of serum, blood or urine [72]. But the drawing of blood is not preferred by the patients and sample handling requires a well-established lab and trained staff.

Breath sampling and analysis provides a non-invasive method to investigate the washout characteristics of drugs and to detect their metabolites. Furthermore, there is an unlimited supply of the sample. One of the first PTR-MS studies to do this was by Harrison et al., who observed the washout of propofol from a patient who had been heavily sedated [4]. Another PTR-MS study was by Beauchamp et al., who undertook an investigation of the washout characteristics of eucalyptol (1, 8-cineol) via exhaled breath [124]. Ruzsanyi et al. followed-up the study by Beachamp, but with a more strict time schedule and using a multi capillary column IMS (Ion mobility spectroemeter) in addition to PTR-MS[125]. The IMS results were found to be in good agreement with those obtained using PTR-MS, with time-concentration curves showing good reproducibility for each volunteer (but less so between volunteers). In addition to that, Fernandez del Rio at al. reported a PTR-MS study dealing with the elimination of isoflurane on patients following a liver transplant [5].

During the 2016 IABR Standardisation Focus Group Meeting in Zurich, Professor Paul Thomas (Loughborough University) proposed a pharmacokinetic benchmarking study, which would compare breath volatile data from different groups using different analytical techniques. This is to aid towards standardised breath analysis and measurement protocols. It was suggested that peppermint oil capsules (readily purchased as health supplements) could be used for this purpose. Dr. Simona Cristescu (Nijmegen University, The Netherlands) became the lead and driver for this programme. The Molecular Physics Group at the University of Birmingham, and the Institute for Breath Research, Austria applied to be part of this European consortium, which is being coordinated by Ben Henderson, University of Nijmegen. In this chapter, preliminary data taken in collaboration with a study at the Institute for Breath Research, University of Innsbruck are presented.

An additional reason for the Molecular Physics Group to be involved was to obtain data for the metabolism of limonene contained in peppermint oil in order to get data through non-invasive breath sampling of liver function for healthy volunteers. This is of interest in relation to their studies on liver disease [2], [126].

Thus in summary the key aims of this study are:

(i) To aid in the benchmarking endeavour to estimate the range of results between participating laboratories

and

(ii) To provide breath data for healthy volunteers which would then be followed-up in a separate study with patients who are suffering from liver disease (a separate ethics approval will be made for that).

The protocol for recruitment and ingestion of the capsules was prepared by Prof. P. Thomas, Dr. S Cristescu, Dr. J Beauchamp, and Dr. S Fowler.

For the measurements reported here, ethical approvals were obtained at the University of Innsbruck and the University of Birmingham. Although ethical approval was gained to do this study in October 2017, in Birmingham, time constraints meant that there was insufficient time to do work there. Instead, the work presented here was done in collaboration with another PhD student, Ms. Michaela Malásková, in the Institute for Breath Research, in Dornbirn, University of Innsbruck in December 2017. Unfortunately, only four people were recruited during the period I was in Dornbirn. Nevertheless, the results are interesting and illustrate the complexity of the use of such measurements for standardization procedures. This work presented in this thesis will be added to those from other groups, leading to a significant database of pharmacokinetic information using breath analysis.

In this study the breath profile of a participant was monitored after he/she swallowed a peppermint oil capsule. The details of the peppermint oil capsule and the protocol will be given in the experimental section below. Once swallowed, the peppermint capsule dissolved in the stomach and the compounds in the capsule were released and entered the blood stream through the stomach and small intestines. Following the absorption of the volatiles into the blood stream, they are distributed throughout the body via the circulatory system, and following this metabolism and excretion of the volatiles occur, which leads to the loss (washout) of the compounds.

Volatiles in the blood stream can exchange in the lungs, and thus be monitored in the breath. Hence the decrease in concentration of the compounds in the blood stream as

a result of the metabolic and excretion processes can be monitored in the breath. Breath thus provides a non-invasive window to monitor these processes.

In summary, the objective of this study is to monitor temporal changes in the body concentrations of key volatiles contained in peppermint oil after the ingestion of a peppermint capsule using PTR-MS.

7.2 Experimental Details and Protocol

All the work presented in this chapter was done in a collaborative programme at the Institute for Breath Research in Dornbirn Austria using a PTR-TOF 8000. Real-time breath samples were analysed using an IONICON buffered end-tidal device (BET) [127] connected to a PTR-TOF 8000 (figure 7.1), so that real time measurements, and hence individual breaths, could be obtained. Details of the BET are given below in Section 7.5. The PTR-MS was operated at 130 Td with the drift tube pressure and temperature maintained at 2.2 mbar and 70 °C, respectively.

A full description of the standardised breath experiment has been prepared by Thomas et al. [private document for IABR]. In brief, a volunteer swallows a 200 mg peppermint food supplement capsule, which dissolves in the stomach. The volatile compounds enter the blood stream, and these and their metabolites are subsequently detected in their breath. Owing to elimination and metabolism the volatile compounds decrease in concentrations, and hence the washout characteristics can be recorded. Breath samples are not monitored continuously, but at set times, e.g. every 30 minutes. A baseline is first taken, however, before the ingestion of a capsule. Typical measurement times for our studies are -30 minutes (background) followed by 0 hr (ingestion), and then every 30 minutes for approximately 6 hours. Samples of the air in the laboratory were also recorded. For each

measurement period, the volunteer supplied 5 breaths using BET. These measurements from these five breaths were then averaged in the subsequent analysis using only the alveolar phase of the breath.

The purpose of the initial sample is to establish baseline levels of VOCS from peppermint oil in exhaled breath from potential dietary or environmental effects.

In addition to the above general protocol, an additional breath measurement was acquired immediately when the volunteer (or his/her colleagues) noticed the taste/smell of peppermint in his/her exhaled breath usually at 15 min intervals until the signal of peppermint decrease gradually. This additional protocol was adopted to make allowances for the volatiles coming up from the gut to the mouth soon after the capsule begins to dissolve, so that we can ascertain when the “true” (blood) volatiles are present in the breath. A continuous observation during one set of breath tests was done until the breath peppermint concentrations rise continuously for each consecutive exhalation. This frequent sampling of exhalations continued until the VOCs from the peppermint concentration reached a peak and then decreased. Subsequently, the standard protocol was once again adapted to continue until reaching the end protocol time (360 minutes) [124]. The integration time was set to 1 Sec.



Figure 7.1 A breath-volunteer exhaling smoothly through the BET which was coupled to a PTR-TOF 8000 (not shown). For each measurement five breaths were collected.

7.3 Peppermint Oil Capsules

This investigation used Boots Pharmaceuticals Digestive Health Peppermint Oil 200 mg capsules. On the information sheet on the health supplement bottle, the main ingredients of the oil are listed only as peppermint and soya. The capsule itself is made from beef gelatine and glycerol. No other information on the ingredients of the peppermint oil is provided.

As with any matrix, without any separation of compounds, it is impossible to ascertain which compounds in the peppermint oil would be contributing to a given m/z in the mass spectrum recorded using PTR-MS. However, from GC/FID and GC-MS studies of peppermint oil by Schmidt et al. [11], the main chemical composition of peppermint oil (summarised in table 7.1) can be identified. Using these results, the main compounds are menthol, menthone, menthyl acetate, 1, 8-cineole, limonene, β -pinene and β -caryophyllene. Hence this gives us a good idea of what the key volatiles in peppermint oil. But some care needs to be taken here, because the concentrations of volatiles and even the actual volatiles can change owing to differences in manufacturer of the peppermint oil.

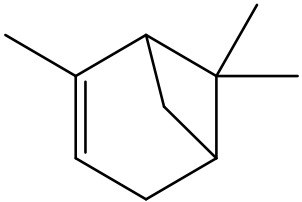
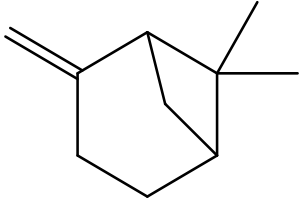
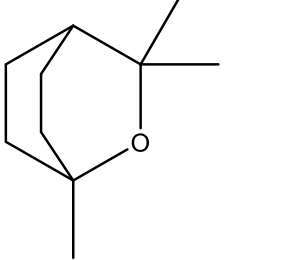
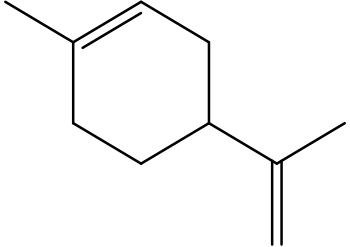
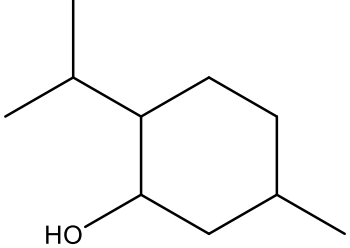
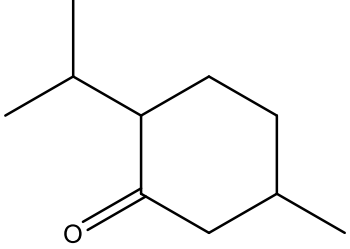
A GC-MS study of the oil contained in the Boots' capsules is currently being undertaken to determine this at the Institute for Breath Research in Dornbirn. Unfortunately, there was no time to do this during the breath measurements. Nevertheless, several of the major compounds identified in the work by Schmidt et al. were separately measured on the PTR-8000 at the reduced electric field of 130 Td in order to determine which compounds could be contributing to a mass spectral peak in the breath and peppermint oil headspace analyses.

Table 7.1 The principle chemical composition of peppermint oil adapted from the GC work reported by Schmidt et al. [11].

Chemical	MW	Protonated <i>m/z</i>	Chemical formula	Relative Conc. (%)	Odour
α -pinene	136	137	C ₁₀ H ₁₆	0.7	pine-like, warm, herbal
β -pinene	136	137	C ₁₀ H ₁₆	1.1	resinous-piney, dry
limonene	136	137	C ₁₀ H ₁₆	2.6	lemon-like, fresh
menthofurane	150	151	C ₁₀ H ₁₄ O	3.7	fresh-minty, herbal, slightly cool
pulegon	152	153	C ₁₀ H ₁₆ O	1.9	herbal-minty, camphorous
menthone	154	155	C ₁₀ H ₁₈ O	23.4	minty
1,8-Cineole	154	155	C ₁₀ H ₁₈ O	5.3	eucalyptus-like, fresh
isomenthone	154	155	C ₁₀ H ₁₈ O	3.7	fresh, cool- minty
menthol	156	157	C ₁₀ H ₂₀ O	40.7	cool-minty
menthyl acetate	198	199	C ₁₂ H ₂₂ O ₂	0.3	ethereal, nearly odourless
β - caryophyllene	204	205	C ₁₅ H ₂₄	1,7	β - Caryophyllene

Using table 7.1 we have selected menthone and menthol to investigate separately on a KORE PTR-ToF-MS. However, just because the concentrations are high in the oil that does not mean that the concentrations will be high in the breath, owing to differences in absorption, metabolism and excretion. (Hence it will therefore be extremely interesting to compare our PTR-MS results (real-time measurements) with those taken by the other groups involved in this study who are using GC-MS (not real-time) for their breath analysis.) Therefore, with this uncertainty some other compounds were selected to measure, namely menthol, menthone, α -pinene, β -pinene, 1, 8-cineole, and limonene. 1,8-cineole in particular is not metabolised efficiently in the body, and is removed from the blood via gas exchange in the lungs, whereas menthol is metabolised into menthol glucuronide in the liver and urinated out of the body [128]. Table 7.2 provides pertinent details on these compounds (molecular weight, CAS number, vapour pressure and molecular structure).

Table 7.2 Details about standard compounds investigated in this study related to peppermint oil capsule in this experiment, including vapour pressure and purity.

Molecular weight of the lightest isotopomer <i>m/z</i>	CAS Number/purity and company	Vapour pressure[129, 130]	Chemical structure
α -Pinene C ₁₀ H ₁₆ 136	7785-70-8 99 % Sigma Aldrich	3 mm Hg (20 °C)	
β -Pinene C ₁₀ H ₁₆ 136	18172-67-3 99 % Sigma Aldrich	2 mm Hg (20 °C)	
1,8-Cineole C ₁₀ H ₁₈ O 154	470-82-6 99% Sigma Aldrich	unknown	
Limonene C ₁₀ H ₁₆ 136	5989-27-5 99% Sigma Aldrich	1.98 mm Hg at (25 °C)	
Menthol C ₁₀ H ₂₀ O 156	89-78-1 99% Sigma Aldrich	7.67 x 10 ⁻³ mm Hg (25 °C)	
Menthone C ₁₀ H ₁₈ O 154	10458-14-7 99% Sigma Aldrich	0.28 mm Hg at (25 °C)	

Given that the pinenes and limonene are isomers, the similar product ions can be expected from these compounds, and hence for the analysis of the breath volatiles, we will be presenting the sum contribution of these for a particular m/z .

To obtain the mass spectra, a 0.1 μ l of each sample was taken using a microsyringe and placed in a 5 ml vial. The vial was connected to nitrogen gas flow using a Teflon tube and peek tube to the inlet line. Background spectra were taken for each vial at 130 Td prior to the sample measurements. The inlet and the drift tube temperature were fixed at 100 °C.

7.4 Participant information

Every participant's details about height (cm), weight (kg), age (years), BMI (Body Mass Index), as well as questions about diet, personal habits and lifestyle were recorded in the participant information form. These details will enable us to exclude possible dietary or lifestyle factors from influencing the results.

Unfortunately, owing to time constraints, only measurements taken of 2 males and 2 females with an age range of 37-58 are reported here. But these illustrate the method and type of results. Details (Age, Sex and quantity of repeated measurement) of each volunteer are listed in table 7.3.

No dietary requirements were required. However, the volunteers were requested to fast for 10 hours prior to the measurements. To make this easier on the volunteer the measurements were started in the morning.

Table 7.3 Details of the age, sex and number of measurements of the volunteers who participated in this peppermint oil study.

Volunteer	Age	Sex	Number of measurements
1	58	Male	1
2	45	Male	1
3	37	Female	4 (sequential days)
4	28	Female	3 (sequential days)

All participants were provided with a volunteer information sheet upon recruitment and informed consent procedures were followed. Participants were asked to breathe normally for up to 5 minutes before beginning the study.

7.5 Buffered End Tidal (BET)

Herbig J et al. introduced a real-time breath- gas sampling method known as buffered end-tidal (BET) on-line sampling. Figure 7.2 shows the BET system which can be easily coupled to a PTR-MS system. There are several advantages for using the BET method compared to conventional direct sampling. In this approach, the end-tidal portion of the breath-gas sample is buffered using a single exhalation of breath delivered via a tailored tube [127]. This helps to increase the sampling time by typically several seconds. Consequently, it improves the signal quality and reduces the total measurement time per participant. Besides that, the participant can maintain a normal breathing style, consequently limiting the risk of hyperventilation. Figure 7.2 shows the volunteer's breath sampling method using BET.

The BET sampling was tested by Herbig J et al. to compare the measurements with direct on-line sampling using PTR-MS. They found a good agreement between acetone and acetonitrile concentrations. The only variabilities observed were high differences in breath to breath isoprene concentrations. This variability could be from the different strength of exhalation and hyperventilation on end tidal concentrations [127].

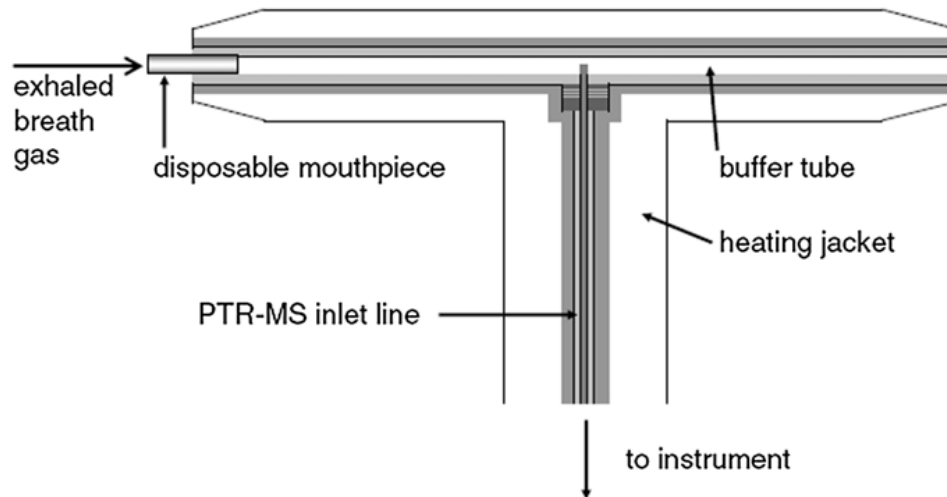


Figure 7.2 Schematic of the buffered end-tidal (BET) sampling apparatus (reproduced from Herbig *et al.* Journal of Breath Research (2008) [127]).

Results and Discussion

7.6 Headspace measurements of compounds associated with peppermint oil

7.6.1 Headspace of α -pinene

The proton affinity for α -pinene is < 854 kJ/mol [131]. Therefore, it efficiently reacts with H_3O^+ , either dissociatively or non-dissociatively [132]. Figure 7.3 presents an overview of the mass spectrum of α -pinene recorded at 130 Td. Table 7.4 provides the product ions resulting from the reaction of α -pinene with H_3O^+ at 130 Td. Eleven product ions were identified at m/z 43 ($\text{C}_2\text{H}_3\text{O}^+$), 57 (C_4H_9^+), 67 (C_5H_7^+), 69 (C_5H_9^+), 81 (C_6H_9^+), 93 (C_7H_9^+), 95 ($\text{C}_7\text{H}_{11}^+$), 109 ($\text{C}_8\text{H}_{13}^+$), 135 ($\text{C}_{10}\text{H}_{15}^+$) and 137 ($\text{C}_{10}\text{H}_{17}^+$). The most dominant product ion from the headspace of α -pinene is at m/z 137 (protonated parent ion) (relative intensity 100). Other ions were observed at m/z 81 contributing 98% to the relative intensity. This was followed by m/z 95 (12), m/z 67 (5), m/z 93 (4), m/z 135 (4), m/z 57 (3), m/z 109 (2), m/z 43 (1) and m/z 69 (1).

Using a drift tube voltage of 580 V (corresponding to about 140 Td) Maleknia et al. observed the following product ions resulting from α -pinene (relative intensities in brackets) [133]; at m/z 81 (100), m/z 137 (44), m/z 93 (21.7), m/z 95 (7.2), m/z 135 (1.5), m/z 107 (1) and m/z 109 (0.9) [133]. We observed similar product ions except m/z 107 but with a different relative abundance. In their measurement, the most dominant ion is at m/z 81, whereas in our study at 130 Td the dominant product ion is at m/z 137, followed by m/z 81, m/z 95 and m/z 67. The disparities of the relative intensity are simply because of different instruments were being used. Materic et al, reported m/z 81 and 137 are the two major fragments from α -pinene. However, Materic et al, have not reported on m/z 135, 95, 93, 67, 69, 57, 57 and 43 in their measurement using PTR-ToF-8000 [132]. This

is purely because two different instruments were used. The instruments have a different transmission factor and transfer optic factor (as mentioned in chapter 6 discussion that branching ratios are very much instrumental dependent).

According to Tani et al. monoterpenes α -pinene produces fragmentation ions such as m/z 67, 81 ($C_6H_8H^+$), and m/z 95, and also protonated m/z 137 ($C_{10}H_{16}H^+$) [134]. These product ions agree with our study.

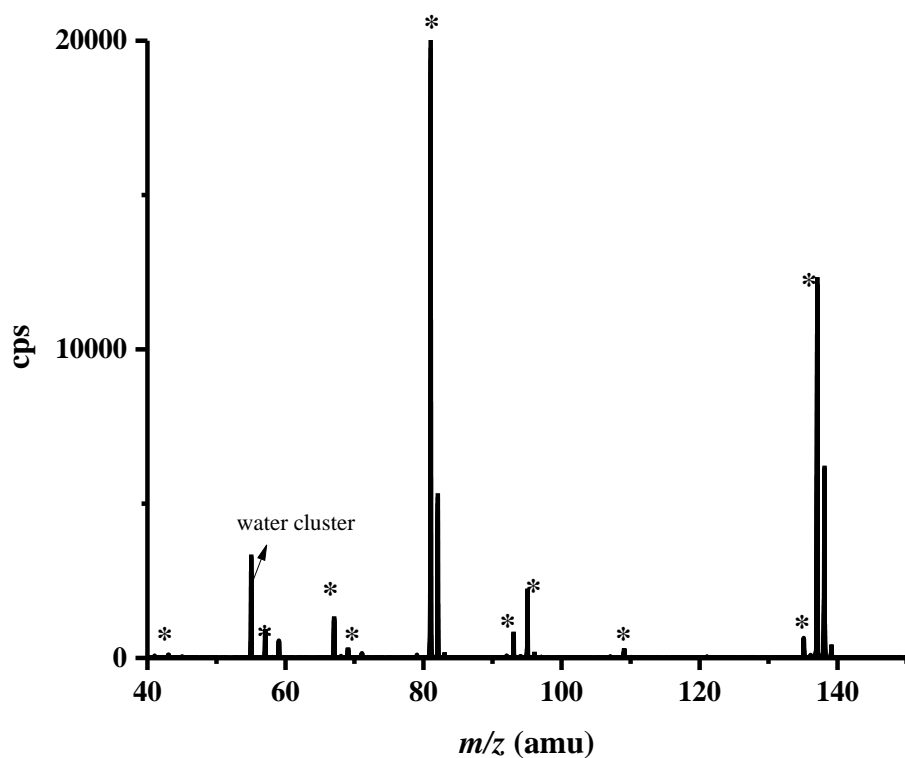


Figure 7.3 A mass spectrum illustrating the product ions (starred) resulting from the reaction of H_3O^+ with α -pinene ($C_{10}H_{17}$) at a reduced electric field of 130 Td.

Table 7.4 Table m/z values of the product ions and their relative intensities (dominant ion given an intensity of 100) resulting from the reaction of α -pinene with H_3O^+ at a reduced electric field of 130 Td.

m/z	Assignments	Relative Intensity (%)
43	$\text{C}_2\text{H}_3\text{O}^+$	1
57	C_4H_9^+	3
67	C_5H_7^+	5
69	C_5H_9^+	1
81	C_6H_9^+	98
93	C_7H_9^+	4
95	$\text{C}_7\text{H}_{11}^+$	12
109	$\text{C}_8\text{H}_{13}^+$	2
135	$\text{C}_{10}\text{H}_{15}^+$	4
137	$\text{C}_{10}\text{H}_{17}^+$	100

7.6.2 Headspace of β -pinene

The proton affinity of β -pinene is unknown. Nevertheless, we assume it will be similar to α -pinene because it is an isomer of α -pinene and hence will readily react with H_3O^+ either dissociatively or non-dissociatively. Figure 7.4 shows an overview of a PTR-MS mass spectrum of β -pinene at 130 Td. Table 7.5 provides the product ions of β -pinene at 130 Td. As shown in table 7.5, there were ten product ions observed as a result of β -pinene reactions with H_3O^+ .

The observed product ions at 130 Td were m/z 57 (C_4H_9^+), 67 (C_5H_7^+), 79 (C_6H_7^+), 81 (C_6H_9^+), 93 (C_7H_9^+), 95 ($\text{C}_7\text{H}_{11}^+$), 107 ($\text{C}_8\text{H}_{11}^+$), 109 ($\text{C}_8\text{H}_{13}^+$), 135 ($\text{C}_{10}\text{H}_{15}^+$) and 137 ($\text{C}_{10}\text{H}_{17}^+$). We observed the m/z 137 protonated parent ion. α -pinene and β -pinene are isomers as pointed out earlier. Therefore, the observed product ions were similar in both compounds. However, the relative intensities for each ion is different although the product ions are similar. The most dominant product ion was m/z 137 (100) which is the protonated parent ion. This was followed by m/z 81 (99), 95 (16), m/z 135 (6), m/z 67 (6), m/z 79 (2), m/z 57 (2), m/z 109 (1), m/z 107 (1) and m/z 93 (1).

Tani et al. mentioned that fragments ions from β -pinene were m/z 67, 81 and 95 and the protonated molecular ion was 137 [134]. Similar ions were detected in our measurements but different relative intensities. Perhaps this also could be related to different instrumentation.

Materic et al reported that the most abundant ions from β -pinene are m/z 137 and m/z 81 [132]. Our results also showed that the most abundant ions are m/z 137 and m/z 81. However, Materic et al have not reported about other product ions related to β -pinene.

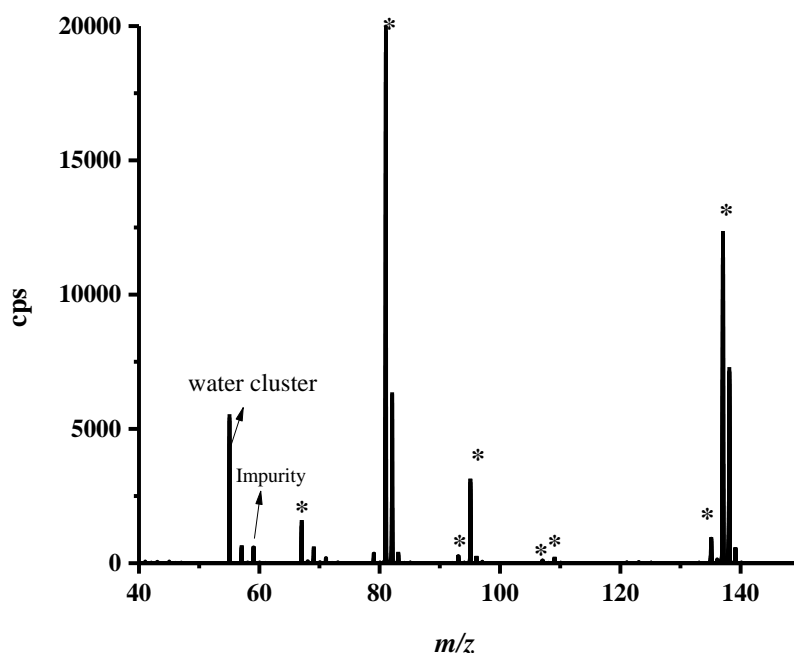


Figure 7.4 A mass spectrum illustrating the product ions (starred) from the reaction of H_3O^+ with β -pinene ($\text{C}_{10}\text{H}_{17}$) whilst operating the drift tube at reduced electric field of 130 Td for 10 second experiment time.

Table 7.5 m/z values of the product ions and their relative intensities (dominant ion given an intensity of 100) resulting from the reaction of β -pinene with H_3O^+ at a reduced electric field of 130 Td.

m/z	Assignments	Relative intensity (%)
57	C_4H_9^+	2
67	C_5H_7^+	6
79	C_6H_7^+	2
81	C_6H_9^+	99
93	C_7H_9^+	1
95	$\text{C}_7\text{H}_{11}^+$	16
107	$\text{C}_8\text{H}_{11}^+$	1
109	$\text{C}_8\text{H}_{13}^+$	1
135	$\text{C}_{10}\text{H}_{15}^+$	6
137	$\text{C}_{10}\text{H}_{17}^+$	100

7.6.3 Headspace of 1,8-cineole

The proton affinity of 1,8-cineole is unknown. However, it can react with water molecule either via dissociatively or non-dissociatively [124]. Figure 7.5 presents the mass spectrum of 1,8-cineole at 130 Td. Table 7.6 summarises the product ions and the relative intensity of 1,8-cineole at 130 Td. The observed product ions are at m/z 81, 95, 137 and 155. m/z 155 is the protonated parent. This indicates that H_3O^+ reacts with 1,8-cineole in a PTR-MS dissociatively and non-dissociatively. The relative intensities of these ions are m/z 137 ($C_{10}H_{17}^+$) (100), m/z 81 ($C_6H_9^+$) (63), m/z 155 ($C_{10}H_{19}O^+$) (11), and m/z 95 ($C_7H_{11}^+$) (1) with the relative intensities are given in the brackets.

According to Maleknia et al. the most abundant compound at 580 V from 1,8-cineole is m/z 81 (100, relative intensity calculated on the basis of ion counts/s), at 480 V it has a relative intensity of 85, whilst at 380 V it has only a relative intensity of 4 [133]. This illustrates the effect of the reduced electric field on collision induced dissociation. The relative intensity for m/z 137 is different from Maleknia et al. compared to our study where we found the contribution from m/z 137 is 100 % at 130 Td. Maleknia et al., also detected m/z 155 with only a relative intensity of 0.3 at 580 V (140 Td), whereas we observe a higher relative intensity of 11 in this study. Moreover, Maleknia et al. have found an additional peak at m/z 95 (7.8), whereas in this study, only 1 was obtained. Tani reported m/z 81, 95, 137, 155 and 173 as fragment ions of 1,8-cineole using PTR-MS in terpenoids (cineole) study [135, 136]. Tani's findings agree with our findings except for m/z 173. Besides that, Steegh et al. found m/z 81 and 137 from their investigation on metabolites emit from a plant (*Arabidopsis*) where 1,8-cineole was identified as one of the metabolite using PTR-MS [135]. We also found m/z 81 and m/z 137 as abundant product ions

from 1,8-cineole. In addition to that, Beauchamp et al. refer m/z 81, 137 and 155 as the product ions detected from headspace of 1,8-Cineole (eucalyptol) [124].

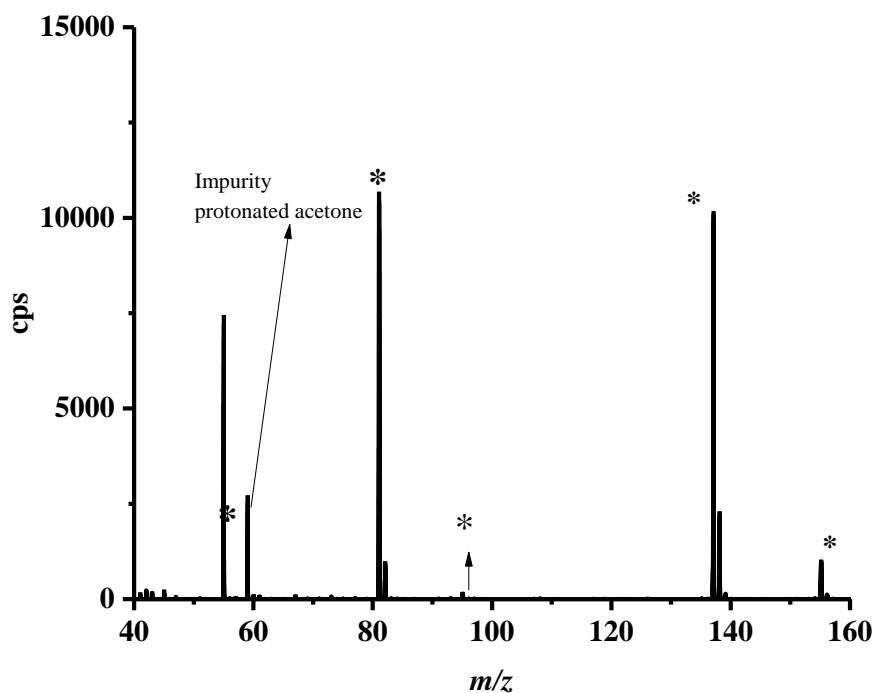


Figure 7.5 A mass spectrum illustrating the product ions (starred) from the reaction of H_3O^+ with 1,8-cineole ($\text{C}_{10}\text{H}_{19}\text{O}$) whilst operating the drift tube at reduced electric field of 130 Td. Other ion such as impurity ion coming from the drift tube is also highlighted.

Table 7.6 m/z values of the product ions and their relative intensity resulting from the reaction of 1,8-cineole with H_3O^+ at a reduced electric field of 130 Td.

m/z	Assignments	Relative Intensity (%)
81	C_6H_9^+	63
95	$\text{C}_7\text{H}_{11}^+$	1
137	$\text{C}_{10}\text{H}_{17}^+$	100
155	$\text{C}_{10}\text{H}_{19}\text{O}^+$	11

7.6.4 Headspace of limonene

The proton affinity of limonene is 875 kJ/mol [29, 137]. Figure 7.6 shows the mass spectrum of limonene, whilst table 7.7 provides the details of the product ions with relative intensity measured at 130 Td resulting from reactions with H_3O^+ . Four product ions are identified at m/z 67 (C_4H_9^+), 81 (C_6H_9^+), 95 ($\text{C}_7\text{H}_{11}^+$) and 137 ($\text{C}_{10}\text{H}_{17}^+$). The protonated parent ion is at m/z 137 (100). Dissociative proton transfer leads to the m/z 81 (76), m/z 95 (11) and m/z 67 (1) product ions.

Using a PTR-Quad-MS, Hewitt et al. reported product ions at m/z 67, 81, 95 and 137 between 120-130 Td [138]. m/z 67 only contributed approximately 0.1 % of total abundance at 120 Td. In our study, m/z 67 has also contributed a small relative intensity of 1 at 130 Td, and hence can be ignored. Also, there was no ion at m/z 67 reported by Fernandez del Rio in her limonene study [2]. Meanwhile, Materic et al, have only found two major ions from limonene which are m/z 137 and 81 [132].

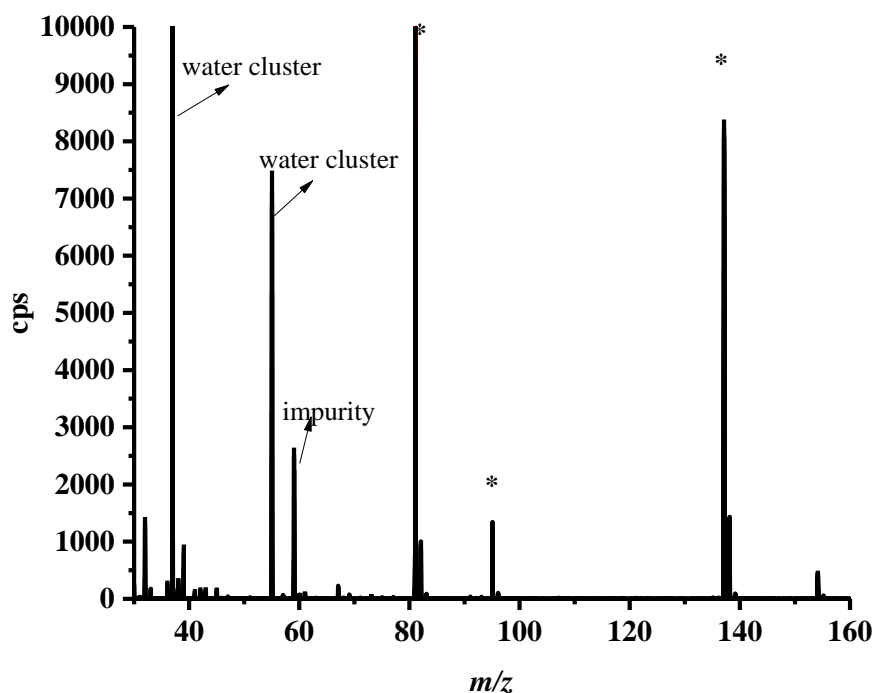


Figure 7.6 A mass spectrum illustrating the product ions (starred) from the reaction of H_3O^+ with limonene ($\text{C}_{10}\text{H}_{17}$) whilst operating the drift tube at reduced electric field of 130 Td. An ion resulting from an impurity of acetone in the drift tube is highlighted, and protonated water clusters (m/z 37 and m/z 55) were observed in this measurement.

Table 7.7 m/z values of the product ions and their relative intensities (dominant ion given an intensity of 100) resulting from the reaction of limonene with H_3O^+ at a reduced electric field of 130 Td.

m/z	Assignments	Relative Intensity (%)
67	C_4H_9^+	1
81	C_6H_9^+	76
95	$\text{C}_7\text{H}_{11}^+$	11
137	$\text{C}_{10}\text{H}_{17}^+$	100

7.6.5 Headspace of menthone

The proton affinity of menthone is unknown. Hence, it reacts with H_3O^+ either dissociatively or non-dissociatively [101]. From the results summarised in figure 7.7 and table 7.8 five product ions result from the reaction of H_3O^+ with menthone at 130 Td. These product ions were observed at m/z 59 ($\text{C}_3\text{H}_7\text{O}^+$), m/z 81 (C_6H_9^+), m/z 95 ($\text{C}_7\text{H}_{11}^+$), m/z 137 ($\text{C}_{10}\text{H}_{17}^+$) and m/z 155 ($\text{C}_{10}\text{H}_{19}\text{O}^+$). The dominant ion observed is at m/z 155, which is the protonated parent. This is followed by m/z 137 (29), m/z 81 (14), m/z 95 (3) and m/z 59 (3).

In an earlier PTR-MS study by Tietz et al. at 140 Td, four product ions associated with menthone were observed at m/z 81 (100), 95 (31), 137 (26) and 155 (11) [139]. In our study, similar product ions are found at 130 Td but the calculated relative intensities are different. This could be due to different instruments being used.

According to a PTR-Quad-MS study by Heenan et al. also at 140 Td, three product ions are associated with menthone, at m/z 81 (100 %), m/z 137 (30 %), m/z 155 (10 %) [101], which are different from our result, again illustrating issues of transmission of ions in different instruments.

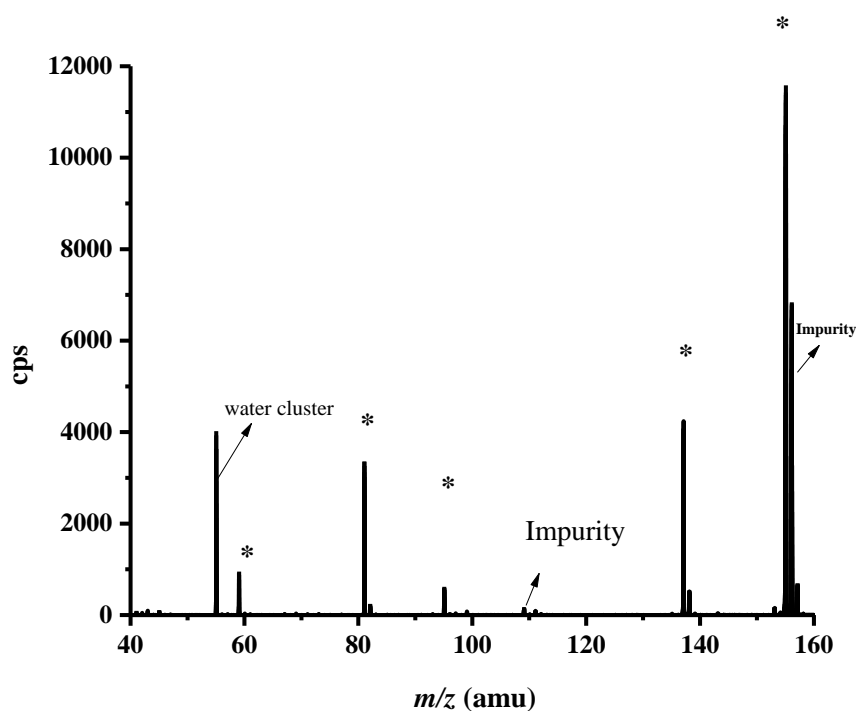


Figure 7.7 A mass spectrum illustrating the product ions (starred) from the reaction of H_3O^+ with menthone ($\text{C}_{10}\text{H}_{19}\text{O}$) whilst operating the drift tube at reduced electric field of 130 Td. An ion resulting from an impurity in the drift tube is identified.

Table 7.8 m/z values of the product ions and their relative intensities (dominant ion given an intensity of 100) resulting from the reaction of menthone with H_3O^+ at a reduced electric field of 130 Td.

m/z	Assignments	Relative Intensity (%)
59	$\text{C}_3\text{H}_7\text{O}^+$	3
81	C_6H_9^+	14
95	$\text{C}_7\text{H}_{11}^+$	3
137	$\text{C}_{10}\text{H}_{17}^+$	29
155	$\text{C}_{10}\text{H}_{19}\text{O}^+$	100

7.6.6 Headspace of menthol

The headspace of menthol was reported in Chapter 5 section 5.3.2. However, that was done on a first generation KORE-PTR-ToF-MS. The plan for the breath analysis in Birmingham was to use a second generation KORE PTR-TOF-MS which has a different drift tube configuration and a smaller TOF tube [140]. Therefore, the headspace analysis was repeated again for comparison with the first generation instrument. Figure 7.8 shows the mass spectrum of the headspace of menthol at 130 Td. Eight product ions are identified (table 7.9) at m/z 55 ($C_4H_7^+$), 57 ($C_4H_9^+$), 69 ($C_4H_5O^+$), 81 ($C_5H_5O^+$), 83 ($C_5H_7O^+$), 97 ($C_6H_9O^+$), 139 ($C_{10}H_{19}^+$) and 155 ($C_{10}H_{19}O^+$). m/z 155 (protonated parent ion) was detected via a non-dissociation process. This indicates that the reaction of menthol with H_3O^+ is via dissociative proton transfer. The most abundant product ion is at m/z 83 (100 relative intensity). This is followed by m/z 139 (88), m/z 57 (48), m/z 81 (34), 97 (25), m/z 69 (9), m/z 155 (1) and m/z 55 (1).

However, the study on headspace of menthol using the first generation KORE-PTR-ToF-MS produced eight product ions with m/z 55, 57, 69, 81, 83, 97, 139 and 155. For the headspace measurement of menthol using the second generation KORE-PTR-ToF-MS has produced seven product ions except m/z 55 which is less than 1. m/z 83 is the dominant ion in both measurement. Obviously, the reason for the difference in relative intensities is due to two different instruments were being used.

A prior E/N study (90-133 Td) using PTR-MS at 133 Td identified four product ions at m/z 55, 81, 83 and 139 [107]. According to Gordon et al. the most abundance product ion (the branching percentage) at 133 Td is m/z 83 (approximately 43 %). This is followed by m/z 55 (approximately 33 %), m/z 81 (approximately 16 %) and m/z 139 (approximately 8 %). Our measurements also find that the dominant product ion at 130

Td is m/z 83 (in relative intensity to 100). However, for the rest, there are significant discrepancies in the product ion intensities, which again relates to the difference in the mass discrimination of quadrupole compared to TOF mass spectrometers. There may also be differences in the transmission of the ions into the mass spectrometer and efficiencies of different ion detectors. Gordon et al. did not observe product ions at m/z 57, 69, and 97.

Similarly, differences are found in the relative intensities of product ions described in another PTR-Quad-MS study of menthol by Saint-Eve et al [106] at an E/N of 140 Td product ions were observed at m/z 81 (100), m/z 55 (62), m/z 83 (42), m/z 137 (22) and m/z 139 (4).

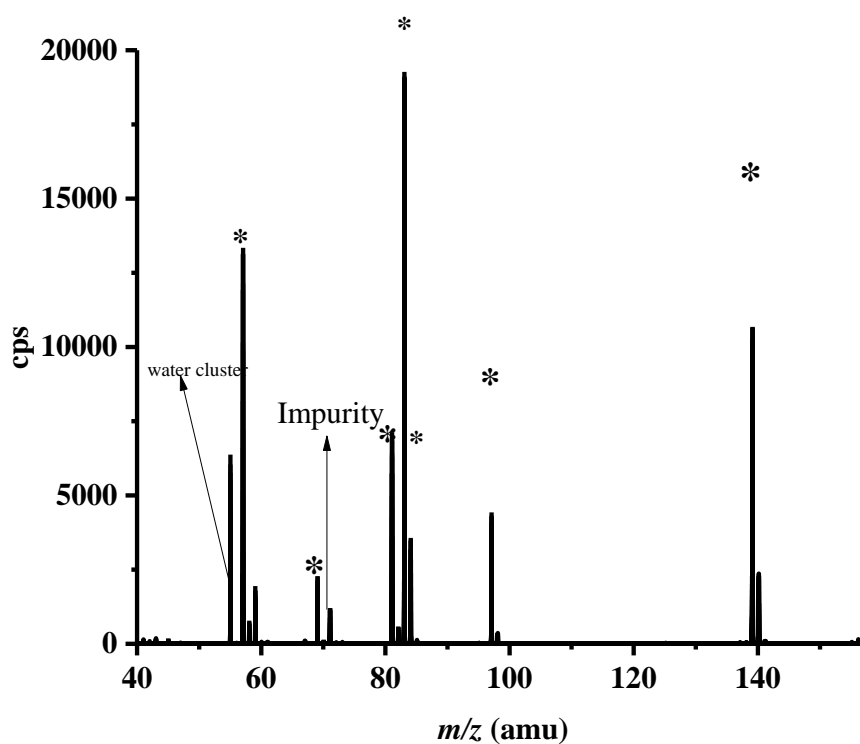


Figure 7.8 A mass spectrum illustrating the product ions from the reaction of H_3O^+ with menthol ($\text{C}_{10}\text{H}_{20}\text{O}$) whilst operating the drift tube at reduced electric field of 130 Td e. Impurity ion was observed in this measurement.

Table 7.9 m/z values of the product ions and their relative intensities (dominant ion given an intensity of 100) resulting from the reaction of menthol with H_3O^+ at a reduced electric field of 130 Td.

m/z	Assignments	Relative intensity (%)
57	C_4H_9^+	48
69	$\text{C}_4\text{H}_5\text{O}^+$	9
81	$\text{C}_5\text{H}_5\text{O}^+$	34
83	$\text{C}_5\text{H}_7\text{O}^+$	100
97	$\text{C}_6\text{H}_9\text{O}^+$	25
139	$\text{C}_{10}\text{H}_{19}^+$	88
155	$\text{C}_{10}\text{H}_{19}\text{O}^+$	1

7.6.7 Headspace of the oil contained in the Boots' Peppermint Capsule

Figure 7.9 presents the headspace mass spectrum of the oil contained in a Boots' peppermint capsule at 130 Td. Table 7.10 provides the relative intensity of peppermint product ions at 130 Td together with an assignment of the compounds that produce these ions following a reaction with H_3O^+ based on the headspace analysis of pure compounds presented in this chapter and upon the results of Schmidt et al [11].

The most abundant product ion is at m/z 155 (which is assigned a relative intensity of 100), as assigned to result from a number of compounds in the peppermint oil, namely menthol (loss of H_2 from the protonated parent), and protonated menthone, 1,8-cineole, and isomenthone. The next intense ion is at m/z 137 (33) which is assigned as to result from either a dissociative proton transfer reaction of H_3O^+ with 1,8-cineole and menthone, or non-dissociative proton transfer which can be contributions from protonated α -pinene, β -pinene and limonene. These are followed by m/z 83 (24) resulting from product fragment ions of menthol and β -pinene. These tentative assignments are based on our headspace study on associated compounds to peppermint oil containing capsules (section 7.6.1-7.6.6). m/z 81 (19) has contributions from α -pinene, β -pinene, limonene, menthol, menthone and 1,8-cineole. m/z 151 (11) most probably has contributions from menthofurane, menthol, methonane and α -pinene. m/z 57 is assigned to result from menthol, α -pinene and β -pinene. m/z 59 is protonated acetone which could be from the drift tube, (7), m/z 153 (5) comes from menthol, menthone fragmentation and pulegon. There were a few ions which have a relative intensity less than 5, including m/z 43 (protonated acetic acid), m/z 45 (protonated acetaldehyde), m/z 69 (protonated isoprene), m/z 95 (fragment ion from menthone, α -pinene and β -pinene), m/z 97 (fragment ion from menthol), m/z 135 (fragment ion from α -pinene and β -pinene), m/z 157 (protonated

menthol) and m/z 205 (protonated sesquiterpene and protonated β -caryophyllene) [11] . If m/z 205 is assigned as a sesquiterpene, it also can produced fragment ions at m/z 137 and 81 following a reaction with H_3O^+ , based on the results presented in a paper by Lee et al. [141].

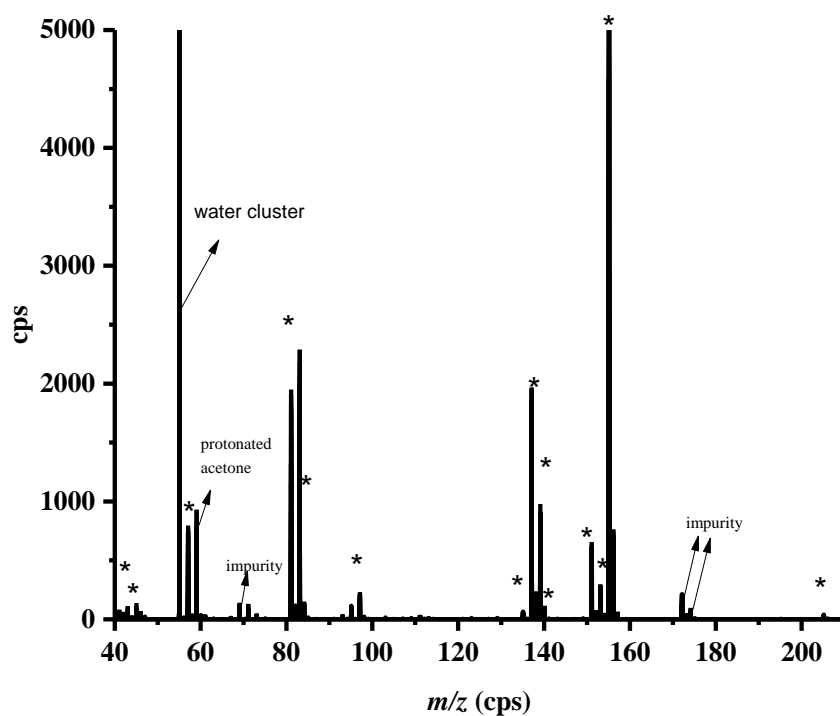


Figure 7.9 A mass spectrum illustrating the product ions and their intensities from the reaction of H_3O^+ with peppermint oil contained capsule whilst operating the drift tube at reduced electric field of 130 Td. Some impurity ions from the sample are highlighted.

Table 7.10 m/z values (tentative identification) of the product ions and their relative intensities (dominant ion given an intensity of 100) resulting from the reaction of peppermint capsule with H_3O^+ at a reduced electric field of 130 Td.

m/z	Compound/ fragment ion resulting from a reaction of H_3O^+	Relative intensity (%)
43	protonated acetic acid	1
45	protonated acetaldehyde	1
57	Menthol, α -pinene, and β -pinene	6
71	unassigned	1
81	α -pinene, β -pinene, limonene, menthol, menthone and 1,8-cineole	19
83	menthol and β -pinene	24
95	menthone, α -pinene and β -pinene	1
97	menthol	2
135	of α -pinene and β -pinene	1
137	α -pinene, β -pinene, limonene, menthone and 1,8-cineole	33
139	menthol	16
141	unassigned	2
151	menthofurane, menthol, methonane and α -pinene	11
153	menthol, menthone and pulegon	5
155	protonated menthone, protonated 1,8-cineole and menthol	100
157	protonated menthol	1
205	protonated sesquiterpene and protonated β -caryophyllene	1

7.6.8 VOCs in the exhaled breath after ingestion of a peppermint capsule

Based on the results presented in the last section, it is clear that the ions to be monitored for the breath analysis are at m/z 81, 137 and 155. These result from a number of compounds in the peppermint oil, and as mentioned it will be interesting to see what the GC-MS study achieves.

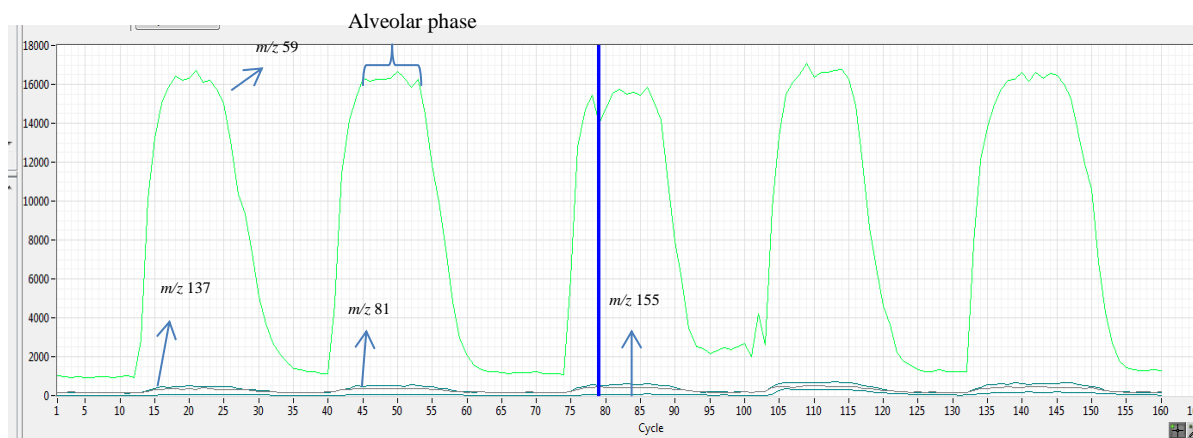


Figure 7.10 Shows five breaths for each measuring period by monitoring *alveolar phase* of m/z 59, 81, 137 and 155.

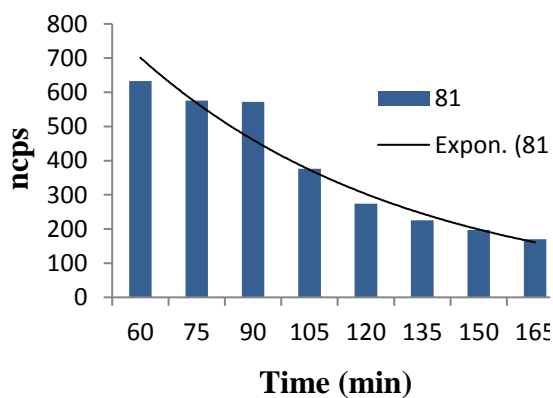
Following the protocol described in section 7.2, five breaths were collected for each measuring period. An illustration of these breaths, whilst monitoring m/z 59, 81, 137 and 155 is given in figure 7.10. The alveolar phase is clearly distinguishable, and from which the intensities of the signals were averaged and standard deviations determined. m/z 59 is a result of acetone which is always in high concentrations in the breath [124], and is used here to illustrate the concentrations of the volatiles from the peppermint oil.

This study confirmed that the peppermint capsule ingestion resulted in VOCs present in exhaled breath, especially at m/z 155, 137 and which could be from menthol, menthone, 1-8-cineole, alpha- pinene, β -pinene and also limonene because similar ions

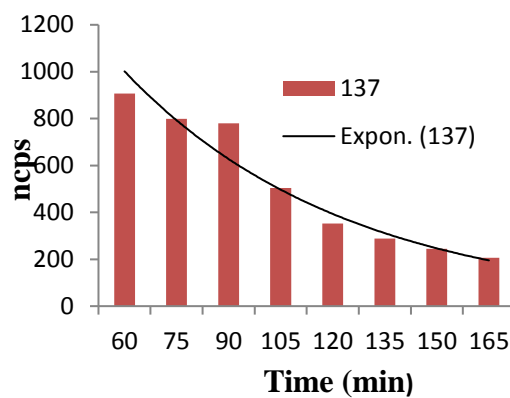
were found in the headspace study investigation which was on pertinent associate compounds.

7.6.9 Washout characteristic of peppermint capsule. Personal and inter-individual variations

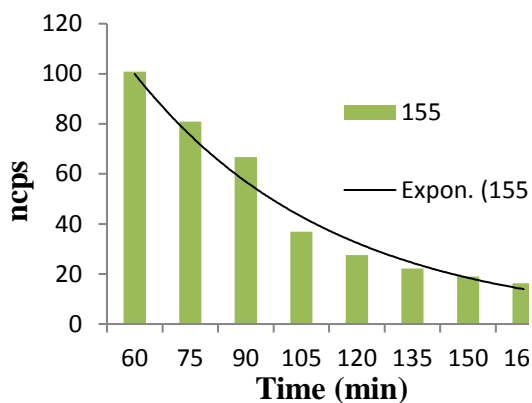
Figure 7.12-7.20 shows the peppermint washout characteristics of volunteers who took part in this study using a PTR-TOF 8000 with BET. The decrease in the ion signals is related to the loss of volatiles in the blood. It can be expected that this loss follows an exponential decay where the concentration decreases as time. In figure 7.11 (a, b, c), ncps (normalised counts per second) for 81, 137 and 155 is presented for one of the studies. A exponential line plot through the data points show that this is in fact the case, and from this a pseudo excretion rate can be calculated. Table 7.12 provides the details about these pseudo excretion rate of volunteers and the excretion rates for the same for different days for repeatability studies.



a)



b)



c)

Figure 7.11 Shows an example of an exponential decay graph of a volunteer for a) m/z 81, b) m/z 137 and c) m/z 155 (normalised counts per second (ncps) versus time) which indicates it is possible to calculate pseudo excretion rate using natural log function.

Figure 7.12 represents the washout characteristics of peppermint capsule for a male age 58 (Volunteer 1). VOCs from the peppermint capsule were detected after 30 minutes of ingestion of the peppermint capsule. The excretion rate for compounds is directly related to the pseudo rates determined from the product ions calculated. m/z 81 ($-0.014 \text{ cps min}^{-1}$), 137 ($-0.015 \text{ cps min}^{-1}$) and 155 ($-0.018 \text{ cps min}^{-1}$) having almost similar excretion rates. The maximum concentration was monitored at 30 minutes. The concentration of the VOCs from the peppermint capsule gradually reduces to the background level after 90 minutes.

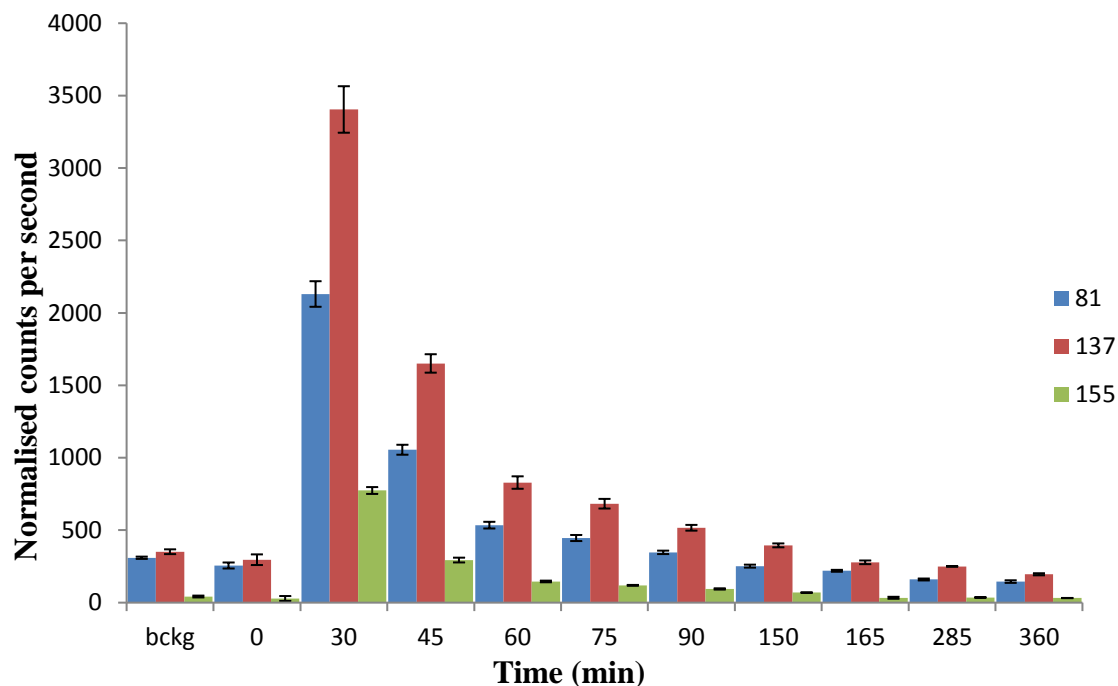


Figure 7.12 The washout characteristics of volatiles in breath recorded at m/z 81, 137, and 155 following the ingestion of a capsule containing 200 mg of peppermint oil for volunteer 1.

One unanticipated finding from volunteer 2 (figure 7.13) was that the result shows the fluctuation of VOCs from the exhaled breath before and after the ingestion of a peppermint capsule. No significant increase of VOCs in exhaled breath was detected. Perhaps, this could be the result of the compounds being metabolised by the volunteer quickly so we are only able to see the VOCs at are almost background levels. This result shows that the chemical reaction, especially the catabolic reaction of peppermint capsule reacted spontaneously which indicates the volunteer is prone to have a fast metabolism.

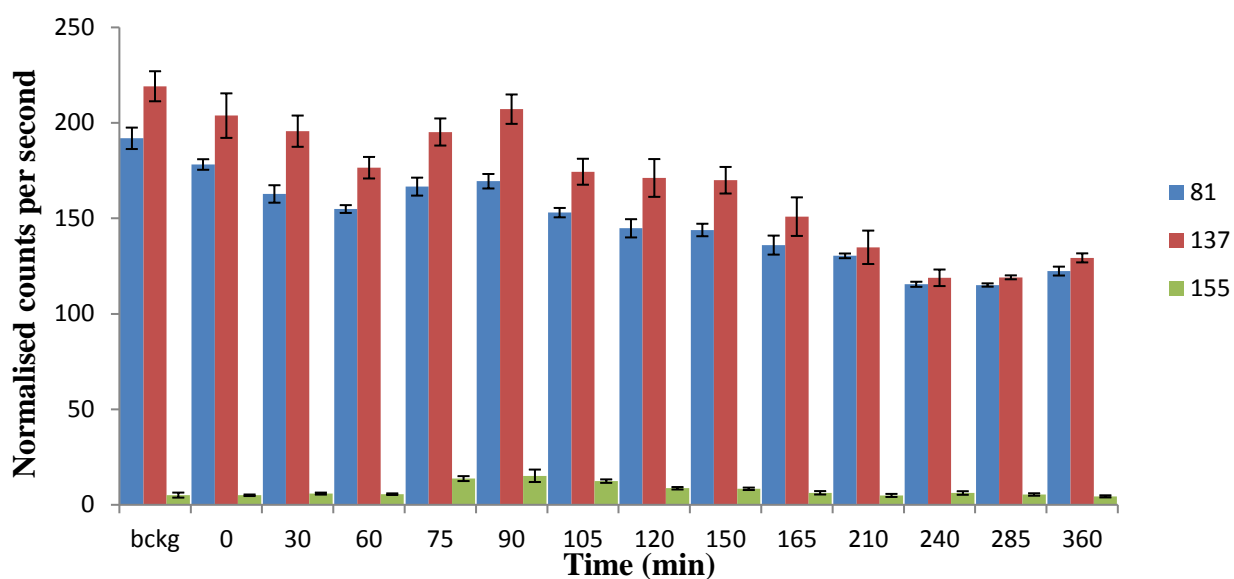


Figure 7.13 The washout characteristics of volatiles in breath recorded at m/z 81, 137, and 155 following the ingestion of a capsule containing 200 mg of peppermint oil for volunteer 2.

For volunteer 3 (female, 37), measurements for four sequential days were undertaken. Surprisingly, for the first measurement the VOCs from the peppermint capsule were only detected after approximately 105 minutes (figure 7.14). The maximum concentration was obtained at 120 minutes. The second measurement on the second day shows a similar trend, where the peppermint compounds were detected at 120 minutes and the maximum concentration was obtained at 150 minutes (figure 7.15). The measurement for the third day showed the maximum concentration at 165 minutes (figure 7.16). From figure 7.15, it can be seen that, for the fourth day, the maximum concentration resulted after just 30 minutes from ingestion of the peppermint capsule.

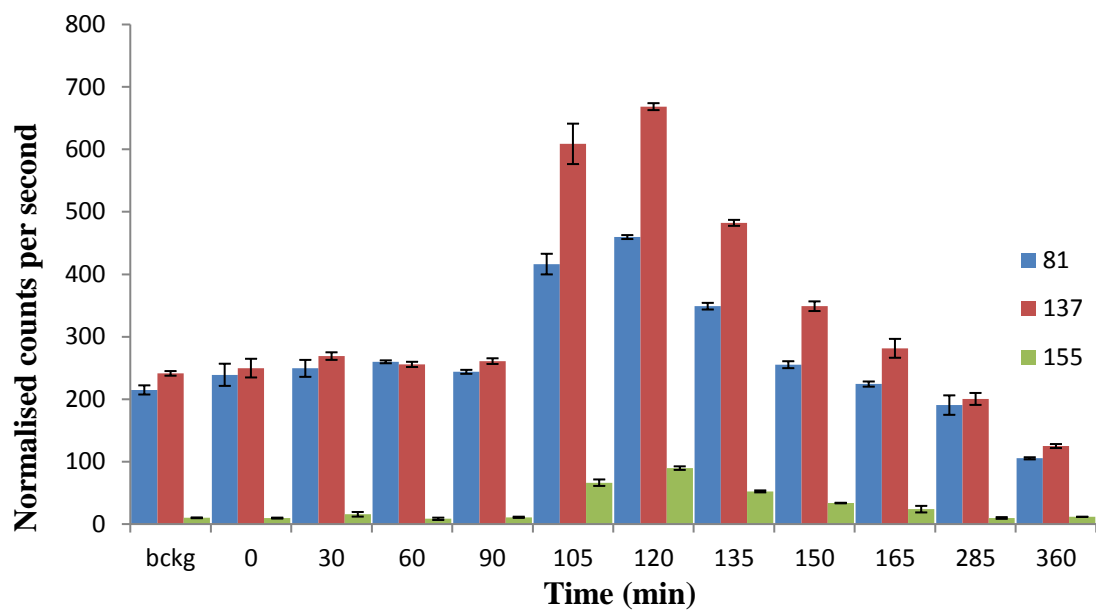


Figure 7.14 The washout characteristics of volatiles in breath recorded at m/z 81, 137, and 155 following the ingestion of a capsule containing 200 mg of peppermint oil for volunteer 3 (day 1).

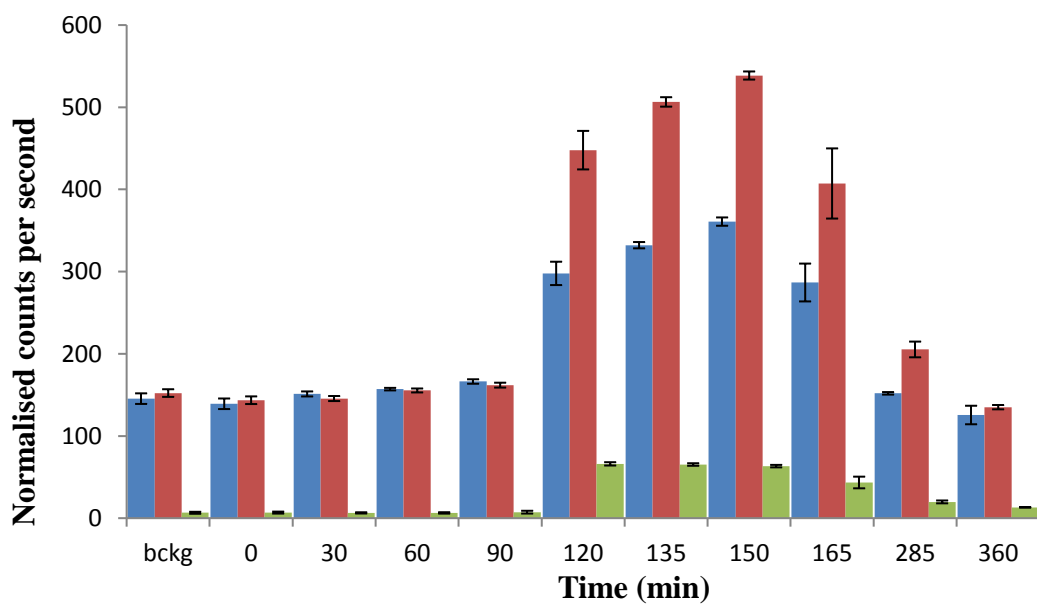


Figure 7.15 The washout characteristics of volatiles in breath recorded at m/z 81, 137, and 155 following the ingestion of a capsule containing 200 mg of peppermint oil for volunteer 3 (day 2).

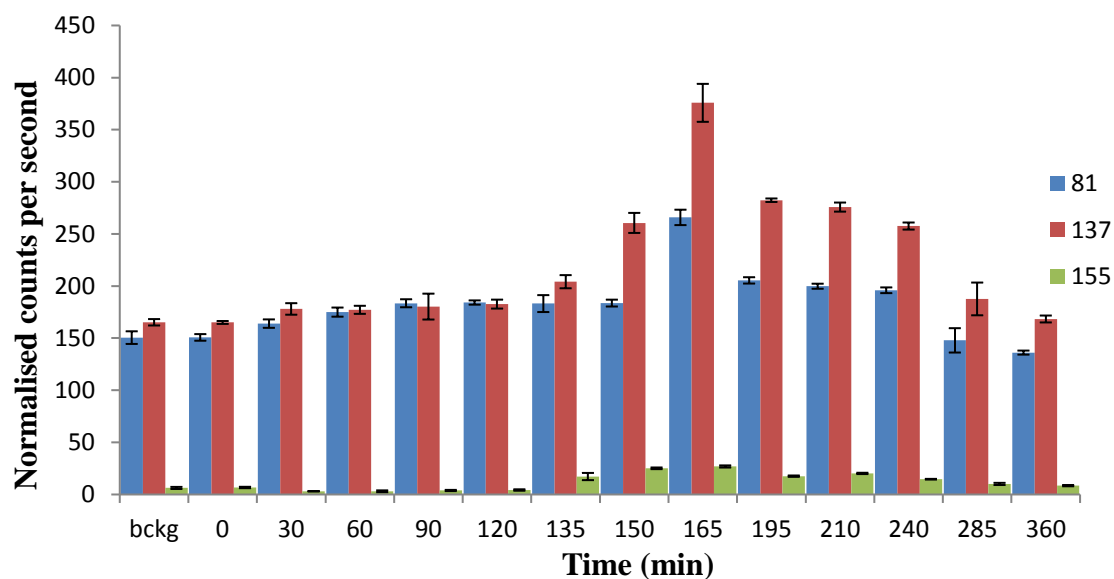


Figure 7.16 The washout characteristics of volatiles in breath recorded at m/z 81, 137, and 155 following the ingestion of a capsule containing 200 mg of peppermint oil for volunteer 3 (day 3)

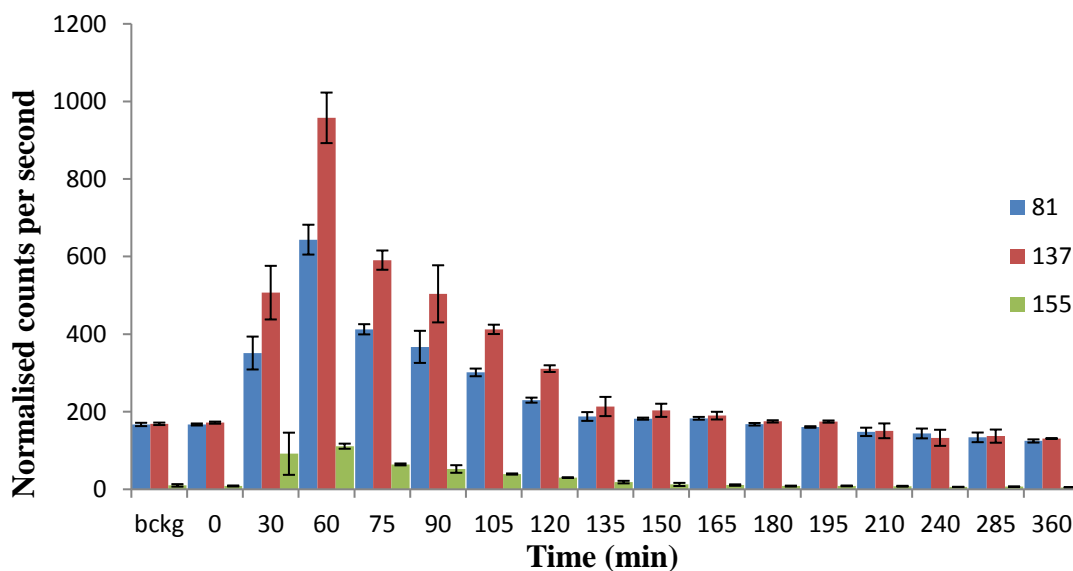


Figure 7.17 The washout characteristics of volatiles in breath recorded at m/z 81, 137, and 155 following the ingestion of a capsule containing 200 mg of peppermint oil for volunteer 3 (day 4).

For volunteer number 4 (Female 28), three measurements were undertaken on different days (figure 7.18-7.20). The maximum concentration monitored from day one was at 90 minutes. For the following days, it was observed at 30 minutes and 60 minutes respectively. The maximum concentration time was not similar for all the measurements. The excretion rate also varies from day to day.

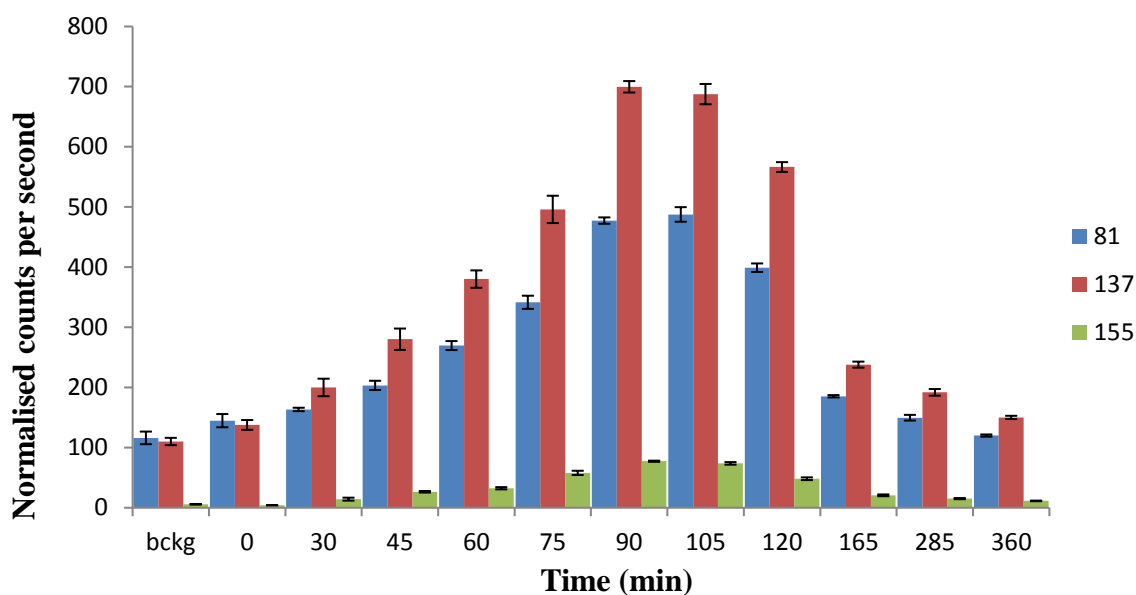


Figure 7.18 The washout characteristics of volatiles in breath recorded at m/z 81, 137, and 155 following the ingestion of a capsule containing 200 mg of peppermint oil for volunteer 4 (day 1).

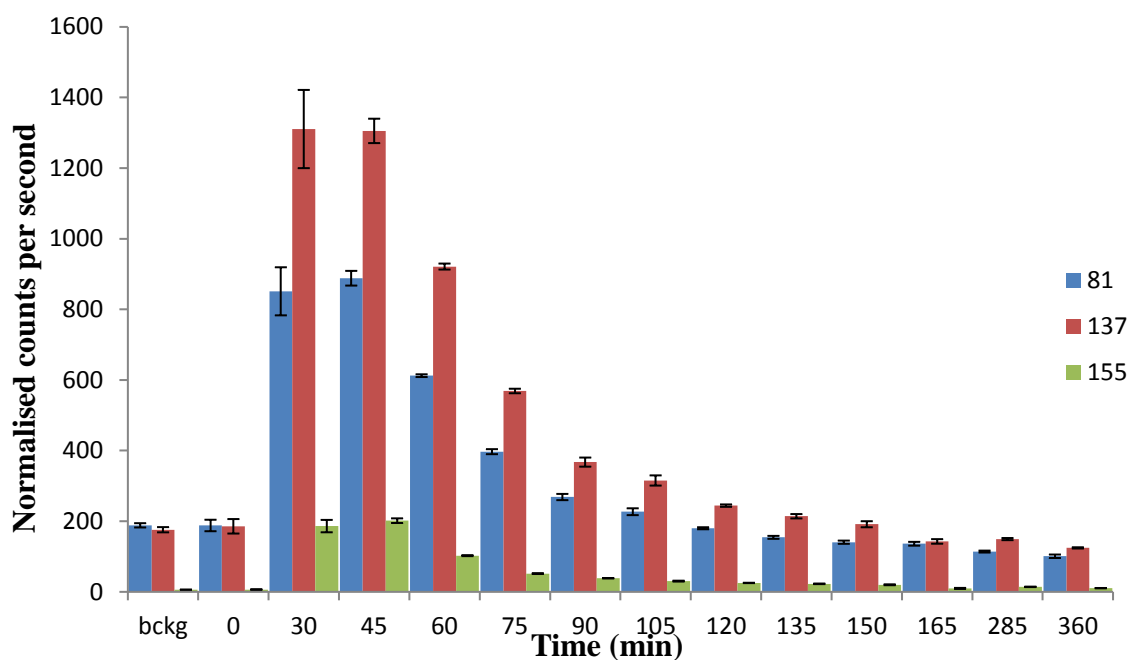


Figure 7.19 The washout characteristics of volatiles in breath recorded at m/z 81, 137, and 155 following the ingestion of a capsule containing 200 mg of peppermint oil for volunteer 4 (day 2).

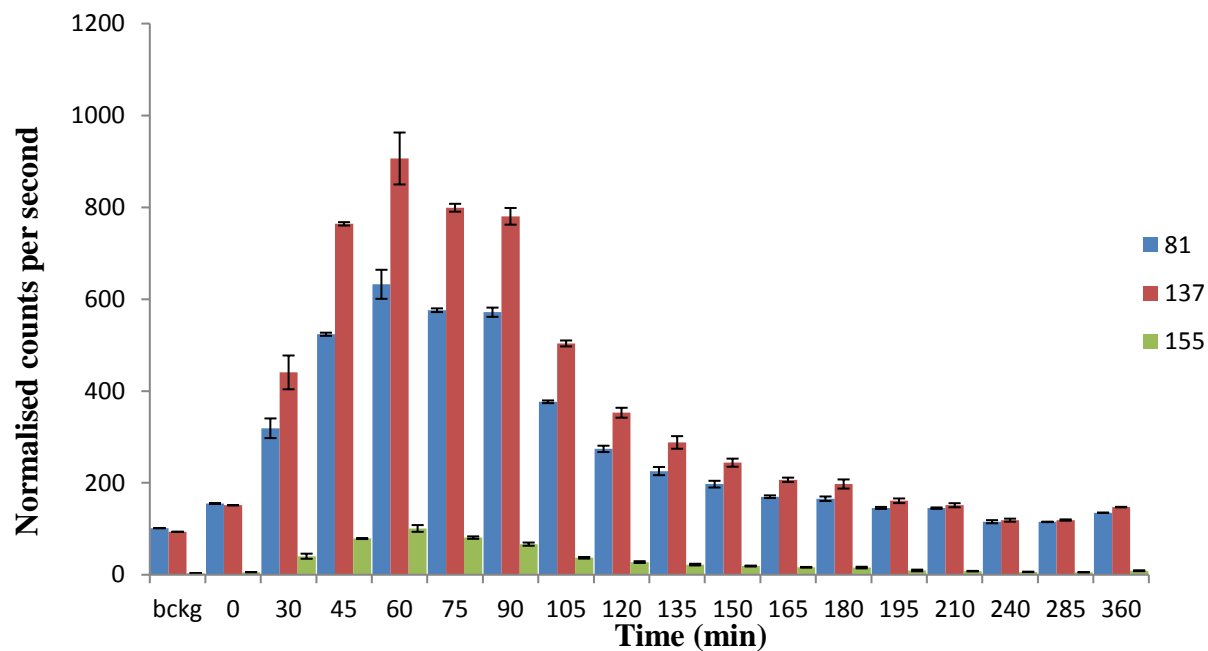


Figure 7.20 The washout characteristics of volatiles in breath recorded at m/z 81, 137, and 155 following the ingestion of a capsule containing 200 mg of peppermint oil for volunteer 4 (day 3).

Table 7.11 Shows the pseudo excretion rate (decrease in the product ions) of volunteers for each product ion measured from the exhaled breath after ingestion of the peppermint capsule for each of the volunteers.

Volunteer	Day	<i>m/z</i> 81 (cps min⁻¹)	<i>m/z</i> 137 (cps min⁻¹)	<i>m/z</i> 155 (cps min⁻¹)
Volunteer 1	Day 1	-0.014	-0.015	-0.018
Volunteer 2	Day 1	-0.002	-0.003	-0.009
Volunteer 3	Day 1	-0.004	-0.005	-0.01
	Day 2	-0.004	-0.004	-0.005
	Day 3	-0.005	-0.006	-0.007
	Day 4	-0.013	-0.017	-0.02
Volunteer 4	Day 1	-0.006	-0.007	-0.001
	Day 2	-0.002	-0.002	0.000
	Day 3	-0.017	-0.019	-0.023

Thus, VOCs from the peppermint oil appeared in the exhaled air approximately 30-60 minutes for some volunteers and for other volunteers it took more than an hour after administration of the capsule.

Almost all the cps versus time bar charts for all the volunteers have shown good washout characteristics. In addition to that, due to the shape of the curves from the washout characteristics, the detected maximal concentration of the same volunteer for different days changed and failed to show a consistent trend. This indicates that the excretion rate for the particular volunteer changes day to day. This perhaps can be linked with their daily activities and food intake. In accordance with the present results, previous studies have also shown differences within individuals in their washout characteristic for 1,8-cineol as reported by Ruzsanyi and Beauchamp [124, 125].

According to Ruzsanyi, this kinetic trend could be observed only with strict consistency to the protocol. She mentioned that when a volunteer was not holding to the 8 hours of fasting prior to the breath sampling, the release of maximal cineol concentration could take up to 18 hours after swallowing the capsule [125]. However, in this peppermint washout study, all the volunteers fasted for a minimum 8-10 hours prior to the capsule ingestion and the maximal signal concentration of volunteers was able to be detected within two to three hours and some within an hour. Therefore, these results provide support for Ruzsanyi's claim.

There are many unknown factors which can have influences on the volatiles in exhaled breath such as physiological influences [124]. Also, it is therefore unlikely that such connections existing between onset time and sex, age or body mass index (BMI) were distinguishable. However, the eating patterns and digestion right after the capsule ingestion could have altered and influenced the exhaled breath volatiles.

7.6.10 Metabolites from Peppermint capsule

In this experiment, there should be some volatile metabolites of the key compounds in peppermint oil in the breath. For examples, for menthol we may expect to observe glucuronide, and for limonene the metabolites are perillyl alcohol, trans-isopiperitenol and trans-carveol. Surprisingly, no metabolites associated with either menthol or limonene were found in this study. Certainly, the metabolites of limonene were observed in the study by Fernandez del Rio et al (this has not been published yet). At present, we have no explanation to this observation. However, we cannot draw any conclusion owing for the limited number of breath samples reported here in this proof-of-principle study.

Somerville et al. have claimed that peppermint (Colpermint) metabolites in spastic colon syndrome volunteers appeared to be glucuronide. Glucuronide is metabolite of menthol from peppermint which was found delayed in the urine [142]. Valente et al. reported that they found glucuronide after 1-2 hours [143].

Meanwhile, for 1,8-Cineole, it has been found that it is oxidized at high rates to 2-*exo*-hydroxy-1,8-cineole by rat and human liver microsomal P450 enzymes [144]. However, there was no metabolites related to 1,8-Cineole found.

According to Miyazawa et al. (-) menthone was metabolized to (p) - neomenthol (2) (via 3-reduction) and 7-hydroxymenthone (3) by human liver microsomes [145]. Also, there were no metabolites detected related to menthone.

Besides that, Sun J has stated that there were a few metabolites (oxygenated metabolites) produced from D-Limonene. The metabolites are perillic acid, dihydroperillic acid, and limonene-1-,2-diol (circulating metabolites) and also metabolites from plasma, such as limonene-8,9-diol and perillic acid isomer [146]. However, there were no metabolites related to limonene detected from the exhaled breath.

These findings raise intriguing questions regarding the nature and extent of production of metabolites from menthol, menthone, 1,8-cineole, limonene, α -pinene and β -pinene via exhaled breath. However, there were no metabolites associated with menthol, 1,8-Cineole, menthone and limonene found in this study.

There were no other breath studies claimed about the metabolites from these associate compounds with peppermint oil capsule. Therefore, detailed separate studies on the metabolisms of these compounds and its metabolites should be done in order to have a better understanding about their washout mechanisms.

7.7 Conclusion

The main objective of the study was to provide a proof-of-principle study to show how PTR-MS can record the washout characteristics of some volatiles present in peppermint capsules via exhaled breath. Although only a small number of volunteers took part, the results are encouraging and will be continued further both in Birmingham and Innsbruck.

In summary, we investigated the breath profiles of four healthy volunteers just prior to and after ingestion of a peppermint capsule. For two of the volunteers repeated measurements were obtained to check for intra-individual variations.

For all studies, a noticeable smell of peppermint was obvious in the breath of all the volunteers shortly after the ingestion of the peppermint capsule, which soon disappeared, and is almost certainly related to the volatiles coming-up from the gut and not from the bloodstream. Thereafter, any volatiles recorded are considered to be from the blood.

The measurement shows that the start of observing these volatiles in the breath coming from the blood varied both in the intra- individual and the inter-individual measurements.

The onset and the peak concentration were typically for 35 minutes, although a broad range of times was involved. The limitations of sampling protocol could be one of the reasons for the maximum peppermint levels being widespread. For example, sampling protocol could lead to underestimation of transience of breath peppermint.

The issue of washout characteristics can be sorted by frequent sampling and analysis using even shorter times (probably within minutes) with sufficient sampling intervals depending on target compounds. In this case, the target compounds were m/z 81, 137 and 155. Also, m/z 137 and 81 are not just from one compound, and hence there may

be differences in washout owing to differences in metabolism of the compounds. It would be interesting to use GC-MS measurements in parallel with PTR-MS measurements for an individual to look for differences.

The concentration levels were different during the different measurement phases for each individual, hence illustrating a large uncertainty in exhaled concentrations. Also, exhaled peppermint concentration can be dependent on the dose rate/body weight [72]. It can be suggested that, probably the concentration of peppermint in each capsule could be different which lead to variations of maximum concentration time within inter- and intra personal.

This study has illustrated how once volatiles enter the blood stream they are eliminated and decrease in concentration rapidly.

In this study, the primary active product ions of the peppermint oil capsule, were observed rather than the metabolites. The immense variability in the breath of peppermint levels proves that there must be a further condition to be understood about the kinetics of this compound in the body after ingestion of peppermint capsule.

Therefore, it can be said that each individual has their own metabolic rate towards the ingestion of peppermint capsule. Probably the metabolic rate for each individual changes day to day. If this is true, perhaps these changes depend on their daily activities and food intake. Besides that, age, sex and BMI factors might play important roles in determining their body metabolism even though we are uncertain about their correlation.

Further studies are required with a larger population and broader spectrum of participants.

This study illustrates the application of breath analysis for investigating pharmacokinetics and washout characteristic studies, showing that on-line breath gas

analysis has advantages compared to blood or urine sampling. Moreover, with breath sampling it is possible to carry out uninterrupted sampling with unlimited samples.

These real-time PTR-MS measurements with BET application have shown prominent and positive results for washout characteristics examination and will benefit future studies on liver diseases.

Chapter 8

8 Breath analysis of Rugby Players who had concussion (controls and injured)

8.1 Introduction

The National Health Service (NHS), has defined concussion as a sudden brain injury causing short-lived loss of mental function [147]. Generally, concussion causes a mixture of signs/symptoms. It does not show any loss of consciousness [147]. Concussion usually can be observed in the presence of one or more symptoms, physical signs, confusion and abnormal behaviour. Sometimes, it can be linked to a severe brain injury. The most common side effects include memory loss, confusion, blurry vision and a blank expression for a short period, although it can be much more serious [147]. The indication for emergency management of a severe brain injury is categorized when a Glasgow Coma Score of less than 15 is achieved with deteriorating mental status and potential spinal injury and also with deteriorating symptoms appearing [148]. Symptoms of a concussion may not be too obvious for several hours after injury. Therefore, most concussions are not identified until 24 hours or even more [149, 150]. Furthermore, most concussion diagnosis is evaluated based on self-reported symptoms [150].

The Standardized Assessment of Concussion (SAC) and Sport Concussion Assessment Tool (SCAT3) or Child SCAT3 is used as a standard protocol to assess injured athletes for concussion. It can be used for athletes from aged 13 years and above. This standardized tool is developed to be used only by a medical professional [148]. However, this evolutionary method to diagnose the concussion is not always effective

because not all concussed athletes will be identified within the expected period of injury [149, 150].

There is no specific diagnostic test or biomarker for a concussion. Currently, the essential and key element of a concussion diagnosis is to confirm the existence of signs and symptoms after any person has experienced a sudden blow to the head or body. A fundamental diagnosis of concussion purely depends on an athlete's self-report of signs and symptoms. This self-based report is made complicated due to insufficient information from the respected individual [151].

Later, multiple evaluation tools were developed such as symptom scales and checklists, balance testing, and neurocognitive assessments to increase the sensitivity and specificity of identification of the concussed athletes [152-155]. Following this, a few conventional neuro imaging techniques are used to diagnose the concussion. The common neuro-imaging techniques which have been used to diagnose the head and brain injuries are conventional computed tomography (CT) which uses ionizing radiation and magnetic resonance imaging (MRI) which uses radio frequency. CT and MRI scanning is usually used to scan severe head trauma injuries to locate the structural (bone and tissue) damages such as fractures and hematoma [156]. However, these techniques have limited diagnostic information on concussion per se because, in most of the cases, the structural imaging appeared to be normal [156]. Furthermore, these techniques involve ionizing and non-ionizing radiation respectively, and are costly and time-consuming [149, 157].

Generally, people who play contact sports such as rugby are at high risk of concussion and the ensuing side effects. This is supported by a recent systematic review on rugby union and rugby league in the UK [158]. Hence, researchers are trying various

methods to diagnose and identify the concussion at an early stage, also taking into account that the blood-brain barrier (BBB) is one of the important components in the brain where it separates the circulating blood and extracellular fluid (includes all body fluids) in the central nervous system) [159]. The disruption of the BBB (having a high possibility to happen) results from a concussion and traumatic brain injury. TBI, a crucial and still unsettled concern is the question of how best to detect possible breakdown in the BBB following neuro-trauma or concussion. Therefore, a new clinical trial was carried out to address this issue where the breath analysis technique has been used. This project is the first clinical trial using breath analysis for a concussion study.

The motive for this study is to measure the alveolar breath from injured players to monitor VOCs from the exhaled breath to see whether there are any differences in exhaled VOCs concentration by comparing with the exhaled breath of healthy rugby players. Also, the common VOCs such as methanol, acetone and isoprene were monitored from exhaled breath of the injured rugby players and healthy rugby players. These compounds can be detected easily via exhaled breath which can be co-related with concentration of blood. Besides that, we wanted to monitor whether there is any biomarker produced associated to N-acetyl aspartate (NAA) (protonated m/z 176) from the exhaled breath due to the concussion. NAA is an amino acid that is present in the vertebrate brain which is primarily being stored in the neurons and secondly in the oligodendrocytes. NAA plays many important roles in the physiology and metabolic processes of the brain [12]. In addition to that, other potential VOCs were investigated.

This project was a collaboration with the Neuro Trauma Department of Queen Elizabeth Hospital (QE), Birmingham and the School of Rehabilitation and Sport Science and School of Physics and Astronomy of the University of Birmingham. If this technique

is successful, it could lead to a development of a non-invasive method to diagnosis the concussion symptoms as early as possible.

The injured players also have undergone other medical tests at the Queen Elizabeth Hospital, Birmingham and the School of Rehabilitation and Sport Science of the University of Birmingham as listed below:

- MRI (T1, T2, functional resting state, DTI, venous BOLD and MR spectroscopy) - *no pre-season screening players have had this.*
- ImPACT computerised test- it is a standardized test to check the absorption of energy during the fracture in the head
- WAIS-IV symbol search and digit span (reversed lists only)- this is a test to examine the association between intellectual function and memory
- 9-hole peg test- it is a standardized test to check the upper extremity function by using a shallow container holding nine pegs and wood which has nine empty holes
- SCAT-3 (Sport Concussion Assessment Tool)- it is a standardized method to evaluate players injury level
- Balance assessment with the Tekscan force plate and Wii Balance Board, using the Modified Balance Error Scoring System protocol- it is a protocol to assess sports concussion
- Neurological exam – it is a test to check the sensory neuron and motor responses
- Transcranial magnetic stimulation- it is a procedure to stimulate the brain cells.
- Blood, urine and saliva sampling for metabolomics and brain tissue damage markers

In this study, breath analysis of healthy rugby players is being utilized as a tool for the study of the physiological process which is mainly focussed on the brain [14].

8.2 Details of analytes measured from exhaled breath of rugby players (healthy and injured players)

Philips et al. [46] stated that different compounds have been found in the exhaled breath. Isoprene, acetone and methanol [160] are the main compounds emitted in human breath which correlated with daily activities and metabolism. This is supported by a few other researchers, who mentioned that major compounds from the healthy individuals exhaled breath are, isoprene and acetone [161] and also methanol [162]. The results of this study encouraged us to do the investigation towards healthy rugby players and rugby players who suffered a concussion to understand whether their sports activities influence these common VOCs or not.

The reasons for these molecules to be selected for this study are: 1) these molecules have been monitored to be existent in human breath and blood at predominant concentrations, and 2) these VOCs are important because they cover a broad range of solubilities where these VOCs concentrations are high in the exhaled breath, and they can be measured using a good signal to noise ratio [163]. Therefore, in this study, we have investigated acetone, isoprene and methanol in healthy and injured players (after 68 hours of injury) to monitor whether there is any difference in the concentration of these VOCs resulting from concussion. Table 8.1 shows the information about in-vitro blood/gas partition coefficients of acetone, isoprene and methanol and details about these molecules are described in section 8.1.

In this study, PTR-MS was used to measure the exhaled breath of healthy rugby players and players who had suffered a concussion, to measure these common VOCs (methanol, acetone, and isoprene) and also other potential VOCs.

Table 8.1 Information about in-vitro blood/gas partition coefficients of the VOCS chosen for this study [60, 164].

VOC	Molecular Formula	Protonated Mass (amu)	*K_{BG}
Acetone	(C ₃ H ₆ O)	59	341
Isoprene	(C ₅ H ₈)	69	0.75
Methanol	(CH ₄ O)	33	2700

*K_{BG} partition coefficient of blood/gas

8.2.1 Isoprene

Isoprene is a common organic compound also known as 2-methyl-1, 3-butadiene and the formula is C_5H_8 (protonated m/z 69). Isoprene can be produced by a biogenic process such as in trees and plants. Isoprene can be categorized as a prominent VOC from the human body as a result of the metabolic pathways. From literature, isoprene which excretes through the lungs has a low water solubility and low boiling point [13].

Recent theory explains that isoprene has been produced by living organisms and is made from isopentenyl pyrophosphate (IPP) and its isomer dimethyl allyl pyrophosphate (DMAPP) [165, 166]. Two important metabolic pathways linked with DMAPP have been found: mevalonic acid pathway (MVA) and the 1-deoxy-D-xylulose-4-phosphate/2-C-methylerythriol 5-phosphate (DOXP/MEP) pathway [13]. The production is related to the isoprenoid biosynthetic pathway. Deneris et al. has mentioned there is a possibility that breath isoprene may be linked to cholesterol genesis (DL-mevalonate pathway) [165]. Besides that, Kennedy et al. reported that breath isoprene level depends on a number of clinical conditions, but the physiological definition of these changes has not been standardized yet [167]. He also mentioned based on some supportive evidence, that isoprene is related to cholesterol biosynthesis and the measurement could be used to monitor lipid disorders [167, 168].

Isoprene concentration from the exhaled breath in the human body is determined by physical activities [166]. Lindinger W et al. and Karl et al. have reported that isoprene concentration from exhaled breath increases within a few seconds after exercise [13, 169]. Karl et al. also stated that increases in heart rate associated with body position such as standing, reclining and sleeping increases isoprene concentration in the breath [170]. His experiment which involved atorvastatin therapy has suggested that isoprene can be used

as a non-invasive marker for cholesterologenesis [170]. J.King et al. has proposed that isoprenoid deficiency linked to muscular dystrophy can be explained by the degeneration of not only skeletal muscle but also cardiac or diaphragmatic muscle which has been affected by Duchenne muscular dystrophy (DMD) [171].

8.2.2 Acetone

Acetone (a type of ketone) also known as propanone is an organic compound with the formula $(\text{CH}_3)_2\text{CO}$ (protonated m/z 59). Acetone could be produced by biogenic emissions e.g. naturally, in plants, forest, trees, fruits and flora and also by anthropogenic emission e.g. vehicles. It also could be found as a breakdown product of animal fat metabolism.

There are three ketone bodies, acetone, acetoacetate, and β -hydroxybutyrate. Acetone in the body is produced via ketogenesis [32]. Ketone bodies are produced from acetyl-CoA, mainly from the mitochondrial matrix of liver cells during the fatty-acid metabolism [32]. Ketone bodies play an important role as a major energy source for brain, heart, and muscle when glucose is not available as a fuel source. Ketoacidosis happens when there is a large amount of accumulation of ketone bodies and acetone helps to maintain the pH buffering capacity [33].

Acetone is produced via spontaneous de carboxylation of acetoacetate. It is produced by the non-enzymatic decarboxylation of acetoacetate or is catalysed by acetoacetate decarboxylase. It is highly volatile. Therefore, it could be found in the breath (because it has a high vapour pressure), urine and blood. Acetone is the most abundant compound in human breath.

A high concentration of acetone is observed in fasting healthy people after a few hours (e.g. 10-15) or after extreme sports activities for 2-3 hours. This happens due to the metabolism of the reserved sugar in the blood and fat to acetone [13]. Wang Z et al. used acetone as a tool to test the breath of Type 1(T1D) and Type 2 (T2D) diabetic patients. He found that acetone could be used as a biomarker for T1D and as an observation tool for T2D. Smith D et al. undertook breath analysis using acetone and other metabolites as a disease marker [172]. This could be used in the future to give a non-invasive technique for glycemic control or for other potential diseases [172].

8.2.3 Methanol

Methanol is the simplest alcohols also known as methyl alcohol. Its chemical formula is CH_3OH (protonated m/z 33). It is a volatile compound which produces a characteristic flavour. Contrary to ethanol, methanol is highly toxic. Methanol is produced naturally via anaerobic metabolism from many types of bacteria. Pectin is a source of methanol [13]. Also, methanol could be considered as a multi-potential carcinogenic agent [173].

A previous study has shown that the concentration of methanol in the body will be increased after the consumption of fruits [35]. This is due to the lack of natural pectin, which is produced in the human colon by bacteria. Pectin is degraded by faecal bacteria and methanol is released by the degradation [35].

According to Bajtarevic et.al., lung carcinoma patients have a lower concentration of methanol compared to healthy volunteers in which a lower concentration could be partially due to age factors and a lower exhalation force [36].

In other studies, Turner C et al. has reported that breath methanol levels are not associated with age and breath ethanol or ethanol consumed [174]. However, he also has

mentioned that it could be probably inversely related to Body Mass Index (BMI). Fruit intake could be the reason for the inverse relation of methanol concentration with BMI [174].

8.3 Experimental details

For the concussion studies, nineteen healthy rugby players' breath samples (Male: age 20-24) were collected before the concussion (as control). Seven players who sustained a head injury had their breath samples collected 2-3 days (68 hours) after the injury to compare with the controls. The players were asked to complete a detailed questionnaire which included information about the home, diet (especially consumption of fruit, fruit juices or any flavoured drinks), smoking status, health condition, and medications. A glass syringe (100 ml, Sigma-Aldrich) was connected to the breath sampling tubing using a stopcock (Braun Medical Limited) to take the breath sample. The volunteers were calm and in a relaxed condition during the breath sampling. Also, they were requested to breath in and breath out normally using a gas-tight respiratory system with an in-line CO₂ mainstream sensor connected to a fast-time response capnometer (Capnogard 1265 Novamatrix Medical Systems Inc) [2]. The breath samples were taken using syringes during the alveolar plateau on the capnograph. 3 to 4 breath samples were collected as replicates to increase the statistical power (precision) of the study and to reduce the statistical errors. In addition, more samples were taken, in case the instrument failed or in case problems arose during handling of the syringes. Also, these samples were served to check the repeatability. For each sample, 3 mass scan cycles were taken. The glass syringes were used in this experiment because they do not contain any volatiles and are easy to clean using an autoclave. The breath samples were sealed in the syringes using a

luer lock fitting. All the samples were kept in an incubator for 30 min at 40 °C to reduce condensation effects. Syringes were covered with a heating bag maintained at 45 °C (figure 3.12). The mass range analysed was from an m/z 20 to 200. The inlet flow was set to 10-15 ml/min and the drift tube voltage was set to 600 V (E/N of 140 Td) to reduce the water clustering. The data were analysed and signal intensities were normalised to H_3O^+ signal of 50 million counts because H_3O^+ can change over the course of a day or may differ from one day to another in the instrument. The room air samples were collected and measured in the same condition as breath. The reason to do this protocol is purely to check any background contamination or contribution to the subject's breath [2].

In addition to that, the headspace of NAA was performed at 140 Td to identify the product ions. NAA was purchased from Sigma Aldrich (CAS Number: 997-55-7). 0.1 mg of NAA was placed in a 20 ml vial. The inlet of a vial containing the compound was connected to a hydrocarbon filter via a 1/8th inch peek tube and nitrogen gas was then flowed through the trap. The vial was wrapped with a heating tape to increase the sample temperature to 80 °C. This was needed because the sample was in the solid form and has a very low vapour pressure.

8.3.1 Details of the players who took part in this breath analysis of concussion study

Nineteen rugby players (male) took part in this study as controls and 7 rugby players who had a concussion during the rugby tournament have taken part as patients. There were two players (see table 8.2) who had given breath samples as controls (RCP13 and RCA23) and also as injured players (RCP22 and RCP23). The rest of the injured players (5 injured players) had not given breath samples as controls. The players and patients were given specific ID (identification code) by the Neuro-trauma Department of QE Hospital, Birmingham.

Table 8.2 Details on healthy male rugby players (controls) and injured male rugby players. This table includes details about age, weight, height, ID (identification code) and healthy rugby player's injured player's ID.

Player ID (Controls)	Player ID (Injured) after 68 hours	Age	Weight (kg)	Height (cm)
*-	RCP31	18	99	190
*-	RCP33	23	95	183
*-	RCP24	25	90	184
RCA09	-	28	94	182
RCA10	-	33	109	201
RCA11	-	26	97	185
RCA12	-	24	99	187
RCA13	RCP22	25	122	187
RCA14	-	27	106	118
RCA15	-	27	114	178
RCA 17	-	27	122	190
RCA18	-	21	87	187
RCA19	-	25	124	185
RCA20	-	27	126	178
RCA21	-	26	92	188
RCA22	-	32	106	183
RCA23	RCP23	21	100	183
RCA24	-	25	117	200
RCA25	-	20	118	189
RCA26	-	18	71	155
RCA27	-	21	126	204
RCA28	-	21	82	175
*	RCP26	21	100	200
*-	RCP18	21	76	187

* The injured rugby players who don't have samples as controls

8.3.2 Data analysis

For breath analysis, the contribution from the room air and surrounding places would influence the concentration of exhaled breath and could lead to confounding variables [16]. For example, in the case of food intake, such as garlic [39] or the intake of orange or citrus juices and also citrus fragrances [175], it can be found in the exhaled breath which could lead to multiple variables.

Besides that, if the analysis produced a significant amount of productions from the surrounding factors such as room air (background), food intake and smoking, strict and extra cautious action should be implemented when using it to find any biomarkers.

The statistical analysis was done using MINITAB version 18. For this study, the Ryan-Joiner test was used to identify the data classification. It assesses the strength of the correlation and found that the data set was not normally distributed. This suggested to use non-parametric tests and therefore, Mann Whitney U-tests were used to determine the m/z values between the healthy players and injured players. There were two volunteers in the group of injured players (RCP13 and RCP23) who had also given breath samples as healthy players. The pre-breath samples (before injury) from these healthy players were collected six months before the collection of their samples as injured players. Therefore, RCP13 and RCP23 have been included as an independent group in the analysis.

8.4 Isoprene calibration

Isoprene, having a boiling point of 34.07°C (307.22K), can be considered as a very volatile organic compound and is emitted in significant quantities into the atmosphere by many species of trees and plays a major role in atmospheric chemistry. It is also an important trace component of human breath as mentioned previously and is involved in many biosynthetic pathways. It is also produced in large quantities by industry.

It is useful to be able to dynamically generate trace vapour standard mixtures of isoprene over a wide range of concentrations for use in calibrating analytical instruments used in the direct analysis in such diverse applications as end-tidal breath analysis and monitoring of atmospheric environments, both outdoors and indoors (occupational and domestic). Static trace gas/vapour standards in cylinders are expensive and limited to just one concentration, unless mixed with an adjustable flow of diluent gas. There is a range of methods for the dynamic generation of standard atmospheres of gas mixtures, especially at trace concentrations.

Isoprene is readily photo-oxidisable and likely to decompose when stored in permeation tubes. Refillable diffusion tubes can be filled freshly just prior to any use in darkened conditions, thus reducing the degradation by such photo-oxidation. Here, the use of refillable diffusion tubes in a tube holder thermostatted at 0°C (273.15K) in a bath containing an ice/water mixture for gravimetric calibration and subsequently in the calibration of Ionicon quadrupole proton transfer reaction mass spectrometer is reported.

8.4.1 Materials and methods

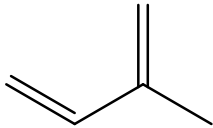
Section 8.4.1, 8.6 and 8.7 were partially elaborated from a draft paper for future publication on isoprene calibration titled, 'Dynamically generating trace standard atmospheres of isoprene vapour in air using refillable diffusion tubes and their use in calibrating Proton Transfer Reaction Mass Spectrometers' (Authors D.J Blenkhorn, P.D Chellayah and J.M Thompson).

Isoprene 99 % purity from Sigma Aldrich was used using oxygen-free nitrogen (99.998% purity) as a carrier gas.

Tracer Cert® refillable diffusion tubes (supplied by Tracer Measurement Systems Ltd.) were used to generate the trace vapour standards of isoprene for gravimetric calibration [176]. The calibration was done over about a 5 hour period with a refillable diffusion tube with a precision bore section of length 2cm and 0.5mm bore (figure 8.1). The refillable diffusion tubes were weighed periodically using a Cole Palmer Symmetry PA120 digital balance (120g x 0.0001mg), recording weight to 0.1mg. Figure 8.3 shows the setup of a diffusion tube using PTR-MS quadrupole.

A diffusion tube with a precision bore section of length 2cm and 0.2mm bore in the calibration of an early version of the Ionicon quadrupole Proton Transfer Reaction mass spectrometer (Ionicon Analytik GmbH, Innsbruck, Austria) was used for breath analysis of isoprene of healthy rugby players and rugby players who suffered concussion. Carrier gas (nitrogen) flows of 150 to 800 ml min⁻¹ produced isoprene concentrations ranging from 0.036 to 0.192 mg l⁻¹.

Table 8.3 Information on isoprene in this experiment, including vapour pressure and purity.

Chemical/Lightest isotopomer weight	CAS Number/purity	Vapour pressure mm Hg	Chemical/Molar Mass
Isoprene C ₅ H ₈	78-79-5, 99 %, Sigma Aldrich	550 at 25 deg C	
Molar Mass 68			isoprene

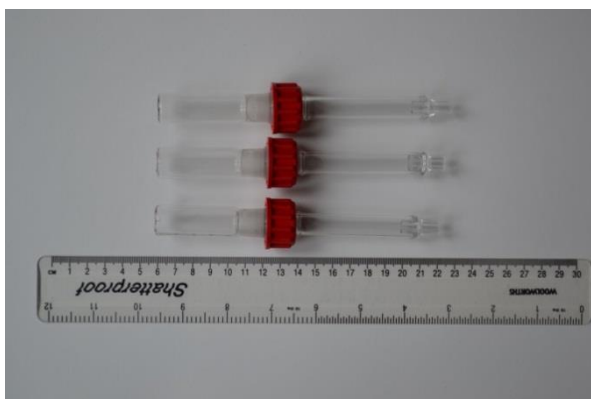


Figure 8.1 Different sizes of diffusion tubes. This picture was reprinted from J.Thompson , 2009, Journal of environmental monitoring [176].

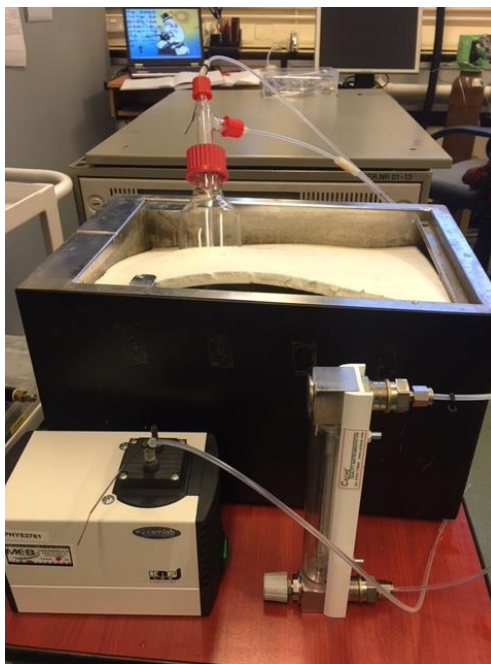


Figure 8.2 The experimental set up of isoprene calibration for Ionicon quadrupole PTR-MS using a diffusion tube (precision bore section of length 2 cm and 0.5mm bore)

8.5 Results

8.5.1 Pre and post injured samples from the same players

Figure 8.3 represents a full mass spectrum of an injured rugby player's exhaled breath using 140 Td. The mass spectrum was the average of three breath cycles.

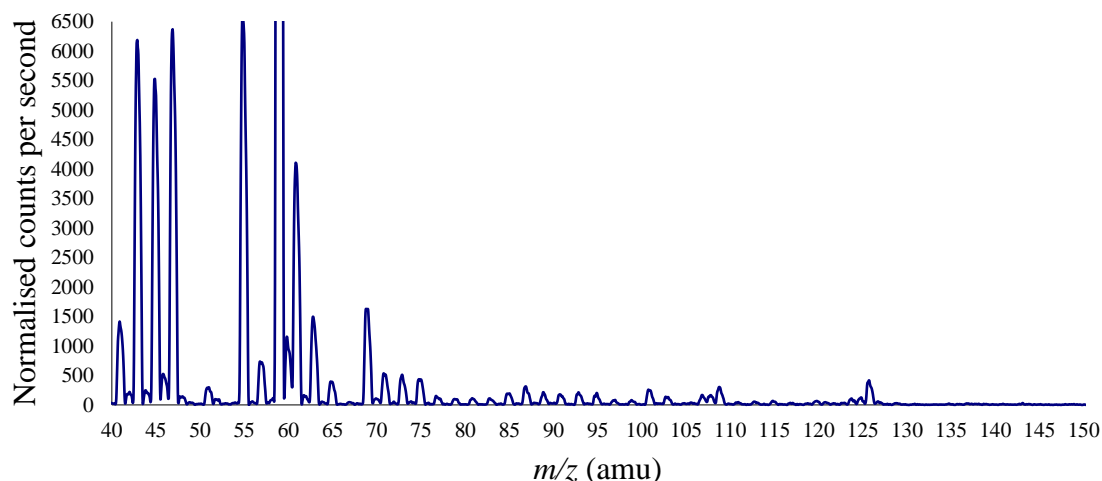


Figure 8.3 An example of a mass spectrum which shows an average of three breath cycle of an injured rugby player measured using Ionicon quadrupole PTR-MS.

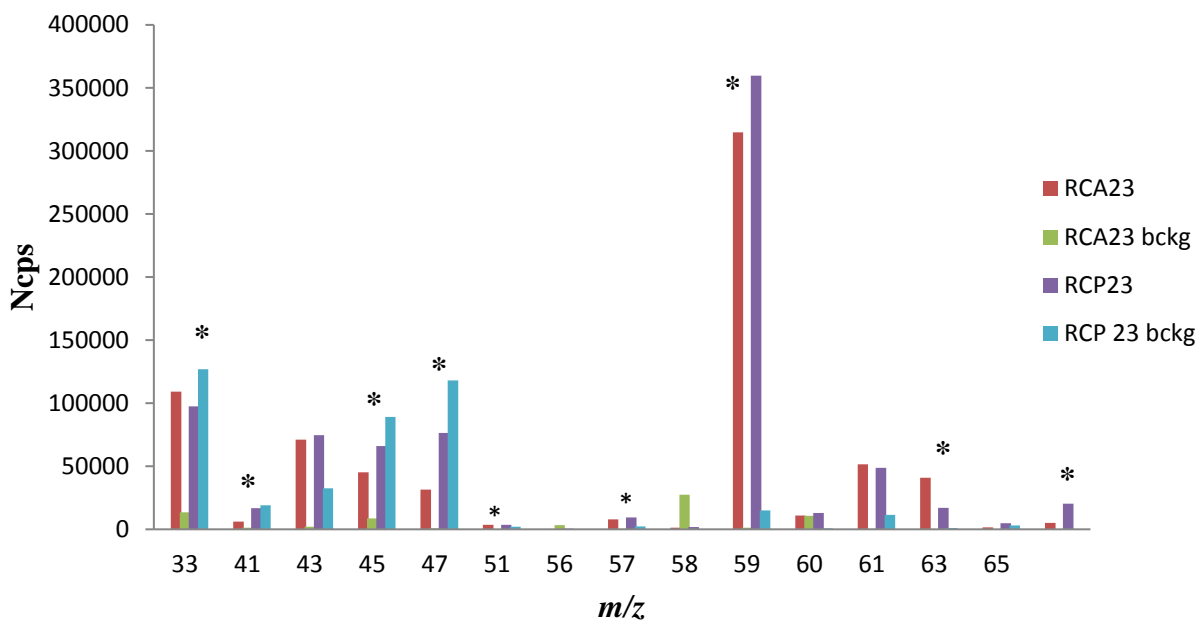
There were two samples taken from the same players who had given the breath sample before and after the concussion and also the respective background. Therefore, there was no statistical analysis performed due to the small number of samples. However, an exploratory study was done for these two players by looking for obvious differences between pre and post-VOCs from the exhaled breath. The first player was given identification as RCA23 for pre-breath sample and RCP23 for the post breath sample. Meanwhile, the second player was given identification as RCP13 for pre-breath sample and RCP22 for the post breath sample.

Figure 8.4 a) and b) show the prominent VOCs which are different in concentration from the exhaled breath of healthy and injured players. There was an increase in the concentration for some VOCs of injured player samples compared to healthy samples such as m/z 45, 47, 51, 57, 59, 69, 75, 77, 79, 89, 93, 97, 107, 109, 124, 125 and 126. Also, there was a decrease in concentration of some VOCs observed for injured player's samples compared to healthy samples. For instance, m/z 33, 41, 61, 63, 71, 73 and 81 were observed to decrease in the concentration in the injured player's breath sample.

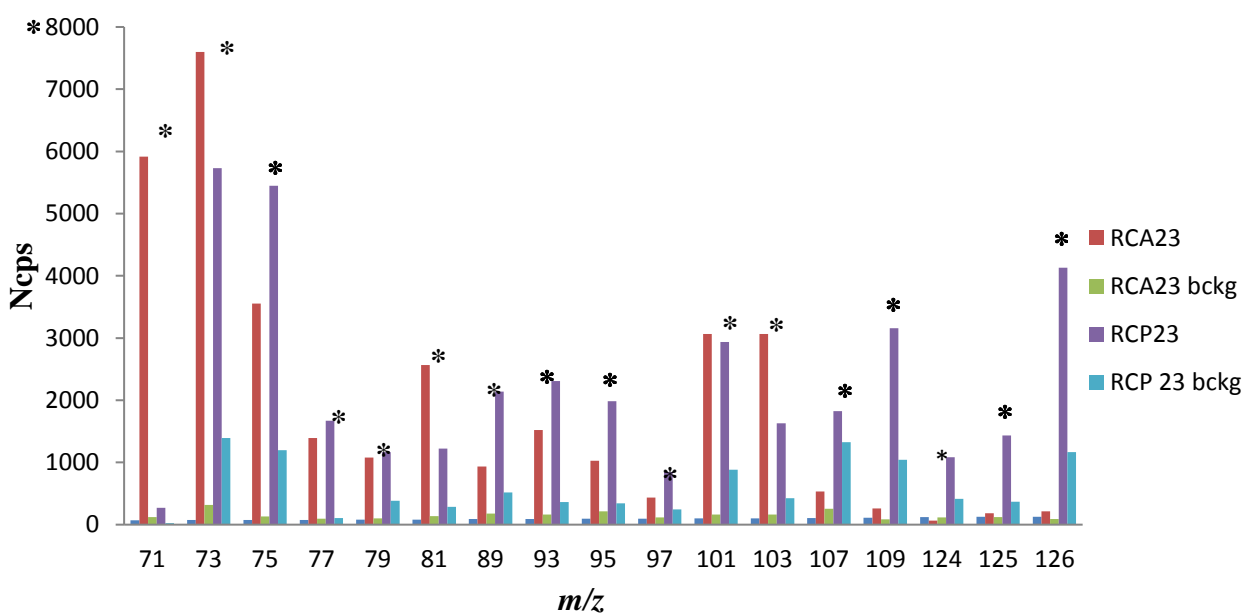
Figure 8.5 a) and b) show the obvious difference in exhaled VOCs obtained from the same rugby player before the injury (RCB13) and after injury (RCB 22) and also the respective background measurements. For example, a decrease in the concentration for some VOCs for the injured player compared to healthy players such as m/z 51, 57, 59, 63, 71, 73, 75, 77, 79, 81 and 101. There was some increase in some of the VOCs such as m/z 41, 47, 69, 89, 93, 95, 107, 109, 124 and 126.

Besides that, there were some common VOCs decreased in the concentration in both injured rugby players obtained when compared to healthy samples. For example, m/z 33, 61, 63, 71, 73, 81, 101 and 103.

In both injured rugby players' samples, there were some common VOCs observed from the exhaled breath as increasing in concentration. The observed common VOCs are m/z 47, 59, 69, 89, 93, 95, 107, 109, 124 and 126.

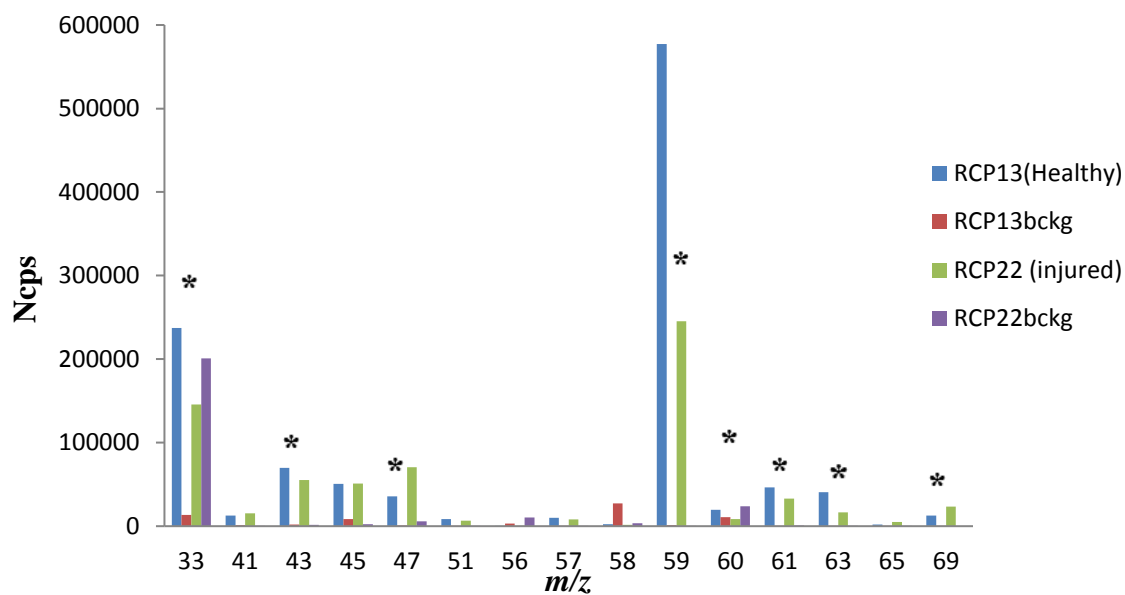


8.4 a)

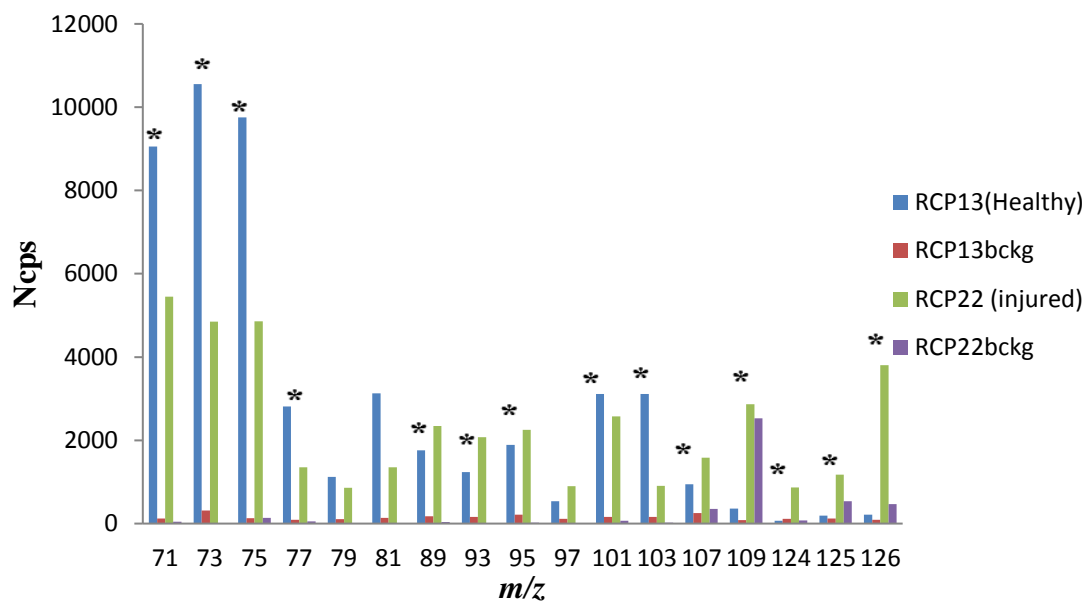


8.4 b)

Figure 8.4 a) and b) Show the differences of obvious VOCs (starred) from the exhaled breath of healthy rugby player (RCA23) and injured rugby players (RCP23) which the samples are from the same player. The background measurement was included for comparison.



8.5 a)



8.5 b)

Figure 8.5 a) and b) Show the differences of obvious VOCs (starred) from the exhaled breath of healthy rugby player (RCB13) and injured rugby players (RCB22) which the samples are from the same player. The background measurement was included for comparison.

8.5.2 Comparison of methanol, acetone and isoprene of healthy players and injured players

Figures 8.6 - 8.8 show the box plots (Origin Software) of methanol, acetone and isoprene respectively for healthy rugby and injured players which summarises the results for healthy rugby players and injured rugby players. The box plot was used to show the median, mean, lower quartile (LQ), and upper quartile (UQ) for respective volatiles.

For the statistical analysis of isoprene and acetone, Minitab software (version 18) was used. The Mann Whitney test was applied to determine whether isoprene and acetone showed a statistical difference between healthy rugby players and injured rugby players. Two product ions have shown significant differences in intensities between healthy rugby players and injured rugby players. The significant p-values for acetone and isoprene are explained in detail later.

For methanol (m/z 33) (figure 8.6) there was no statistical test performed for both healthy and injured players because the methanol concentration in the room air for the injured players were considerably high compared to the healthy players' room air sample. From the box plot, it is clear that the presence of the volatiles in the room air is not negligible. Taking into account the confounding variables, the data for methanol was presented using a box-plot which included room air to show that there was methanol contamination during the injured player breath sampling. Meanwhile, for acetone and isoprene, the room air contribution was subtracted for the box plot presentation because it has the negligible effect on the concentration in the breath samples of healthy and injured rugby players.

For acetone results, the null hypothesis states that the difference in the median for two groups of rugby players is 0. The achieved confidence level was 95.08 % and the median for acetone scores was higher for healthy rugby players compared to injured rugby players. The p-value is 0.014, which is less than 0.05, where the decision is to the null hypothesis and concludes that there is a statistical difference in median engagement between two independent groups which consist of healthy players and injured players.

Meanwhile, the median engagement for isoprene (m/z 69) scores is higher for injured rugby players compared to healthy rugby players (controls). The achieved confidence level for isoprene is 95.06 % .The P value is 0.015 which is less than 0.05 (i.e $p < 0.05$), where the decision is to the null hypothesis and it can be concluded that there is a statically difference in median engagement between two groups.

The box plot presentation clearly shows the presence of the volatiles are negligible either in the room air of the School of Sports Science, University of Birmingham or the Brain Imaging centre of the QE Hospital. In addition to that, this analysis is based on comparisons of the injured players and healthy players affected similarly by the room air contaminations except for methanol.

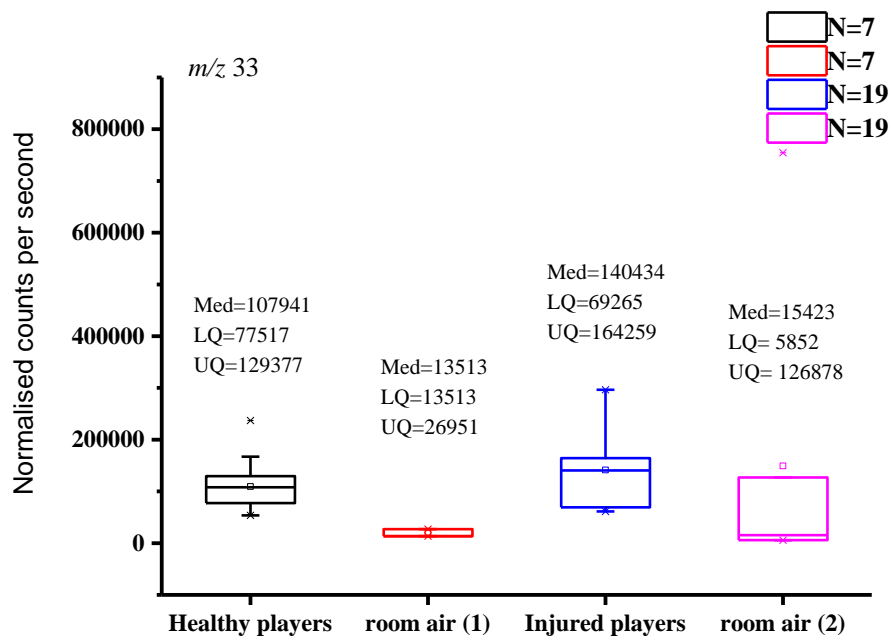


Figure 8.6 Boxplot showing lower quartile (LQ), median, mean and upper quartile (UQ) normalised counts per second for exhaled methanol from a healthy rugby player and an injured player.

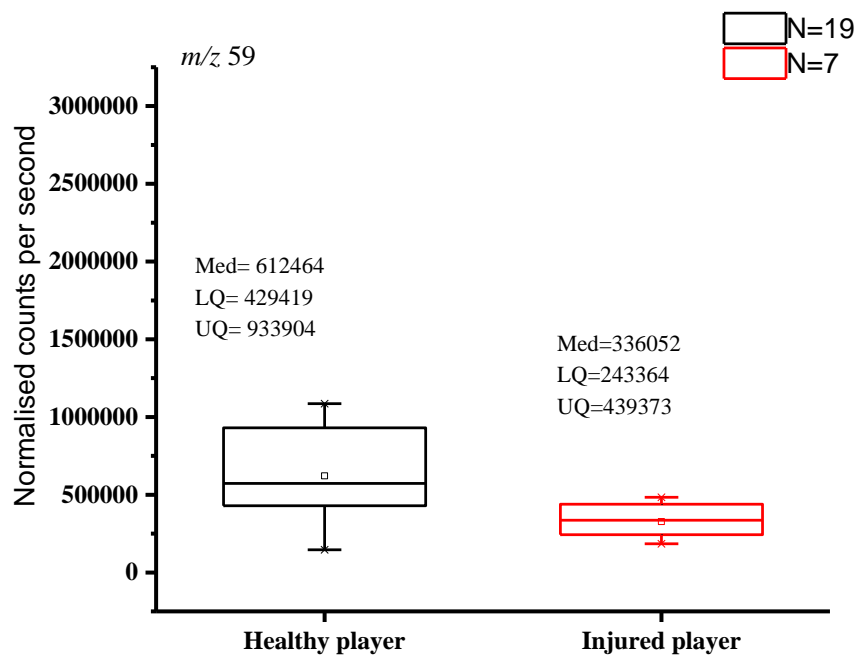


Figure 8.7 Boxplot (acetone) showing lower quartile (LQ), median, mean and upper quartile (UQ) normalised counts per second for exhaled acetone from a healthy rugby player and an injured player.

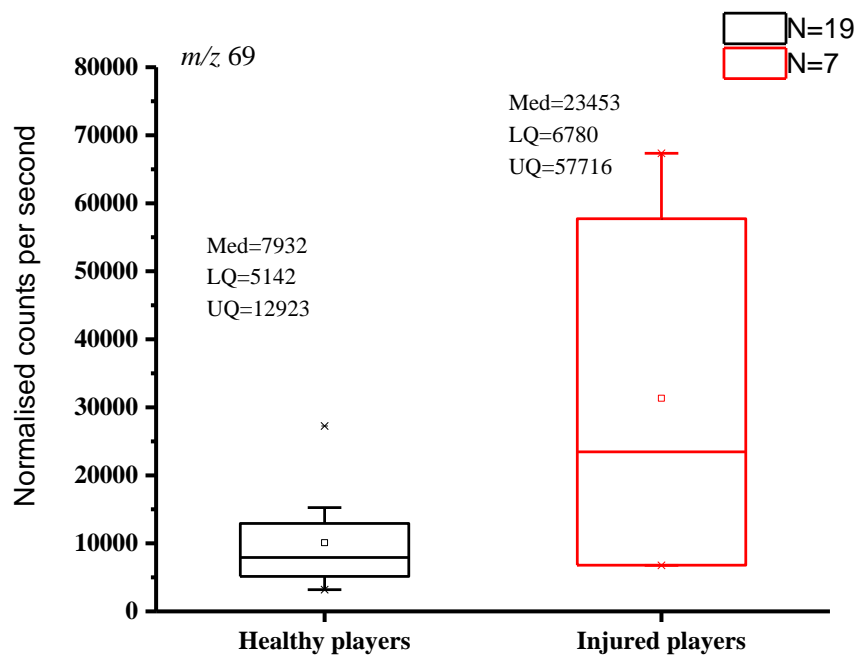


Figure 8.8 Boxplot (isoprene) showing lower quartile (LQ), median, mean and upper quartile (UQ) normalised counts per second for exhaled isoprene from healthy rugby player and injured player.

8.6 Gravimetric calibration and the use of scaling for using different sized Tracer Cert® diffusion tubes

Figure 8.9 represents a weight loss of isoprene versus time (min), figure 8.10 shows isoprene calibration (normalised data) and figure 8.11 shows isoprene calibration (un-normalised data) using the Ionicon quadrupole instrument.

By applying a statistical design of regression experiments, better estimation on the rate of emission of any vapour trace was achieved from diffusion tubes. Figure 8.9 shows the excellent robust rank regression method of Hettmansperger and McKean is available in Minitab® 18 [177]. In this graph, weight changes were monitored from the start of the experiment. For the first reading, we obtained a larger change compared to other points because of the initial loss of more volatile impurities. This might influence and leverage the fitted line. However, estimating emission rates by applying a fitted line just for five points would give a straight line and the influence and leverage of the first point in the plot will be “down-weighted” using robust and resistant linear regression. This has produced good and close fits between weight loss versus time concentration. On this fitted line plot [177], the points generally follow the regression line. The points adequately cover the entire range of weight (mg) values and the confidence envelope [177]. There was no curvature in the data and also there was no appearance of outlier except the contribution from the impurities on the surface of the diffusion tube which were emitted fast and later produced a steady emission rate.

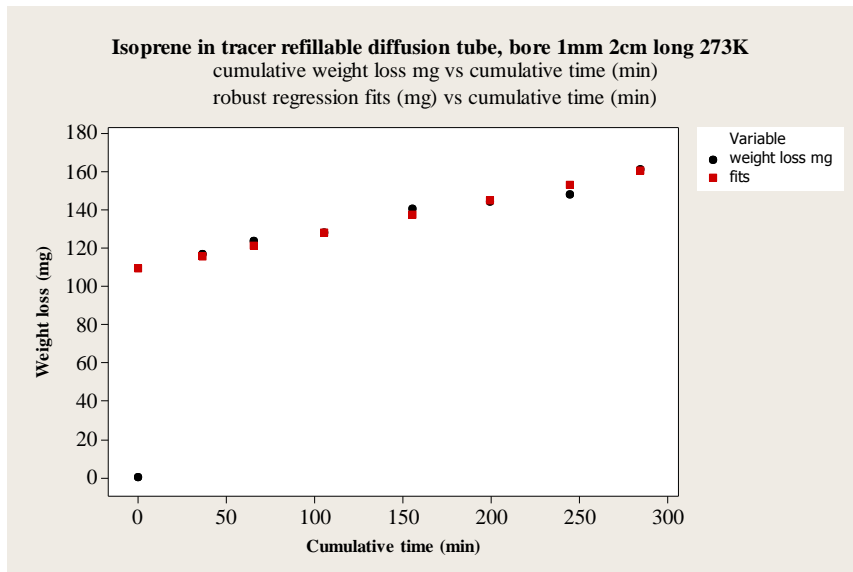


Figure 8.9 Isoprene in tracer refillable 0.2 mm bore 2cm long diffusion tube using gravimetric method.

8.7 Using calibrated diffusion tubes and other Tracer Cert® diffusion tubes with scaling for calibration for of PTR-MS quadrupole

The same principles and considerations as the gravimetric calibration were applied in designing experiments for the calibration of analytical measurement using the refillable diffusion tubes.

For the isoprene calibration of PTR-MS using a diffusion tube, we used robust regression statistics and a linear regression plot (fitted linear model). From the results, we were 95 % confident that the confidence interval contains the population where the p-value is less than 0.05 for both normalised and non-normalised data (figure 8.10 and figure 8.11). Besides that, for prediction interval, we achieved 95 % confidence that observations fall within the interval indicated by the green line. However, this is only true for the concentration values that are within the range included in the analysis. The regression equation for normalised data is $\text{cps} = 21420 + 1468320 \text{ mg/l}$ and for not normalised data is $\text{cps} = 23784 + 1460648 \text{ mg/l}$. As you can see from both graphs (normalised and not normalised), the regression plot shapes are very similar, except that the vertical scale (cps or normalised cps) is different by a factor of four.

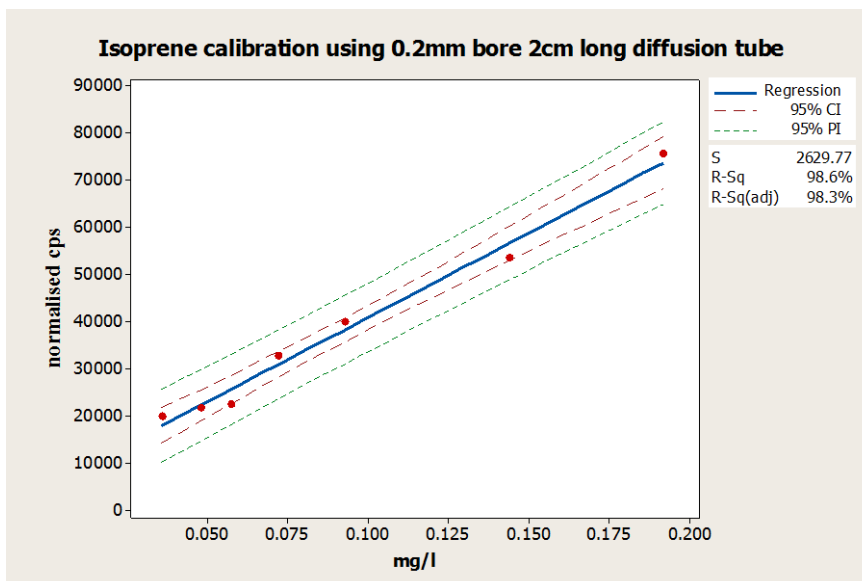


Figure 8.10 Isoprene calibration (normalised data) of PTR-MS (Ionicon) using 0.2 mm bore 2 cm long diffusion tube

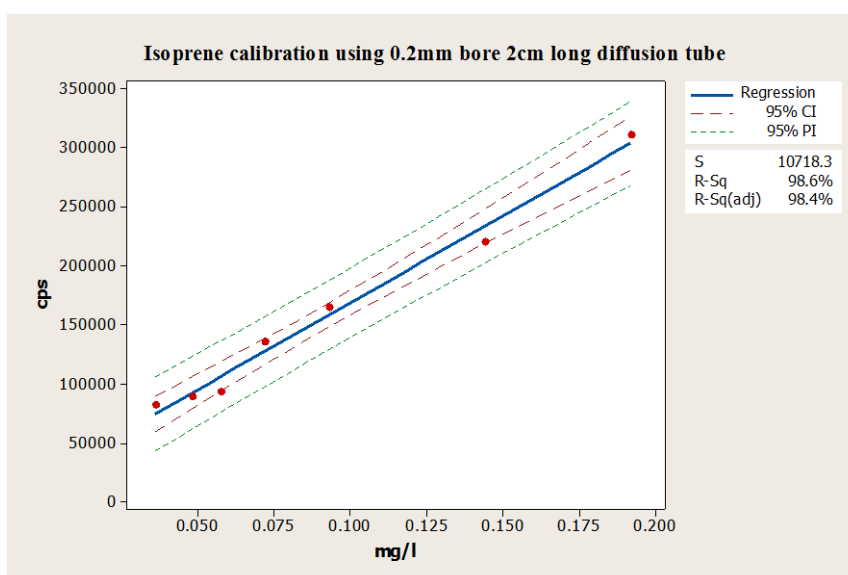


Figure 8.11 Isoprene calibration of PTR-MS Ionicon for non-normalised data (robust rank regression) using refillable diffusion tube

8.8 Discussion

It should be taken into account that the number of days collecting the injured players' breath samples is variable because it is impossible to determine when the concussion would happen and when the subjects would be available to do further medical tests and give their breath samples. There were no products found from the headspace of NAA. Therefore, the fragmentation pattern of NAA was unknown. Perhaps, it could be possible that NAA does not fragment.

For the comparison of pre and post breath samples of the same rugby players, (RCA23(pre)-RCP23(post)) and (RCB13(pre)-RCB22(post)), there were some VOCs found to increase in concentration and some VOCs were found to decrease in concentration from the injured players VOCs compared to healthy players. Unfortunately, these findings may be somewhat limited by the number of players who had given pre and post samples. Although there were some differences in the VOCs concentration of two of the healthy players and injured players, the precise causes of these changes remain unclear. This needs further investigation by taking more samples of pre and post injury of the same player to monitor the correlation and consistency of difference in concentration of VOCs from the exhaled breath.

From figure 8.7, the methanol (m/z 33) concentration in the room air was higher for the injured rugby players' room air compared to the healthy rugby players' room air. Therefore, it was complicated to do any statistical analysis. Methanol has been used in a variety of commercial products, especially as cleaning and purification materials [178]. Besides that, methanol also has been used to prepare some medicines [178]. Possibly, methanol would have been used in the cleaning or purification material in the Brain Imaging centre or places nearby the MRI room. This would have contributed to high

concentrations in the room air of the Brain Imaging Centre. It clearly shows that there was a high possibility that the players' breath was contaminated with this room air condition during the MRI imaging and the biological half-life of the methanol is unknown [160]. Therefore, methanol is pointless to be used as an indicator to evaluate any physiological condition of the players who had concussion.

According to the Mann Whitney statistical analysis for isoprene, there is a significant difference between the healthy and injured players. The isoprene concentration of the injured players is higher compared to the healthy rugby players. The healthy rugby players have a lower concentration of isoprene most probably because they were engaged with the exercise and training program for the rugby matches. Also, they were on a strict diet schedule.

However, due to concussion, the players had undergone some cognitive symptoms. These would have caused the players to be unfit to perform their normal activities such as training, exercise and also diet. Also, some evidence has linked isoprene levels to different physiological states [25]. According to King et al, isoprene tends to react sensitively associated to an increase in ventilation during the exercise session (isoprene is strongly lipophilic) [168]. For example, isoprene level is low during sleep [179] and increases when there is change in body posture. Also, during the physical exercise, a drastic increase in isoprene level was reported [169]. Hence, in our study, the injured players were in the calm state and did not perform any activities before and during breath sampling.

Dahl et al, have reported that non-metabolic isoprene clearance occurs through the lungs [180]. This perhaps can be linked to the abnormal health condition and abnormal metabolic activities in injured players. The high excretion of isoprene via breath from the

injured players could be due to the accumulation of non-metabolic isoprene after the concussion.

Acetone in the human body depends on biological variability, diet and natural daily activity of an individual [181]. In addition to that, the concentration of acetone is influenced by fasting or performing strong exercise for a few hours [13]. Therefore, these factors have to be taken into account in order to determine the correlation of the differences in the concentration of acetone from the exhaled breath of healthy players and injured players. From the statistical analysis, the results show that there is a significant difference between healthy players and injured players. The concentration of acetone of the injured players was significantly lower compared to healthy rugby players. Due to concussion, injured players potentially tend to have abnormal metabolism, especially an abnormality in the conversion of acetoacetate or isopropanol to acetone [182]. However, since diet is one of the important factors which affects the concentration of acetone, this concerns an uncertainty in the use of breath acetone as an indicator to monitor the concussion.

The Tracer Cert® Diffusion Tube has provided a significant advantage with the ease and quickness of calibration. A significant weight loss can be measured easily using a wide bore capillary of short length in a shorter period (few hours or days) using an electronic balance weighing to 0.1mg. The isoprene calibration result shows that calibration using diffusional tubes was in good agreement with the gravimetric method.

8.9 Conclusion

This study has shown the non-invasive application of PTR-MS by detecting significant differences of acetone and isoprene produced by healthy and injured rugby players via exhaled breath. For those rugby players with the concussion, the measurements were taken after 2-4 days of the injury.

Whilst the breath sampling was carried out, the players were healthy and conscious after the concussion. Although a significant difference was obtained for healthy and injured rugby players, it is crucial to understand about a low concentration of acetone in exhaled breath. Acetone concentration in humans depends on variable factors. Therefore, it will be challenging to use it for concussion monitoring purposes.

For isoprene, although this current study is based on a small number of injured rugby players, it gives some clue that it could have an impact on injured players. This is essentially a Phase 1 clinical trial of a potentially interesting new medical diagnostic test. Therefore, further investigations by doing longitudinal studies are compulsory as this result is sufficiently encouraging to go onto a Phase 2 clinical trial. This longitudinal study also will aid the interpretation of other VOCs which can be correlated with the concentration of VOCs before and after the concussion in order to obtain concrete and conclusive results. Also, these VOCs can be potential indicators of concussion in the near future.

For future work, it's been suggested to get the breath samples of the injured player immediately after the concussion to monitor the immediate effects on VOCs from exhaled breath.

CHAPTER 9

9 CONCLUSIONS AND FURTHER DISCUSSION

The research work reported in this thesis has highlighted the potential of applying Proton Transfer Mass Spectrometry in the health sciences. The main aims of this chapter are to summarise the key outcomes and to discuss future directions.

9.1 Key Conclusions and Summary of Chapters

9.1.1 Volatile Organic Compounds Associated with Shisha Paste and Shisha Smoking

This thesis presented the first PTR-MS study of shisha. Many VOCs were detected, either from the headspace of shisha paste, or from the volatiles coming out of the water pipe following the combustion of charcoal and shisha paste. Many harmful VOCs were found, predominantly from the headspace of the burning charcoal, namely benzene, toluene, propene and acetaldehyde.

9.1.2 Investigation of the product ions resulting from the reactions of H_3O^+ with menthol and vanillin and associated compounds (cyclohexanol, phenol, anisole, benzaldehyde and guaiacol).

The main objective of this investigation was to identify the vanillin and menthol product ions as a continuation investigation of Chapter 4 (VOCs from shisha smoking) where VOCs emitted from vanilla and mint flavoured shisha paste were measured. The key compound for vanilla is vanillin and menthol for mint. Vanillin and menthol product ions were investigated as a function of the important PTR-MS parameter E/N . The investigations on vanillin and menthol product ions have led us to investigate the reactions of H_3O^+ with associated compounds which have differences in the functional groups,

namely, cyclohexanol, phenol, anisole, benzaldehyde and guaiacol. Some similar ions associated to menthol were identified from cyclohexanol such as m/z 55, 57, 67, 81 and 83.

Of relevance to the shisha investigation, our results have shown that menthol has been used to prepare mint flavoured shisha paste but no vanillin was used in vanilla flavoured shisha paste.

9.1.3 PTR-ToF-MS studies of the reactions of H_3O^+ and O_2^+ with the anaesthetic gases halothane, isoflurane, enflurane, sevoflurane, desflurane and methoxyflurane

This study on anaesthetics has identified product ions from the reactions of H_3O^+ and O_2^+ as a function of reduced electric field for a number of commonly used (isoflurane and sevoflurane) and less commonly used (halothane, enflurane, sevoflurane, desflurane and methoxyflurane) anaesthetics. All the details on possible channels were described and identified. Although this study focuses on identifying the product ions resulting from the anaesthetics, the findings will have a bearing on a further investigation of on-line monitoring by applying mass spectrometry techniques to investigate changes of anaesthesia in breath post-surgery via longitudinal studies. Moreover, this study can provide supporting data which can be used to improve guidance on occupational safety and health for personnel who work in the operating theatres. This is important because the personnel working in operating theatres and intensive care units are exposed to toxic agents particularly volatile anaesthetics which can cause adverse effects.

9.1.4 Washout Characteristics of the Peppermint capsule

In this study, the data indicated that there is a great variability in breath VOCs released from peppermint oil which contains various volatiles (namely 1,8-cineole, menthol, menthone, limonene, with α -pinene and β -pinene) between inter-individual and intra-individual after ingestion of the peppermint capsule. The reason for these great differences could be the way the capsule is dissolved in the gut and the effect of diet. Perhaps metabolism is different for different people due to different BMI (Body Mass Index). Also, potentially, each peppermint oil capsule would have different concentrations of peppermint oil in the capsule. This probably would have an influence on the peppermint washout characteristics result of each individual who took part in this study.

Further studies, which involve correlation measurements of expected VOCs in exhaled breath and blood, will need to be undertaken to monitor the variability of concentration between blood and breath washout characteristics. This could lead to *in vivo* studies in which in future breath sampling can be used to illuminate the pharmacokinetics of peppermint oil containing capsules which contains many volatile compounds.

This study has identified that, m/z 155 is associated with menthol, menthone and 1,8-cineole, whereas, m/z 137 associated with α -pinene, β -pinene, limonene, fragments of menthone and fragments of 1,8-cineole, and m/z 81 is associated with α -pinene, β -pinene, limonene, menthone and 1,8-cineole.

Although VOCs from exhaled breath after ingestion of the peppermint oil capsule were identified using PTR-MS, further parallel monitoring of the breath washout

characteristics of the peppermint oil containing capsule using GC-MS is needed. This will aid the investigation to confirm and support the identification of VOCs and washout characteristics of the peppermint capsule from exhaled breath.

9.1.5 Breath analysis of Rugby Players who have had concussion (control and injured)

This study is purely an exploratory study using breath analysis for healthy and injured rugby players (after suffering a concussion). Methanol, acetone and isoprene were used to investigate the healthy and injured rugby players. One source of weakness in this study, which has affected the measurements of methanol from the exhaled breath, was the contamination of the room air where the background level of methanol was higher than the exhaled breath of injured players. This was probably due to the use of cleaning materials in the MRI room. Therefore, methanol was not considered to be used as an indicator in this study. However, this contamination does not affect acetone and isoprene as the background level of acetone and isoprene were low in comparison to the exhaled breath of the injured player.

For acetone and isoprene, the results have shown a significant difference between the healthy and injured rugby players. Although acetone has shown a significant difference between healthy and injured players, this has thrown up many questions, as the concentrations of acetone from exhaled breath are influenced by many known factors such as diet, metabolism activities and routine physiological activities.

The result of isoprene following concussion of rugby players' research, supports the idea that isoprene can be used as a potential indicator to evaluate protocols for monitoring the condition of the injured player for the next level of a clinical trial by doing a longitudinal study.

Also, this longitudinal study would provide some clues on the consistency of other VOCs' concentration which can be correlated with concentration of VOCs before and after suffering a concussion.

9.2 Limitations of the Investigations

For the shisha smoking investigation, the only limitation was in identifying the VOCs being emitted from the headspace of the shisha paste and also headspace of shisha paste and charcoal. Although, we used GC-MS to aid in identifying many of the compounds, some product ions observed with PTR-MS could not be assigned to any compound. Therefore, certain compounds were recorded as unassigned.

The main limitation of breath analysis (regarding the rugby player concussion study and the peppermint washout characteristics study) was the difficulty in recruitment where only a limited number of participants took part. For example, only two players had breath samples taken for pre and post-concussion. Besides that, the exhaled breath of injured rugby players was collected and measured after a few days of concussion. More importantly, we need to investigate the instant effects of concussion, i.e. taking the breath samples immediately after the concussion. This may provide stronger evidence of biochemical changes in the brain due to injury.

Similarly, in this case, the samples were only allowed to be taken with the collaboration of the Neuro-trauma Department, Queen Elizabeth Hospital, Birmingham with limited permitted time following the ethical guidelines.

Also it has to be noted that it was difficult to recruit more volunteers for peppermint washout characteristics because the measurement took more than 6 hours and required a volunteer to fast for approximately 10 hours prior to the measurement.

Despite promising results from concussion and peppermint washout characteristic studies, a larger sample size study is required to provide more conclusive results. However, the proof-of-principle studies presented in this thesis clearly demonstrate the usefulness and potential of using PTR-MS for medical purposes/assessment. In light of that, multi clinical research centres are involved in an EU (European Union) funded project which this project is being coordinated by Dr Simona Cristescu and Professor Paul Thomas. This project should provide more samples from multiple ethnic, gender and age groups in order to get a better understanding. Owing to having a larger number of samples, the confounding factors from the investigations can be limited.

9.3 Future work related to current studies

In this section, some suggestions and recommendations are proposed to improve the methodology, sampling, and also the importance of findings.

For future work, the existing current studies need to be extended. For example, further investigation of shisha smoking can be done using breath analysis of shisha smokers by taking pre and post shisha smokers breath samples to monitor the VOCs before shisha smoking and breath after shisha smoking. This combination of findings provides some support for the conceptualization of shisha smoking by taking into account VOCs being produced and being absorbed in the body, especially the lungs. It will be more prominent and accurate if we used online breath sampling rather than off line sampling which can be influenced by a lot of environmental factors such as exposure to sun light and extreme weather conditions.

Meanwhile, for anaesthetics investigation, based on the data base of product ions from this work, it is possible to carry out further work to monitor the washout

characteristics of each anaesthetic compound and the metabolites using the PTR-MS technique.

For the peppermint oil containing capsules washout study, a larger scale European study is being carried out (coordinated by Prof. P. Thomas and Dr. S Cristescu) to establish a standardized breath protocol. Also, given that limonene is an ingredient in peppermint oil, its washout characteristics from a large number of healthy volunteers will be extremely useful for comparison with the limonene washout characteristics from patients who are suffering from liver disease [2].

For concussion studies, it has been suggested to get immediate breath sample after the concussion and also, the significant difference of exhaled isoprene between two groups (healthy and injured) suggests that this is worth investigating further in a Phase 2 trial.

9.4 Summary

This thesis provides fundamental groundwork on PTR-MS applications in the health sciences and the evaluation of breath samples. This research work has contributed significantly to showing how PTR-MS can be used in the medical sciences. More intense clinical trials using PTR-MS relating to the screening and diagnoses of early stage disease are required.

In this thesis it has been shown how the analysis of shisha smoke extends our knowledge of the volatiles being emitted and their threat to health. For the flavour compound, Vanillin, expected to be the main flavour compound in vanilla shisha paste, was investigated using PTR-MS for the first time. This led to original PTR-MS studies

on guaiacol and anisole to aid in the understanding of the reactions of H_3O^+ with vanillin owing to changes in the functional groups.

The investigation of product ions from the reactions of anaesthetics with H_3O^+ and O_2^+ has provided a large data base of product ions for halothane, isoflurane, enflurane, sevoflurane, methoxyflurane, and desflurane. This will be used in a future investigation of the elimination of anaesthetics from the body; which surprisingly is lacking. This has consequences to possible cognitive awareness after an operation and could be used to determine liver function. For the first time product ions of halothane, enflurane, methoxyflurane and desflurane are presented.

The study of washout characteristics of peppermint oil via exhaled breath results showed that there were inter-personnel and intra-personal variation. The VOCs from the peppermint oil contained in the capsule and the exhaled VOCs after the peppermint capsule ingestion were tentatively identified using PTR-MS. GC-MS is needed to conclusively assign the compounds.

For the concussion clinical trial, breath sampling and analysis were used for the first time to investigate the VOCs in the breath of healthy and head-injured rugby players.

To summarize, the large amount of work presented in this thesis has highlighted the versatility of using PTR-MS for medical applications.

REFERENCES

- [1] A.M. Ellis, C.A. Mayhew, *Proton Transfer Reaction Mass Spectrometry: Principles and Applications*, John Wiley & Sons, Ltd 2014.
- [2] R. Fernández del Río, M.E. O'Hara, A. Holt, P. Pemberton, T. Shah, T. Whitehouse, C.A. Mayhew, *Volatile Biomarkers in Breath Associated With Liver Cirrhosis — Comparisons of Pre- and Post-liver Transplant Breath Samples*, *EBioMedicine* 2 (2015) 1243-1250.
- [3] P.B. Lirk, F.; Rieder, J., *Medical applications of proton transfer reaction-mass spectrometry: ambient air monitoring and breath analysis*, *International Journal of Mass Spectrometry* 239 (2004) 221-226.
- [4] G.R. Harrison, A.D.J. Critchley, C.A. Mayhew, J.M. Thompson, *Real-time breath monitoring of propofol and its volatile metabolites during surgery using a novel mass spectrometric technique: a feasibility study*, *British Journal of Anaesthesia* 91 (2003) 797-799.
- [5] R. Fernández del Río, M. E. O'Hara, P. Pemberton, T. Whitehouse, C.A. Mayhew., *Elimination characteristics of post-operative isoflurane levels in alveolar exhaled breath via PTR-MS analysis*, *Journal of Breath Research* 10 (2016) 046006.
- [6] N. Yasuda, S.H. Lockhart, E.I. Eger, 2nd, R.B. Weiskopf, J. Liu, M. Laster, S. Taheri, N.A. Peterson, *Comparison of kinetics of sevoflurane and isoflurane in humans*, *Anesthesia and analgesia* 72 (1991) 316-324.
- [7] S.F. Solga, T.H. Risby, *Chapter 2 - Issues and Challenges in Human Breath Research: Perspectives from Our Experience*, in: A. Amann, D. Smith (Eds.), *Volatile Biomarkers*, Elsevier, Boston, 2013, pp. 19-24.
- [8] A. Jordan, A. Hansel, R. Holzinger, W. Lindinger, *Acetonitrile and benzene in the breath of smokers and non-smokers investigated by proton transfer reaction mass spectrometry (PTR-MS)*, *International Journal of Mass Spectrometry and Ion Processes* 148 (1995) L1-L3.
- [9] S.L. Blair, S.A. Epstein, S.A. Nizkorodov, N. Staimer, *A Real-Time Fast-Flow Tube Study of VOC and Particulate Emissions from Electronic, Potentially Reduced-Harm, Conventional, and Reference Cigarettes*, *Aerosol science and technology : the journal of the American Association for Aerosol Research* 49 (2015) 816-827.
- [10] S. Colard, G.O. Connell, P. Sulzer, K. Breiev, X. Cahours, S.S. Biel., *An Experimental Method to Determine the Concentration of Nicotine in Exhaled Breath and its Retention Rate Following Use of an Electronic Cigarette*, *Journal of Environmental Analytical Chemistry* 02 (2015).
- [11] E. Schmidt, S. Bail, G. Buchbauer, I. Stoilova, T. Atanasova, A. Stoyanova, A. Krastanov, L. Jirovetz, *Chemical composition, olfactory*

- evaluation and antioxidant effects of essential oil from *Mentha x piperita*, *Natural product communications* 4 (2009) 1107-1112.
- [12] M.H. Baslow, N-acetylaspartate in the vertebrate brain: metabolism and function., *Neurochem Res* (2003).
- [13] W. Lindinger, A. Hansel, A. Jordan., Proton-transfer-reaction mass spectrometry (PTR-MS): on-line monitoring of volatile organic compounds at pptv levels, *Chemical Society reviews* volume 27 (1998).
- [14] M. Munson, F. Field, Chemical Ionisation Mass Spectrometry, *Journal of American Chemical Society* 88 (1966) 2621.
- [15] M.E. Jennings W, *Analytical gas chromatography*, Academic Press 1997.
- [16] R.L Grob, E.F Barry, *Modern Practise of Gasd Chromatography*, John Wiley & Sons Inc, USA, 2004.
- [17] G. Eiceman, Z. Karpas, J.H. Hill., *Ion Mobility Spectrometry*, Boca Raton: CRC Press, USA, 2014.
- [18] Syft Technologies, USA, 2012.
- [19] R.S. Blake, P S. Monks, A.M. Ellis, Proton-Transfer Reaction Mass Spectrometry, *Chem. Rev* Vol. 109, (2009) 861–896.
- [20] A. Hansel, A. Jordan, R. Holzinger, P. Prazeller, W. Vogel, W. Lindinger, Proton transfer reaction mass spectrometry: on-line trace gas analysis at the ppb level, *International Journal of Mass Spectrometry and Ion Processes* 149 (1995) 609-619.
- [21] J.A. Hansel A , Holzinger R, Prazeller P, Vogel W, Lindinger W., Proton transfer reaction mass spectrometry: on-line trace gas analysis at the ppb level *International Journal of Mass Spectrometry and Ion Processes* (1995) 609-619
- [22] Proton Transfer Reactor Time-of-Flight Mass Spectrometry (PTR-TOF-MS), Kore Technology Limited United Kingdom, 2014.
- [23] S.M. Y. Ikezoe , M. Takebe , A. Viggiano *Gas Phase Ion Molecule Reaction Rate-Constants Through Maruzan*, Tokyo, 1987.
- [24] E.P.L. Hunter, S.G. Lias, Evaluated Gas Phase Basicities and Proton Affinities of Molecules: An Update, *Journal of Physical and Chemical Reference Data* 27 (1998) 413-656.
- [25] N.G. Adams, D. Smith, E.E. Ferguson, Comparative effects of temperature and kinetic energy change on the reaction of O_2^+ with CH_4 and CD_4 ., *International Journal of Mass Spectrometry and Ion Processes* (1985) 67-74.
- [26] C. Warneke, J.A. de Gouw, W.C. Kuster, P.D. Goldan, R. Fall, Validation of Atmospheric VOC Measurements by Proton-Transfer-

- Reaction Mass Spectrometry Using a Gas-Chromatographic Preseparation Method, *Environmental Science & Technology* 37 (2003) 2494-2501.
- [27] S. Kato, Y. Miyakawa, T. Kaneko, Y. Kajii, Urban air measurements using PTR-MS in Tokyo area and comparison with GC-FID measurements, *International Journal of Mass Spectrometry* 235 (2004) 103-110.
- [28] NIST Chemistry WebBook, US Secretary of Commerce, USA, 2008.
- [29] M. Tereza Fernandez, C. Williams, R. S. Mason, B. J. Costa Cabral, Experimental and theoretical proton affinity of limonene, *Journal of the Chemical Society, Faraday Transactions* 94 (1998) 1427-1430.
- [30] V.G. Anicich, Evaluated Bimolecular Ion-Molecule Gas Phase Kinetics of Positive Ions for Use in Modelling Planetary Atmospheres, Cometary Comae, and Intersellar Clouds, *J.Phys. Chem* 22, No 6 (1993).
- [31] M.E. O'Hara, R. Fernandez Del Rio, A. Holt, P. Pemberton, T. Shah, T. Whitehouse, C.A. Mayhew, Limonene in exhaled breath is elevated in hepatic encephalopathy, *J Breath Res* 10 (2016) 046010.
- [32] T.A. Popov, Human exhaled breath analysis, *Annals of Allergy, Asthma & Immunology* 106 (2011) 451-456.
- [33] L. Pauling, A.B. Robinson, Teranish.R, P. Cary, Quantitative Analysis of Urine Vapor and Breath by Gas-Liquid Partition Chromatography, *Proceedings of the National Academy of Sciences of the United States of America* 68 (1971) 2374-&.
- [34] M. Phillips, J.P. Boehmer, R.N. Cataneo, T. Cheema, H.J. Eisen, J.T. Fallon, P.E. Fisher, A. Gass, J. Greenberg, J. Kobashigawa, D. Mancini, B. Rayburn, M.J. Zucker, Prediction of heart transplant rejection with a breath test for markers of oxidative stress, *American Journal of Cardiology* 94 (2004) 1593-1594.
- [35] J.K. Schubert, W. Miekisch, Chapter 9 - Breath Analysis in Critically Ill Patients—Potential and Limitations, *Volatile Biomarkers*, Elsevier, Boston, 2013, pp. 155-176.
- [36] A.J. Scott-Thomas, M. Syhre, P.K. Pattemore, M. Epton, R. Laing, J. Pearson, S.T. Chambers, 2-Aminoacetophenone as a potential breath biomarker for *Pseudomonas aeruginosa* in the cystic fibrosis lung, *BMC pulmonary medicine* 10 (2010).
- [37] A.J. Scott-Thomas, M. Epton, S. Chambers, Validating a breath collection and analysis system for the new tuberculosis breath test, *J Breath Res* 7 (2013) 037108.
- [38] M. Phillips, R.N. Cataneo, B.A. Ditkoff, P. Fisher, J. Greenberg, R. Gunawardena, C.S. Kwon, O. Tietje, C. Wong, Prediction of breast cancer using volatile biomarkers in the breath, *Breast Cancer Research and Treatment* 99 (2006) 19-21.

- [39] J. Taucher, A. Hansel, A. Jordan, W. Lindinger, Analysis of Compounds in Human Breath after Ingestion of Garlic Using Proton-Transfer-Reaction Mass Spectrometry, *Journal of Agricultural and Food Chemistry* 44 (1996) 3778-3782.
- [40] C. Warneke, J. Kuczynski, A. Hansel, A. Jordan, W. Vogel, W. Lindinger, Proton transfer reaction mass spectrometry (PTR-MS): Propanol in human breath, *International Journal of Mass Spectrometry and Ion Processes* 154 (1996) 61-70.
- [41] J. Taucher, A. Lagg, A. Hansel, W. Vogel, W. Lindinger, Methanol in Human Breath, *Alcoholism-Clinical and Experimental Research* 19 (1995) 1147-1150.
- [42] J. Taucher, A. Hansel, A. Jordan, R. Fall, J.H. Futrell, W. Lindinger, Detection of isoprene in expired air from human subjects using proton-transfer-reaction mass spectrometry, *Rapid Communications in Mass Spectrometry* 11 (1997) 1230-1234.
- [43] E.S. Deneris, R.A. Stein, J.F. Mead, Invitro biosynthesis of isoprene from mevalonate utilizing a rat liver cytosolic fraction, *Biochemical and Biophysical Research Communications* 123 (1984) 691-696.
- [44] M. Phillips, J. Greenberg, J. Awad, Metabolic and environmental origins of volatile organic compounds in breath, *J Clin Pathol* 47 (1994) 1052-1053.
- [45] B. Buszewski, M. Kesy, T. Ligor, A. Amann, Human exhaled air analytics: Biomarkers of diseases, *Biomedical Chromatography* 21 (2007) 553-566.
- [46] M. Phillips, J. Herrera, S. Krishnan, M. Zain, J. Greenberg, R.N. Cataneo, Variation in volatile organic compounds in the breath of normal humans, *Journal of Chromatography B* 729 (1999) 75-88.
- [47] P.J. Mazzone, Analysis of Volatile Organic Compounds in the Exhaled Breath for the Diagnosis of Lung Cancer, *Journal of Thoracic Oncology* 3 (2008) 774-780.
- [48] L. Learning, The respiratory system, Creative Commons Attribution, Portland, The United State, 2017.
- [49] D.A. Sibernagal S, *Color Atlas of Physiology*, 6 edition ed., Thieme Publishing Group, Germany, 2006.
- [50] ClicalGate, Respiratory system, iKnowledge, Internet, 2015.
- [51] A. Tangerman, M.T. Meuwese-Arends, J.H.M. van Tongeren, A new sensitive assay for measuring volatile sulphur compounds in human breath by Tenax trapping and gas chromatography and its application in liver cirrhosis, *Clinica Chimica Acta* 130 (1983) 103-110.

- [52] J.J. Van Berkel, J.W. Dallinga, G.M. Moller, R.W. Godschalk, E.J. Moonen, E.F. Wouters, F.J. Van Schooten, A profile of volatile organic compounds in breath discriminates COPD patients from controls, *Respir Med* 104 (2010) 557-563.
- [53] J. Kwak, M. Fan, S.W. Harshman, C.E. Garrison, V.L. Dershem, J.B. Phillips, C.C. Grigsby, D.K. Ott, Evaluation of Bio-VOC Sampler for Analysis of Volatile Organic Compounds in Exhaled Breath, *Metabolites* 4 (2014) 879-888.
- [54] O. Lawal, W.M. Ahmed, T.M.E. Nijsen, R. Goodacre, S.J. Fowler, Exhaled breath analysis: a review of 'breath-taking' methods for off-line analysis, *Metabolomics* 13 (2017) 110.
- [55] N. Peled, M. Hakim, P.A. Bunn, Jr., Y.E. Miller, T.C. Kennedy, J. Mattei, J.D. Mitchell, F.R. Hirsch, H. Haick, Non-invasive breath analysis of pulmonary nodules, *Journal of thoracic oncology : official publication of the International Association for the Study of Lung Cancer* 7 (2012) 1528-1533.
- [56] Z.Q. Xu, Y.Y. Broza, R. Ionsecu, U. Tisch, L. Ding, H. Liu, Q. Song, Y.Y. Pan, F.X. Xiong, K.S. Gu, G.P. Sun, Z.D. Chen, M. Leja, H. Haick, A nanomaterial-based breath test for distinguishing gastric cancer from benign gastric conditions, *British journal of cancer* 108 (2013) 941-950.
- [57] T.Y. Khalid, B.D. Costello, R. Ewen, P. White, S. Stevens, F. Gordon, P. Collins, A. McCune, A. Shenoy, S. Shetty, N.M. Ratcliffe, C.S. Probert, Breath Volatile Analysis for the Recognition of Harmful Drinking, Cirrhosis and Hepatic Encephalopathy, *Gut* 61 (2012) A414-A415.
- [58] W. Filipiak, A. Filipiak, A. Sponring, T. Schmid, B. Zelger, C. Ager, E. Klodzinska, H. Denz, A. Pizzini, P. Lucciarini, H. Jamnig, J. Troppmair, A. Amann, Comparative analyses of volatile organic compounds (VOCs) from patients, tumors and transformed cell lines for the validation of lung cancer-derived breath markers, *J Breath Res* 8 (2014) 027111.
- [59] P. Mochalski, J. King, M. Haas, K. Unterkofler, A. Amann, G. Mayer, Blood and breath profiles of volatile organic compounds in patients with end-stage renal disease, *BMC Nephrol* 15 (2014) 43.
- [60] J.C. Anderson, A.L. Babb, M.P. Hlastala, Modeling soluble gas exchange in the airways and alveoli, *Annals of Biomedical Engineering* 31 (2003) 1402-1422.
- [61] J.C. Anderson, M.P. Hlastala, Breath tests and airway gas exchange, *Pulmonary Pharmacology & Therapeutics* 20 (2007) 112-117.
- [62] M.E. O'Hara, S. O'Hehir, S. Green, C.A. Mayhew, Development of a protocol to measure VOCs in human breath: a comparison of rebreathing and

- on-line single exhalations using PTR-MS, *Physiological Measurement* (2008) 309-330.
- [63] T.H. Risby, S.F. Solga, Current status of clinical breath analysis, *Applied Physics B* 85 (2006) 421-426.
- [64] B. Jonathan, H. Jens, G. Rene, H. Armin, On the use of Tedlar® bags for breath-gas sampling and analysis, *Journal of Breath Research* 2 (2008) 046001.
- [65] M.E. O'Hara, T.H. Clutton-Brock, S. Green, C.A. Mayhew, Endogenous volatile organic compounds in breath and blood of healthy volunteers: examining breath analysis as a surrogate for blood measurements, *Journal of Breath Research* 3 (2009).
- [66] J. Herbig, J. Beauchamp, Towards standardization in the analysis of breath gas volatiles, *J Breath Res* 8 (2014) 037101.
- [67] Recommendations for Standardized Procedures for the Online and Offline Measurement of Exhaled Lower Respiratory Nitric Oxide and Nasal Nitric Oxide in Adults and Children—1999, *American Journal of Respiratory and Critical Care Medicine* 160 (1999) 2104-2117.
- [68] ATS/ERS recommendations for standardized procedures for the online and offline measurement of exhaled lower respiratory nitric oxide and nasal nitric oxide, 2005, *Am J Respir Crit Care Med* 171 (2005) 912-930.
- [69] W. Miekisch, J.K. Schubert, D.A. Vagts, K. Geiger, *Analysis of volatile disease markers in blood*, *Clinical Chemistry* 47 (2001) 1053-1060.
- [70] B. Krauss, D.R. Hess, Capnography for Procedural Sedation and Analgesia in the Emergency Department, *Annals of Emergency Medicine* 50 172-181.
- [71] J. Spiegel, End-Tidal Carbon Dioxide: The most Vital of Vital Signs, *AnesthesiologyNews.com* (2013) 21-27.
- [72] http://www.anesthesia2000.com/physics/Chemistry_Physics/physics15.htm, *Anesthesia Fundamentals*, 2000.
- [73] Al Rashidi, M. Shihadeh, A. Saliba, N.A., Volatile aldehydes in the mainstream smoke of the narghile waterpipe, *Food Chem Toxicol* 46 (2008) 3546-3549.
- [74] M. Chaaya, Z. El-Roueiheb, H. Chemaitelly, G. Azar, J. Nasr, B. Al-Sahab, Argileh smoking among university students: a new tobacco epidemic, *Nicotine Tob Res* 6 (2004) 457-463.
- [75] R.A. Al-Naggar, Saghir, F.S., Water Pipe (Shisha) Smoking and Associated Factors Among Malaysian University Students, *Asian Pacific journal of cancer prevention* 12 (2011) 3041-3047.

- [76] W. Maziak, F.M. Fouad, T. Asfar, F. Hammal, E.M. Bachir, S. Rastam, T. Eissenberg, K.D. Ward, Prevalence and characteristics of narghile smoking among university students in Syria, *Int J Tuberc Lung Dis* 8 (2004).
- [77] D. Jackson, P. Aveyard, Waterpipe smoking in students: Prevalence, risk factors, symptoms of addiction, and smoke intake. Evidence from one British university, *BMC Public Health* 8 (2008) 174.
- [78] T. Eissenberg, A. Shihadeh, Waterpipe Tobacco and Cigarette Smoking: Direct Comparison of Toxicant Exposure, *American Journal of Preventive Medicine* 37 (2009) 518-523.
- [79] K. Chaouachi, More rigor needed in systematic reviews on "waterpipe" (hookah, narghile, shisha) smoking, *Chest* 139 (2011) 1250-1251; author reply 1251-1252.
- [80] A. Apsley, K.S. Galea, A. Sánchez-Jiménez, S. Semple, H. Wareing, MTongerren., Assessment of polycyclic aromatic hydrocarbons, carbon monoxide, nicotine, metal contents and particle size distribution of mainstream Shisha smoke PDF, *Journal of Environmental Health Research* 11.
- [81] R.T. Nakkash, J. Khalila, R.A. Afifi, The rise in narghile (shisha, hookah) waterpipe, *BMC Public Health* 11 (2011).
- [82] M.V. Carroll, A. Shensa, B.A. Primack, A comparison of cigarette- and hookah-related videos on YouTube, *Tobacco control* 22 (2013) 319.
- [83] Y.A. Shafagoj, Mohammed, F.I, Following Levels of maximum end-expiratory carbon monoxide and certain cardiovascular parameters following hubble-bubble smoking, *Saudi medical journal* 23 953-958.
- [84] K.-H. Kim, E. Kabir, S.A. Jahan, Waterpipe tobacco smoking and its human health impacts, *Journal of Hazardous Materials* 317 (2016) 229-236.
- [85] C. Cobb, K.D. Ward, W. Maziak, A.L. Shihadeh, T. Eissenberg, Waterpipe tobacco smoking: an emerging health crisis in the United States, *Am J Health Behav* 34 (2010) 275-285.
- [86] A. Shihadeh, R. Salman, E. Jaroudi, N. Saliba, E. Sepetdjian, M.D. Blank, C.O. Cobb, T. Eissenberg, Does switching to a tobacco-free waterpipe product reduce toxicant intake? A crossover study comparing CO, NO, PAH, volatile aldehydes, "tar" and nicotine yields, *Food and Chemical Toxicology* 50 (2012) 1494-1498.
- [87] J. Schubert, F.D. Müller, R. Schmidt, A. Luch, T.G. Schulz, Waterpipe smoke: source of toxic and carcinogenic VOCs, phenols and heavy metals?, *Archives of Toxicology* 89 (2015) 2129-2139.
- [88] E. Kabir, K.H. Kim, J.W. Ahn, O.F. Hong, J.R. Sohn, Barbecue charcoal combustion as a potential source of aromatic volatile organic compounds and carbonyls, *Journal of hazardous materials* 174 (2010) 492-499.

- [89] K. Breiev, K.M.M. Burseg, G. O'Connell, E. Hartungen, S.S. Biel, X. Cahours, S. Colard, T.D. Märk, P. Sulzer, An online method for the analysis of volatile organic compounds in electronic cigarette aerosol based on proton transfer reaction mass spectrometry, *Rapid Communications in Mass Spectrometry* 30 (2016) 691-697.
- [90] C.J. Ennis, J.C. Reynolds, B.J. Keely, L.J. Carpenter, A hollow cathode proton transfer reaction time of flight mass spectrometer, *International Journal of Mass Spectrometry* 247 (2005) 72-80.
- [91] R. González-Méndez, D.F. Reich, S.J. Mullock, C.A. Corlett, C.A. Mayhew, Development and use of a thermal desorption unit and proton transfer reaction mass spectrometry for trace explosive detection: Determination of the instrumental limits of detection and an investigation of memory effects, *International Journal of Mass Spectrometry* 385 (2015) 13-18.
- [92] R.A. Philip, *Food flavorings*, Springer, USA, 1999.
- [93] Acrolein and Methacrolein, *Ullmann's Encyclopedia of Industrial Chemistry*.
- [94] F. Roth-Walter, C. Bergmayr, S. Meitz, S. Buchleitner, C. Stremnitzer, J. Fazekas, A. Moskovskich, M.A. Muller, G.A. Roth, K. Manzano-Szalai, Z. Dvorak, A. Neunkirchner, E. Jensen-Jarolim, Janus-faced Acrolein prevents allergy but accelerates tumor growth by promoting immunoregulatory Foxp3+ cells: Mouse model for passive respiratory exposure, *Scientific reports* 7 (2017) 45067.
- [95] Toxicology Data Network (Toxnet), National Institute of Health, Health & Human Services, USA, 2005.
- [96] A. Vale, *Methanol*, *Medicine* 35 (2007) 633-634.
- [97] National Center for Biotechnology Information. PubChem Compound Database; CID=527, <https://pubchem.ncbi.nlm.nih.gov/compound/527> (accessed May 31, 2018). US National Library of Medicine National Institutes of Health, USA, 2004.
- [98] Acetone, Canadian Centre for Occupational Health & Safety, Canada, 1997-.
- [99] F.E. Ahmed, Toxicological effects of ethanol on human health, *Critical reviews in toxicology* 25 (1995) 347-367.
- [100] Chemical Summary For Acetaldehyde, in: U.E.P. Agency (Ed.), *US Environmental Protection Agency*, USA, 2018.
- [101] S. Heenan, C. Soukoulis, P. Silcock, A. Fabris, E. Aprea, L. Cappellin, T.D. Märk, F. Gasperi, F. Biasioli, PTR-TOF-MS monitoring of in vitro and in vivo flavour release in cereal bars with varying sugar composition, *Food Chemistry* 131 (2012) 477-484.

- [102] R. Nakkash , J. Khalil Health warning labelling practices on narghile (shisha, hookah) waterpipe tobacco products and related accessories, *Tobacco control* 19 (2010) 235-239.
- [103] M.T. Belay, C.F. Poole, Determination of vanillin and related flavor compounds in natural vanilla extracts and vanilla-flavored foods by thin layer chromatography and automated multiple development, *Chromatographia* 37 (1993) 365-373.
- [104] M.D. Sharp, N.A. Kocaoglu-Vurma, V. Langford, L.E. Rodriguez-Saona, W.J. Harper, Rapid discrimination and characterization of vanilla bean extracts by attenuated total reflection infrared spectroscopy and selected ion flow tube mass spectrometry, *Journal of food science* 77 (2012) C284-292.
- [105] K. Klausner, Menthol cigarettes and smoking initiation: a tobacco industry perspective, *Tobacco control* 20 (2011) ii12-ii19.
- [106] A. Saint-Eve, I. Déléris, E. Aubin, E. Semon, G. Feron, J.-M. Rabillier, D. Ibarra, E. Guichard, I. Souchon, Influence of Composition (CO₂ and Sugar) on Aroma Release and Perception of Mint-Flavored Carbonated Beverages, *Journal of Agricultural and Food Chemistry* 57 (2009) 5891-5898.
- [107] S.M. Gordon, M.C. Brinkman, R.Q. Meng, G.M. Anderson, J.C. Chuang, R.R. Kroeger, I.L. Reyes, P.I. Clark, Effect of cigarette menthol content on mainstream smoke emissions, *Chem Res Toxicol* 24 (2011) 1744-1753.
- [108] S. Jürschik, A. Tani, P. Sulzer, S. Haidacher, A. Jordan, R. Schottkowsky, E. Hartungen, G. Hanel, H. Seehauser, L. Märk, T.D. Märk, Direct aqueous injection analysis of trace compounds in water with proton-transfer-reaction mass spectrometry (PTR-MS), *International Journal of Mass Spectrometry* 289 (2010) 173-176.
- [109] P. Brown, P. Watts, T.D. Märk, C.A. Mayhew, Proton transfer reaction mass spectrometry investigations on the effects of reduced electric field and reagent ion internal energy on product ion branching ratios for a series of saturated alcohols, *International Journal of Mass Spectrometry* 294 (2010) 103-111.
- [110] R. Winterhalter, F. Herrmann, B. Kanawati, T.L. Nguyen, J. Peeters, L. Vereecken, G.K. Moortgat, The gas-phase ozonolysis of [small beta]-caryophyllene (C₁₅H₂₄). Part I: an experimental study, *Physical Chemistry Chemical Physics* 11 (2009) 4152-4172.
- [111] A. Feilberg, P. Bildsoe, T. Nyord, Application of PTR-MS for Measuring Odorant Emissions from Soil Application of Manure Slurry, *Sensors* 15 (2015) 1148.

- [112] A. Romano, G.B. Hanna, Identification and quantification of VOCs by Proton Transfer Reaction Time of Flight Mass Spectrometry: an experimental workflow for the optimization of specificity, sensitivity and accuracy, *Journal of mass spectrometry : JMS* (2018).
- [113] P. Spanel, D. Smith, SIFT studies of the reactions of H_3O^+ , NO^+ and O_2^+ with a series of alcohols, *International Journal of Mass Spectrometry and Ion Processes* 167-168 (1997) 375-388.
- [114] González-Méndez R, Watts P, Reich D.F, Mullock S.J, Cairns S, Hickey P, Brookes M, M. C.A, Use of Rapid Reduced Electric Field Switching to Enhance Compound Specificity for Proton Transfer Reaction-Mass Spectrometry *Analytical Chemistry* (2018).
- [115] T. Wang, D. Smith, P. Spaněl, Selected ion flow tube studies of the reactions of H_3O^+ , NO^+ and O_2^+ with the anaesthetic gases halothane, isoflurane and sevoflurane, *Rapid Commun Mass Spectrom* 16 (2002) 1860-1870.
- [116] J.M. Dumans, P. Dupuis, G. Pfister-Guillouzo, C. Sandorfy, 'Ionization Energetics Data' NIST Chemistry WebBook, SRD 69, U.S. Secretary of Commerce on behalf of the United States of America, USA, 2017.
- [117] A.J. Sanyal, A.M. Freedman, P.P. Purdum, 3rd, TIPS-associated hemolysis and encephalopathy, *Annals of internal medicine* 117 (1992) 443-444.
- [118] R. González-Méndez, P. Watts, F.D. Reich, S.J. Mullock, S. Cairns, P. Hickey, M. Brookes, C.A. Mayhew, Use of Rapid Reduced Electric Field Switching to Enhance Compound Specificity for Proton Transfer Reaction-Mass Spectrometry, *Analytical Chemistry* 90 (2018) 5664-5670.
- [119] Isoflurane, National Center for Biotechnology Information, USA, 2017.
- [120] I.S. Ltd, Sevoflurane, Ion Science Ltd, United Kingdom, 2018.
- [121] L.P. Summer G, Hoerauf K, Riccabona U, Bodrogi F, Raifer H, Deibl M, Rieder, S.W. J, Sevoflurane in exhaled air of operating room personnel., *Anesthesia and analgesia* 97 (2003) 1070-1073.
- [122] A. Critchley, T.S. Elliott, G. Harrison, C.A. Mayhew, J.M. Thompson, T. Worthington, The proton transfer reaction mass spectrometer and its use in medical science: applications to drug assays and the monitoring of bacteria, *International Journal of Mass Spectrometry* 239 (2004) 235-241.
- [123] D.B. Milligan, P.F. Wilson, C.G. Freeman, M. Meot-Ner, M.J. McEwan, Dissociative Proton Transfer Reactions of H_3^+ , N_2H^+ , and H_3O^+ with Acyclic, Cyclic, and Aromatic Hydrocarbons and Nitrogen

- Compounds, and Astrochemical Implications, *The Journal of Physical Chemistry A* 106 (2002) 9745-9755.
- [124] J. Beauchamp, F. Kirsch, A. Buettner, Real-time breath gas analysis for pharmacokinetics: monitoring exhaled breath by on-line proton-transfer-reaction mass spectrometry after ingestion of eucalyptol-containing capsules, *J Breath Res* 4 (2010) 026006.
- [125] V. Ruzsanyi, Ion mobility spectrometry for pharmacokinetic studies – exemplary application, *Journal of breath research* 7 (2013) 10.1088/1752-7155/1087/1084/046008.
- [126] M.E. O’Hara, R. Fernández del Río, A. Holt, P. Pemberton, T. Shah, T. Whitehouse, C.A. Mayhew, Limonene in exhaled breath is elevated in hepatic encephalopathy, *Journal of Breath Research* 10 (2016) 046010.
- [127] J. Herbig, T. Titzmann, J. Beauchamp, I. Kohl, A. Hansel, Buffered end-tidal (BET) sampling-a novel method for real-time breath-gas analysis, *J Breath Res* 2 (2008) 037008.
- [128] D. Sanders, Peppermint Pill – Terpene washout: Frequent Alternating Direct Breath Sampling via mouth and nose, G.A.S. Gesellschaft für analytische Sensor systeme mbH BioMedizin Zentrum Dortmund, Germany, 2016.
- [129] PubChem open Chemistry Database, National Center for Biotechnology Information, USA, 2004.
- [130] Sigma-Aldrich, 2018.
- [131] W. Lindinger, A. Jordan, Proton-transfer-reaction mass spectrometry (PTR-MS): on-line monitoring of volatile organic compounds at pptv levels, *Chemical Society reviews* 27 (1998) 347-375.
- [132] D. Materić, M. Lanza, P. Sulzer, J. Herbig, D. Bruhn, V. Gauci, N. Mason, C. Turner, Selective reagent ion-time of flight-mass spectrometry study of six common monoterpenes, *International Journal of Mass Spectrometry* 421 (2017) 40-50.
- [133] S.D. Maleknia, T.L. Bell, M.A. Adams, PTR-MS analysis of reference and plant-emitted volatile organic compounds, *International Journal of Mass Spectrometry* 262 (2007) 203-210.
- [134] A. Tani, S. Hayward, C.N. Hewitt, Measurement of monoterpenes and related compounds by proton transfer reaction-mass spectrometry (PTR-MS), *International Journal of Mass Spectrometry* 223-224 (2003) 561-578.
- [135] M. Steeghs, H.P. Bais, J. de Gouw, P. Goldan, W. Kuster, M. Northway, R. Fall, J.M. Vivanco, Proton-Transfer-Reaction Mass Spectrometry as a New Tool for Real Time Analysis of Root-Secreted Volatile Organic Compounds in Arabidopsis, *Plant Physiology* 135 (2004) 47-58.

- [136] A. Tani, Fragmentation and Reaction Rate Constants of Terpenoids Determined by Proton Transfer Reaction-mass Spectrometry, *Environmental Control in Biology* 51 (2013) 23-29.
- [137] A. Tani, S. Hayward, A. Hansel, C.N. Hewitt, Effect of water vapour pressure on monoterpene measurements using proton transfer reaction-mass spectrometry (PTR-MS), *International Journal of Mass Spectrometry* 239 (2004) 161-169.
- [138] C.N. Hewitt, S. Hayward, A. Tani, The application of proton transfer reaction-mass spectrometry (PTR-MS) to the monitoring and analysis of volatile organic compounds in the atmosphere, *Journal of Environmental Monitoring* 5 (2003) 1-7.
- [139] M. Tietz, A. Buettner, B. Conde-Petit, Interaction between starch and aroma compounds as measured by proton transfer reaction mass spectrometry (PTR-MS), *Food Chemistry* 108 (2008) 1192-1199.
- [140] R. González-Méndez, P. Watts, D. Olivenza-León, D.F. Reich, S.J. Mullock, C.A. Corlett, S. Cairns, P. Hickey, M. Brookes, C.A. Mayhew, Enhancement of Compound Selectivity Using a Radio Frequency Ion-Funnel Proton Transfer Reaction Mass Spectrometer: Improved Specificity for Explosive Compounds, *Analytical Chemistry* 88 (2016) 10624-10630.
- [141] A. Lee, G.W. Schade, R. Holzinger, A.H. Goldstein, A comparison of new measurements of total monoterpene flux with improved measurements of speciated monoterpene flux, *Atmos. Chem. Phys.* 5 (2005) 505-513.
- [142] K.W. Somerville, C.R. Richmond, G.D. Bell, Delayed release peppermint oil capsules (Colpermin) for the spastic colon syndrome: a pharmacokinetic study, *British journal of clinical pharmacology* 18 (1984) 638-640.
- [143] A. Valente, A.E. Carrillo, M.N. Tzatzarakis, E. Vakonaki, A.M. Tsatsakis, G.P. Kenny, Y. Koutedakis, A.Z. Jamurtas, A.D. Flouris, The absorption and metabolism of a single L-menthol oral versus skin administration: Effects on thermogenesis and metabolic rate, *Food and Chemical Toxicology* 86 (2015) 262-273.
- [144] M. Miyazawa, M. Shindo, T. Shimada, Oxidation of 1,8-Cineole, the Monoterpene Cyclic Ether Originated From *Eucalyptus Polybractea*, by Cytochrome P450 3A Enzymes in Rat and Human Liver Microsomes, *Drug Metabolism and Disposition* 29 (2001) 200-205.
- [145] M. Miyazawa, S. Marumoto, T. Takahashi, H. Nakahashi, R. Haigou, K. Nakanishi, Metabolism of (+)- and (-)-menthols by CYP2A6 in human liver microsomes, *Journal of oleo science* 60 (2011) 127-132.
- [146] J. Sun, D-Limonene: safety and clinical applications, *Alternative medicine review : a journal of clinical therapeutic* 12 (2007) 259-264.

- [147] Concussion, www.nhs.uk/Conditions/Concussion/Pages/Introduction.aspx (2014) .
- [148] Sport concussion assessment tool - 5th edition, *British Journal of Sports Medicine* 51 (2017) 851-858.
- [149] P. McCrory, W.H. Meeuwisse, M. Aubry, B. Cantu, J. Dvořák, R.J. Echemendia, L. Engebretsen, K. Johnston, J.S. Kutcher, M. Raftery, A. Sills, B.W. Benson, G.A. Davis, R.G. Ellenbogen, K. Guskiewicz, S.A. Herring, G.L. Iverson, B.D. Jordan, J. Kissick, M. McCrea, A.S. McIntosh, D. Maddocks, M. Makdissi, L. Purcell, M. Putukian, K. Schneider, C.H. Tator, M. Turner, Consensus statement on concussion in sport: the 4th International Conference on Concussion in Sport held in Zurich, November 2012, *British Journal of Sports Medicine* 47 (2013) 250-258.
- [150] A.C. Duhaime, J.G. Beckwith, A.C. Maerlender, T.W. McAllister, J.J. Crisco, S.M. Duma, P.G. Brolinson, S. Rowson, L.A. Flashman, J.J. Chu, R.M. Greenwald, Spectrum of acute clinical characteristics of diagnosed concussions in college athletes wearing instrumented helmets: clinical article, *Journal of neurosurgery* 117 (2012) 1092-1099.
- [151] M.S. Dziemianowicz, M.P. Kirschen, B.A. Pukenas, E. Laudano, L.J. Balcer, S.L. Galetta, Sports-Related Concussion Testing, *Current Neurology and Neuroscience Reports* 12 (2012) 547-559.
- [152] S.P. Broglio, S.N. Macciocchi, M.S. Ferrara, Sensitivity of the concussion assessment battery, *Neurosurgery* 60 (2007) 1050-1057; discussion 1057-1058.
- [153] K.M. Guskiewicz, J.K. Register-Mihalik, Postconcussive impairment differences across a multifaceted concussion assessment protocol, *PM & R : the journal of injury, function, and rehabilitation* 3 (2011) S445-451.
- [154] K.G. Harmon, J.A. Drezner, M. Gammons, K.M. Guskiewicz, M. Halstead, S.A. Herring, J.S. Kutcher, A. Pana, M. Putukian, W.O. Roberts, American Medical Society for Sports Medicine position statement: concussion in sport, *Br J Sports Med* 47 (2013) 15-26.
- [155] J.K. Register-Mihalik, K.M. Guskiewicz, J.P. Mihalik, J.D. Schmidt, Z.Y. Kerr, M.A. McCrea, Reliable change, sensitivity, and specificity of a multidimensional concussion assessment battery: implications for caution in clinical practice, *The Journal of head trauma rehabilitation* 28 (2013) 274-283.
- [156] I.o. Medicine, N.R. Council, Sports-Related Concussions in Youth: Improving the Science, Changing the Culture, The National Academies Press, Washington, DC, 2014.
- [157] C.C. Giza, J.S. Kutcher, S. Ashwal, J. Barth, T.S. Getchius, G.A. Gioia, G.S. Gronseth, K. Guskiewicz, S. Mandel, G. Manley, D.B. McKeag,

- D.J. Thurman, R. Zafonte, Summary of evidence-based guideline update: evaluation and management of concussion in sports: report of the Guideline Development Subcommittee of the American Academy of Neurology, *Neurology* 80 (2013) 2250-2257.
- [158] G. Kirkwood, N. Parekh, R. Ofori-Asenso, A.M. Pollock, Concussion in youth rugby union and rugby league: a systematic review, *British journal of sports medicine* 49 (2015) 506-510.
- [159] R. Sahyouni, P. Gutierrez, E. Gold, R.T. Robertson, B.J. Cummings, Effects of concussion on the blood–brain barrier in humans and rodents, *Journal of Concussion* 1 (2017) 2059700216684518.
- [160] J. Beauchamp, Inhaled today, not gone tomorrow: pharmacokinetics and environmental exposure of volatiles in exhaled breath, *J Breath Res* 5 (2011) 037103.
- [161] M.E. O'Hara, C.-B.T. H., S. Green, S. O'Hehir, C.A. Mayhew, Mass spectrometric investigations to obtain the first direct comparisons of endogenous breath and blood volatile organic compound concentrations in healthy volunteers, *International Journal of Mass Spectrometry* (2008) (accepted for publication).
- [162] J.D. Fenske, S.E. Paulson, Human Breath Emissions of VOCs, *Journal of the Air & Waste Management Association* 49 (1999) 594-598.
- [163] M.E. O'Hara, The Use of Proton Transfer Reaction Mass Spectrometry For Analysis of Volatile Organic Compounds in Breath and Microbial Headspace, School of Physics and Astronomy, University of Birmingham, United Kingdom, 2009, pp. 167.
- [164] J.G. Filser, C. Hutzler, V. Meischner, V. Veereshwarayya, G.A. Csanády, Metabolism of 1,3-butadiene to toxicologically relevant metabolites in single-exposed mice and rats, *Chemico-Biological Interactions* 166 (2007) 93-103.
- [165] E.S. Deneris, R.A. Stein, J.F. Mead, In vitro biosynthesis of isoprene from mevalonate utilizing a rat liver cytosolic fraction, *Biochem. Biophys. Res. Commun.* 123 (1984) 691-696.
- [166] J. King, P. Mochalski, K. Unterkofler, G. Teschl, M. Klieber, M. Stein, A. Amann, M. Baumann, Breath isoprene: Muscle dystrophy patients support the concept of a pool of isoprene in the periphery of the human body, *Biochemical and Biophysical Research Communications* 423 (2012) 526-530.
- [167] R. Salerno-Kennedy, K.D. Cashman, Potential applications of breath isoprene as a biomarker in modern medicine: a concise overview, *Wien. Klin. Wochenschr.* 117 (2005) 180-186.

- [168] J. King, A. Kupferthaler, K. Unterkofler, H. Koc, S. Teschl, G. Teschl, W. Miekisch, J. Schubert, H. Hinterhuber, A. Amann, Isoprene and acetone concentration profiles during exercise on an ergometer, *Journal of Breath Research* 3 (2009).
- [169] T. Karl, P. Prazeller, D. Mayr, A. Jordan, J. Rieder, R. Fall, W. Lindinger, Human breath isoprene and its relation to blood cholesterol levels: new measurements and modeling, *Journal of Applied Physiology* 91 (2001) 762-770.
- [170] T. Karl, P. Prazeller, D. Mayr, A. Jordan, J. Rieder, R. Fall, W. Lindinger, Human breath isoprene and its relation to blood cholesterol levels: new measurements and modeling, *Journal of applied physiology* (Bethesda, Md. : 1985) 91 (2001) 762-770.
- [171] G. Siciliano, M. Mancuso, D. Tedeschi, M.L. Manca, M.R. Renna, V. Lombardi, A. Rocchi, F. Martelli, L. Murri, Coenzyme Q10, exercise lactate and CTG trinucleotide expansion in myotonic dystrophy, *Brain research bulletin* 56 (2001) 405-410.
- [172] S. David, Š. Patrik, A.F. Anthony, H. Fahmy, A.A.F. Gordon, Can volatile compounds in exhaled breath be used to monitor control in diabetes mellitus?, *Journal of Breath Research* 5 (2011) 022001.
- [173] W. Lindinger, J. Taucher, A. Jordan, A. Hansel, W. Vogel, Endogenous production of methanol after the consumption of fruit, *Alcoholism-Clinical and Experimental Research* 21 (1997) 939-943.
- [174] C. Turner, P. Spanel, D. Smith, *A longitudinal study of methanol in the exhaled breath of 30 healthy volunteers using selected ion flow tube mass spectrometry, SIFT-MS*, *Physiological Measurement* 27 (2006) 637-648.
- [175] J. Sun, D-limonene: Safety and clinical applications, 2007.
- [176] J.M. Thompson, D.B. Perry, A new system of refillable and uniquely identifiable diffusion tubes for dynamically generating VOC and SVOC standard atmospheres at ppm and ppb concentrations for calibration of field and laboratory measurements, *Journal of environmental monitoring : JEM* 11 (2009) 1543-1544.
- [177] Minitab, Minitab Ltd, United Kingdom, 2017.
- [178] Survey of methanol (Cas no. 67-56-1), Denmark, 2013, pp. 64.
- [179] A. Amann, S. Telsler, L. Hofer, A. Schmid, H. Hinterhuber, Exhaled breath gas as a biochemical probe during sleep, 2005.
- [180] A.R. Dahl, L.S. Birnbaum, J.A. Bond, P.G. Gervasi, R.F. Henderson, The fate of isoprene inhaled by rats: comparison to butadiene, *Toxicology and applied pharmacology* 89 (1987) 237-248.

- [181] P. Spanel, K. Dryahina, A. Rejskova, T.W.E. Chippendale, D. Smith, Breath acetone concentration; biological variability and the influence of diet, *Physiological Measurement* 32 (2011) N23-N31.
- [182] R. Veronika, K. Miklós Péter, Breath acetone as a potential marker in clinical practice, *Journal of Breath Research* 11 (2017) 024002.

APPENDIX 1- GC-MS measurements of various shisha pastes

Supplementary Table 1. GC-MS measurements of various shisha pastes

Compound	CAS	MW	Retention Time	Strawberry	Mint (new)	Double Apple	Mint (old)	Vanilla
Methanol	67-56-1	32	6.7	x	x	x	x	x
Acetaldehyde	75-07-0	44	7.6	x	x	x	x	x
Ethanol	64-17-5	46	11.42	H				HH
Oxirane, methyl-, (S)-	16088-62-3	58	13.23	x		x		x
2-Propenal	107-02-8	56	13.65	x	x	x	x	x
Propanal	67-64-1	58	14.21	x	x	x	x	H
Acetone	67-64-1	58	14.5	x	x		x	
Ethyl formate	109-94-4	74	15.92	x				
Isoprene	78-79-5	68	17.29			x		
1,3-Pentadiene, (E)-	2004-70-8	68	18.34	x		x		
1,3-Pentadiene, (Z)-	1574-41-0	68	18.45	x		x		
Furan, 2-methyl-	534-22-5	82	20.29	x	x	x	x	x
2,3-Butanedione	431-03-8	86	20.6	H			x	HH
Ethyl Acetate	141-78-6	88	21.44	x				x
Acetic acid	64-19-7	60	22.74	H	HH	HH	H	HH
2-Propanone, 1-hydroxy-	116-09-6	74	22.98	H	x	x		x
3-Hexene, (Z)-	03/09/7642	84	23.02	x				
Benzene	71-43-2	78	23.44	x				
2,4-Hexadiene	592-46-1	82	23.75	x				
2,3-Pentanedione	600-14-6	100	26.11	x				
Propylene Glycol	57-55-6	76	26.33	HH		HH		HH
Propylene Glycol	57-55-6	76	27		H			
Propanoic acid	79-09-4	74	28			x		
Toluene	108-88-3	92	28.95	x	x	x	x	
3(2H)-Furanone, dihydro-2-methyl-	3188-00-9	100	29.41		x		x	
Furfural	98-01-1	96	29.69	x	x	x	x	x
Butanoic acid	107-92-6	88	30.8	HH				
Hexanal	66-25-1	100	30.96			x	x	
2-Furanmethanol	98-00-0	98	31.24			x		

Appendices

Butyrolactone	96-48-0	86	32.08		x	x	x	x
3-Octene, (E)-	14919-01-8	112	32.35				x	
3-Hexen-1-ol, (Z)-	928-96-1	100	32.94	HH	x	x	H	
1-Hexanol	111-27-3	102	33.43			HH	x	
1,2-Propanediol, 2-acetate	03/01/6214	118	33.94	x		x		x
Butanoic acid, 2-propenyl ester	2051-78-7	128	34.46	x				
Furan, 2,5-diethyltetrahydro-	41239-48-9	128	35.66				x	
Benzaldehyde	100-52-7	106	35.94	HH	x	HH	x	x
Cyclohexanone, 3-methyl-	591-24-2	112	36.75		x		x	
Phenol	108-95-2	94	37			x		
alpha-Pinene??		136	37.2		x			
Butanoic acid, 2-methyl-, methyl ester	868-57-5	116	37.6			x		
1,2-Cyclopentanedione, 3-methyl-	765-70-8	112	38					x
1,3-Dioxolane, 2,2,4-trimethyl-	1193-11-9	116	38.37	x				HH
Benzene, 1-methoxy-4-methyl-	104-93-8	122	38.44			x		
Benzyl Alcohol	100-51-6	108	38.53			HH		
3-Octanone	106-68-3	128	38.59				x	
beta-pinene	127-91-3	136	38.63		x			
Benzyl Alcohol	100-51-6	108	38.88	HH				
Acetic acid, hexyl ester	142-92-7	144	39.27			x		
3-Octanol??	589-98-0	130	39.45				x	
Cyclohexene, 4-methyl-1-(1-methylethyl)-	500-00-5	138	39.48		x			
o-Cymene	527-84-4	134	40.14	x	x	x	x	x
Limonene	138-86-3	136	40.34		H	x	H	
Pentanoic acid, 4-oxo-, ethyl ester	539-88-8	144	40.33	H				
Pyrazine, tetramethyl-	1124-11-4	136	40.62					x
Propanoic acid, 2-methyl-, methyl ester	547-63-7	102	41	HH	x			
n-Hexyl propionate	2445-76-3	158	42.98			x		

Appendices

p-Methoxystyrene	637-69-4	134	43.43			x		
Benzyl acetate	140-11-4	150	44.07	x		x		
Menthofuran	494-90-6	150	44.65		x		x	
1,6-Octadien-3-ol, 3,7-dimethyl-	78-70-6	154	44.78	x		x		
Estragole	140-67-0	148	46.55			x		
2-Cyclohexen-1-one, 5-methyl-2-(1-methylethyl)-	5113-66-6	152	46.8		x			
Menthone	10458-14-7	154	47.25		HH		HH	x
Benzaldehyde, 4-methoxy-	123-11-5	136	47.89			x		
DL-Menthol	15356-70-4	156	49		HH	x	HH	x
Benzene, 1-methoxy-4-(1-propenyl)-	104-46-1	148	48.62				x	
2(3H)-Furanone, 5-butyldihydro-	104-50-7	142	50	x				
Anisole, p-propenyl-	104-46-1	148	50.2			HH		
Piperonal	120-57-0	150	52.48					x
2-Cyclohexen-1-one, 3-methyl-6-(1-methylethyl)-	89-81-6	152	52.8		x		x	
γ -Decanolactone	706-14-9	170	56.28				x	
1,3-Dioxolane-2-propanoic acid, 2,4-dimethyl-, ethyl ester	5413-49-0	202	58.17	x	x			

APPENDIX 2 - Chapter 6

Ion Molecule Density Functional Calculation for isoflurane and enflurane (PTR-MS)

6.3.2.1 Isoflurane reaction with H_3O^+

There are three sites for protonation on the ISOFL molecule. These are shown below with the sites being labelled in decreasing proton affinity – see Table 1.

It is important to note that no protonated Isoflurane is observed as is to be expected from the calculated PA's (proton affinities) and GBs. But if sufficient energy (probably from the field) is introduced into the system, the traces of protonated Isoflurane, which must be formed, will fragment. Rather than consider the formation of the fragment ions in isolation, the possible fragmentations occurring from each of the three protonation sites will be explored.



Figure 1 Shows the possible protonated sites

Table 1 Possible protonation of isoflurane.

Site	PA kJ mol ⁻¹	GB kJ mol ⁻¹
1	670	655
2	637	608
3	573	552

Table 2 The energetics for the proton transfers.

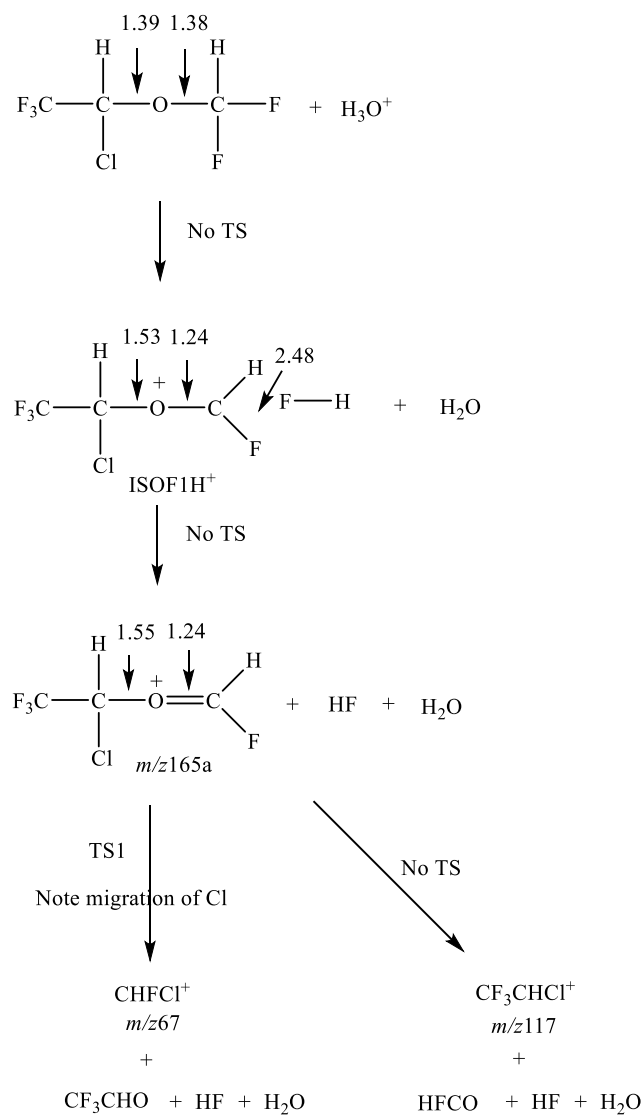
Reaction	Product	ΔH kJ mol ⁻¹	ΔG kJ mol ⁻¹
ISOF + H ₃ O ⁺	ISOF1H ⁺ + H ₂ O	+15	-2
	ISOF2H ⁺ + H ₂ O	+47	+45
	ISOF3H ⁺ + H ₂ O	+112	+101

a) ISOF1H⁺

Scheme 1 shows the formation and fragmentation of ISOF1H⁺. It can be seen that following proton transfer a major change in bond lengths (given in Å) has occurred and the formation of *m/z* 165a is well underway and proceeds to completion without going through a Transition State (TS). The suffix in *m/z* 165a should be noted as the ion with *m/z* 165b formed via ISOF3H⁺ has a different structure. Further fragmentation to *m/z* 117 is also a barrierless process i.e. no TS. A pathway for an alternative fragmentation via a Transition State (TS1) has been found and leads to the ion with *m/z* 67. The energetics for these processes is given in Table 3.

Table 3 Shows the formation and fragmentations of ISOF1H⁺. All energies are relative to ISOF + H₃O⁺.

Products	ΔH kJ mol ⁻¹	ΔG kJ mol ⁻¹
ISOF1H ⁺ + H ₂ O	+15	-2
<i>m/z</i> 165a + HF + H ₂ O	+54	+8
<i>m/z</i> 117 + HFCO + HF + H ₂ O	+167	+68
TS1 + HF + H ₂ O	+182	+143
<i>m/z</i> 67 + CF ₃ CHO + HF + H ₂ O	+174	+77



Scheme 1 Formation and fragmentations of ISOF1H⁺.

c) ISOF3H⁺

Scheme 3 shows the formation and fragmentation of ISOF3H⁺. Loss of HF following protonation occurs without TS which is perhaps surprising as there is a concomitant migration of the Cl to the carbon from which HF is lost. Concurrently, there is a shortening of the CO bond as it approaches the carbonyl bond (1.20 Å) of the resultant aldehyde.

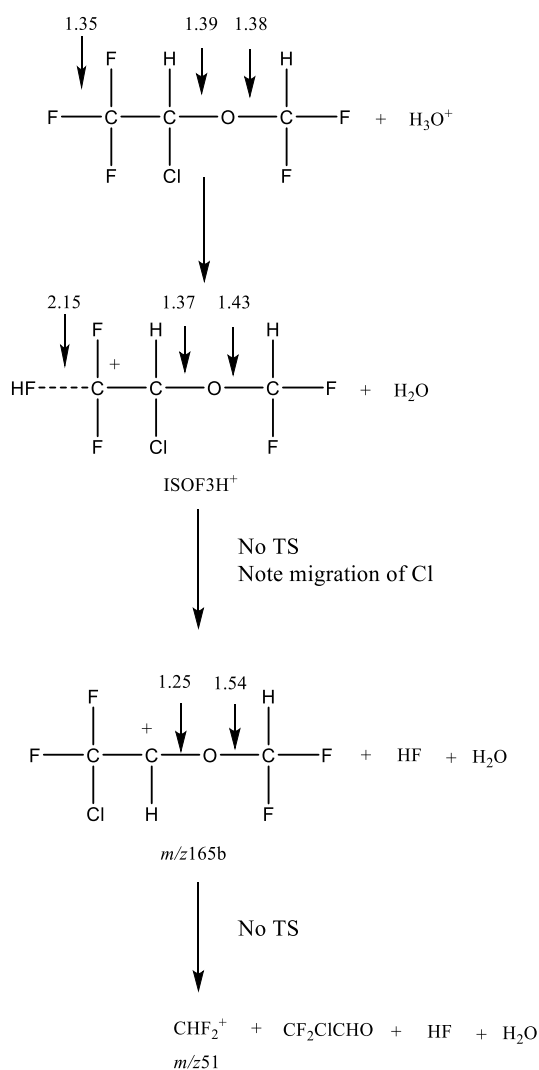
Scheme 3 Formation and fragmentations of ISOF3H⁺.

Table 5 Formation and fragmentations of all energies which are relative of ISOF3H⁺.

Products	ΔH kJ mol ⁻¹	ΔG kJ mol ⁻¹
ISOF3H ⁺ + H ₂ O	+112	+101
<i>m/z</i> 165b + HF + H ₂ O	+82	+36
<i>m/z</i> 51 + CF ₂ ClCHO + HF + H ₂ O	+238	+140

d) *m/z*163 C₃F₄OCl⁺

Before a mechanism for the formation of this fragment ion it is necessary to explore its possible structures. There are two likely candidates as shown in Figure 2. The cyclic structure is the more stable with ΔH (cyclic – linear) -34 kJ mol⁻¹ and ΔG (cyclic – linear) -37 kJ mol⁻¹. The overall reaction thermodynamics assuming the neutral products are H₂ and HF are given in Table 6. The most likely mechanism of formation is a concerted loss of HF and H₂ from ISOF3H⁺ as a sequential loss would not yield either of the two proposed structures.

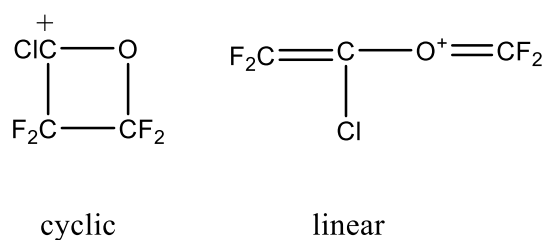
Figure 2 Two possible structures for the ion C₃F₄OCl

Table 6 All energies are relative to ISOF + H₃O⁺.

Products	ΔH kJ mol ⁻¹	ΔG kJ mol ⁻¹
<i>m/z</i> 163(cyclic) + H ₂ + HF + H ₂ O	+221	+146
<i>m/z</i> 163(linear) + H ₂ + HF + H ₂ O	+266	+183

Whilst these calculations (DFT B3LYP 6-31+G9d,p) have given some insight into the feasibility, both mechanistically and thermodynamically, of the various fragmentations, they have failed to throw much light on the branching ratios. This is probably because the majority of the fragmentations occur via barrierless processes i.e. no transition states, that proceed via multiple conformations the probability distribution being unknown. Also, it should be noted that even at the lowest values of E/N the ions must have considerable excess energy as formation two of the three dominant ions require additional energies of at least ca. 150 kJ mol⁻¹. More thought required here – particularly the excess energy.

Table 7 Summary of thermodynamics for the various fragmentations.

Ions	Dominance	ΔH kJ mol ⁻¹	ΔG kJ mol ⁻¹	Notes
<i>m/z</i> 165a	Major	+54	+8	formed via ISOF1H ⁺
<i>m/z</i> 165b		+82	+36	formed via ISOF3H ⁺
<i>m/z</i> 163	Major	+221	+146	formed via ISOF3H ⁺
<i>m/z</i> 117	Minor	+167	+68	formed via ISOF1H ⁺
<i>m/z</i> 67	Major	+174	+77	formed via ISOF1H ⁺ and TS1
TS1		+182	+143	
<i>m/z</i> 51	Minor	+172	+121	formed via ISOF2H ⁺
		+238	+140	Formed via ISOF3H ⁺

6.3.4.2.1 Enflurane reaction with H_3O^+

There are four sites for protonation on the ENF molecule. These are shown in the table 1 below. It is important to note that no protonated ENF is observed as is to be expected from the calculated PAs and GBs. But if sufficient energy (probably from the field) is introduced into the system, the traces of protonated ENFF, which must be formed, will fragment. Rather than consider the formation of the fragment ions in isolation, the possible fragmentations occurring from each of the four protonation sites will be explored.



Figure 1 Protonation site of enflurane.

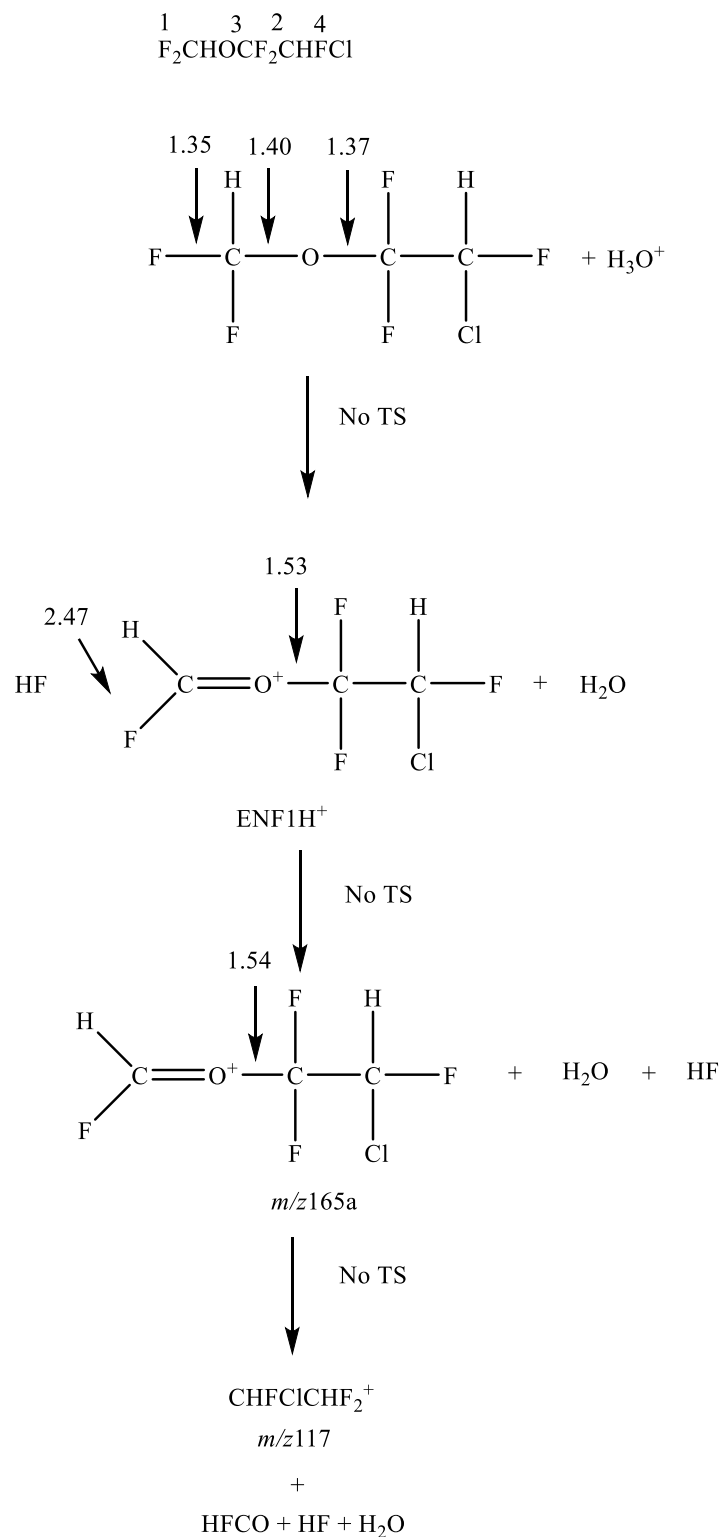
Table 1 Shows the details of protonation sites of enflurane.

Site	PA kJ mol ⁻¹	GB kJ mol ⁻¹
1	657	638
2	662	646
3	625	596
4	594	574

Table 2 The energetics for the proton transfers of enflurane.

Reaction	Product	ΔH kJ mol ⁻¹	ΔG kJ mol ⁻¹
ENF + H ₃ O ⁺	ENF1H ⁺ + H ₂ O	+27	+15
	ENF2H ⁺ + H ₂ O	+23	+7
	ENF3H ⁺ + H ₂ O	+59	+58
	ENF4H ⁺ + H ₂ O	+90	+80

a) ENF1H⁺



Scheme 1 Shows the formation and fragmentation of ENF1H⁺

Table 3 Formation and fragmentation of ENF1H⁺ and all energies are relative to ENF + H₃O⁺.

Products	ΔH kJ mol ⁻¹	ΔG kJ mol ⁻¹
ENF1H ⁺ + H ₂ O	+27	+15
<i>m/z</i> 165a + HF + H ₂ O	+69	+28
<i>m/z</i> 117 + HFCO + HF + H ₂ O	+158	+63

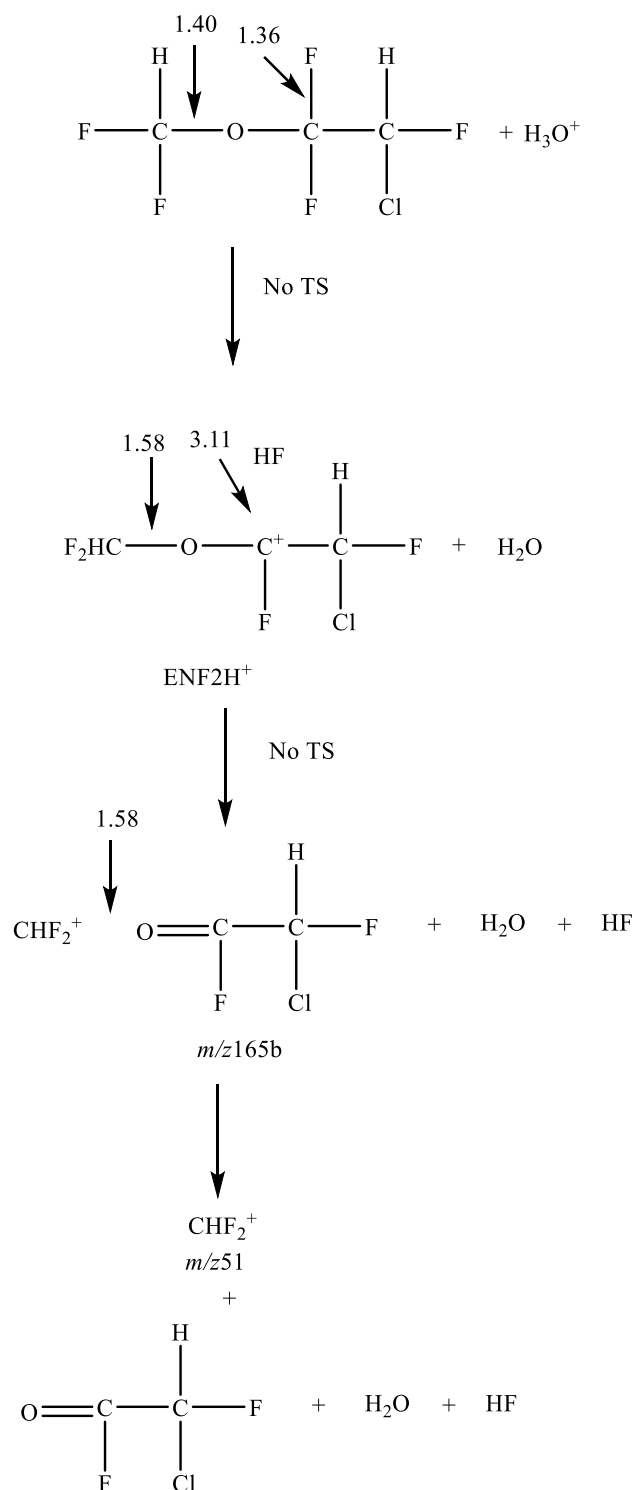
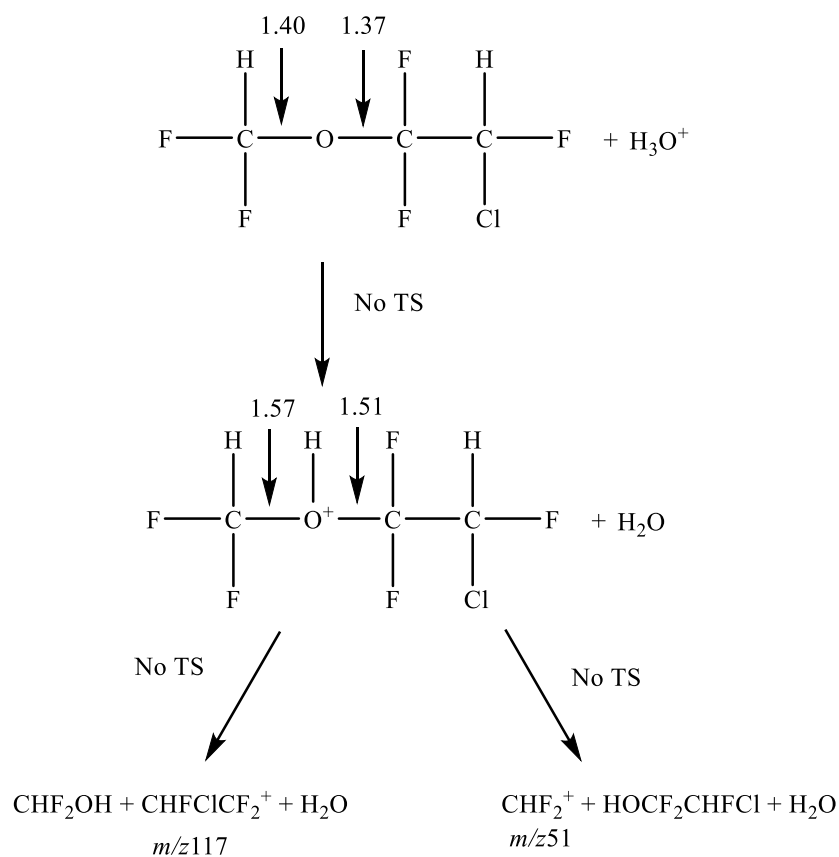
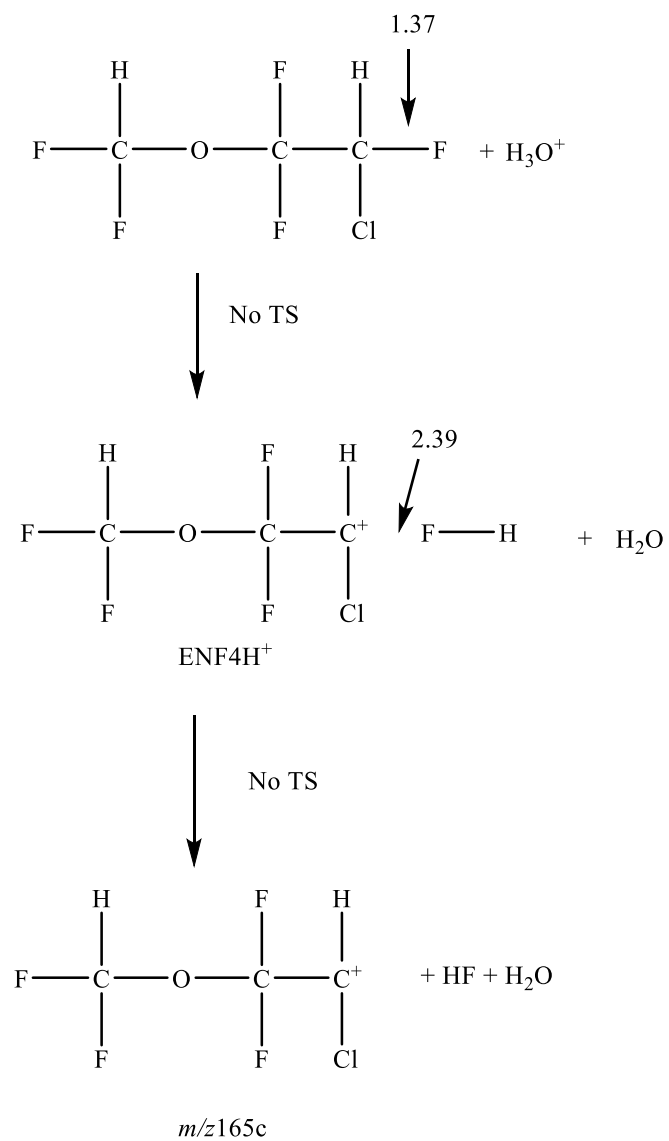
b) ENF2H⁺Scheme 2 Show the formation and fragmentation of ENF2H⁺.

Table 4 Formation and fragmentation of ENF2H⁺ and all energies are relative to ENF + H₃O⁺.

Products	ΔH kJ mol ⁻¹	ΔG kJ mol ⁻¹
ENF2H ⁺ + H ₂ O	+23	+7
<i>m/z</i> 165b + HF + H ₂ O	+60	+14
<i>m/z</i> 51 + CHFClCFO ⁺ + HF + H ₂ O	+184	+89

c) ENF3H⁺Scheme 3 Show the formation and fragmentation of ENF3H⁺.Table 5 Formation and fragmentation of ENF3H⁺ and all energies are relative to ENF+H₃O⁺.

Products	$\Delta\text{H kJ mol}^{-1}$	$\Delta\text{G kJ mol}^{-1}$
ENF3H ⁺ + H ₂ O	+59	+58
<i>m/z</i> 51 +HOCF ₂ CHFCI + H ₂ O	+169	+120
<i>m/z</i> 117 + CHF ₂ OH + H ₂ O	+158	+63



Scheme 4 Show the formation and fragmentation of ENF3H⁺

Table 6 Shows the formation and fragmentation of ENF4H⁺ and all energies are relative to ENF + H₃O⁺.

Products	ΔH kJ mol ⁻¹	ΔG kJ mol ⁻¹
ENF4H ⁺ + H ₂ O	+90	+80
<i>m/z</i> 165c + HF + H ₂ O	+169	+120

APPENDIX 3 – Chapter 7 (Peppermint Washout Characteristics studies)

Ethical Review

<p style="text-align: center;">UNIVERSITY OF BIRMINGHAM</p> <p style="text-align: center;">APPLICATION FOR ETHICAL REVIEW</p>

Who should use this form:

This form is to be completed by PIs or supervisors (for PGR student research) who have completed the University of Birmingham's Ethical Review of Research Self Assessment Form (SAF) and have decided that further ethical review and approval is required before the commencement of a given Research Project.

Please be aware that all new research projects undertaken by postgraduate research (PGR) students first registered as from 1st September 2008 will be subject to the University's Ethical Review Process. PGR students first registered before 1st September 2008 should refer to their Department/School/College for further advice.

Researchers in the following categories are to use this form:

1. The project is to be conducted by:
 - staff of the University of Birmingham; or
 - postgraduate research (PGR) students enrolled at the University of Birmingham (to be completed by the student's supervisor);
2. The project is to be conducted at the University of Birmingham by visiting researchers.

Students undertaking undergraduate projects and taught postgraduate (PGT) students should refer to their Department/School for advice.

NOTES:

- An electronic version of the completed form should be submitted to the Research Ethics Officer, at the following email address: aer-ethics@contacts.bham.ac.uk. Please **do not** submit paper copies.
- If, in any section, you find that you have insufficient space, or you wish to supply additional material not specifically requested by the form, please it in a separate file, clearly marked and attached to the submission email.
- If you have any queries about the form, please address them to the [Research Ethics Team](#).

Before submitting, please tick this box to confirm that you have consulted and understood the following information and guidance and that you have taken it into account when completing your application:

- **The information and guidance provided on the University's ethics webpages**
- **(<https://intranet.birmingham.ac.uk/finance/accounting/Research-Support-Group/Research-Ethics/Ethical-Review-of-Research.aspx>)**
- **The University's Code of Practice for Research (http://www.as.bham.ac.uk/legislation/docs/COP_Research.pdf)**

UNIVERSITY OF BIRMINGHAM APPLICATION FOR ETHICAL REVIEW	<i>OFFICE USE ONLY:</i> Application No: Date Received:
--	--

1. TITLE OF PROJECT

Breath Profiles and Washout Characteristics for Peppermint Oil
--

1. THIS PROJECT IS:

- University of Birmingham Staff Research project
- University of Birmingham Postgraduate Research (PGR) Student project X
- Other (Please specify):

2. INVESTIGATORS

a) PLEASE GIVE DETAILS OF THE PRINCIPAL INVESTIGATORS OR SUPERVISORS (FOR PGR STUDENT PROJECTS)

b) PLEASE GIVE DETAILS OF ANY CO-INVESTIGATORS OR CO-SUPERVISORS (FOR PGR STUDENT PROJECTS)

c) In the case of PGR student projects, please give details of the student

Principal			
	C A Mayhew		

**1. ESTIMATED
START OF PROJECT**

ESTIMATED END OF PROJECT

2. FUNDING

List the funding sources (including internal sources) and give the status of each source.

3.1 Funding Body	3.1.1 Approved/Pending /To be submitted
EU	Approved

If you are requesting a quick turnaround on your application, please explain the reasons below (including funding-related deadlines). You should be aware that whilst effort will be made in cases of genuine urgency, it will not always be possible for the Ethics Committees to meet such requests.

The student has only a limited time to complete her PhD. This proposed study will provide her with sufficient original data to satisfactorily complete her studies.

3. SUMMARY OF PROJECT

Describe the purpose, background rationale for the proposed project, as well as the hypotheses/research questions to be examined and expected outcomes. This description should be in everyday language that is free from jargon. Please explain any technical terms or discipline-specific phrases.

This study is in part based on a larger one proposed by was proposed by Prof Paul Thomas (Loughborough University, UK), during the 2016 International Association of Breath Research (IABR) Standardisation Focus Group Meeting at Zurich, with the ultimate aim of standardising breath analysis across Europe. However, another objective for us is to obtain data for metabolism of key volatiles contained in peppermint oil in order to get data through non-invasive breath sampling of liver function for healthy volunteers.

This study entails the comparison of breath volatile organic compounds (VOC) data between different groups acquired by different analytical platforms after a standardised intervention of ingesting peppermint oil sweet. Preliminary studies have been performed previously by the group at Loughborough University. Peppermint oil capsules will be provided to the volunteers willing to participate within this study. Subjects will swallow the peppermint oil capsule. Breath samples will then be taken to monitor the subsequent release of menthone/menthol and other volatiles over time recorded.

The aims of this particular study are

- (i) To aid in the benchmarking endeavour to estimate the range of results between participating laboratories
- (ii) To provide breath data for healthy volunteers which would then be followed-up in a separate study with patients who are suffering from liver disease (a separate ethics approval will be made for that).

Why are we interested in taking breath samples and how are we approaching this?

Exhaled breath analysis of volatile chemicals offers the potential to develop more effective biomarkers or diagnosing disease non-invasively. This study is original and important as it aims to standardise breath analysis across Europe and to obtain details on healthy liver function. There are no previous published research papers evaluating the benchmarking of breath analysis. We consider that washout characteristics following breath profiles may be

able to provide sensitive information with regards to liver or kidney functions in a non-invasive way.

4. CONDUCT OF PROJECT

Please give a description of the research methodology that will be used

We will be collecting breath samples after a volunteer has ingested a peppermint capsule (these are health supplements available over the counter at Boots, Holland and Barret etc. see <http://www.boots.com/boots-peppermint-oil-200mg-60-capsules-10115320>). The instruments used to analyse the breath will be a Proton Transfer React Mass Spectrometer. Proton-Transfer Reaction Mass Spectrometry (PTR-MS): this platform allows the direct and real-time detection of volatile organic compounds (VOCs) that are present in the exhaled human breath. It requires no sample preparation or handling and offers on-line and off-line measurements. For real-time measurements the volunteer will be provided with a mouthpiece connected to a one-way non re-breathing valve. For off-line measurements, a CO2 sensor will be used to collect alveolar air.

All participants will be provided with a volunteer information sheet upon recruitment and Informed consent procedures will be followed. Participants will be provided with the needed breath sampling and asked to breathe normally for up to 5 minutes before commencing the study.

Participants will be asked to take a peppermint oil 200 mg supplement tablet and provide breath samples using the different instruments (nsampling point = 7, nbreath samples= 7 per platform, time for washout sampling = -30, 30, 60, 90, 120, and 150 up to 5 hours)

Also, participants will be asked to answer a designed questionnaire to determine the factors that could affect the quality of breath VOCs samples at the end of sampling duration.

5. DOES THE PROJECT INVOLVE PARTICIPATION OF PEOPLE OTHER THAN THE RESEARCHERS AND SUPERVISORS?

Yes No

Note: 'Participation' includes both active participation (such as when participants take part in an interview) and cases where participants take part in the study without their knowledge and consent at the time (for example, in crowd behaviour research).

If you have answered NO please go to Section 18. If you have answered YES to

this question please complete all the following sections.

6. PARTICIPANTS AS THE SUBJECTS OF THE RESEARCH

Describe the number of participants and important characteristics (such as age, gender, location, affiliation, level of fitness, intellectual ability etc.). Specify any inclusion/exclusion criteria to be used.

<p>Up to 50 participants will be recruited (this number has been selected to provide a good statistical number for analysis). Criteria:</p> <p>Healthy adults (18-80 years old), with no history of chronic or recent acute illnesses.</p> <p>People who associate with any of the following categories will not take part in the study</p> <ul style="list-style-type: none">People with serious allergiesPeople who smoke or vapePregnant womenPeople who use anti-inflammatory drugs regularlyPeople with metabolic diseaseVegetarians/people who do not eat beef products (gelatine is present in the capsule shell) <p>Initial meeting to take a peppermint oil capsule; a total of 360 minutes of sampling.</p>

7. RECRUITMENT

Please state clearly how the participants will be identified, approached and recruited. Include any relationship between the investigator(s) and participant(s) (e.g. instructor-student).

Note: Attach a copy of any poster(s), advertisement(s) or letter(s) to be used for recruitment.

Campaign, e-mails and social media to the staff, students, and their social networks, of the University of Birmingham.

Interested participants will be given a participant information sheet and a consent form.

8. CONSENT

a) Describe the process that the investigator(s) will be using to obtain valid consent. If consent is not to be obtained explain why. If the participants are minors or for other reasons are not competent to consent, describe the proposed alternate source of consent, including any permission / information letter to be provided to the person(s) providing the consent.

See attached sheets.

Note: Attach a copy of the Participant Information Sheet (if applicable), the Consent Form (if applicable), the content of any telephone script (if applicable) and any other material that will be used in the consent process.

b) Will the participants be deceived in any way about the purpose of the study?

Yes No

If yes, please describe the nature and extent of the deception involved. Include how and when the deception will be revealed, and who will administer this feedback.

9. PARTICIPANT FEEDBACK

Explain what feedback/ information will be provided to the participants after participation in the research. (For example, a more complete description of the purpose of the research, or access to the results of the research).

No feedback is planned. However, participants will be given the opportunity to request a copy of any paper that results from the study.

10. PARTICIPANT WITHDRAWAL

- a) Describe how the participants will be informed of their right to withdraw from the project.

Participants will be informed verbally and by written information that they are free to withdraw from the study at any point, without reason, and can request that their data is destroyed. They will be able to withdraw up until the completion of the study. The final deadline for the completion of the study will be the 30th September 2018. After this time the participants will not be able to withdrawal from the project.

- b) Explain any consequences for the participant of withdrawing from the

study and indicate what will be done with the participant's data if they withdraw.

None. Participant's data can be destroyed if requested before the deadline above.

11. COMPENSATION

Will participants receive compensation for participation?

i) Financial

Yes No **X**

ii) Non-financial

Yes No **X**

If **Yes** to **either** i) or ii) above, please provide details.

If participants choose to withdraw, how will you deal with compensation?

12. CONFIDENTIALITY

a) Will all participants be anonymous?

Yes

No

b) Will all data be treated as confidential?

Yes **No**

Note: Participants' identity/data will be confidential if an assigned ID code or number is used, but it will not be anonymous. Anonymous data cannot be traced back to an individual participant.

Describe the procedures to be used to ensure anonymity of participants and/or confidentiality of data both during the conduct of the research and in the release of its findings.

<p>It is important to note that your information will be anonymised and none of the researchers will be able to trace the information back to you or anyone. The index of the participants and their identifier codes is kept under lock and key by the principle investigator, who does not work directly with individual records.</p>

If participant anonymity or confidentiality is not appropriate to this research project, explain, providing details of how all participants will be advised of the fact that data will not be anonymous or confidential.

13. STORAGE, ACCESS AND DISPOSAL OF DATA

Describe what research data will be stored, where, for what period of time, the measures that will be put in place to ensure security of the data, who will have access to the data, and the method and timing of disposal of the data.

The index of the participants and their identifier codes is kept under lock and key by the principle investigator, who does not work directly with individual records.

14. OTHER APPROVALS REQUIRED?

e.g. Criminal Records Bureau (CRB) checks or NHS R&D approvals.

YES NO X NOT APPLICABLE

If yes, please specify.

15. SIGNIFICANCE/BENEFITS

Outline the potential significance and/or benefits of the research

Two key benefits:

1. Detailed washout characteristics of chemicals in the body will lead to a database for use at a later stage for comparison with patients suffering from liver disease. This could lead to a non-invasive method for determining liver function and severity of liver disease.
2. We are seeking to standardise breath analysis and measurement to accelerate the development of new and more sensitive tests for serious diseases. Many different breath methods have been developed to sample and analyse breath. At the moment little is known about the differences between them. This study will contribute towards a larger study aimed at a standardised breath experiment that will enable benchmark data to be collected by different researchers using their own methods. The data that will be produced will allow researchers to evaluate and compare their methods in an evidential manner for the first time.
This is important because the speed at which research in breath diagnostics is progressing is hindered because it is difficult for researchers to compare and share data. This study is intended to improve this situation.

16. RISKS

a) Outline any potential risks to **INDIVIDUALS**, including research staff, research participants, other individuals not involved in the research and the measures that will be taken to minimise any risks and the procedures to be adopted in the event of mishap

This study poses little to no risk of discomfort to the volunteers. Peppermint oil capsules can be purchased over the counter and are used as health supplements. If the volunteer does not like the taste of the capsule, the volunteer can stop immediately.

Breath samples are acquired using different types of mouthpieces or masks, and the volunteer may find these unfamiliar and uncomfortable to being with. If this is the case the participant can stop immediately.

There are no risks to the research staff.

- b) Outline any potential risks to **THE ENVIRONMENT and/or SOCIETY** and the measures that will be taken to minimise any risks and the procedures to be adopted in the event of mishap.

None

16. ARE THERE ANY OTHER ETHICAL ISSUES RAISED BY THE RESEARCH?

Yes No

If yes, please specify

17. EXPERT REVIEWER/OPINION

You may be asked to nominate an expert reviewer for certain types of project, including those of an interventional nature or those involving significant risks. If you anticipate that this may apply to your work and you would like to nominate an expert reviewer at this stage, please provide details below.

3.2 Name
3.3 Contact details (including email address)
Brief explanation of reasons for nominating and/or nominee's suitability

18. CHECKLIST

Please mark if the study involves any of the following:

- Vulnerable groups, such as children and young people aged under 18 years, those with learning disability, or cognitive impairments
- Research that induces or results in or causes anxiety, stress, pain or physical discomfort, or poses a risk of harm to participants (which is more than is expected from everyday life)
- Risk to the personal safety of the researcher
- Deception or research that is conducted without full and informed consent of the participants at time study is carried out
- Administration of a chemical agent or vaccines or other substances (including vitamins or food substances) to human participants. X
- Production and/or use of genetically modified plants or microbes
- Results that may have an adverse impact on the environment or food safety
- Results that may be used to develop chemical or biological weapons

Please check that the following documents are attached to your application.

	ATTACHED	NOT APPLICABLE
Recruitment advertisement	X	<input type="checkbox"/>
Participant information sheet	X	<input type="checkbox"/>
Consent form	X	<input type="checkbox"/>
Questionnaire	<input type="checkbox"/>	X
Interview Schedule	<input type="checkbox"/>	X

19. DECLARATION BY APPLICANTS

I submit this application on the basis that the information it contains is confidential and will be used by the

University of Birmingham for the purposes of ethical review and monitoring of the research project described

herein, and to satisfy reporting requirements to regulatory bodies. The information will not be used for any

other purpose without my prior consent.

I declare that:

- The information in this form together with any accompanying information is complete and correct to the best of my knowledge and belief and I take full responsibility for it.
- I undertake to abide by University Code of Practice for Research (http://www.as.bham.ac.uk/legislation/docs/COP_Research.pdf) alongside any other relevant professional bodies' codes of conduct and/or ethical guidelines.
- I will report any changes affecting the ethical aspects of the project to the University of Birmingham Research Ethics Officer.
- I will report any adverse or unforeseen events which occur to the relevant Ethics Committee via the University of Birmingham Research Ethics Officer.

03/09/2017

Please now save your completed form, print a copy for your records, and then email a copy to the Research Ethics Officer, at aerethics@contacts.bham.ac.uk. As noted above, please do not submit a paper copy.

PARTICIPANT INFORMATION SHEET
BREATH PROFILES AND WASHOUT CHARACTERISTICS FOR
PEPPERMINT OIL

4 Investigators:

Professor Dr. Chris Mayhew

Ms. Prema Devi Chellayah

University of Birmingham

5 What is the purpose of the study?

Primary aim:

To benchmark and standardise breath analysis across Europe.

Secondary aims:

- To compare breath volatile organic compounds (VOC) data between different groups.
- To evaluate breath volatile organic compounds (VOC) data from different analytical platforms.
- To perform multivariate statistical analysis on the collected data from all partners.
- To estimate the range of results between participating laboratories.
- To provide a database for washout characteristics of volatiles in peppermint oil from healthy volunteers, which will later be used to compare with washout characteristics from patients suffering from liver disease (not this study)

6 What are we doing, and why is this study important?

This study has been proposed by Prof. Paul Thomas (Loughborough University, UK) and developed by an international team of researchers who met during the 2016 International Association of Breath Research (IABR) Standardisation Focus Group meeting at Zurich.

They are seeking to standardise breath analysis and measurement to accelerate the development of new and more sensitive tests for serious diseases.

- Many different breath methods have been developed to sample and analyse breath.
- At the moment little is known about the differences between them.
- This study will provide a standardised breath experiment that will enable benchmark data to be collected by different researchers using their own methods.

- The data that will be produced will allow researchers to evaluate and compare their methods in an evidential manner for the first time.
- This is important because the speed at which research in breath diagnostics is progressing is hindered because it is difficult for researchers to compare and share data.
- This study is intended to improve this situation.

6.1 Description of the standardised breath experiment: Peppermint

The peppermint breath experiment is designed to produce a temporary and well-defined change in the breath profile of a participant that will reduce over time. The change is defined by the participant swallowing a peppermint oil 200 mg food supplement¹ capsule and drinking 150 ml of water afterwards. The capsule dissolves and releases peppermint oil into the stomach of the participant. The volatile (aroma) compounds in the oil (e.g. menthone/menthol) enter the bloodstream of the participant and are subsequently detectable in their breath. As the participant metabolises and eliminates these compounds their concentrations in breath reduce over several hours. Although the peppermint oil washout profiles vary between participants, the way the levels of the volatiles in breath change over time is similar and statistical analysis of the washout profiles provides useful information about the reproducibility (precision) and sensitivity (limit of detection) of the analysis.

All participants will be provided with a patient information sheet upon recruitment and Informed Consent procedures will be followed. Also, participants will be asked to answer a designed questionnaire to determine all the factors that could affect the quality of breath volatile samples.

Who is doing this research and why?

¹ Peppermint oil is claimed by the manufacturers and suppliers to support a healthy digestive system and aid the normal functioning of the digestive tract.

This study is original and important as it aims to standardise breath analysis across Europe. There are no previous published research papers evaluating the benchmarking of breath analysis.

Who are we asking to participate in this research?

Healthy adults (18-80 years old), with no history of chronic or recent acute illnesses.

7

8 Are there any people who should not take part?

People who associate with any of the following categories should not take part in the study

- People with serious allergies
- People who smoke or vape
- Pregnant women
- People who use anti-inflammatory drugs regularly
- People with metabolic disease
- Vegetarians or people who don't eat beef products (Beef Gelatine is present in the capsule shell)

9 If I agree to take part can I change my mind and stop?

- Yes.
- You will be asked to complete a participant Informed Consent Form after reading this information sheet.
- Any questions you may have must be answered to your satisfaction before you give your consent to participate.
- You may withdraw at any time before, during or after the study.
- You will not be asked to give any reasons for your withdrawal.
- If you wish to withdraw, please just tell the investigator.
- Even after you have finished participating in this study you can instruct us to destroy all data about you and excluded it from future analysis. You can do this at any time up to the final deadline for the completion of the study, which is the 30th September 2018. After that you will not be able to withdraw the data from the project.

10 How long will it take?

Please study the experiment schedule notes below. These show that that the study is planned to take 6.5 hours. Once you have given your first two breath samples and completed the questionnaire you can come and go between giving further samples.

You will give between 6 and 18 breath samples depending on the instruments and techniques allocated to your test. Each breath sample will take no more than 15 minutes. Some of the instruments collect a breath sample in a few seconds.

11 Is there anything I need to do before the experimental session?

- The day before the experimental session we ask you not to use any perfume or fragrances until after the experimental session.
- We ask you not to eat or use anything that contains mint flavour or fragrance (e.g., toothpaste or chewing gum).

12 What will I be asked to do during the experimental session?²

- We will provide a mouthpiece or a mask for you to breath into. The breath sampling is easy and effortless, allowing only allow collection of alveolar air.
- You will be asked to breathe normally for up to 10 minutes and during this time your breath will be sampled automatically; you need do nothing.
- You will be asked to provide a preliminary breath sample and then complete a questionnaire about your diet and personal habits.
- After this you will be asked to take a peppermint oil 200 mg supplement capsule and then provide more breath samples at 30 minutes intervals for up to 5 hours.
- We will ask you not to eat or drink dairy products throughout this time as this may interfere with the release of the peppermint oil into your circulatory system.

² See detailed experiment description at the end of this document.

13 What is in the peppermint oil capsule?

- Peppermint oil (200 mg) soya/sunflower oil and a capsule shell of beef gelatine and glycerol.
- The peppermint oil capsule is a digestive health food supplement manufactured and supplied by Boots Pharmaceuticals or by Obbekjaers.

14 Are there any risks with taking part?

This study poses little to no risk of discomfort to you.

Breath samples are acquired using different types of mouthpieces or masks, and you may find these unfamiliar and uncomfortable to begin with.

If this is the case you can stop immediately.

If you feel unwell or uncomfortable at any time just say so and the experiment will be stopped immediately.

You may not enjoy the taste of the peppermint oil capsule. There are no listed side effects. The capsule is marketed to help support healthy digestion and function of the digestive tract.

15 What personal information will be required from me?

We will ask questions about your height (cm), and weight (kg), age (years), as well as questions about your diet, personal habits and life style. Your answers will enable us to exclude possible dietary or life style factors from skewing the results.

It is important to note that your information will be anonymised and none of the researchers will be able to trace the information back to you or anyone. The index of the participants and their identifier codes is kept under lock and key by the principle investigator, who does not work directly with individual records.

16 Will my taking part in this study be kept confidential?

- Yes.
- We will use an ID code (e.g. P001) to refer to your data.

- The originals containing the index with your name and ID code will be held by Dr. Chris Mayhew in a closed locker.
- No one else will have access to this information and it is kept so that we can contact you if we need to (perhaps you leave something behind when you visit) or if you want to leave the project and have your information destroyed (we will need to identify all the data that relates to you).

17 What will happen to my data and the results of the study?

- The data we obtain from you and your breath samples will be consolidated and combined with data from other research centres to enable us to compare and evaluate different sampling and breath measurement methods. It will be safely stored in a repository at Loughborough University following the safety and privacy university's rules.
- We will publish our findings as a research article in a scientific journal. (No personal information will be used with or for the publication)
- We will also present this study at a conference organised by the International Association of Breath Research and copies of the slides will be available for anyone to download from our data repository. (No personal information will be used with or for the presentation)

18 What if I am not happy with how the research was conducted?

19 In the first instance, please contact:

Dr. Chris Mayhew

Email: c.mayhew@bham.ac.uk

Tel: 0121-4144729

Experiment Schedule

1. Participant preparation
 - a. Provide information sheet and obtain informed consent.
 - b. -24 hr from capsule ingestion. Excluding peppermint and peppermint associated products from diet and personal care routines until completion of peppermint washout. Participants can follow their normal dietary requirements, no restrictions are being made, and this includes dairy products.
2. Peppermint Washout experiment. This is based on a 1-D central composite design across an approximate exponential washout profile. Breath samples/measurements are to be taken at 30 min, 60 min, 90 min, 120 min, 150 min, etc. . Sample alveolar air.
 - a. -0.5 hr from capsule ingestion.
 - i. Baseline sample measurement.
 - ii. Start completion of participant information sheet and diet/lifestyle questionnaire.
 - iii. Remind the participants about dairy products and provide them with a list of items to avoid eating (Participant information sheet).
 - b. 0 hr
 - i. capsule is ingested and 150 ml is swallowed as quickly as is comfortable.
 - ii. Participant information sheet and diet/lifestyle questionnaires are completed.
 - c. 30 min
 - i. Washout sample
 - d. 60 min
 - i. Washout sample
 - e. 90 min
 - i. Washout sample
 - f. 120 min
 - i. Washout sample
 - g. 150 min
 - i. Washout sample

Participants will be able to leave or remain in the laboratory in between measurements. A desk will be made available for participants.

And so on up to 5 hours

3. Environmental/ambient air sample.
 - a. Select at random one of the sample points $t = 60 \text{ min}, 90 \text{ min}, 165 \text{ min}, 285 \text{ min}$ and 360 min .
 - b. On completion of the breath sampling of that chosen sample point, collect an environmental/ambient air sample, or make a measurement.

- c. Use the same sample/measurement volume as the breath samples/measurements while the researcher and participant are still present in the room.
4. Collect an air supply/instrument blank sample after completion of a breath sampling.

INFORMED CONSENT FORM
BREATH PROFILES AND WASHOUT CHARACTERISTICS FOR
PEPPERMINT OIL

(The researcher should guide the participant through the participant information sheet and ensure that all queries or questions are answered to the participant's satisfaction before completing this informed consent form.)

1. Taking Part

Please initial box

The purpose and details of this study have been explained to me. I understand that this study is designed to further scientific knowledge and that all procedures have been approved by the University of Birmingham's Ethics Committee.

I have been given a copy of the participant information sheet and I have read and understood the information sheet and this consent form.

I have had an opportunity to ask questions about my participation.

I understand that I am under no obligation to take part in the study, have the right to withdraw from this study at any stage for any reason, and will not be required to explain my reasons for withdrawing.

I agree to take part in this study.

2. Use of Information

I understand that all the personal information I provide will be treated in strict confidence and will be kept anonymous and confidential to the researchers unless (under the statutory obligations of the agencies which the researchers are working with), it is judged that confidentiality will have to be breached for the safety of the participant or others or for audit by regulatory authorities.

I agree for the data I provide to be securely archived at the end of the project.

3. Data

I agree that the Data obtained during this study can be stored for future use in research associated with the aims and objectives theme as this study.

Name of participant

[printed] Signature

Date

Researcher [printed] Signature Date

Participant Code:

APPENDIX 4- Chapter 8 (Concussion of Rugby players)

Questionnaire



20 Health Status Questionnaire for BREATHE study

Participant identification number:

Date:

Time:

All the information you give in this questionnaire will be treated with confidence and will not be divulged to any third parties.

Age

Sex

Height

Weight

1. Are you now, or have you in the past ever suffered from any of the following?
 - a. Severe asthma
 - b. COPD
 - c. Emphysema
 - d. Any other serious lung condition
 - e. Serious heart condition
 - f. Are you pregnant?

If the answer to any of the above questions is yes, then you may not take part in the study.

2. Do you have any other medical conditions

3. Do you smoke?

If yes: How many cigarettes a day?

For how long have you smoked?

PTO...

4. Have you ever smoked in the past?

If yes: How long ago did you stop?

a. How many cigarettes a day?

b. For how long did you smoke?

5. Have you been exposed to other people smoking in the past week?

6. Do you have an open fire, or have you recently been exposed to any other source of open fire?

7. Are you taking any prescribed medication other than the Pill? Please give details.

8. Are you taking any preparations or medications that have not been prescribed eg herbal remedies? Please give details.

9. Are you taking any food supplements such as vitamin pills, cod liver oil etc? Please give details.

10. Have you been eating normally in recent days? Eg would you say your appetite is normal?

11. When did you last have something to eat or drink?

12. What did you last eat or drink?

13. Have you eaten or drunk any of the following things in the past 24 hours?

20.1.1 Garlic

Coffee

Alcoholic drinks

14. Have you used nasal decongestants or any product containing menthol eg chewing gum, cigarettes, in the past 24 hours?

15. Do you normally eat food or drink with citrus flavours eg orange, lemon, grapefruit, including artificially flavoured drinks? Please give details.

16. Have you eaten citrus fruit or any food/drink with citrus flavour in the past 24 hours? Please give details.

17. Have you been anywhere where citrus or pine scented air fresheners have been used in the past week? Please give details.

P
T
O
...

Your signature